Accurate approximations for nonlinear vibrations

Alexander J Elliott

Submitted in fulfilment of the requirements for the

Degree of Doctor of Philosophy

School of Engineering

College of Science and Engineering

University of Glasgow

August 2019

Abstract

As global issues such as climate change and overpopulation continue to grow, the role of the engineer is forced to adapt. The general population now places an emphasis not only on the performance of a mechanical system, but also the efficiency with which this can be achieved. In pushing these structures to their maximum efficiency, a number of design and engineering challenges can arise. In particular, the occurrence of geometric nonlinearities can lead to failures in the linear modelling techniques that have traditionally been used.

The aim of this thesis is to increase the understanding of a number of widely-used, nonlinear methods, so that they may eventually be used with the same ease and confidence as traditional linear techniques.

A key theme throughout this work is the notion that nonlinear behaviour is typically approximated in some way, rather than finding exact solutions. This is not to say that exact solutions cannot be found, but rather that the process of doing so, or the solutions themselves, can be prohibitively complicated. Across the techniques considered, there is a desire to accurately predict the frequency-amplitude relationship, whether this be for the free or forced response of the system.

Analytical techniques can be used to produce insight that may be inaccessible through the use of numerical methods, though they require assumptions to be made about the structure. In this thesis, a number of these methods are compared in terms of their accuracy and their usability, so that the influence of the aforementioned assumptions can be understood. Frequency tuning is then used to bring the solutions from three prominent methods in line with one another.

The Galerkin method is used to project a continuous beam model into a discrete set of modal equations, as is the traditional method for treating such a system. Motivated by microscale beam structures, an updated approach for incorporating nonlinear boundary conditions is developed. This methodology is then applied to two example structures to demonstrate the importance of this procedure in developing accurate solutions.

The discussion is expanded to consider non-intrusive reduced-order modelling techniques, which are typically applied to systems developed with commercial finite element software. By instead applying these methods to an analytical nonlinear system, it is possible to compare the approximated results with exact analytical solutions. This allows a number of observations to be made regarding their application to real structures, noting a number of situations in which the static cases applied or the software itself may influence the solution accuracy.

Contents

List of Tables

List of Figures

Acknowledgements

I would like to take this opportunity to express my sincere gratitude to the people who have both enabled me to undertake such an interesting project and made the experience hugely rewarding and enjoyable.

Firstly, and most importantly, I would like to extend my deepest thanks to my supervisor, Dr Andrea Cammarano, for his expertise, guidance, patience, and passion for the field. Not only have these characteristics been invaluable from a technical viewpoint, but they have allowed me to develop into an enthusiastic and motivated researcher. I would also like to thank my co-supervisor, Prof. Simon Neild, for his guidance and wisdom in my research and for the numerous opportunities he has given me to expand my work.

I have been very lucky to work with a number of very informed and passionate people, including Dr Thomas Hill, Prof. David Wagg, and Dr Irene Tartaruga. I am grateful to have been able to work alongside them and have no doubt that my thesis is much stronger having done so.

Thanks must also be given to the friends that have encouraged me along the way, both outside the academic setting, who have provided me with both support and distraction when they have been required, and those on the inside, who have helped me on a daily basis. In particular, I would like to thank Graeme Hunt, Loizos Christodoulou, and Tata Sutardi, with whom I have been lucky enough to work alongside and coffee with since the outset.

To my family, and particularly my parents, brother, and sister, I thank you wholeheartedly for your support and understanding throughout this project, even if has not always been obvious what it is I have been doing.

Finally, I would like to express my heartfelt thanks to my wife, Tash, for her understanding, kindness, and, perhaps most importantly, patience throughout this process. Preparing this thesis has been no easy task, and it would not have been possible without her unwavering encouragement and support.

Author's Declaration

I declare that the work in this this was carried out in accordance with the regulations of the University of Glasgow. The work is original except where indicated by special reference in the text and no part has been submitted for any other degree.

Any views expressed in the dissertation are those of the author and in no way represent those of the University of Glasgow.

The thesis has not been presented to any other University for examination either in the United Kingdom or overseas.

Signed:

Dated:

Publications

As a result of the work undertaken in this thesis, the following publications have been produced.

Journal publications

- Elliott, A. J., Cammarano, A., Neild, S. A., Hill, T. L., and Wagg, D.J. (2018). Comparing the direct normal form and multiple scales methods through frequency detuning. *Nonlinear Dynamics*, 94(4):2919–2935.

- Tartaruga, I., Elliott, A. J., Cammarano, A., , Hill, T. L., and Neild, S. A. (2019). The effect of nonlinear cross-coupling on reduced-order modelling. *International Journal of Non-Linear Mechanics*, 116:7-17.

- Elliott, A. J., Cammarano, A., Neild, S. A., Hill, T. L., and Wagg, D.J. (2019, accepted). Using frequency detuning to compare analytical approximations for forced responses. *Nonlinear Dynamics*.

Conference publications

- Elliott, A. J., Cammarano, A., and Neild, S. A.. (2017). Comparing Analytical Approximation Methods with Numerical Results for Nonlinear Systems. In *Nonlinear Dynamics, Volume 1*, Kerschen, G., ed., Conference Proceedings of the Society for Experimental Mechanics Series, 37–49.

- Elliott, A. J., Cammarano, A., and Neild, S. A.. (2018). Investigating Modal Contributions Using a Galerkin Model. In *Nonlinear Dynamics, Volume 1*, Kerschen, G., ed., Conference Proceedings of the Society for Experimental Mechanics Series, 199-210.

- Elliott, A. J., Tartaruga, I., Cammarano, A., Dobson, P. S., and Neild, S. A.. (2018). Investigating reduced order models for nanoscale nonlinear structures. In *Proceedings of ISMA2018*.

Nomenclature

General nonlinear system

t	Time
$\dot{\bullet}$	First derivative of $\bullet$, with respect to time
$\ddot{\bullet}$	Second derivative of $\bullet$, with respect to time
N	Number of degrees-of-freedom
e	Euler's number
j	Imaginary unit, i.e. $\sqrt{-1}$
ε	A bookkeeping parameter denoting smallness
$\mathbf{x}$	An $N \times 1$ vector of physical displacements
$\mathbf{q}$	An $N \times 1$ vector of linear modal displacements
$\bullet^{\mathrm{T}}$	The transverse of matrix $\bullet$
$\mathbf{I}$	An $N \times N$ identity matrix
$\mathbf{M}$	An $N \times N$ mass matrix
$\mathbf{C}$	An $N \times N$ linear damping matrix
$\mathbf{K}$	An $N \times N$ linear stiffness matrix
$\mathbf{\Lambda}$	A diagonal $N \times N$ matrix of squared natural frequencies
$\mathbf{\Phi}$	An $N \times N$ mode shape matrix
ϕ_k	The k^{th} mode shape of a system
$\mathbf{\Gamma_x}$	An $N \times 1$ vector of nonlinear terms in physical coordinates
$\hat{\mathbf{P}}_\mathbf{x}$	An $N \times 1$ vector of excitation amplitudes in physical coordinates
$\mathbf{P_x}$	An $N \times 2$ matrix of excitation amplitudes in physical coordinates
$\mathbf{\Gamma_q}$	An $N \times 1$ vector of nonlinear terms in modal coordinates
$\mathbf{P_q}$	An $N \times 2$ matrix of excitation amplitudes in modal coordinates
$\mathbf{r}$	A 2×1 vector of complex exponential functions defining the sinusoidal nature of forcing

$\mathbf{F}_{\text{NL}}$	An $N \times 1$ vector of nonlinear forcing terms in physical coordinates
$\mathbf{F}$	An $N \times 1$ vector of external forcing terms in physical coordinates
$\mathbf{F}_{\text{NL},q}$	An $N \times 1$ vector of nonlinear forcing terms in physical coordinates
$\mathbf{F}_q$	An $N \times 1$ vector of external forcing terms in physical coordinates
ω_r	The response frequency of a structure
ω_n	The linear natural frequency of a structure
Ω	The forcing frequency applied to a structure
c.c.	Complex conjugate

Chapter 3

Harmonic balance

n	Number of harmonics in trial solution
$\bar{\bullet}$	Complex conjugate of $\bullet$
x_k	The k^{th} physical displacement of vector **x**
$A_{k,i}$	Coefficient of the i^{th} harmonic of the trial solution for x_k
ϕ_k	Phase of the fundamental harmonic of x_k

Multiple scales

Derivative-expansion

T_k	The k^{th} component of the perturbation of time (t), equal to $\varepsilon^k t$
D_k	First derivative with respect to T_k, equal to $\frac{\partial}{\partial T_k}$
$\mathbf{x}_k$	The k^{th} component of the perturbation of the physical displacement vector (**x**)
$\mathbf{q}_k$	The k^{th} component of the perturbation of the modal displacement vector (**q**)
$\nabla_\bullet$	The gradient of vector $\bullet$
$q_{k,n}$	The n^{th} element of $\mathbf{q}_k$
$\phi_{k,n}$	Phase of the n^{th} component of $\mathbf{q}_k$
$\Gamma_{q,k}$	The k^{th} component of $\mathbf{\Gamma_q}$

Two-timing

τ	Fast time scale, assumed to respond at frequency ω
T	Slow time scale

T_s	Extra slow time scale
$\bullet^{\dagger}$	First derivative, with respect to τ
$\bullet^{\ddagger}$	First derivative, with respect to T
$\bullet^{*}$	First derivative, with respect to T_s

Direct normal form

$\mathbf{v}$	An $N \times 1$ vector of force-transformed displacements
$[e]$	An $N \times 2$ matrix used to isolate the resonant terms in $\mathbf{v}$
$[e]_k$	The k^{th} row of $[e]$
$\mathbf{W}$	An 2×2 diagonal matrix with entries $+\text{j}\Omega$ and $-\text{j}\Omega$
$\mathbf{\Gamma_v}$	An $N \times 1$ vector of nonlinear and damping terms in force-transformed coordinates
$\mathbf{P_v}$	An $N \times 2$ matrix of excitation amplitudes in force-transformed coordinates
$\mathbf{u}$	An $N \times 1$ vector of displacements in resonant coordinates
$\mathbf{\Gamma_u}$	An $N \times 1$ vector of nonlinear and terms in resonant coordinates
$\mathbf{P_u}$	An $N \times 2$ matrix of excitation amplitudes in resonant coordinates
$\mathbf{h}$	An $N \times 1$ vector of harmonic components of displacements in resonant coordinates
$\mathbf{h}_k$	The k^{th} component of the perturbation of $\mathbf{h}$
u_k	The k^{th} component of $\mathbf{u}$
u_{kp}	The positive component of the complex conjugate pair that comprise u_k
u_{km}	The negative component of the complex conjugate pair that comprise u_k
A_k	Amplitude of u_k
ϕ_k	Phase of u_k
$\omega_{r,k}$	Response frequency of u_k
$\mathbf{\Upsilon}$	An $N \times N$ diagonal matrix of squared response frequencies
N_k	Number of combinations of the elements that comprise $\mathbf{u}_p$, $\mathbf{u}_m$, and $\mathbf{r}$
$\mathbf{u}_k^*$	An $N_{\times}1$ vector all possible combinations of the elements that comprise $\mathbf{u}_p$, $\mathbf{u}_m$, and $\mathbf{r}$
$\mathbf{\Gamma_{v,k}}$	An $N \times 1$ vector containing the components of $\mathbf{\Gamma_v}$ that respond at $\omega_{r,k}$
$\mathbf{\Gamma_{u,k}}$	An $N \times 1$ vector containing the components of $\mathbf{\Gamma_u}$ that respond at $\omega_{r,k}$

$\mathbf{n}_{\mathbf{u},k}$	An $N \times 1$ vector containing the resonant components of the k^{th} homological equation
$[\Gamma_{v,k}]$	An $N \times N_k$ vector containing the time-independent coefficients of the terms in $\mathbf{\Gamma}_{\mathbf{v},\mathbf{k}}$
$[\Gamma_{u,k}]$	An $N \times N_k$ vector containing the time-independent coefficients of the terms in $\mathbf{\Gamma}_{\mathbf{u},\mathbf{k}}$
$[h_k]$	An $N \times N_k$ matrix containing the time-independent coefficients of the terms in $\mathbf{h}_k$
$u^*_{k,\ell}$	The ℓ^{th} element of $\mathbf{u}^*_k$
U_k	The amplitude of the fundamental component of the k^{th} linear mode
$\boldsymbol{\beta}_k$	An $N \times N_k$ matrix used to determine the resonance of the terms of the k^{th} homological equation
$P^+_{u,k}$	The time-invariant component of the k^{th} element of $\mathbf{P}_\mathbf{u}$, corresponding to the positive conjugate of the forcing term
$P^-_{u,k}$	The time-invariant component of the k^{th} element of $\mathbf{P}_\mathbf{u}$, corresponding to the negative conjugate of the forcing term
$\Gamma^+_{u,k}$	The time-invariant component of the k^{th} element of $\mathbf{P}_\mathbf{u}$, corresponding to the positive conjugate of the resonating term
$\Gamma^-_{u,k}$	The time-invariant component of the k^{th} element of $\mathbf{P}_\mathbf{u}$, corresponding to the negative conjugate of the resonating term

Frequency detuning

δ	A detuning parameter applied to the square of the natural frequency
$\omega_{d,k}$	The k^{th} detuning frequency
$\mathbf{\Upsilon}_\mathbf{d}$	An $N \times N$ diagonal matrix of squared detuning frequencies
δ_d	Arbitrary detuning parameter
γ	Parameter used to vary the arbitrary detuning

Duffing oscillator

x	Physical displacement of the mass
q	Modal displacement of the mass
v	Force-transformed displacement of the mass
u	Resonant component of the displacement of the mass
h	Harmonic component of the displacement of the mass

ζ	Damping coefficient
ω_n	Natural frequency of the oscillator
α	Coefficient of the cubic nonlinear term
P	Forcing level applied to the system
A	Oscillator amplitude
Ω	Frequency of the sinusoidal forcing
ψ	Linear transformed phase angle
σ	Detuning of the natural frequency

Chapter 4

Beam definition

ℓ	Undeformed beam length
E	Young's modulus
I	Second moment of inertia
ρ	Density
$\hat{A}$	Cross-sectional area
M	Bending moment
x	Position along the beam
w	Transverse displacement
V	Shearing force
f	Continuous load
a	Parameter used to compile the influence of the physical properties of the beam
ϕ_k	The k^{th} linear mode shape
q_k	Contribution of ϕ_k to the physical beam displacement
p_k	Assumed frequency of the sinusoidal response of ϕ_k
κ	Parameter used to compile p_k and a
c_n	Coefficients of the trigonometric components of ϕ
T	Tension force
Δs	Small length of beam
L	Deformed beam length
F_z	Combined external and internal forces
P	Compressive loading of the beam at the boundary conditions

ψ	Beam rotation
N	Number of linear modes in the truncated model
$\alpha_{2,n,k}$	Parameter used to denote the integral of the product of ϕ_n and the second derivative of ϕ_k, with respect to x
$\alpha_{4,k}$	Parameter used to denote the integral of the product of ϕ_k and its fourth derivative, with respect to x
$\beta_{i,j}$	Parameter used to denote the integral of the product of derivatives of ϕ_i and ϕ_j, with respect to x
$\hat{k}$	Rotational spring stiffness
δ	Dirac delta function
k_L	Linear compression spring constant
$\hat{K}_L$	Non-dimensionalised linear compression spring constant
$\mathbf{c}$	Vector of coefficients c_n
$\mathbf{A}$	Matrix of coefficients got $\mathbf{c}$

Non-classical boundary conditions

$\bullet'$	First derivative of $\bullet$, with respect to x
BC	Boundary condition, either $x = 0$ or $x = \ell$
f_{BC}	Function defining the boundary condition at $x =$ BC
C^k	Set of functions that are k-times differentiable
N_{BC}	Order of f_{BC}
$\mu_{\text{BC},k}$	The k^{th} coefficient that arises in the Taylor expansion of f_{BC}
λ_{BC}^n	Coefficient of c_n in ϕ''' at BC
$\mu_{\text{BC}}^{k_1,k_2}$	Coefficient of $c^{k_1}c^{k_2}$ in the expansion of f_{BC}
(X, Y)	Assumed solution to the system of equations defined by the boundary conditions
z	Dummy variable to allow the system to be defined by only one of X and Y
$\hat{\mu}_{\text{BC}}^{k_1,k_2}$	Updated version $\mu_{\text{BC}}^{k_1,k_2}$ to include linear boundary conditions
N_{max}	Maximum order of boundary condition functions
ν_{BC}	Coefficient tensor for system of equations defined by the boundary conditions
$\mathcal{R}_{n\|s}(\bullet)$	Tensor resultant of a system, $\bullet$, of n polynomials of order s
$\hat{K}_n^{(\text{BC})}$	The n^{th}-order spring stiffness at $x =$ BC

Cantilever beam with magnetic tip interaction

q_i	Point charge on the beam
q_j	Point charge on the stator
$\mathbf{F}_{i,j}$	Attractive force between q_i and q_j
K_m	Constant accounting for the characteristics of the magnets
$\mathbf{d}_{i,j}$	Radius vector applied to q_i and q_j
$d_{i,j}$	Distance between q_i and q_j
δ_i	Distance of q_i from he vertical centre of the beam
δ_j	Distance of q_j from he vertical centre of the stator
D	Horizontal distance between the beam and stator
h_b	Beam thickness
h_s	Stator thickness
w	Vertical distance between the centres of the beam and the stator
w_b	Beam width
w_s	Stator width
F_M	Net force arising from magnetic boundary condition
σ_{BC}^k	Coefficient of the linear component of the equation for $x = \text{BC}$
μ_{BC}^{ijk}	Coefficient of the cubic component of the equation for $x = \text{BC}$
$\phi_{\text{BC},n}$	The n^{th} mode shape for particular set of boundary conditions
$\mathbf{\Phi}_{\text{comb},n}$	An $N \times 2$ matrix defined by the n^{th} mode shapes of cantilevers with free and pinned tips

Chapter 5

N	Order of truncation for the Galerkin model
$A_{ijk}^{(n)}$	Coefficient of $q_i q_j q_k$ in the n^{th} modal equation of motion
$B_{ij}^{(n)}$	Coefficient of $q_i q_j$ in the n^{th} modal equation of motion
Γ_2	Number of quadratic coefficients
Γ_3	Number of cubic coefficients
L	Lagrangian function
T	Kinetic Energy
U	Potential energy
σ	Generic combination of modal shapes, applied as either a force or a displacement

a_n	Contribution of ϕ_n to σ
Γ_{static}	Number of prescribed static cases
F	Applied modal force in the implicit condensation method
C_k	Scale factor of the k^{th} mode shape in F
N_{th}	Number of modes with non-zero contributions to F
t_R	Variable, referential scale factor used in defining $\{C_k\}$
$\tilde{\bullet}$	Notation to highlight approximate nature of ROM
$\hat{\bullet}$	Notation for exact modal displacements
k_3	Cubic stiffness coefficient
k_5	Quintic stiffness coefficient
$\gamma_{i,j,k,l}$	Cross-coupling term between mode shapes ϕ_i, ϕ_j, ϕ_k, and ϕ_l
η_J	Coefficient of $\prod_{x\in J} q_x$
N_y	The number of elements of the set $A = \{a, b, c, d\}$ that are equal to y
$(N_{\{a,b,c,d\}})!$	Parameter equal to $N_a!N_b!N_c!N_d!$
$\setminus$	Set difference operator

Chapter 6

u_k	The k^{th} node of a discretised beam
F_k	Sum of force experienced by u_k from the elements either side of it
F_k^e	Contribution to F_k from element e
$\delta_{i,j}$	The proportion of the response force $-F_j$ experienced at u_i
f_k	Sum of force experienced by displaced node u'_k from the elements either side of it
$N^{(k)}$	Shape function for element e_k
w_{inc}	Incrementally increasing beam displacement
w_{lin}	Linearly increasing beam displacement
w_i	Beam displacement defined as $iw_{\text{inc}} + (1-i)w_{\text{inc}}$, for some $i \in [0, 1]$
$F_{q,n}$	Modal forcing for iteration n
x_{des}	Desired maximum physical beam displacement
q_{des}	Desired maximum modal beam displacement
α_n	Updating parameter for iteration n
$\bullet^+$	Moore-Penrose pseudo-inverse

Chapter 1

Introduction

The understanding and modelling of nonlinear vibrations continues to grow in importance as mechanical structures are designed to perform outside the region in which the observed behaviour is effectively linear. While the assumption of linear behaviour has traditionally been dependable, this tends not to be the case in next-generation technology that requires structures that are ultralight and flexible, or on a scale that is significantly larger or smaller than previous systems. As a result of this traditional assumption, a useful framework for modal analysis and testing has been developed and widely applied as a methodology to predict the response of a system. At the time of writing, the complex behaviours and models for nonlinear structures have prevented an equivalent scheme from being satisfactorily developed. That is, in the ideal scenario, it would be possible to be able to understand nonlinear systems with the same speed and accuracy as traditional modal analysis provides for linear structures.

The complexity introduced by nonlinearity can be observed both in the system behaviour and the equations of motion through which this is captured. Naturally, the two are inherently linked. From a modelling perspective, many of the challenges arise from the fact that a number of key properties exhibited by linear systems are not guaranteed for the nonlinear case. Principal among these properties is the orthogonality of the linear modes; the practical implication of this is that energy contained in one mode will remain in this mode, regardless of the behaviour of other modes. A direct result of this characteristic is that the overall system response can be found simply by the superposition of the modal responses. Thus, if the practitioner is able to deduce which modes will contribute significantly to the oscillatory response, it is possible to produce an accurate model using a very small modal basis.

In contrast to this relatively simple case, a defining feature of nonlinear systems is the possibility of energy being transferred from one mode to another; this is typically referred to as *modal interaction* or *internal resonance*. Thus, the development of a low-order system of equations is inhibited by the fact that the inclusion of one mode in the modal basis may lead to the activation of other modes that have not been included. A number of reduced-order modelling techniques have been considered for nonlinear structures, though the confidence that can be placed in their results remains somewhat unclear. This thesis will aim to further the fundamental understanding of these methodologies, representing an important step towards a nonlinear equivalent to modal analysis.

As well as this focus on modal bases, it must be noted that models of just a single mode may also exhibit nonlinear behaviour. In particular, it can no longer be assumed that the natural frequency is independent of the response amplitude. The literature has provided a wide range of examples in which this frequency is seen to change at higher amplitudes, which can introduce a number of challenges for the aforementioned flexible systems that continue to be pursued; further details of this will be provided in Chapter 2. As well as providing further complexity to analytical models, this phenomenon introduces a number of hysteretic behavioural traits that could cause serious damage to these structures, if they are not accurately predicted. Examples of this hysteresis include amplitude jumping as the frequency varies and also contributes to isolated components of the frequency response, as will be outlined in the following chapter.

Given that models of such a small scale can exhibit nonlinear behaviour, the techniques involved in their modelling remain an active area of interest. It is often possible to treat these systems through the numerical continuation of a periodic orbit from the linear regime, though this can be restrictive in cases that have isolated sections of the response. Furthermore, it has been observed that the computational expense of such techniques can rapidly increase with the number of degrees-of-freedom (DOFs), and, in continuous structures (with an infinite number of DOFs), hyperdimensional torus bifurcations can occur, which are particularly difficult to continue numerically. To overcome these challenges, a number of analytical methods have been developed to create an approximation of the response in a more reasonable timescale. Each technique utilises a number of assumptions in developing a model and, as such, there can be notable variation in the accuracy of their results. Thus, the choice of the most appropriate technique can be somewhat unclear for the user. To overcome this issue, the work of this thesis will thoroughly compare the techniques both in terms of their accu-

racy and their applicability, with the intention of providing the user with a clear choice as to the most practical way of meeting their modelling requirements.

In general terms, the aim of this thesis is to contribute to the development and understanding of techniques for approximating nonlinear responses, so that they may eventually be applied with the same degree of confidence as their linear counterparts. This includes the comparison of these methods as they currently exist, as well as establishing ways in which they can be developed to give a more accurate response. The more specific research aims are explored in the following section.

The major novel contributions of this work can be summarised as follows:

- The performance of the multiple scales technique has been improved through the use of the frequency detuning applied in the direct normal form method.
- An investigation of the correlation between modal coupling terms and the occurrence of modal interactions has been undertaken, highlighting trends that could indicate such behaviour.
- A methodology for the incorporation of nonlinear boundary conditions in the Galerkin method has been developed, allowing their influence on modal properties to be explored.
- A fundamental investigation of the implicit condensation and enforced displacement techniques has been undertaken to further the understanding of their respective merits and shortcomings, as well as highlighting the influence of commercial software.
- An investigation into disparities between the implicit condensation (IC) and enforced displacement (ED) techniques in the literature has explained the reasons for this phenomenon, allowing suggestions to be made regarding how this could be overcome.

1.1 Research aims

The aims for this thesis can be summarised as follows:

1. To extend and align the usage of analytical techniques used to approximate nonlinear system response.

Given the scope of behaviour that could be predicted using these methods, particularly in reduced-order models (ROMs), it is important that the practitioner of these techniques is aware of their potential shortcomings, both in terms of accuracy and usability. To this end, a thorough comparison of three of the most widely used of these methods will be given, initially assessing the accuracy of each method. From this assessment, attempts will be made to pinpoint the reasons for accuracy in these techniques and apply these in the others, so that the user has the option of selecting any technique and producing equally accurate results.

2. To further the understanding and application of the Galerkin method, particularly for micro-/nanoscale electromechanical system (M/NEMS) devices.

   As discussed above, the Galerkin method has a key role to play in the understanding of M/NEMS devices. In this thesis, a new methodology for modelling nonlinear BCs is introduced and the influence this has on the nonlinear behaviour of the structure is assessed. The generality of this methodology will allow the modelling of complicated BC relationships (such as those seen in an atomic force microscope (AFM)), so long as the mathematical definition of this relationship can be approximated using a Taylor expansion. Through this, the prediction of complex behaviour, such as modal interaction, will be possible; an initial assessment of this behaviour will be given in this thesis.

3. To investigate the performance of non-intrusive ROM techniques and contribute to their development.

   Although widely used, techniques such as the IC and ED methods require significant further testing if they are to be applied beyond the academic sphere. In this thesis, they will first be investigated using the Galerkin method as a “full” model, so that their coefficients can be directly compared to those in the full system of equations. The correlation between this prediction and the behaviour of the ROM will then be investigated. The results from this somewhat artificial implementation of the IC and ED methods will then be compared with the results from the true application in an attempt to resolve certain issues that may currently occur in their usage.

1.2 Thesis outline

Chapter 2 - Literature review

A thorough review of the literature associated with nonlinear vibrations is provided, highlighting the areas in which the contributions of this work are necessary. This chapter will not only review the studies that defined, developed, and applied the techniques studied throughout the thesis, but will also provide wider context in terms of observed nonlinear behaviour and methods that are not explicitly considered in this work.

Chapter 3 - Analytical approximation methods

The comparison and alignment of methods used to create analytical approximations of the system response is a key motivation for this thesis. In Chapter 3, three widely-applied methods are introduced and derived; namely, these are the harmonic balance, multiple scales, and direct normal form techniques. To aid the comparison, each of these methods will be applied to both a single-degree-of-freedom Duffing equation and to a more general two-degree-of-freedom, lumped-mass oscillator. Based on observations made in the literature, the frequency detuning applied in the DNF method will be further applied in the MS technique, to show that it is possible for the two techniques to give identical results with a single, relatively simple change. This discussion of frequency detuning is further investigated using a general formulation.

Chapter 4 - The Galerkin method

The recent resurgence of the Galerkin method in the field of M/NEMS modelling has occurred, in part, due to the relative structural simplicity of these devices. That being said, the often significant slenderness of these structures and increased influence of atomic forces require careful consideration, if this methodology is to be used accurately. Building on classical boundary conditions for these structures, these models are initially adapted to be asymmetrical, so that the prediction of modal interaction behaviour can be assessed. Following this, a novel, nonlinear algebraic approach is proposed to develop models in which the BCs themselves are nonlinear.

Chapter 5 - Non-intrusive reduced-order modelling

Chapter 5 introduces two non-intrusive reduced-order modelling techniques; namely, these are the implicit condensation and enforced displacement methods. While the techniques are

typically applied to models developed using specialist finite element software, to provide further insight into the effect of the underlying assumptions on the final implementation, they are applied to analytical models in this section. First, they are applied to lumped-mass systems with cubic nonlinearities, before being used to predict the behaviour of a continuous Galerkin model for an asymmetric beam configuration at cubic order. This discussion is then expanded by considering both models up to quintic order, mirroring the more realistic case in which the order of the approximation is not equal to that of the full model.

Chapter 6 - Understanding reduced-order modelling techniques

In Chapter 6, the nature of the results from the two methods applied in Chapter 5 is observed to be qualitatively different from results in the literature for similar structures that are modelled using finite element software. The primary focus of this chapter is to investigate these differences and provide insight that may explain this. Particular attention is given to the manner in which the static cases associated with each method are implemented in the finite element software, and the effect that this has on the result.

Chapter 7 - Conclusions and future work

This final chapter presents the conclusions that are drawn from the work of this thesis, outlining their potential importance in terms of nonlinear vibrations generally and for the more specific field of M/NEMS design. The possible ways in which this research could be expanded and applied are also discussed.

Chapter 2

Literature Review

2.1 Overview

Throughout the engineering disciplines, the pursuit of efficiency remains an important and active goal. As the world looks to engineers for solutions to the rapidly-growing issues of climate change [3, 4] and population growth [5], this objective becomes increasingly relevant and substantial. As such, the research and development of mechanical solutions has recently seen a noticeable shift in focus; where once the aim was solely to push the limits of performance, there is now a marked interest in the ability to do so in the most energy-efficient manner. This has been recognised as a key motivation in the field of aeronautics [6, 7].

The engineering challenges associated with developing these highly-efficient structures are numerous, as the systems are frequently pushed past the performance envelope that has historically been experienced. Significant decreases in the mass of a mechanical component can often be associated with dramatic increases in its flexibility, as has been demonstrated and investigated in a recent collaborative project between researchers at NASA and MIT investigating fuel-efficient aeroplane wings [8].

Recent developments such as these undoubtedly have the potential to make meaningful and sustainable changes to countless problems around the globe, but they are frequently observed to push the behaviour of the structures beyond the limits of traditional modelling methods. In particular, the classical approach focuses on *linear* dynamic behaviour and assumes that the nonlinear characteristics of the response are negligible. This strategy has the potential to overlook potentially destructive behaviour such as hysteresis and frequency shifting phenomena that can occur at high-amplitude vibrations of nonlinear systems (see, for

instance, [9]). A real-world example to illustrate the destructive nature of these phenomena can be observed in the former NASA Hyper-X programme [10], the failure of which has largely been ascribed to shortcomings of linear modelling techniques [11]. This highlights the need for accurate, usable methods for calculating the nonlinear dynamics of engineering structures.

The potential for nonlinear behaviour continues to grow in a number of engineering applications, such as the development and study of wind turbine blade performance. An example of this can be found in the study of Ataya and Ahmed [12], which investigated damage to wind turbine blades on their trailing edge, studying eighty-one 100 kW-rated turbines and eighteen with a rating of 300 kW. This survey motivated a comprehensive study into the causes of such a failure [13], concluding that:

> *"It was shown, both experimentally and numerically, that a geometric nonlinear longitudinal trailing-edge wave can occur in blades, which are designed to prevent local buckling. Such a wave can have serious consequences for the integrity of the adhesive trailing-edge joint."*

Failures relating to the aforementioned joints have been observed in failures of the Siemens B53 wind turbine blade observed at the Ocotillo and Eclipse wind farms [14].

As alluded to above, lightweight, flexible vehicles that require less fuel are actively sought as a direct consequence of the issues discussed in [6, 7]. The blade vibration observed in these vehicles is qualitatively very similar to the behaviour of the aforementioned wind turbine blades. As such, the nonlinear behaviour of high-aspect ratio wings remains a key area of research; a summary of findings in this area is presented in [15].

The aerospace industry provides a number of examples where nonlinear behaviour must be carefully monitored to ensure that structural failure is not encountered. For example, the occurrence of landing gear shimmy oscillations, as reviewed in [16], has been connected to the failure of the Fokker MK-100 aircraft in November 1999 [17]. Further complexity can be experienced in the consideration of the *rotating* components of aerospace systems, such as rotor and blades of a helicopter, as invsetigated in [18].

Even without the addition of long blade components, rotating structures are often seen to exhibit geometric nonlinearities. Manufacturing and drilling processes often experience

nonlinear responses, particularly when considered in conjunction with friction effects. The coupling of the axial and torsional vibration modes is identified as the root cause of the occurrence of self-excited oscillations in a drill bit, in [19], and chatter in machining processes, in [20]. In both cases, the shutdown of the entire process would be required to stop this unwanted vibration.

Recently, the development of micro- and nanoelectromechanical systems (M/NEMS) has provided further motivation for investigating nonlinear behaviour. It is often the case that this behaviour is more pronounced than in similar macroscale structures; for instance, in [21], a MEMS device with behaviour defined by the nonlinear Mathieu equation is seen to exhibit five parametric resonances, whereas only one has been observed in larger structures. As has been reported in the review paper of Rhoads *et al.* [22], nonlinear behaviour has been observed in a wide variety of micro- and nanoscale structures and there are a number of factors that contribute to this.

As can be seen from this discussion, the behavioural traits associated with nonlinear structures have the potential to cause a great amount of damage. The modelling requirements to accurately capture and understand these phenomena continue to be of active interest to the field of mechanical engineering research. One of the key goals is to develop techniques that avoid giving analytical solutions that are prohibitively complex. It must be noted that strategies for modelling nonlinearities have been developed both for purely analytical systems and those developed in finite element software. In some cases, it is possible that the structure could be modelled either numerically or analytically, though the most suitable method is not always apparent. This thesis aims to contribute to the understanding of a number of these techniques, allowing the user to make a more informed decision as to the most applicable methodology for their structure.

2.2 Nonlinear vibrations in engineering structures

As has been observed in §2.1, the potential scope for structures exhibiting nonlinear characteristics is extremely broad, both in terms of the variety and the scale of these mechanical systems. These range from large, lightweight wind turbines [13, 23] to increasingly small and intricate micro- and nanoscale devices [22]. Whether this behaviour is desired or not, the accurate modelling of the associated phenomena presents a significant challenge to engineers.

In linear dynamic structures, there is an underlying assumption that each linear normal mode has a natural frequency for its vibration, and that the value of this is invariant to the behaviour of the system [24]. It can be further observed that these linear modes are orthogonal to one another. Mathematically speaking, this means that it is not possible for one mode to be written as a linear combination of the others, but the practical implication of this is that the contribution of one mode to the response has no influence on that of the others. As such, linear systems follow the principle of superposition, by which the full system response can simply be found through the summation of the contributions of the linear modes. These modelling techniques and assumptions undoubtedly provide a useful framework, which has been used to great effect in the modelling of classical engineering structures. However, the assumptions of uncoupled modes and of invariant natural frequencies do not hold for nonlinear structures, so this approach must be developed or replaced to accommodate more complicated behaviour.

Nonlinearity can be introduced to mechanical structures in a number of ways. The focus of this thesis will be on *geometric* nonlinearity, in which the geometry of the structure changes in deformation, leading to changes in the structural properties and, hence, the system response. These systems are typically characterised using polynomial expressions, though the approach differs depending on the size of the deformation, as summarised in [9]. It must be noted that, although not discussed in this thesis, it is possible for the material of a structure, or any contact it may have with other bodies (such as impact or friction), may also lead to nonlinear behaviour. However, in contrast with geometric nonlinearities, it may not be possible to use a polynomial expression in terms of the displacement to model these nonlinear effects, particularly in the case of contact nonlinearities. Further details of such phenomena may be found, for example, in [25]. From this point forward, any references to 'nonlinear' behaviour will be taken to refer to geometric nonlinearity.

In nonlinear structures, the natural frequencies have been observed to shift as the response amplitude changes [26]. Therefore, the resonance peak will appear at different frequencies for different excitation levels. Although this difference may appear simple, it can add a great deal of complexity to both the response itself and the mathematical tools required to capture it. For a linear model, the peak of the response will be exactly at the linear natural frequency, regardless of the amplitude. Therefore, the locus defined by the peak of the curve at different displacements is simply a straight, vertical line. In the nonlinear case, the aforementioned shifting of the natural frequency at higher amplitudes creates

a locus (or *backbone curve*) that can move away from the linear natural frequency at higher displacement levels. This can lead to the phenomenon of multistability, in which a single forcing frequency may induce a stable periodic orbit for more than one amplitude, leading to systems that exhibit hysteretic behaviour [26]. An example of this has been observed in the 'jumping' phenomenon in aircraft dynamics, as addressed in [27]. Furthermore, if the modes are not uncoupled, it is possible for an internal resonance to occur between them, in which energy may transfer from one to another, as remarked in [28].

These behavioural phenomena correspond to nonlinear terms in the equations of motion. These terms typically result in analytical approximations that are extremely complicated and, hence, require a great deal of further manipulation to allow the system to be understood. As such, the typical approach is to approximate the response in some way, either using an analytical method or by employing a numerical strategy. In either case, the solutions are no longer exact, and their accuracy is dependent on the assumptions made in the creation of the approximation. There are a number of methods that may be applied, and the user must decide which assumptions will lead to an accurate approximation of the system behaviour. The most suitable and applicable method, and the implications of its assumptions, are not necessarily known *a priori*.

For the methods discussed in this thesis to become as reliable as their linear counterparts, it is important to remove the uncertainty associated with their accuracy and usability. As summarised in Chapter 1, a key aim of this thesis is to extend the understanding of a number of nonlinear techniques. As such, the current chapter will address the historical and recent developments in the field, as well as highlighting those areas in which further research may be beneficial to the practitioner.

2.3 Numerical approaches

2.3.1 Response approximation techniques

The ability to accurately capture and predict the response of nonlinear structures is an important challenge in theoretical and modelling studies. This has been illustrated by the example structures in §2.1, the success of which can not be guaranteed without a sufficient understanding of the system dynamics.

The atypical physical characteristics observed in these structures translate to nonlinear terms in the equations of motion. It is the inclusion of such terms that leads to overly com-

plex analytical solutions that provide little insight without significant extra algebraic manipulation. This leaves the practitioner with two options to predict the behaviour of these structures. On one hand, an analytical method could be used to approximate the behaviour, as will be discussed in §2.4.1. Alternatively, the periodic response across a certain frequency range can be created numerically by selecting an initial periodic orbit in the linear regime and applying a continuation method. The latter of these options is discussed here.

Numerical continuation programmes, such as the *AUTO-07p* package[1] [29, 30], *MatCont* [31, 32], and *Continuation Core (COCO)* [33, 34], have been widely applied to nonlinear structures. In particular, the work of [18] utilises numerical continuation to assess the nonlinear dynamics of an autogyro beyond the parameter window that can be achieved experimentally. A similar methodology was applied in [35], in which experimental results were supplemented with numerical responses. The lack of detailed knowledge of the basins of attraction led to some stable solutions being experimentally inaccessible.

Due to the multitude of experimentally-observed nonlinear behaviour in M/NEMS structures, as addressed above, the use of numerical continuation methods for such systems has become increasingly common.

A series of studies by Caruntu *et al.* has utilised AUTO-07p to predict bifurcation behaviour in both MEMS cantilever beams [36–38] and circular plates [39, 40]. However, the continuation had to be applied to a reduced-order model of the structures, since the process can be extremely computationally expensive for larger systems. A similar microarch structure, modelled as a pinned-pinned beam and reduced using the Galerkin method, is investigated using the same software in [41], which observed both internal resonance and softening-to-hardening behaviour in the structure. The work of [42] utilised the MatCont package to analyse the lumped-mass model of a MEMS oscillator; in this case, the multiple scales method was required to reduce the order of the system. The examples of this paragraph highlight the fact that, while it is possible to apply numerical continuation techniques to a variety of real-world structures, it is typically necessary to first approximate the system dynamics using a small number of equations. This is a result of the rapid increase in computational expense associated with the continuation of large systems of nonlinear equations and provides motivation both for the pursuit of reduced-order modelling techniques and of analytical approximation methods that do not have such a steep increase in computation time.

[1] AUTO-07p is the current version of this software, but the programme has been in development since the 1970s.

The effectiveness of these general numerical continuation software packages in nonlinear vibration applications has inspired the development of a number of methodologies that are aimed specifically at predicting nonlinear behaviour in mechanical structures. The *NNMcont* programme is one such example of these [43]; its methodology is described in [44]. The programme employs a shooting strategy that allows the continuation of NNMs to be achieved. Recently, this method has been used to investigate the NNMs of a gong [45], in which the nonlinear model was shown to match well with experimental results, though only when a large number of modes was included.

One potential drawback of the NNMcont programme is its dependence on extensive numerical solutions that would introduce a large computational expense for complex structures, a point which is addressed by Peeters *et al.* in [44]. To address this, in [46, 47], Kuether *et al.* expanded the algorithm through the use of a predictor-corrector step, so that only a single period was required to be calculated in the finite element software. The methodology begins by using a single linear mode of the system to produce the required period and expands the modal basis once the error becomes too great. The results generated using this technique showed good agreement with those found using the original NNMcont method, but were found in a matter of minutes, whereas the full model required over four days of calculation to create.

It should be noted that the continuation concept has also been pursued outside of numerical and analytical systems, with an experimental strategy being applied in the development of control-based continuation methods. The theoretical framework for this technique was initially outlined in [48], which provided a strategy for the continuation of periodic orbits and bifurcations. The methodology was then successfully applied to a nonlinear energy harvester in [49] and a cantilever beam with magnetic interaction at the tip in [50]. The application and understanding of this technique continues to be expanded. In [51], the optimisation of an impact oscillator was investigated through the introduction of a tuning scheme. The same system was used to investigate the possibility of calculating the stability of each periodic oscillation in [52], with further analysis of both stability and bifurcation for a SDOF oscillator given in [53]. This discrete system has also been used to calculate the backbone curve of a physical structure in [54].

2.3.2 Finite element models and reduced-order modelling

Across the field of engineering, it is common practice to use computer-aided design software to develop finite element models for real structures. In such systems, the continuous model is discretised into a set of nodes and elements with well-defined behaviour. The user is typically given the choice of the most suitable elements to fully characterise the physical structure. However, the most widely-used and robust finite element software packages tend to be commercial, which means that the source code is not accessible; in this respect, these packages must be considered as "black box" systems. While this is not a problem in and of itself, it does mean that the user interested in the nonlinear behaviour of the system does not have direct access either to the nonlinear parameters themselves or the process in which the nonlinearity is treated.

Although these finite element software packages are capable of modelling extremely complicated structures, the number of elements required to accurately capture the behaviour can often lead to computations that are prohibitively time-consuming. As such, it is common practice to approximate this behaviour using a reduced-order model (ROM). In the linear regime, this is typically achieved by simply retaining the modes that oscillate within the expected frequency range [24]. However, when nonlinearity arises in the structure, there is the possibility that energy can transfer between the modes, leading to internal resonances and vibrations at higher or lower frequencies than those actuated [55]. It is not always clear as to which modes should be retained; this can be addressed in a number of ways. Often, only the response of the first mode is of interest, so only one mode will be retained. For higher-order ROMs, it is possible to select a representative modal basis based on previous numerical or experimental data. Alternatively, a convergence approach can be taken, with modes continually added to the basis until the difference from the full-model data is below some tolerance. When the source code of the software is available, it is possible to create an *intrusive* or *direct* ROM, named as such due to the fact that information regarding the nonlinearity calculations is taken directly from the finite element source code.

For most commercial software, however, this information is inaccessible and a *non-intrusive* or *indirect* ROM technique is required; a useful overview of such methods is given in [56]. Broadly speaking, these methods use a series of representative, static cases to approximate the nonlinear behaviour as a polynomial in terms of the modal displacements. Hence, they can be used in conjunction with any finite element software or nonlinear solver. The overarching aim of these indirect methods is to find an analytical approximation for the

force-amplitude relationship of the structure. It follows that there are two obvious ways in which this can be achieved. Either a known set of displacements can be applied to the structure and the forces can be measured, known as the *Enforced Displacement* (ED) method, or vice versa, known as the *Implicit Condensation* (IC) method. In both methods, the nonlinear component of the ROM is typically approximated by a cubic-order polynomial.

The IC method was originally proposed in [57, 58] and applies a series of static modal forcing cases. By ensuring that these static forces are of a great enough magnitude, it is possible to induce the triggering of modes that have not been directly forced, as a result of the nonlinear nature of the structure. The outputted modal displacements can then be assessed and applied in a regression analysis to approximate the quadratic and cubic coefficients in the ROM. The IC method is so called due to the fact that the membrane effects (i.e. deformation in the plane of the beam) are implicitly condensed into the nonlinear coefficients; this is possible as the forcing of the linear bending modes leads to both bending and membrane displacements. More recently, the IC method has been expanded to include membrane modes [59], which are those normal modes that primarily deform in the plane of the beam or plate; this updated version is referred to as the implicit condensation *and expansion* (ICE) method. Considerable investigation of this method is given in [60], in which it was shown that the ROMs found can produce results that very closely agree with full-order simulations. A common theme in the validation of ROMs is through the use of the full finite element model. This tends to be done on a case-by-case basis, with the literature lacking more fundamental investigations into the general cases in which the method can be accurately applied and the range over which the solutions will be valid.

The ED method – introduced in [61] – imposes a series of static displacements comprised of linear combinations of the modes contained in the ROM basis. Again, it is assumed that displacements of sufficient magnitude will ensure that the resulting force will consist of more than one modal contribution, though this displacement level is not necessarily known without extra testing. These sets of displacements and forces can be considered using regression analysis that is identical to that used in the IC method. Thus, it can be noted that a large amount of the methodology of the two techniques is common to both, with the only real difference arising in the creation of the sets of static cases.

These similarities have, naturally, led to extensive comparison between the two methods. As well as the aforementioned review paper [56], this comparison is expanded in [62],

which uses NNMs as a method of evaluating the quality of the ROMs produced. This paper highlights the influence of the static scale factors used. However, a characterisation of the relationship between the static cases applied and the accuracy achieved was not given. The paper considers the convergence of the ROMs, further details of which are given in [63, 64]. The use of a convergence test is often necessary to ensure the accuracy of the ROM, but this can be a time-consuming process and the dependence upon it should be removed if these methods are to become widely applied. In the related work of [46, 47], these results are compared with NNMs found using the full model, with the IC method being shown to give the more accurate curve. It should be noted that this seems to arise from a key difference between the methods: when the bending modes are displaced, rather than forced, there is no activation of the membrane effects. The impact of this is negligible for the systems in this thesis and is not considered, but provides a potential difficulty for more complex structures.

Although the initial development of the IC method focused on nonlinear beams [57], a driving force for related research has been the thermo-acoustic loading of aircraft. This has been motivated by the development of hypersonic vehicles, as it is possible for sonic fatigue to arise as a result of high temperatures and fluctuating pressures [65]. In contrast, the ED method was created with this motivation in mind [61]. Historically, investigations of thermo-acoustic loading have been considered in terms of linear theory [66]. However, this single-mode approach taken does not allow for modal interaction behaviour to be captured, so has largely been replaced by the use of the non-intrusive ROM techniques presented in this section. A further evaluation of these methods can be found in [67], in which the non-linear ROMs are compared in terms of their power spectral densities and coefficients for a clamped-clamped beam. Both methods have been shown to provide useful results, with the IC methods showing good agreement with experimental data in [59], and the ED method showing agreement with full-order model results in [68]. Once more, the validation of models must be done on a case-by-case basis.

Hypersonic vehicles often experience very high temperatures and fluctuating pressures, and must be designed with these conditions taken into consideration. The non-intrusive methods discussed have also been applied in conjunction with thermal and acoustic models, allowing the response of hypersonic vehicle panels to be more completely investigated. Initial research in this area focused on the integration of acoustic effects into ROMs, primarily doing so by introducing random acoustic loading, as in [69]. Of particular interest in this study was the selection of the modal basis, confirming the notion that additional membrane

modes may need to be added in the ED method to capture the behaviour in large-deformation systems; further investigation is provided in [70]. This work was expanded in [71], developing the methodology so that acoustic fatigue could be predicted. These ROM techniques continue to be applied to structural fatigue problems, such as monitoring of cracked panels in [72]. These studies emphasise the fact that modern engineering structures are not only designed with nonlinear structural properties, but may also need to be considered as multiphysics problems. This adds further complexity to the problem, and requires a complete understanding of the ranges in which they can be considered accurate.

In [73], the ED method is combined with thermal effects for a plate on elastic foundations, demonstrating that the ROM is able to accurately recreate the full model behaviour at a range of temperatures. However, there is greater deviation between the solutions when this temperature is increased, an example of the reduction in accuracy that can arise in a multiphysics problem. The results mirrored those seen in [74, 75], though these also note that there is also a slight decrease in accuracy at higher frequencies. Further validation of this model has been provided in [76]. This work was expanded in [77], in which an oscillating heat flux was introduced to model the thermal effects of an oscillating shock on a panel.

Another key motivating factor for researching these ROM techniques has been the modelling of aircraft with high aspect ratio wings, such as the NASA Helios prototype, which failed, in part, due to failures in the modelling of nonlinear behaviour [78]. A review of research in this area can be found in [15]. In [79], the IC method is used to investigate the tip response of such a wing, modelled through the use of a relatively simple beam model [80]. Once more, a simplification of a real structure is required as the full finite element model is restrictively complex. A similar system was also considered in [81], which applied the IC method to investigate modal coupling. The ED method has also been applied to complicated slender wing models in [82], though this required the model to be reduced first.

In addition to the studies discussed thus far, these techniques have been applied to model periodic vibrations with large displacements [83, 84] (as well as coupling these with thermoelastic effects [85]), and also to investigate acoustic excitation of cylindrical plates [86], joints [87], and piezoelectric NEMS [88]. They have also been applied in conjunction with characteristic constraint modes in modal substructuring applications [89–91]. These academic studies demonstrate industrial applications where these ROM techniques could be applied. As has already been highlighted, this will require further testing to develop a more

universal understanding of their accuracy and limitations.

2.4 Analytical approaches

2.4.1 Response approximation techniques

As has been discussed in §2.3.1, numerical techniques are extremely competent in continuing the periodic response of nonlinear systems of equations. In spite of this, there a number of cases in which this ability is not sufficient or able to fully comprehend and predict the full scope of nonlinear behavioural characteristics. These numerical continuation techniques are extremely well-suited for predicting the response of small systems of equations, but there can be a marked increased in the computational expense when larger systems of equations are required [63]. As such, those users hoping to use this numerical methodology for real-world structures may have to either invest in a great deal of computational power or apply some type of model reduction prior to investigating its response.

Furthermore, since these numerical techniques are typically arclength continuation methods, they require an initial periodic orbit and then incrementally adapt certain parameters to develop the locus of the frequency response. Therefore, an issue arises in the prediction and modelling of isolated periodic solution branches that are not attached to the main response curve, such as those observed experimentally in [92]. The prediction of such responses is difficult to detect using only numerical techniques, as they tend to require knowledge of the system dynamics that is not known *a priori*. However, their prediction can be aided by the use of techniques that produce analytical approximations of the response curves. For instance, the work of [93] develops a detection technique based on the direct normal forms (DNF) method, an analytical technique that will be applied in this thesis. In fact, this method is one of a number of such analytical techniques. Here, the most widely applied of these methods are introduced and discussed.

In this work, the focus will be on those systems that are weakly nonlinear, which still leaves an expansive list of possible approximation methods; an introduction and overview of these can be found in [94]. In the majority of these techniques, a trial solution is applied to the system, which allows the equations of motion to be expressed analytically in terms of both frequency and amplitude. Across these techniques, there is a desire to obtain accurate predictions with the smallest possible amount of calculation. As addressed in [1], this aim typically leads to an application of these methods with only one or two iterations of the steps. Beyond this, not only is the refinement of the solution often negligible, but the analytical expressions can become overly complicated and may require the use of symbolic software

or numerical methods to be solved. This would defeat the purpose of using the analytical methods.

Perhaps the most widely applied of these is the harmonic balance (HB) method, which obtains information about the system response by recognising that the coefficients of time-dependent terms in the equations of motion that respond at the same frequency must be balanced to obtain a valid solution. An introduction to its use can be found, for example, in [95–97]. This strategy has proved effective, with the HB method being used to aid the solution of nonlinear normal modes [98], identify system parameters for nonlinear structures [99–104], accurately predict the behaviour of very stiff systems [105], model energy harvesting devices [106], and identify bifurcations in large systems [107]. This final reference highlights a number of key issues regarding the application of the HB method. The study investigates the dynamics of the highly complicated *SmallSat* spacecraft structure, which required a reduction to a 37DOF model and the understanding of a large number of harmonics. In cases such as these, the HB method requires any harmonics of interest to be included in the trial solution; in [107], five harmonics for each DOF were necessary to achieve an error of less than 1%. This complexity required the HB solutions to be calculated numerically. In most cases, the necessary number of harmonics is not known, so they are either required to assume that the higher-order response is negligible or use a complicated trial solution. This introduces an uncertainty to the methodology that is not present in the methods discussed below.

The method of averaging takes a similar approach to that of the HB method, though it averages first-order differential equations over a cycle of oscillation to remove higher-frequency vibrations [9, 108, 109]. As such, the method is limited to those cases in which the higher-order harmonics are negligible; this information may not be known to the user. For instance, in [110], the method compares favourably to experimental results for a base-excited cantilever beam, which is a simple model with relatively low contributions from the harmonics. Although the approach is, in many ways, similar to that of the HB method, it is possible to introduce time-dependent displacement and phase terms, which would allow the user to consider transient behaviour.

The multiple scales (MS) method applies perturbations to the time scale, displacements, and, in some cases, the response frequency. This perturbation is achieved by introducing a bookkeeping parameter, which is used to track the relative size of each term; further discus-

sions on the development of this methodology can be found in [9, 25, 94, 111–113]. Despite some added complexity added by this parameter, the ability to monitor the contribution of each term and omit those that are negligible can be extremely useful. The user is also able to capture higher-order dynamics than those present in the trial solution. This capability has been applied in the investigation of internal resonances in [114–116]. In each of studies, a single-mode trial solution is used to capture the behaviour of a number of harmonics; as has already been identified, these would implicitly be considered negligible in the HB method. Similar remarks can be made regarding the work in [117–119]. More recently, the MS approach has been used to investigate bifurcations in a system exhibiting a 1:3 internal resonance in [120], drawing similar conclusions. Despite its wide application, the accuracy of MS solutions has been brought into question by studies such as [121], which observed that the solutions obtained for the Duffing oscillator were less accurate than those from the HB and normal form techniques.

As can be seen, the MS method has been widely applied, and its similarities with the more classical Lindstedt-Poincaré technique has led to a comparison of the methods in [122]. This comparison considers two distinct versions of the MS method, reflecting the variable nature in which this method can be applied. For instance, it is possible to apply the method using either the derivative expansion [94, 111, 112] or two-timing [9, 26] version of the method, with the differences arising in which variables are perturbed and to what extent.

Another important family of techniques, which has been widely used for investigating periodic solutions in nonlinear structures, is that of normal form methods. An overview of these can be found in [123]. These techniques have typically been applied to the first-order differential equations, as discussed in [124] and with further examples in [125–128], but have more recently been applied directly to the second-order equations of motion. For instance, in [129], such a method was used to accurately capture the nonlinear normal modes of both discrete and continuous systems, though it could be argued that the complexity of the analytical coefficients is somewhat limiting. This was overcome by the matrix-based methodology proposed in [130], referred to henceforth as the *direct* normal form (DNF) method. This technique applies a series of coordinate transformations so that only those resonant terms with a non-negligible contribution to the total system dynamics are retained. Despite being developed more recently than the other techniques discussed, there have still been a number of applications of the DNF method. As well as modelling nonlinear behaviour in complex analytical systems, such as taut cables [131], and identifying such behaviour in

real structures [55, 132], the technique has also been extensively applied in the investigation of modal interactions [124, 133–135]. Although the notation used to derive and explain the DNF technique can often be expansive, the application of the method itself requires a similar amount of algebraic manipulation as the MS method.

It can be noted that there is a large overlap in the areas of application for this method and the HB/MS methods, which has led to comparisons being made between their accuracy and applicability [1, 121]. This is an important theme in the development of this thesis. The work undertaken aims to offer the user an informed decision into the most suitable method for their application, as this is not always apparent from the literature. Of particular interest to this comparison are the results of [136], in which it is noted that it is the detuning of the DNF method which leads to more accurate results than the first-order normal form method. Similar discussions regarding frequency detuning in the MS method have been initiated [137, 138]. These applications used an arbitrary frequency tuning and lacked the physical motivation observed in [136].

2.4.2 Finite element models

As discussed in §2.3.2, finite element models are ubiquitous in understanding the structural dynamics of physical structures. While the section above discussed this modelling technique in terms of software-based methods, it must be noted that finite element models were originally derived analytically. A thorough guide to the technical implementation of these is given in [139]. As this reference shows, there are a number of different implementations of the finite element method. The primary focus of this thesis is the study of beam-like structures, which can be accurately modelled using the Galerkin method [2, 140]. As such, this will be the only finite element methodology investigated in this section.

Accurate beam models are of great importance to this thesis, due to their historic use in modelling macroscale structures and their more recent prominence in M/NEMS devices. As such, it is necessary to understand the development of various beam theories and the applicability of each. Note that these are continuous models for beams, which will then be discretised using the Galerkin method. There are two leading linear methodologies employed, each with its own set of assumptions and associated advantages and disadvantages; namely, these are the theories of Euler-Bernoulli, as applied in [2], and Timoshenko, as defined in [140]. The principal difference between the two methodologies is that the Euler-Bernoulli theory assumes that the cross section of the beam remains perpendicular to the neutral axis,

whereas Timoshenko theory allows a shear deformation, so that these are no longer perpendicular. As a result of their prevalence, the two methods are regularly compared, for instance in [141], concluding that there are a number of cases in which the difference in accuracy resulting from their assumptions is negligible. An example of this can be observed in the modelling of rotating wind turbine and helicopter blades in [142]. However, the inclusion of shear deformations and the associated rotation allows a more accurate solution at high deflections. Note that a number of nonlinear beam methodologies have been developed (see [143], for a comparison of these), but these are beyond the scope of this thesis, which will focus on weakly nonlinear structures.

As with the software-based finite element methods above, the analytical structures must be discretised and appropriately treated. Across the literature, this is commonly achieved through the use of the Ritz-Galerkin method, henceforth referred to simply as the Galerkin method [2, 140]. The underlying assumption of this technique is that a continuous function in terms of two variables can be discretised as an infinite series of products of projection functions, each of which is then defined in terms of only one variable. For beams, the transverse displacement, w, is typically expressed as a function of the position along the beam, x, and time, t. Applying the Galerkin approximation, this displacement is expressed as

$$w(x,t) = \sum_{k=1}^{\infty} \phi_k(x) q_k(t),$$

where the ϕ_k and q_k terms are functions defining the shape and magnitude of the deflection, respectively. By truncating this expansion[2] and utilising the orthogonality of the linear mode shapes, it becomes possible to express the equations of motion as a finite system of second-order differential equations. This approach was used to model coupled-bending torsion vibrations of an asymmetric aerofoil in [144].

The Galerkin approximation is particularly useful for modelling simple continuous systems, such as beams, plates, shells, and pipes. Extensive consideration has been given to developing Galerkin models for these structures with a number of *classical* BCs, an expression that typically refers to clamped, pinned, free, and sliding beam tips. Derivations

[2] As an interesting aside, the HB technique discussed above is actually a specific application of the Galerkin method. By writing

$$y(t) = \sum_{k=1}^{N} A_k \mathrm{e}^{+jk\omega_n t} + \bar{A}_k \mathrm{e}^{-jk\omega_n t},$$

the displacement x is expressed in terms of Fourier coefficients, A_k, and time varying components, $\mathrm{e}^{\pm jk\omega_n t}$. These are truncated in the same way as the expansion of the displacement.

and discussions of these cases can be readily found, for example, in [2, 140, 145]. These BCs have been widely used in the literature. For instance, circular plates have been considered with free BCs in [146] and with clamped conditions in [39]. This variation can be seen to noticeably alter the mode shapes and natural frequencies of the plate. Further, the Galerkin method has been developed to include fluid-structure interactions, largely building upon these classical BCs [147–152]. While this provides a relatively uncomplicated model, this technique does not take into account the influence that the pressure induced by the fluid would have on the accuracy of these BCs.

In spite of this, there are a number of cases in which it is inaccurate to use these classical BCs, as doing so does not truly reflect the resonant behaviour of the system. The development of this approach has been somewhat incremental and has primarily been achieved by adapting or adding to the traditional cases. For instance, in [153], a cantilever bar model is expanded with a horizontal spring at its tip, leading to more pronounced hysteretic behaviour. In [154], a cantilever beam is considered with a rotational spring at some point along its length, and this concept is expanded, in [155], through the addition of a linear compressive spring. These papers derive the mode shapes and frequencies for these configurations, though an investigation into the influence this has on the system dynamics was prohibited by the lack of sufficient computing power at the time they were written. Similar statements can be made regarding the system considered in [156, 157], in which both beam tips are supported by two springs, one rotational and the other translational. In [158], a compressive axial load is added to a number of classical beam configurations, revealing that the relative critical buckling load is consistent across a large number of these combinations, despite the differences in their resonant behaviour. Furthermore, systems such as these have been shown to exhibit interactions between the modes [159].

While undoubtedly more complex, the non-classical BCs discussed thus far have a relative simplicity due to the fact that any additional components have been defined linearly. Of course, this is not guaranteed to be the case and the inclusion of nonlinear terms leads to solvability conditions that are markedly more complicated. This has been addressed in the work of [160], which considers the normal modes of a number of beams with non-classical, nonlinear BCs. However, the inclusion of a nonlinear term requires the updating of the standard procedure for finding the mode shapes, instead applying Hamilton's principle to find an approximate solution for the mode shapes. This use of an approximation adds some uncertainty to the model, which could be avoided if the exact mathematical definitions of the

BCs were used. An important aspect of this work is the conclusion that these nonlinear BCs influence the mode shapes and natural frequencies of the system. This concept could be developed further, as will be shown in this thesis.

The methodology of [160] has been expanded to allow the considerations of thin plates [161, 162], thick plates [163], and complex shell structures [164], as well as to consider the implications of non-local effects in the free vibrations of M/NEMS in [165]. These complex expansions increase the uncertainty related to the use of an approximation for the mode shape. In each of these cases, as opposed to assuming that the solution to the fourth-order equations of motion will comprise some combination of $\cos$, $\sin$, $\cosh$, and $\sinh$ functions, it is proposed that this could be approximated through a truncated Fourier series. The validation of this proposition would need to be done either numerically or experimentally, which increases the workload of the user.

Alternatively, it has been demonstrated that, should the cubic term be assumed to be small, then the analytical approximation methods of the previous section can be used to calculate the system behaviour. For example the MS method has been used to predict the behaviour of a beam supported by a nonlinear cubic spring in [166] and a spring with a magnetic interaction at the tip in [167]. In fact, the application of Hamilton's principle in [160] is originally presented as an implementation of the HB method. As has already been discussed, these methods are themselves approximations based on a series of assumptions, so it is possible that excessive testing would be required to validate the model.

Numerical solutions for a beam with one nonlinear BC are provided in [168], which applies an iterative method that converges to a numerically correct mode shapes. This approach is also applied in [169], which assumes that both BCs can be nonlinear. This iterative method initially considers the problem from a purely mathematical standpoint, similar to that in [170]. However, the latter study focuses on the existence of solutions, defining criteria to ensure that it is possible to obtain a number of mode shapes. This work is expanded in [171] to demonstrate that infinitely many solutions exist, as is expected from the more traditional engineering approach. These mathematical studies offer comfort to the engineering user of these techniques, but do not offer any great insight for their successful application.

2.5 Nonlinear behaviour in micro- and nanoscale systems

A key aim for this thesis is the development and investigation of nonlinear modelling techniques that can be applied to M/NEMS. The motivation for this is briefly addressed in §2.1, but is more thoroughly outlined in this section. This discussion includes both occurrence of nonlinear behaviour in physical structures, as well as the advances that have been made in modelling these.

2.5.1 Observed nonlinear phenomena

Similarly to the thin, lightweight systems discussed in §2.1, M/NEMS are inherently slender and typically have very low masses. As such, they exhibit a high degree of flexibility and this can lead to nonlinear behaviour. When these slender structures are created at the micro- or nanoscale, this nonlinearity can be further exacerbated by the relative strength of atomic forces, such as the Casimir force modelled in [172], which can lead to higher deflections than may be seen in similar macroscale structures. This paper assumes the linear mode shapes of the structure as basis functions, though it is possible that the boundary reaction may reduce the accuracy of this methodology. As well as this increased propensity for nonlinear behaviour, it has also been observed – for instance, in [173] – that M/NEMS can have a particularly high quality factor (or Q factor). Given that the damping of a structure is inversely proportional to this factor, this suggests that it is possible to gain a great deal understanding of its dynamics simply by computing the free response. This is true to a greater extent than at the macroscale.

The use of M/NEMS is increasingly widespread. Perhaps primary among the application of these devices is their use in sensing and measurements, with their negligible influence on the host structure driving the miniaturisation of measurement devices across the field of engineering. Progress in this area has been reviewed in [174]. In addition, by reducing the size of a sensor, it is possible to make accurate measurements of a much smaller scale. To be able to achieve this accuracy, the behaviour and properties of the sensor must be fully understood. This is made more challenging by the fact that some forces, which are typically ignored at the macroscale, can no longer be assumed to be negligible. These forces can strongly contribute to nonlinear behaviour. When the influence of electrostatic interactions and thermal expansion forces must be considered, it is necessary to use a multiphysics approach. As has been discussed in §2.4.2, this approach can greatly increase the complexity of the problem, so the reliability of using linear mode shapes must be thoroughly assessed.

One noteworthy example of such behaviour can be found in the use of dynamic atomic force microscopes (AFMs). This is particularly true when the method is applied to measure the surface forces along the liquid-solid interface, as has been summarised in [175]. Initial observations of this nonlinearity have been made in [176], which observed a hardening behaviour of the system as the distance between the sample and the cantilever became very small. This force is observed at the boundary, so it is possible that it not only hardens the structure, but also changes the mode shapes themselves. In addition to this, [177] observed the amplification of higher harmonics due to interaction between the first and second modes. More recently, in [178], a wide variety of nonlinear behaviour in dynamic AFM has been reported, including hardening behaviour in the forced response and the separation of the resonance peak into two distinct peaks. Both of these phenomena occur due to interaction forces between the tip and the sample, which is not typically considered at the macroscale. As such, it is important that the traditional modelling methods for these sensors are updated to accommodate such behaviour.

Due to the intrinsically small dimensions of M/NEMS, they typically have natural frequencies that are several orders of magnitude above those seen in macroscale engineering structures. This has been utilised in the development of M/NEMS resonators (alternatively referred to as *oscillators*) that use the stable nature of these resonant vibrations as a method for precisely measuring time. This has been recently reviewed in [179]. The stable nature of these vibrations has seen M/NEMS resonators used in mass detection [180], strain gauges [181], optical scanning [182], and neurocomputers [183], along with a number of applications in biological and motion sensing. Thus, it can be seen that there is a broad scope of measurements that can be made with M/NEMS devices. For these to be reliably applied in academic and industrial settings, it is necessary for their behaviour to be fully comprehended. This provides a strong motivation for the development and refinement of modelling techniques to predict their system dynamics.

An example of this continuing research is presented in [184], in which it was observed that polysilicon resonators exhibit unwanted stiffening behaviour about the resonance frequency if the superposition of the d.c. polarization voltage and a.c. drive voltage are incorrectly configured or the quality factor was too high. This study assessed these structures experimentally, but also modelled the behaviour using a Galerkin model. The behaviour was investigated further in [181], in which a hysteresis criterion has been developed to aid the design of resonant microbridges without hysteretic characteristics. Building on these initial

studies, the frequency shift that occurs as a result of a hardening nonlinearity has been exploited, in [180], to monitor the loading of a resonator. The repeated investigation of these polysilicon resonators has not only continued to reveal nonlinear behaviour that must be accurately captured, but has also led to novel applications of M/NEMS structures.

The hysteretic properties of M/NEMS resonators continue to be of interest to researchers, though the focus has shifted away from avoiding the behaviour entirely, with more recent research attempting to understand it more thoroughly, so that these attributes can be embraced. In [182], a cantilever-type test device was investigated for use in optical scanner applications; in such structures, higher deflections allow a greater optical scanning window by increasing the maximum achievable angle of incidence for the laser spot. Given the magnitude of the deflections, a cubic stiffening effect was observed and this was accurately captured by finite element simulations. However, the large size of the model restricted the ability to predict the frequency response. Similar large deflections were explored for a clamped-clamped beam configuration in [185]. This paper further considered the importance of incorporating the influence of the Casimir force (as discussed above) and surface energy of the structure into the model, concluding that these nonlinear effects must be included in the model to accurately capture the fundamental frequencies of the system and its nonlinear behaviour. This provides further evidence that the boundary effects can have a large influence on the vibration frequency and shape of a model, a phenomenon that may require inclusion in the eigenanalysis used in the modal analysis.

Another key application of this hysteretic behaviour is in the measurement and processing of time and frequency variables themselves. To this end, in [183], hysteresis has been used in the experimental synchronisation of two coupled beams, as the stiffening effect is associated with a widening of the Arnold tongues that characterise the synchronised state. This is an important result in the development of neurocomputers, which would be expected to characterise a number of physical properties. Hardening behaviour was again observed in [186], in which experimental results observing noise squeezing were obtained, which could be used for noise reduction and signal amplification at high frequencies. The reduction of noise has also been achieved in [187], where the level of noise in a nonlinear resonator was seen to be significantly lower than in an equivalent linear system. Along with a large reduction in noise, the nonlinearity of M/NEMS has also been used to stabilise the frequencies themselves, as has been demonstrated in [188]. In this study, the coupling of the first two modes is used to stabilise the first natural frequency; this is only achievable as a result of

the hardening nonlinearity observed in the first mode. A more general investigation into the noise reduction and frequency stabilisation of the resonator from [187] is presented in [189], in which the experimental results not only demonstrate significant noise reduction, but also provide extensive tunability of the frequency. The examples presented in the paragraph highlight the precision that can be achieved using M/NEMS and, hence, the importance that should be placed on the understanding of their nonlinear vibrations.

The tuning of M/NEMS oscillators remains an active area of research, as this ability would allow the aforementioned nonlinear effects to be either avoided or exploited, depending on the application. In [190], two parametrically-excited MEMS oscillators are considered and tuned to have both hardening and softening behaviour, which greatly expands the number of applications of this technology. Note that parametric excitation is an area of research that continues to be developed for a number of nonlinear structures [191, 192]. This ability to tune oscillators has been used to adapt design parameters in [193], so that the linear behaviour can be maintained in a case where doing so increases the resolution of the sensor. These studies primarily utilise SDOF models in the tuning process, and it is possible that these could be enhanced through the consideration of interactions between the modes.

Along with these studies into particular applications of hysteresis, a number of works have considered M/NEMS more generally. Both hardening and softening behaviour were observed in [194]; this work provided initial insight into the observation and modelling of such trends. A similar study was undertaken in [35], in which a combined experimental and numerical approach is taken to investigate properties such as hysteresis and internal resonance in electroelastic crystals. Although these structures have been studied less than the more traditional microbeams of [194] (and the discussion above), this work presents users with the ability to model a system with both geometric and material nonlinearities, and that can be used in a number of optical applications. The complexity added by material nonlinearities may require further refinement of the theoretical models, similarly to the consideration of the multiphysics models discussed in this chapter.

2.5.2 Modelling techniques for M/NEMS devices

The Galerkin method has been widely applied in the modelling of M/NEMS devices, in part due to the relative simplicity of the structures themselves. In these cases, it is possible to obtain a strong understanding of the system behaviour analytically, the benefits of which are addressed in §2.4. An introduction to the application of the Galerkin method in M/NEMS

cases can be found in [174]. For example, the technique plays an explicit role in the development of micro resonant force gauges, as reviewed in [195]. While a number of studies have used a Duffing equation to characterise the nonlinear behaviour of M/NEMS devices [196–199], such a model would only ever be able to characterise the hysteretic behaviour of the device and would not be able to capture internal resonances between the modes.

The study of [200] notes that internal resonances could potentially damage the structure. A Galerkin approach capable of modelling this phenomenon is applied in conjunction with the MS method, and the clamped-clamped model is shown to exhibit a 1:3 internal resonance. This could see energy being transferred to a destructive mode, if the behaviour is not captured in the modelling process. A similar technique was applied to a microcantilever beam in [201, 202], though it was only the hysteretic behaviour recorded, as the method of averaging was applied. The modelling of this behaviour was also the primary focus of the studies in [203, 204], which utilised the MS method to generate frequency responses.

The use of the Galerkin method to create ROMs for M/NEMS structures has been further pursued in [205]. This study considered an electrically-actuated MEMS to investigate the influence of the modal basis size. A similar approach was again applied to an electrically-actuated microbeam in [206], which investigated the influence of both mechanical shock and voltage on the stability of the response. More recent investigations of this manner include the work of Ruzziconi *et al.*, which introduce imperfections to a microbeam in [207] and validate these results experimentally in [208]. This renewed interest in beam-type structures is a motivating factor in the decision to primarily pursue this type of system in this thesis, as it can be seen that they must continually be refined and adapted to meet new engineering requirements.

As discussed in §2.5.1, the large forces encountered by the tip of AFMs and similar beam models can easily lead to nonlinear behaviour. The analytical modelling of this behaviour is outlined in [209] and is investigated both analytically and experimentally using a cantilever beam model with a tip mass in [210]. The alteration of the BC with a tip mass is an approach that could be taken for other non-classical boundary interactions. The Galerkin model applied in the latter study was shown to give good agreement with experimental results. A review of research in this area is provided in [211].

2.6 Research motivations

2.6.1 Analytical methods for response approximation

This chapter has included detailed discussions regarding the relative merits of the HB, MS, and DNF techniques for producing analytical approximations for the free and forced response of nonlinear structures. Despite the focus on these techniques, it has also been noted that there are a number of further techniques that can also provide similar results. While there have been a number of comparison studies [1, 121, 136–138], it must still be concluded that it is still not obvious to the user as to which technique they should use. This arises from the fact that the HB, MS, and DNF method – among others – have been widely applied in the literature, though there is rarely justification for using one method over others. The general user could potentially conclude that any method could be used without the decision influencing the accuracy of their results. However, they may not be aware of, for instance, the fact that the HB method implicitly disregards harmonics outside of the trial solution. Such assumptions also exist in other methods, with the accuracy of the MS method dependent on the frequency detuning applied and the DNF method requiring extensive matrix manipulation.

In reality, it is unlikely that there is one technique that should be considered and it is more plausible that the differences in assumptions and methodologies may be better suited to different cases. A key motivation of this thesis is to begin to answer this question, in an attempt to present the practitioner with an informed choice, depending on whether they want to prioritise accuracy, speed, or any number of other characteristics.

With regard to accuracy, the work presented here aims to expand the results of [136], which noted that the frequency tuning present in the second-order version of the normal form method has previously lead to results that are more accurate than the first-order technique. Given that the use of frequency tuning is not uncommon in the MS method, this thesis will investigate the introduction of the DNF detuning to the method. As has been discussed, the MS technique has been observed to be less accurate than the HB and DNF methods at higher amplitudes and the use of the DNF detuning will be considered as a method for increasing accuracy.

2.6.2 The Galerkin method

The Galerkin method has been applied across a number of structures, but its recent application to M/NEMS beam-type devices motivates a thorough investigation into this type of

structure. Furthermore, a number of studies have shown that alterations to the system boundary can alter the nonlinear behaviour of a structure, whether this be through the introduction of a tip mass [210] or an electrostatic interaction [185]. The observations made have typically been regarding the possible changes to the frequency. Given the inherent link between natural frequency and mode shape, this thesis aims to address the possibility that these novel interactions at the boundary may also change the shape in which the system responds. In M/NEMS settings, the force at the tip of a beam can be dependent on the distance from some exterior structure. This would lead to a BC that is dependent on the deflection.

As has been observed in a number of studies [155, 160], interactions such as these can be incorporated to give a more accurate mode shape. However, to the knowledge of the author, any nonlinear dependence on deflection has only been treated via an approximation, such as the use of a Fourier series. This thesis will investigate the expansion of this concept through the use of nonlinear algebra techniques, with the aim of creating more accurate analytical models for M/NEMS devices. This will allow a greater understanding of the causes and characteristics of nonlinear behaviour in the rapidly-expanding field of microscale measurement devices.

2.6.3 Non-intrusive reduced-order modelling techniques

Chapter 2 has detailed a wide variety of complex structures in which nonlinear behaviour has been exhibited. These systems are typically designed and tested through the use of computational finite element analysis, which can often in result in very large models and computationally expensive simulations. Attempts to reduce the order of these models in a way that maintains the nonlinear properties is often inhibited by the fact that commercial finite element software does not allow the user access to the methodologies used to treat such phenomena. This chapter has outlined the non-intrusive methods that can be used to create such ROMs, focussing on the IC and ED techniques. These methods have shown a great deal of promise in recreating nonlinear behaviour, but require a more fundamental understanding, if they are to be applied in an industrial setting.

Among the issues that need addressing are the dependence of the solution on the magnitude of the static cases, and the number of modes required in the basis to ensure that the behaviour is accurately captured. Some initial investigations have been made in this area [62], but this thesis aims to take a more fundamental approach using analytical nonlinear systems to eliminate the uncertainty associated with commercial finite element software. By

understanding the assumptions made in the application of these methods, the user will be given more confidence in the ROM. This will remove the necessity of extensive comparisons with cumbersome full-order models.

Finally, it has been frequently noted that the ED method produces a less accurate response curve, should the two methods be applied to the same order. Given the similarities between the two methods, this observation appears unusual. This thesis will investigate the reasons behind this through close examination of the static cases from both methods and will then address possible ways in which this disparity could be overcome.

Chapter 3

Analytical approximation methods

In this chapter:

- The harmonic balance, multiple scales, and direct normal form methods are derived for a general forced, damped, nonlinear system.
- These methods are applied to a single-degree-of-freedom system, namely the Duffing oscillator, to assess the practicalities of their application, as well as considering their accuracy.
- The intricacies and difficulties of comparing perturbative solutions with differences in their analytical form are discussed.
- The detuning of the direct normal form method is applied to the multiple scales method, to bring their respective frequency responses in line with one another.
- A variable detuning is applied to investigate the impact of specifically selecting the detuning from the direct normal form.

3.1 Introduction

While it is possible to use numerical techniques to provide solutions to nonlinear problems that can be considered exact up to numerical tolerances, often, this does not provide the user with sufficient information to fully understand the behaviour of a nonlinear dynamical system. To address this issue, it is common practice to apply an analytical approximation method, which can be used to develop a more thorough appreciation of the influence that

the system parameters have on the system response. In particular, the use of numerical continuation can produce both the stable and unstable branches of the frequency response, but requires an initial periodic solution to do so; these techniques typically apply a predictor-corrector methodology to an initial linear periodic orbit, as outlined in [212, 213]. As such, it can be extremely difficult to predict phenomena such as isolated branches of the response (referred to as *isolas*) [93]. These analytical methods typically require the use of an assumed trial solution, which can then be applied in the governing equations to determine how the approximate solution relates to the characteristics of the structure. A key attribute of such methods is that they include the repetition of a number of steps, which can be iteratively applied to develop an increasingly accurate solution. Assuming a stable numerical scheme, it is widely accepted that, as the number of repetitions grows, the error of the solution reduces, though it is desirable to be able to achieve a sufficiently accurate solution with a minimal number of these repetitions.

In this work, the focus will be on those systems that are *weakly* nonlinear, in which the perturbation from the underlying linear equations is assumed to be small. This somewhat narrows the selection of analytical approximations which could be considered, but still leaves a relatively expansive list; further information on this can be found in [94] and has been discussed at length in Chapter 2. Following this discussion and given their wide applications in the literature, the HB, MS, and DNF methods have been selected for the examination. The focus of this discussion will be placed on their respective ability to capture the free and forced responses of nonlinear systems. Initial consideration of these methods has been given in [121], though this only considers the free response of the system, and only applies the steps of these methods once. Here, the forced response is used for a more in-depth discussion, with two applications of these steps used for the free response.

In this chapter, the results of [136] are brought to the forefront of the discussion, as it is noted here that it is the detuning of the DNF method which leads to more accurate results than the first-order normal forms method. This raises an important issue regarding the comparison of these methods, in that each is dependent on a certain set of assumptions that, naturally, will influence the accuracy of the results. To address this, the work of this chapter will consider the possibility of adapting these assumptions and applying the detuning of the DNF method in the MS technique.

To establish a framework for this comparison, the three methods are first derived and

discussed in §3.2. The second part of this section will introduce the aforementioned frequency detuning to the MS method, initially considering a general MDOF nonlinear system. This comparison is then extended to the SDOF Duffing oscillator in §3.3. Both the free and forced vibrations are initially investigated, with a single iteration of each method being applied. The backbone curves are then considered after a second iteration of the method, so that the convergence and accuracy of the techniques can be assessed further.

Publications resulting from this work

Elliott, A. J., Cammarano, A., and Neild, S. A.. (2017). Comparing Analytical Approximation Methods with Numerical Results for Nonlinear Systems. In *Nonlinear Dynamics, Volume 1*, Kerschen, G., ed., Conference Proceedings of the Society for Experimental Mechanics Series, 37–49.

– This paper compares the HB, MS, and DNF methods for a 2DOF lumped-mass system. As in§3.2, the techniques are compared in terms of both their accuracy and their usability, noting that the divergence of the MS solution at higher amplitudes is as a result of its linearisation of the frequency.

Elliott, A. J., Cammarano, A., Neild, S. A., Hill, T. L., and Wagg, D.J. (2018). Comparing the direct normal form and multiple scales methods through frequency detuning. *Nonlinear Dynamics*, 94(4):2919–2935.

– This paper compares the HB, MS, and DNF methods in terms of their frequency detuning, as is presented in §3.3.6. It is demonstrated that, if the detuning from the DNF method is applied in the MS method, the solutions from the two are identical.

Elliott, A. J., Cammarano, A., Neild, S. A., Hill, T. L., and Wagg, D.J. (2019, accepted). Using frequency detuning to compare analytical approximations for forced responses. *Nonlinear Dynamics*.

– This paper again compares the HB, MS, and DNF methods in terms of their frequency detuning, but expands the discussion to a forced, damped oscillator. The conclusions from this paper are consistent with the above work, as discussed in §3.2.4.

3.2 Overview of considered techniques

This chapter presents a thorough outline of the involved techniques. The key reason for doing so is that, particularly for the HB and MS methods, a number of implementations exist in the literature, which could potentially lead to confusion in the discussion. In addition, across the methods discussed, attempts will be made to unify the symbols used, as this will further simplify the comparison.

The equations of motion for a nonlinear mechanical system can be expressed, in physical coordinates $\mathbf{x}$, as

$$\mathbf{M}\ddot{\mathbf{x}} + (\varepsilon)\mathbf{C}\dot{\mathbf{x}} + \mathbf{K}\mathbf{x} + (\varepsilon)\mathbf{\Gamma}_{\mathbf{x}}(\mathbf{x}, \mathbf{r}) = (\varepsilon)\mathbf{P}_{\mathbf{x}}\mathbf{r}, \tag{3.1}$$

where $\mathbf{M}$, $\mathbf{C}$, and $\mathbf{K}$ define the $N \times N$ linear mass, damping, and stiffness matrices, respectively, $\mathbf{\Gamma}_{\mathbf{x}}$ is an $N \times 1$ vector of the nonlinear terms, and the dot notation represents derivatives with respect to time, t. Here, $\mathbf{r}^{\mathrm{T}} = [r_p \;\; r_m] = [\mathrm{e}^{+\mathrm{j}\Omega t} \;\; \mathrm{e}^{-\mathrm{j}\Omega t}]$ represents the periodic nature of the forcing generally applied to nonlinear systems, where $\mathbf{P}_{\mathbf{x}} = \left[\frac{\hat{\mathbf{P}}_{\mathbf{x}}}{2}, \frac{\hat{\mathbf{P}}_{\mathbf{x}}}{2}\right]$ and $\hat{\mathbf{P}}_{\mathbf{x}}$ is an $N \times 1$ vector of scalar terms defining the magnitude of this forcing. The bookkeeping parameter, ε – used to denote the relatively small nature of the damping, nonlinear, and forcing terms – is bracketed to denote the fact that it is not necessarily used in the HB method.

If the $\mathbf{\Gamma}_{\mathbf{x}}$ term is removed from Eq. (3.1), the system of equations will be completely linear. This will be referred to as the *underlying* linear system.

3.2.1 Harmonic balance

The HB method is perhaps the most established technique, with both the MS and DNF methods applying its core approach of balancing similar terms as part of their steps. As such, only a brief description will be given, with more thorough details found in the literature [95–97]. The initial assumption made in this technique is that the response is sinusoidal, with each component of the displacement taking the form

$$x_k(t) = \sum_{i=1}^{n} \frac{A_{k,i}}{2}\mathrm{e}^{+\mathrm{j}i(\omega_{r,k}t+\phi_k)} + \frac{\bar{A}_{k,i}}{2}\mathrm{e}^{-\mathrm{j}i(\omega_{r,k}t+\phi_k)}, \tag{3.2}$$

where $A_{k,i}$ denotes the response amplitude and ϕ_k the phase; n denotes the number of harmonics in the trial solution. $\omega_{r,k}$ denotes the k^{th} response frequency, which is typically assumed to be equal to the forcing frequency, should the system be forced. Note that there are some cases in which this will not be the case, such as the occurrence of period-doubling

bifurcations.

The displacement expression defined in Eq. (3.2) can then be applied in Eq. (3.1) to give a system of equations in terms of $A_{k,i}$, ϕ_k, and $\mathrm{e}^{+\mathrm{j}\omega_r t}$. It is at this stage that the harmonics are balanced; the $\mathrm{e}^{+\mathrm{j}\omega_r t}$ terms are time-dependent, so their coefficients must be balanced for the equality to hold. Thus, those terms responding at integer multiples of ω_r are collected and equated separately. These new equations govern the harmonic response of the system and can be algebraically manipulated to produce the amplitude-frequency relationships of interest. Further, Eq. (3.2) gives a complex definition of the displacement components, hence the balancing of coefficients can be divided into two equations, for the real and imaginary parts, respectively. Once these new equations have been defined, it is simply a case of solving them analytically; further details on the implementation of this will be given for a real example in Section 3.3.1.

It is worth noting that nonlinear systems are characterised by exponents of ω_r that are greater than 1. As such, the expansion of these terms, when the expressions in Eq. (3.2) are applied, can result in the emergence terms of the form $\mathrm{e}^{+jk\omega t}$, with $k > n$. However, since these terms are not present in the trial solution, they will only be present in the nonlinear terms, so their coefficients in the aforementioned expansion will be set to zero. Thus, there is an implicit assumption that the harmonics of a higher order than n are negligible. This can be assessed through the inclusion of these harmonics, though this is not common practice. Again, this will be further illustrated in Section 3.3.1.

3.2.2 Multiple scales

As discussed in §3.1, the MS method has been widely used throughout the literature, which has led to some variation in its definition and implementation. Although the underlying concept remains the same, the fact that it is a perturbation method allows for variation in both the variables that are perturbed, and the order of these perturbations. In this overview of the technique, the *derivative-expansion* version [112] will be used. However, it is first noted that, while less commonly used, other versions have been applied in the literature. In particular, the *two-timing* version of the MS method (see, for example, [26]) makes the assumption that, while it may be advantageous to perturb the displacement in the typical way, it is sufficient to define only two time-scales, referred to as slow- and fast-time. During this investigation of the equivalence of analytical techniques, both techniques have been used. Initially, the derivative-expansion method is applied to the general system, and is also used to investigate

the ε^1-order MS solutions. An expanded version of the two-timing methodology will be used to find the ε^2 solution, to demonstrate the fact that the choice of implementation does not influence the discussion.

In the derivative-expansion version, the following standard perturbations (in terms of bookkeeping parameter, ε) of displacement and time are used:

$$t = t + \varepsilon t + \varepsilon^2 t + \dots = T_0 + T_1 + T_2 + \dots . \tag{3.3}$$

$$\mathbf{x} = \mathbf{x}_0 + \varepsilon \mathbf{x}_1 + \varepsilon^2 \mathbf{x}_2 + \dots , \tag{3.4}$$

Here, the notation $T_n = \varepsilon^n t$ has been introduced. As such, the time perturbation given in Eq. (3.3) leads to the following expressions for the derivatives

$$\begin{aligned} \tfrac{\mathrm{d}}{\mathrm{d}t} &= D_0 + \varepsilon D_1 + \varepsilon^2 D_2 + \dots , \\ \tfrac{\mathrm{d}^2}{\mathrm{d}t^2} &= D_0^2 + \varepsilon(2D_0 D_1) + \varepsilon^2(D_1^2 + 2D_0 D_2) + \dots . \end{aligned} \tag{3.5}$$

where $D_k = \frac{\partial}{\partial T_k}$.

Although the MS technique is typically applied directly to the physical coordinates of a system, the matrix formulation for a general system, such as that in Eq. (3.1), can quickly become unwieldy. To prevent the discussion from becoming overly complicated, it is possible to consider the same system projected onto modal coordinates, without loss of generality. This step will be explained in the description of the DNF method.

The conversion into modal coordinates results in equations of motion given by

$$\ddot{\mathbf{q}} + \mathbf{\Lambda}\mathbf{q} + \varepsilon \mathbf{\Gamma}_{\mathbf{q}}(\mathbf{q}, \dot{\mathbf{q}}, \mathbf{r}) = \varepsilon \mathbf{P}_{\mathbf{q}} \mathbf{r}, \tag{3.6}$$

where $\mathbf{q}$ denotes the transformed modal form of $\mathbf{x}$, $\mathbf{\Lambda}$ is the modal stiffness matrices, with i^{th} diagonal $\omega_{n,i}^2$, $\mathbf{\Gamma}_{\mathbf{q}}(\mathbf{q}, \dot{\mathbf{q}}, \mathbf{r})$ collects the modal projections of $\mathbf{\Gamma}_{\mathbf{x}}(\mathbf{x}, \mathbf{r})$ and $\mathbf{C}\dot{\mathbf{x}}$, and $\mathbf{P}_{\mathbf{x}}\mathbf{r}$. These terms are more thoroughly outlined in the definition of the DNF method.

The modal coordinates are now perturbed in the same way as the physical coordinates in Eq. (3.4) to give

$$\mathbf{q} = \mathbf{q}_0 + \varepsilon \mathbf{q}_1 + \varepsilon^2 \mathbf{q}_2 + \dots . \tag{3.7}$$

In Eq. (3.6), the forcing term is assumed to be *weak*, i.e. small in comparison to the acceler-

ation and displacement terms; this is denoted using ε. Similar assumptions have been made for the damping and nonlinear terms, which are collected in $\varepsilon\mathbf{\Gamma_q}(\mathbf{q},\dot{\mathbf{q}},\mathbf{r})$.

By applying the perturbations given by Eqs. (3.3), (3.5), and (3.7) in Eq. (3.6) leads to the equation

$$\begin{aligned}&((D_0^2+\varepsilon(2D_0D_1)+\varepsilon^2(D_1^2+2D_0D_2)+\dots)+\mathbf{\Lambda})(\mathbf{q}_0+\varepsilon\mathbf{q}_1+\varepsilon^2\mathbf{q}_2+\dots)\\&+\varepsilon\mathbf{\Gamma_q}(\mathbf{q}_0+\varepsilon\mathbf{q}_1+\varepsilon^2\mathbf{q}_2+\dots,\\&\quad(D_0+\varepsilon D_1+\varepsilon^2D_2+\dots)(\mathbf{q}_0+\varepsilon\mathbf{q}_1+\varepsilon^2\mathbf{q}_2+\dots),\mathbf{r})=\varepsilon\mathbf{P_q}\mathbf{r},\end{aligned}\tag{3.8}$$

It is immediately apparent that the perturbed parameters in $\mathbf{\Gamma_q}$ would lead to a complex set of calculations. To simplify this, a Taylor expansion is applied, leading to the following ε-expansion for the equations of motion:

$$\varepsilon^0: \quad (D_0^2+\mathbf{\Lambda})\mathbf{q}_0=0, \tag{3.9}$$

$$\varepsilon^1: \quad (D_0^2+\mathbf{\Lambda})\mathbf{q}_1=-2D_0D_1\mathbf{q}_0-\mathbf{\Gamma_q}(\mathbf{q}_0,\frac{\mathrm{d}}{\mathrm{d}t}(\mathbf{q}_0),\mathbf{r})+\mathbf{P_q}\mathbf{r}, \tag{3.10}$$

$$\begin{aligned}\varepsilon^2: \quad (D_0^2+\mathbf{\Lambda})\mathbf{q}_2=&-2D_0D_1\mathbf{q}_1-(D_1^2+2D_0D_2)\mathbf{q}_2-\left[\frac{\partial}{\partial\mathbf{q}_0}\mathbf{\Gamma_q}\right]\mathbf{q}_1\\&-\left[\frac{\partial}{\partial\dot{\mathbf{q}}_0}\mathbf{\Gamma_q}\right]\dot{\mathbf{q}}_1,\end{aligned}\tag{3.11}$$

$$\vdots$$

This equation makes use of the notation $\frac{\partial}{\partial\mathbf{q}_0}=\nabla_{\mathbf{q_0}}\mathbf{\Gamma_q}(\mathbf{q}_0,\dot{\mathbf{q}}_0,\mathbf{r})$ and $\frac{\partial}{\partial\dot{\mathbf{q}}_0}=\nabla_{\dot{\mathbf{q}}_\mathbf{0}}\mathbf{\Gamma_q}(\mathbf{q}_0,\dot{\mathbf{q}}_0,\mathbf{r})$. Similarly to the HB method, the MS technique assumes a sinusoidal form for the response, which is found by solving the ε^0-order equation and is given by

$$q_{0,k}=\frac{A_{0,k}(T_1,T_2,\dots)}{2}\left(\mathrm{e}^{+\mathrm{j}(\omega_{r,k}T_0+\phi_{0,k}(T_1,T_2,\dots))}+\mathrm{e}^{-\mathrm{j}(\omega_{r,k}T_0+\phi_{0,k}(T_1,T_2,\dots))}\right), \tag{3.12}$$

where $A_{0,k}$ and $\phi_{0,k}$ denote the amplitude and phase of the fundamental response, respectively. The trial solution used for the MS method takes a similar form to that in the HB method, with the key difference being that the amplitude and phase terms are functions of the slower time scales, allowing transient behaviour to be captured; this feature is undoubtedly useful, but is not pursued further in this thesis.

Applying the solution defined in Eq. (3.12) in Eq. (3.10) leads to the following form for

the ε^1-order equation:

$$\begin{aligned}
&(D_0^2+\omega_{n,k}^2)q_{1,k}+2D_0D_1\Big(\frac{A_{0,k}}{2}\Big(\mathrm{e}^{+\mathrm{j}(\omega_{n,k}T_0+\phi_{0,k})}+\mathrm{e}^{-\mathrm{j}(\omega_{n,k}T_0+\phi_{0,k})}\Big)\Big)\\
&\quad+\Gamma_{q,k}\Big(\frac{A_{0,k}}{2}\Big(\mathrm{e}^{+\mathrm{j}(\omega_{n,k}T_0+\phi_{0,k})}+\mathrm{e}^{-\mathrm{j}(\omega_{n,k}T_0+\phi_{0,k})}\Big),\\
&\qquad\mathrm{j}\omega_{n,k}\frac{A_{0,k}}{2}\Big(\mathrm{e}^{+\mathrm{j}(\omega_{n,k}T_0+\phi_{0,k})}-\mathrm{e}^{-\mathrm{j}(\omega_{n,k}T_0+\phi_{0,k})}\Big),\mathrm{e}^{+\mathrm{j}\Omega t}+\mathrm{e}^{-\mathrm{j}\Omega t}\Big)=P_{q,k}\\
&\Leftrightarrow(D_0^2+\omega_{n,k}^2)q_{1,k}+\mathrm{j}\omega_{n,k}\Big((D_1A_{0,k}+A_{0,k}D_1\phi_{0,k})\mathrm{e}^{+\mathrm{j}(\omega_{n,k}T_0+\phi_{0,k})}\\
&\qquad\qquad+(D_1A_{0,k}-A_{0,k}D_1\phi_{0,k})\mathrm{e}^{-\mathrm{j}(\omega_{n,k}T_0+\phi_{0,k})}\Big)\\
&\quad+\Gamma_{q,k}\Big(\frac{A_{0,k}}{2}\Big(\mathrm{e}^{+\mathrm{j}(\omega_{n,k}T_0+\phi_{0,k})}+\mathrm{e}^{-\mathrm{j}(\omega_{n,k}T_0+\phi_{0,k})}\Big),\\
&\qquad\mathrm{j}\omega_{n,k}\frac{A_{0,k}}{2}\Big(\mathrm{e}^{+\mathrm{j}(\omega_{n,k}T_0+\phi_{0,k})}-\mathrm{e}^{-\mathrm{j}(\omega_{n,k}T_0+\phi_{0,k})}\Big),\mathrm{e}^{+\mathrm{j}\Omega t}+\mathrm{e}^{-\mathrm{j}\Omega t}\Big)=P_{q,k}.
\end{aligned}\tag{3.13}$$

Here, to simplify the expression, the dependence of the amplitude and phase on the faster time scales is not displayed. Considering the homogeneous case of Eq. (3.13), given by $(D_0^2+\omega_{n,k}^2)q_{1,k}=0$, it can be seen that the complementary function will take the same form as that of $q_{0,k}$. The presence of this form in the particular integral will result in terms that will grow with time and, therefore, will no longer represent the steady-state dynamics required. This is easily resolved by setting these resonant, or *secular*, terms to zero. For the general system under consideration here, this is given by

$$\begin{aligned}
&\mathrm{j}\omega_{n,k}\Big((D_1A_{0,k}+A_{0,k}D_1\phi_{0,k})\mathrm{e}^{+\mathrm{j}(\omega_{n,k}T_0+\phi_{0,k})}+(D_1A_{0,k}-A_{0,k}D_1\phi_{0,k})\mathrm{e}^{-\mathrm{j}(\omega_{n,k}T_0+\phi_{0,k})}\Big)\\
&\quad+\mathrm{Res}\Big\{\Gamma_{q,k}\Big(\frac{A_{0,k}}{2}\Big(\mathrm{e}^{+\mathrm{j}(\omega_{n,k}T_0+\phi_{0,k})}+\mathrm{e}^{-\mathrm{j}(\omega_{n,k}T_0+\phi_{0,k})}\Big),\\
&\qquad\mathrm{j}\omega_{n,k}\frac{A_{0,k}}{2}\Big(\mathrm{e}^{+\mathrm{j}(\omega_{n,k}T_0+\phi_{0,k})}-\mathrm{e}^{-\mathrm{j}(\omega_{n,k}T_0+\phi_{0,k})}\Big),\mathrm{e}^{+\mathrm{j}\Omega t}+\mathrm{e}^{-\mathrm{j}\Omega t}\Big)-P_{q,k}\Big\}=0,
\end{aligned}\tag{3.14}$$

where Res$\{\bullet\}$ denotes the resonant terms of $\bullet$. By first separating the real and imaginary parts of the equation, then setting the coefficients of $\mathrm{e}^{\pm j(\omega_{n,k}T_0+\phi_{0,k})}$ in each of those to zero, it is possible to solve Eq. (3.14) to define the frequency-amplitude relationship and phase information. Once these equations have been solved, the values of $A_{0,k}$ and $\phi_{0,k}$ can be applied in the non-resonant equation:

$$\begin{aligned}
(D_0^2+\omega_{n,k}^2)q_{1,k}=-\mathrm{NRes}\Big\{&\Gamma_{q,k}\Big(\frac{A_{0,k}}{2}\Big(\mathrm{e}^{+\mathrm{j}(\omega_{n,k}T_0+\phi_{0,k})}+\mathrm{e}^{-\mathrm{j}(\omega_{n,k}T_0+\phi_{0,k})}\Big),\\
&\mathrm{j}\omega_{n,k}\frac{A_{0,k}}{2}\Big(\mathrm{e}^{+\mathrm{j}(\omega_{n,k}T_0+\phi_{0,k})}-\mathrm{e}^{-\mathrm{j}(\omega_{n,k}T_0+\phi_{0,k})}\Big),\mathrm{e}^{+\mathrm{j}\Omega t}+\mathrm{e}^{-\mathrm{j}\Omega t}\Big)\Big\},
\end{aligned}\tag{3.15}$$

where NRes$\{\bullet\}$ denotes the non-resonant terms of $\bullet$. This equation can then be solved to find an expression for $q_{1,k}$. The process for solving Eq. (3.15) is not expanded upon here, as it is dependent on the definition of $\mathbf{\Gamma_q}$. To find solutions for a higher order of ε, it is simply necessary to repeat the above steps.

3.2.3 Direct normal forms

The final method under consideration here is a normal form method. In particular, the *direct* normal form method will be used, so called due to its direct application to the second-order differential equations. The use of normal form techniques is common in the field of nonlinear dynamics and, in earlier applications, it was first necessary to convert the equations into first-order form before applying the technique [130]. However, more recent developments have seen the method applied directly to the second-order equations; as such, the DNF method has also been referred to as the *second-order* normal forms method. This nomenclature is avoided here as there is potential for confusion when ε-order is also considered.

The initial stages of this method comprises three coordinate transforms that ensure that only the resonant modal responses are calculated. These transforms are summarised as:

- Modal transform
  - The physical equations of motion are projected onto the coordinate system defined by the mode shapes of the underlying linear system.
- Forcing transform
  - The terms in the response which oscillate at frequencies close to the forcing frequency are isolated.
- Nonlinear near-identity transform
  - The non-resonant nonlinear terms are removed.

These steps are now illustrated using the general nonlinear system considered above.

First-order normal form method

For the sake of completeness, a brief overview of how the first-order version of the normal form technique differs from the DNF method is given. In this case, Eq. (3.1) must be first written as a

first-order differential equation. This is achieved by the introduction of the phase-space parameter $\mathbf{y} = [\mathbf{x}, \dot{\mathbf{x}}]$. The equations of motion are then given by

$$\dot{\mathbf{y}} = \mathbf{A}\mathbf{y} + \mathbf{\Gamma}_{\mathbf{y}}(\mathbf{y}, \mathbf{r}) + \mathbf{P}_{\mathbf{y}}\mathbf{r}, \tag{3.16}$$

where

$$\mathbf{A} = \begin{bmatrix} 0 & I \\ -\mathbf{M}^{-1}\mathbf{K} & -\mathbf{M}^{-1}\mathbf{C} \end{bmatrix}, \quad \mathbf{\Gamma}_{\mathbf{y}} = \begin{bmatrix} 0 \\ -\mathbf{M}^{-1}\mathbf{\Gamma}_{\mathbf{x}}(\mathbf{y}, \mathbf{r}) \end{bmatrix}, \quad \text{and} \quad \mathbf{P}_{\mathbf{y}} = \begin{bmatrix} 0 \\ -\mathbf{M}^{-1}\mathbf{P}_{\mathbf{x}} \end{bmatrix}. \tag{3.17}$$

Once the system has been transformed into this form, the steps are the same as those of the DNF method, so are not repeated here.

Modal Transform: This step makes use of the linear modeshape matrix, $\mathbf{\Phi}$, found by solving the eigenanalysis problem defined by $\mathbf{\Lambda\Phi} = \mathbf{M}^{-1}\mathbf{K\Phi}$. The matrix is applied as a change of basis matrix to project the physical coordinates onto a set of modal displacements. Thus, the transform is written as $\mathbf{x} = \mathbf{\Phi q}$, where $\mathbf{q}$ is an $N \times 1$ vector of modal contributions. This can be applied in Eq. (3.1) and the resultant equation can be pre-multiplied by $\mathbf{\Phi}^{\mathrm{T}}$ to give

$$(\mathbf{\Phi}^{\mathrm{T}}\mathbf{M\Phi})\ddot{\mathbf{q}} + (\varepsilon)(\mathbf{\Phi}^{\mathrm{T}}\mathbf{C\Phi})\dot{\mathbf{q}} + (\mathbf{\Phi}^{\mathrm{T}}\mathbf{K\Phi})\mathbf{q} + (\varepsilon)\mathbf{\Phi}^{\mathrm{T}}\mathbf{\Gamma}_{\mathbf{x}}(\mathbf{\Phi q}, \mathbf{r}) = (\varepsilon)\mathbf{\Phi}^{\mathrm{T}}\mathbf{P}_{\mathbf{x}}\mathbf{r}. \tag{3.18}$$

In this dicussion, it will be assumed that $\mathbf{\Phi}$ is mass-normalised. In this case, $\mathbf{\Phi}^{\mathrm{T}}\mathbf{M\Phi} = \mathbf{I}$ and $\mathbf{\Phi}^{\mathrm{T}}\mathbf{K\Phi} = \mathbf{\Lambda}$, where $\mathbf{\Lambda}$ is a diagonal matrix with the k^{th} diagonal element given by $\omega_{n,k}^2$, the square of the k^{th} linear natural frequency. This leads to the simplified equation:

$$\ddot{\mathbf{q}} + \mathbf{\Lambda q} + \varepsilon\mathbf{\Gamma}_{\mathbf{q}}(\mathbf{q}, \dot{\mathbf{q}}, \mathbf{r}) = \varepsilon\mathbf{P}_{\mathbf{q}}\mathbf{r}, \tag{3.19}$$

Here, the function $\mathbf{\Gamma}_{\mathbf{q}} = \mathbf{\Phi}^{\mathrm{T}}[\mathbf{C\Phi}\dot{\mathbf{q}} + \mathbf{\Gamma}_{\mathbf{x}}(\mathbf{\Phi q}, \mathbf{r})]$ now includes both the projection of $\mathbf{\Gamma}_{\mathbf{x}}$ into modal space and the projected damping term. $\mathbf{P}_{\mathbf{q}} = \mathbf{\Phi}^{\mathrm{T}}\mathbf{P}_{\mathbf{x}}$ is the modal projection of the forcing amplitudes.

Forcing transform: This takes the form $\mathbf{q} = \mathbf{v} + [e]\mathbf{r}$, where $\mathbf{v}$ is an $N \times 1$ vector of resonant forced terms and $[e]$ is an $N \times 2$ matrix that isolates the resonant forcing terms. The transform can then be applied in the modal equations of motion to give

$$\ddot{\mathbf{v}} + [e]\mathbf{WWr} + \mathbf{\Lambda v} + \mathbf{\Lambda}[e]\mathbf{r} + \varepsilon\mathbf{\Gamma}_{\mathbf{v}}(\mathbf{v}, \dot{\mathbf{v}}, \mathbf{r}) = \varepsilon\mathbf{P}_{\mathbf{v}}\mathbf{r}, \tag{3.20}$$

where $\mathbf{W}$ is a 2×2 diagonal matrix with entries $+\mathrm{j}\Omega$ and $-\mathrm{j}\Omega$. The purpose of this step is to monitor which forcing terms are close to resonance, which, for the k^{th} mode, will be taken to mean $\omega_{n,k} \approx \Omega$.

It is desirable to write Eq. (3.20) in a similar form to Eq. (3.19), i.e. with the non-resonant forcing terms have been removed. As suggested by its name, this type of *normal form* is repeatedly used in the DNF method. In the current coordinate system, this would be written as

$$\ddot{\mathbf{v}} + \mathbf{\Lambda}\mathbf{v} + \varepsilon\mathbf{\Gamma}_{\mathbf{v}}(\mathbf{v}, \dot{\mathbf{v}}, \mathbf{r}) = \varepsilon\mathbf{P}_{\mathbf{v}}\mathbf{r}. \tag{3.21}$$

In order to achieve this normal form, the following functions are defined:

$$\mathbf{\Gamma}_{\mathbf{v}}(\mathbf{v}, \dot{\mathbf{v}}, \mathbf{r}) = \mathbf{\Gamma}_{\mathbf{q}}(\mathbf{v} + [e]\mathbf{r}, \dot{\mathbf{v}} + [e]\mathbf{W}\mathbf{r}, \mathbf{r}) \tag{3.22}$$

$$\mathbf{P}_{\mathbf{v}} = \mathbf{P}_{\mathbf{q}} - (\mathbf{\Lambda}[e] - [e]\mathbf{W}\mathbf{W}). \tag{3.23}$$

These expressions assure that $\mathbf{\Gamma}_{\mathbf{v}}$ and $\mathbf{P}_{\mathbf{v}}$ contains only the resonant entries of $\mathbf{\Gamma}_{\mathbf{q}}$ and $\mathbf{P}_{\mathbf{q}}$, respectively. The second definition in Eq. (3.22) can be rewritten using the definition of $\mathbf{W}$ to give the k^{th} row as

$$P_{v,k} = P_{q,k} - (\omega_{n,k}^2 - \Omega^2)[e]_k. \tag{3.24}$$

From this, it is possible to define the k^{th} row of $[e]$ as

$$[e]_k = \begin{cases} [0 \;\; 0] & \text{if } \omega_{n,k} \approx \Omega, \\ P_{q,k}/(\omega_{n,k}^2 - \Omega^2) & \text{otherwise.} \end{cases} \tag{3.25}$$

Therefore, $P_{v,k}$ can be defined as

$$P_{v,k} = \begin{cases} P_{q,k} & \text{if } \omega_{n,k} \approx \Omega, \\ [0 \;\; 0] & \text{otherwise.} \end{cases} \tag{3.26}$$

Nonlinear near-identity transform: In this step, the response is separated into its fundamental and harmonic components. This is achieved by implementing the following expression for $\mathbf{v}$:

$$\mathbf{v} = \mathbf{u} + \mathbf{h}(\mathbf{u}, \dot{\mathbf{u}}, \mathbf{r}), \;\; \text{where} \;\; \mathbf{h}(\mathbf{u}, \dot{\mathbf{u}}, \mathbf{r}) = \varepsilon\mathbf{h}_1(\mathbf{u}, \dot{\mathbf{u}}, \mathbf{r}) + \varepsilon^2\mathbf{h}_2(\mathbf{u}, \dot{\mathbf{u}}, \mathbf{r}) + \dots \;. \tag{3.27}$$

Here, $\mathbf{u}$ is an $N \times 1$ vector of resonant nonlinear terms and $\mathbf{h}$ captures the remaining harmonic content of the response. Similarly to the nonlinear and damping terms, the harmonics have been perturbed, which formalises the assumption that higher-frequency harmonics will be of less consequence to the behaviour of the system.

Furthermore, the assumption is made that the expression for $\mathbf{u}$ is sinusoidal. In the DNF method, this is written in exponential form, with separate vectors for the positive and negative exponents; this is expressed as $\mathbf{u} = \mathbf{u}_p + \mathbf{u}_m$, where the subscripts denote the sign of the exponent. Furthermore, the k^{th} element of $\mathbf{u}$ is now written as

$$u_k = u_{pk} + u_{mk} = \frac{A_k}{2} \mathrm{e}^{+\mathrm{j}(\omega_{r,k} t + \phi_k)} + \frac{A_k}{2} \mathrm{e}^{-\mathrm{j}(\omega_{r,k} t + \phi_k)}, \tag{3.28}$$

where A_k, ϕ_k, and $\omega_{r,k}$ denote the amplitude, phase, and response frequency of u_k, respectively.

Once again, the desired form for the equations of motion in this step, with the non-resonant nonlinear terms removed, is given by

$$\ddot{\mathbf{u}} + \mathbf{\Lambda u} + \varepsilon \mathbf{\Gamma}_{\mathbf{u}}(\mathbf{u}, \dot{\mathbf{u}}, \mathbf{r}) = \varepsilon \mathbf{P}_{\mathbf{u}} \mathbf{r}. \tag{3.29}$$

By differentiating Eq. (3.28) twice and then applying it in Eq. (3.29), it is possible to remove the differential term and write the system as

$$(\mathbf{\Lambda} - \mathbf{\Upsilon})\mathbf{u} + \varepsilon \mathbf{\Gamma}_{\mathbf{u}}(\mathbf{u}, \dot{\mathbf{u}}, \mathbf{r}) = \varepsilon \mathbf{P}_{\mathbf{u}} \mathbf{r}, \tag{3.30}$$

where $\mathbf{\Upsilon}$ is an $N \times N$ diagonal matrix with k^{th} diagonal term $\omega_{r,k}^2$. Thus, once the system defined by Eq. (3.29) has been obtained, it is possible to reduce the equations to a set of time-independent expressions.

By applying the transform defined in Eq. (3.27) to Eq. (3.21), and implementing the expression in Eq. (3.29), it is possible to eliminate the $\ddot{\mathbf{u}}$ to give

$$\begin{aligned}(\varepsilon \ddot{\mathbf{h}}_1 + \varepsilon^2 \ddot{\mathbf{h}}_2 + \dots) + (\varepsilon \mathbf{\Upsilon} \mathbf{h}_1 + \varepsilon^2 \mathbf{\Upsilon} \mathbf{h}_2 + \dots) + \varepsilon \mathbf{\Gamma}_{\mathbf{v}} - (\varepsilon \mathbf{\Gamma}_{\mathbf{u},1} + \varepsilon^2 \mathbf{\Gamma}_{\mathbf{u},2} + \dots) \\ + \varepsilon \mathbf{P}_{\mathbf{u}} \mathbf{r} - \varepsilon \mathbf{P}_{\mathbf{v}} \mathbf{r} = 0.\end{aligned} \tag{3.31}$$

This equation applies the perturbation $\mathbf{\Gamma}_{\mathbf{u}}(\mathbf{u}, \dot{\mathbf{u}}, \mathbf{r}) = \mathbf{\Gamma}_{\mathbf{u},1}(\mathbf{u}, \dot{\mathbf{u}}, \mathbf{r}) + \varepsilon \mathbf{\Gamma}_{\mathbf{u},2}(\mathbf{u}, \dot{\mathbf{u}}, \mathbf{r}) + \dots$. The perturbed variables in the $\mathbf{\Gamma}_{\mathbf{v}}$ expression inhibit the ability to balance the ε terms in this

current state. As such, a Taylor expansion is applied:

$$\begin{aligned}\boldsymbol{\Gamma}_{\mathbf{v}}(\mathbf{u}+&\varepsilon\mathbf{h}_1+\dots,\dot{\mathbf{u}}+\varepsilon\dot{\mathbf{h}}_1+\dots,\mathbf{r})\\ &=\boldsymbol{\Gamma}_{\mathbf{v}}(\mathbf{u},\dot{\mathbf{u}},\mathbf{r})+\varepsilon[\nabla_{\mathbf{u}'}\boldsymbol{\Gamma}_{\mathbf{v}}(\mathbf{u}',\dot{\mathbf{u}},\mathbf{r})]_{\mathbf{u}'=\mathbf{u}}\mathbf{h}_1+\varepsilon[\nabla_{\dot{\mathbf{u}}'}\boldsymbol{\Gamma}_{\mathbf{v}}(\mathbf{u},\dot{\mathbf{u}}',\mathbf{r})]_{\dot{\mathbf{u}}'=\dot{\mathbf{u}}}\dot{\mathbf{h}}_1+\dots,\end{aligned} \tag{3.32}$$

where $\nabla_{\mathbf{y}}$ represents the gradient of some vector $\mathbf{y}$.

Implementing this Taylor expansion and Eq. (3.30) allows Eq. (3.31) to be written, up to ε^2-order, as

$$\begin{aligned}\varepsilon\ddot{\mathbf{h}}_1+\varepsilon^2\ddot{\mathbf{h}}_2+\varepsilon\boldsymbol{\Upsilon}\mathbf{h}_1+\varepsilon^2\boldsymbol{\Upsilon}\mathbf{h}_2+\varepsilon^2(\boldsymbol{\Lambda}-\boldsymbol{\Upsilon})\mathbf{h}_1+\varepsilon\boldsymbol{\Gamma}_{\mathbf{v}}+\varepsilon^2\left[\frac{\partial}{\partial\mathbf{u}}\boldsymbol{\Gamma}_{\mathbf{v}}\right]\mathbf{h}_1\\ +\varepsilon^2\left[\frac{\partial}{\partial\dot{\mathbf{u}}}\boldsymbol{\Gamma}_{\mathbf{v}}\right]\dot{\mathbf{h}}_1-\varepsilon\boldsymbol{\Gamma}_{\mathbf{u},1}-\varepsilon^2\boldsymbol{\Gamma}_{\mathbf{u},2}+\varepsilon\mathbf{P}_{\mathbf{u}}\mathbf{r}-\varepsilon\mathbf{P}_{\mathbf{v}}\mathbf{r}=0.\end{aligned} \tag{3.33}$$

This equation makes use of the notation $\frac{\partial}{\partial\mathbf{u}}\boldsymbol{\Gamma}_{\mathbf{v}}=\nabla_{\mathbf{u}}\boldsymbol{\Gamma}_{\mathbf{v}}(\mathbf{u},\dot{\mathbf{u}},\mathbf{r})$ and $\frac{\partial}{\partial\dot{\mathbf{u}}}\boldsymbol{\Gamma}_{\mathbf{v}}=\nabla_{\dot{\mathbf{u}}}\boldsymbol{\Gamma}_{\mathbf{v}}(\mathbf{u},\dot{\mathbf{u}},\mathbf{r})$, and also applies the perturbation $\varepsilon\boldsymbol{\Gamma}_{\mathbf{u}}(\mathbf{u},\dot{\mathbf{u}},\mathbf{r})=\varepsilon\boldsymbol{\Gamma}_{\mathbf{u},1}(\mathbf{u},\dot{\mathbf{u}},\mathbf{r})+\varepsilon^2\boldsymbol{\Gamma}_{\mathbf{u},2}(\mathbf{u},\dot{\mathbf{u}},\mathbf{r})+\dots$.

Furthermore, the following detuning expression has been employed:

$$\boldsymbol{\Lambda}=\boldsymbol{\Upsilon}+\varepsilon\boldsymbol{\Delta}=\boldsymbol{\Upsilon}+\varepsilon(\boldsymbol{\Lambda}-\boldsymbol{\Upsilon}). \tag{3.34}$$

This step is traditionally applied in the DNF method and is explored in [130, 136]. The first equality here demonstrates the fact that, instead of simply detuning around the natural frequency, its square is detuned. This is consistent with the form in which the frequency arises in the equations of motion. The second expression makes use of the fact that, although $\boldsymbol{\Lambda}$ is not necessarily equal to $\boldsymbol{\Upsilon}$, the dynamics are considered within some close neighbourhood of the natural frequency. Therefore, their difference will be small (and hence of order ε).

The resultant ε balance of Eq. (3.33), the components of which are referred to as the *homological* equations, is now given by

$$\begin{aligned}\varepsilon^0:&\quad\mathbf{P}_{\mathbf{u}}\mathbf{r}=\mathbf{P}_{\mathbf{v}}\mathbf{r},\\ \varepsilon^1:&\quad\ddot{\mathbf{h}}_1(\mathbf{u},\dot{\mathbf{u}},\mathbf{r})+\boldsymbol{\Upsilon}\mathbf{h}_1(\mathbf{u},\dot{\mathbf{u}},\mathbf{r})+\boldsymbol{\Gamma}_{\mathbf{v},1}(\mathbf{u},\dot{\mathbf{u}},\mathbf{r})=\boldsymbol{\Gamma}_{\mathbf{u},1}(\mathbf{u},\dot{\mathbf{u}},\mathbf{r}),\\ \varepsilon^2:&\quad\ddot{\mathbf{h}}_2(\mathbf{u},\dot{\mathbf{u}},\mathbf{r})+\boldsymbol{\Upsilon}\mathbf{h}_2(\mathbf{u},\dot{\mathbf{u}},\mathbf{r})+\boldsymbol{\Gamma}_{\mathbf{v},2}(\mathbf{u},\dot{\mathbf{u}},\mathbf{r})=\boldsymbol{\Gamma}_{\mathbf{u},2}(\mathbf{u},\dot{\mathbf{u}},\mathbf{r}),\\ &\quad\vdots\end{aligned} \tag{3.35}$$

where $\boldsymbol{\Gamma}_{\mathbf{v},1}(\mathbf{u},\dot{\mathbf{u}},\mathbf{r})=\boldsymbol{\Gamma}_{\mathbf{v}}(\mathbf{u},\dot{\mathbf{u}},\mathbf{r})$ and $\boldsymbol{\Gamma}_{\mathbf{v},2}(\mathbf{u},\dot{\mathbf{u}},\mathbf{r})=(\boldsymbol{\Lambda}-\boldsymbol{\Upsilon}+\frac{\partial}{\partial\mathbf{u}}\boldsymbol{\Gamma}_{\mathbf{v}})\mathbf{h}_1+(\frac{\partial}{\partial\dot{\mathbf{u}}}\boldsymbol{\Gamma}_{\mathbf{v}})\dot{\mathbf{h}}_1$.

Balancing the ε^0 terms in Eq. (3.35), it can be seen that $\mathbf{P_u} = \mathbf{P_v}$. In the ε^1-order balance, the $\mathbf{\Gamma}_{\mathbf{u},k}$ terms are used to manage resonant terms, which respond at $\omega_{r,k}$. The $\mathbf{h}_k$ terms are included to denote harmonic terms. Naturally, these contain those components which do *not* respond at $\omega_{r,k}$. These expressions typically comprise polynomials in terms of $\mathbf{u}_p = \{u_{pk}\}, \mathbf{u}_m = \{u_{mk}\}$, and $\mathbf{r}$. As such, the expanded forms of Eq. (3.35) can quickly become unwieldy and it is convenient to represent them in terms of the vector $\mathbf{u}_k^*(\mathbf{u}_p, \mathbf{u}_m, \mathbf{r})$, which is an $N_k \times 1$ vector consisting of all the potential product combinations of these elements. In doing so, the expressions in Eq. (3.35) can now be written as

$$\begin{aligned} \mathbf{\Gamma}_{\mathbf{v},k}(\mathbf{u}, \dot{\mathbf{u}}, \mathbf{r}) &= [\Gamma_{v,k}]\mathbf{u}_k^*(\mathbf{u}_p, \mathbf{u}_m, \mathbf{r}), \\ \mathbf{\Gamma}_{\mathbf{u},k}(\mathbf{u}, \dot{\mathbf{u}}, \mathbf{r}) &= [\Gamma_{u,k}]\mathbf{u}_k^*(\mathbf{u}_p, \mathbf{u}_m, \mathbf{r}), \\ \mathbf{h}_k(\mathbf{u}, \dot{\mathbf{u}}, \mathbf{r}) &= [h_k]\mathbf{u}_k^*(\mathbf{u}_p, \mathbf{u}_m, \mathbf{r}), \end{aligned} \tag{3.36}$$

where $[\Gamma_{v,k}]$, $[\Gamma_{u,k}]$, and $[h_k]$ are $N \times N_k$ matrices of time-invariant coefficient for the products of parameters that comprise $\mathbf{u}_k^*$. Thus, for $k \geq 1$, the ε^k homological equation is given by

$$[h_k]\ddot{\mathbf{u}}_k^* + \Upsilon[h_k]\mathbf{u}_k^* + [\Gamma_{v,k}]\mathbf{u}_k^* = [\Gamma_{u,k}]\mathbf{u}_k^*. \tag{3.37}$$

Careful consideration of the $\mathbf{u}_k^*$ vectors is necessary to find a solution for $\mathbf{u}$. This begins by writing the ℓ^{th} element of $\mathbf{u}_k^*$ as

$$u_{k,\ell}^* = r_p^{m_{p,k,\ell}} r_m^{m_{m,k,\ell}} \prod_{n=1}^{N} u_{pn}^{s_{p,k,\ell,n}} u_{mn}^{s_{m,k,\ell,n}} = U_{k,\ell}^* \mathrm{e}^{j(\omega_{k,\ell}^* t + \phi_{k,\ell}^*)}, \tag{3.38}$$

where

$$U_{k,\ell}^* = \prod_{n=1}^{N} \left(\frac{U_n}{2}\right)^{(s_{p,k,\ell,n} + s_{m,k,\ell,n})},$$

$$\phi_{k,\ell}^* = \sum_{n=1}^{N} (s_{m,k,\ell,n} - s_{p,k,\ell,n})\phi_n,$$

and

$$\omega_{k,\ell}^* = (m_{p,k,\ell} - m_{m,k,\ell})\Omega + \sum_{n=1}^{N} (s_{p,k,\ell,n} - s_{m,k,\ell,n})\omega_{r,n}.$$

These new variables can be applied in Eq. (3.37) so that element $\{i, \ell\}$ of $[\Gamma_{v,k}]$ to be written as

$$[\Gamma_{v,k}]_{i,\ell} = [\Gamma_{u,k}]_{i,\ell} + \beta_{k,i,\ell}[h_k]_{i,\ell}, \tag{3.39}$$

where

$$\beta_{k,i,\ell} = [\omega^*_{k,\ell}]^2 - \omega^2_{r,k} \tag{3.40}$$

defines the $N \times N_k$ matrix $\boldsymbol{\beta}_k$. Therefore, if $[\omega^*_{k,\ell}]^2 = \omega^2_{r,k}$, then $\beta_{k,i,\ell} = 0$. This allows $\boldsymbol{\beta}_k$ to be considered as a matrix that determines whether the elements of $[\Gamma_{v,k}]$ are coefficients of resonant or harmonic terms. Now,

$$[\Gamma_{v,i}]_{k,\ell} = [\Gamma_{u,i}]_{k,\ell}, \;\; [h_i]_{k,\ell} = 0, \qquad \text{if } \beta_{i,k,\ell} = 0, \tag{3.41}$$

$$[\Gamma_{v,i}]_{k,\ell} = 0, \;\; [h_i]_{k,\ell} = \frac{[\Gamma_{u,i}]_{k,\ell}}{\beta_{i,k,\ell}}, \qquad \text{otherwise.} \tag{3.42}$$

These expressions can be applied in Eq. (3.36) to find $\boldsymbol{\Gamma}_u$, and hence $\boldsymbol{\Gamma}_v$, leading to the k^{th} resonant equation

$$\begin{aligned}\Big[(\omega^2_{n,k} - \omega^2_{r,k})A_k \mathrm{e}^{-\mathrm{j}\phi_k} + \Gamma^+_{u,k} - P^+_{u,k}\Big]\mathrm{e}^{+\mathrm{j}\omega_{r,k}t} \\ + \Big[(\omega^2_{n,k} - \omega^2_{r,k})A_k \mathrm{e}^{+\mathrm{j}\phi_k} + \Gamma^-_{u,k} - P^-_{u,k}\Big]\mathrm{e}^{-\mathrm{j}\omega_{r,k}t} = 0,\end{aligned} \tag{3.43}$$

where $P^+_{u,k}$ and $P^-_{u,k}$ denote elements $\{k,1\}$ and $\{k,2\}$ of $\mathbf{P_u}$, respectively. The variables $\Gamma^+_{u,k}$ and $\Gamma^-_{u,k}$ arise in the decomposition

$$\Gamma_{u,k} = \Gamma^+_{u,k}\mathrm{e}^{+\mathrm{j}\omega_{r,k}t} + \Gamma^-_{u,k}\mathrm{e}^{-\mathrm{j}\omega_{r,k}t}. \tag{3.44}$$

The square bracketed terms in Eq. (3.43) are complex conjugates of one another and, for the equality to hold, it is necessary for both of these to be equal to zero. As such, the frequency-amplitude relationship is simply given by

$$(\omega^2_{n,k} - \omega^2_{r,k})A_k \mathrm{e}^{-\mathrm{j}\phi_k} + \Gamma^+_{u,k} = P^+_{u,k}, \tag{3.45}$$

which can be solved to find the frequency-amplitude relationship of the system once values for A_k and ϕ_k are found.

Additionally, the harmonics can be found using Eqs. (3.27) and (3.35), allowing the physical response to be given by

$$\mathbf{x} = \boldsymbol{\Phi}(\mathbf{u} + \mathbf{h}(\mathbf{u}, \dot{\mathbf{u}}, \mathbf{r}) + [e]\mathbf{r}). \tag{3.46}$$

Note that the bookkeeping term, ε, has been dropped, as it is no longer necessary to keep

track of the relative size of each term.

3.2.4 Comparison through frequency detuning

It is common practice to apply a frequency detuning to increase the accuracy of the MS method, although it is not strictly an integral part of its methodology. In the literature [122, 214–216], these detunings are proposed as arbitrary perturbations:

$$\omega = \omega_0 + \varepsilon\omega_1 + \varepsilon^2\omega_2 + \dots. \tag{3.47}$$

However, although it is rarely used, a detuning of the square of the linear natural frequency has also been suggested [214]:

$$\omega^2 = \omega_0^2 + \varepsilon\omega_1 + \varepsilon^2\omega_2 + \dots. \tag{3.48}$$

Once the expression in Eq. (3.48) has been truncated to ε^1-order, it takes the same form as the detuning given in Eq. (3.34). The difference between Eq. (3.48) and the DNF detuning is the physical motivation and interpretation of that in the DNF method. As opposed to using the arbitrarily defined frequency ω_0, Eq. (3.34) can be interpreted as a series expansion about the stiffness term, which is expressed as the square of the linear natural frequency:

$$\omega_{r,k}^2 = \omega_{n,k}^2 + \varepsilon\delta = \omega_{n,k}^2 + \varepsilon(\omega_{n,k}^2 - \omega_{r,k}^2), \tag{3.49}$$

as has been seen in the previous section. The procedure for applying this detuning in the MS method (henceforth referred to as the detuned Multiple Scales (dMS) method) is identical to the previous section up to the ε-expansion given in Eq. (3.9), which now takes the form

$$\begin{aligned}
&\varepsilon^0 : (D_0^2 + \boldsymbol{\Upsilon})\mathbf{q}_0 = 0,\\
&\varepsilon^1 : (D_0^2 + \boldsymbol{\Upsilon})\mathbf{q}_1 = -2D_0D_1\mathbf{q}_0 - (\boldsymbol{\Lambda} - \boldsymbol{\Upsilon})\mathbf{q}_0 - \Gamma_{q,k}(\mathbf{q}_0, D_0\mathbf{q}_0, \mathbf{r}) + \mathbf{P}_\mathbf{q}\mathbf{r},\\
&\varepsilon^2 : (D_0^2 + \boldsymbol{\Upsilon})\mathbf{q}_2 = -2D_0D_1\mathbf{q}_1 - (\boldsymbol{\Lambda} - \boldsymbol{\Upsilon})\mathbf{q}_1\\
&\qquad\qquad -(D_1^2 + 2D_0D_2)\mathbf{q}_2 - \left[\tfrac{\partial}{\partial\mathbf{q}_0}\Gamma_{q,k}\right]\mathbf{q}_1 - \left[\tfrac{\partial}{\partial\dot{\mathbf{q}}_0}\Gamma_{q,k}\right]\dot{\mathbf{q}}_1,\\
&\quad\vdots
\end{aligned} \tag{3.50}$$

It remains necessary to remove the secular terms, initially from the ε^1-order equation, and set them to zero. These are now given by

$$\begin{aligned}
&\mathrm{j}\omega_{r,k}\Big((D_1A_{0,k}+A_{0,k}D_1\phi_{0,k})\mathrm{e}^{+\mathrm{j}(\omega_{n,k}T_0+\phi_{0,k})}\\
&\quad+(D_1A_{0,k}-A_{0,k}D_1\phi_{0,k})\mathrm{e}^{-\mathrm{j}(\omega_{n,k}T_0+\phi_{0,k})}\Big)\\
&\quad+(\omega_{n,k}^2-\omega_{r,k}^2)\Big(A_{0,k}\Big(\mathrm{e}^{+\mathrm{j}(\omega_{n,k}T_0+\phi_{0,k})}+\mathrm{e}^{-\mathrm{j}(\omega_{n,k}T_0+\phi_{0,k})}\Big)\\
&\qquad+\mathrm{Res}\{\Gamma_{q,k}\Big(\frac{A_{0,k}}{2}\Big(\mathrm{e}^{+\mathrm{j}(\omega_{n,k}T_0+\phi_{0,k})}+\mathrm{e}^{-\mathrm{j}(\omega_{n,k}T_0+\phi_{0,k})}\Big),\\
&\qquad\quad\mathrm{j}\omega_{r,k}\frac{A_{0,k}}{2}\Big(\mathrm{e}^{+\mathrm{j}(\omega_{n,k}T_0+\phi_{0,k})}-\mathrm{e}^{-\mathrm{j}(\omega_{n,k}T_0+\phi_{0,k})}\Big),\\
&\qquad\qquad\mathrm{e}^{+\mathrm{j}\Omega T_0}+\mathrm{e}^{-\mathrm{j}\Omega T_0}\Big)\}=P_{q,k}\Big(\mathrm{e}^{+\mathrm{j}(\Omega T_0)}+\mathrm{e}^{-\mathrm{j}(\Omega T_0)}\Big).
\end{aligned}\tag{3.51}$$

Comparing Eq. (3.51) with Eq. (3.14), it can be seen that, by no longer assuming that the response frequency is equal to the linear natural frequency, new terms arise in the ε^1-order equation. The inclusion of the term $(\omega_{n,k}^2-\omega_{r,k}^2)\big(A_{0,k}\big(\mathrm{e}^{+\mathrm{j}(\omega_{n,k}T_0+\phi_{0,k})}+\mathrm{e}^{-\mathrm{j}(\omega_{n,k}T_0+\phi_{0,k})}\big)\big)$ can be thought of as a detuning term that accounts for the influence that those terms which are close to resonance have on the free vibrations of the system.

Collecting coefficients for the $\mathrm{e}^{\pm\mathrm{j}\omega_{r,k}T_0}$, Eq. (3.51) can be written as

$$\begin{aligned}
&\Big[A_{0,k}(\omega_{n,k}^2-\omega_{r,k}^2)\Big(\mathrm{e}^{+\mathrm{j}\phi_{0,k}}\Big)+(D_1A_{0,k}+\mathrm{j}\omega_{r,k}A_{0,k}D_1\phi_{0,k})\mathrm{e}^{+\mathrm{j}\phi_{0,k}}\\
&\quad+\mathrm{Res}\{\Gamma_{q,k}\Big(\frac{A_{0,k}}{2}\Big(\mathrm{e}^{+\mathrm{j}(\omega_{n,k}T_0+\phi_{0,k})}\Big),\mathrm{j}\omega_{r,k}\frac{A_{0,k}}{2}\Big(\mathrm{e}^{+\mathrm{j}(\omega_{n,k}T_0+\phi_{0,k})}\Big),\\
&\qquad\mathrm{e}^{+\mathrm{j}\Omega T_0}\Big)\}-P_{q,k}\Big]\mathrm{e}^{+\mathrm{j}(\omega_{r,k}T_0)}\\
&\quad+\Big[A_{0,k}(\omega_{n,k}^2-\omega_{r,k}^2)\Big(\mathrm{e}^{-\mathrm{j}\phi_{0,k}}\Big)+(D_1A_{0,k}-\mathrm{j}\omega_{r,k}A_{0,k}D_1\phi_{0,k})\mathrm{e}^{-\mathrm{j}\phi_{0,k}}\\
&\qquad+\mathrm{Res}\{\Gamma_{q,k}\Big(\frac{A_{0,k}}{2}\Big(\mathrm{e}^{-\mathrm{j}(\omega_{n,k}T_0+\phi_{0,k})}\Big),\mathrm{j}\omega_{r,k}\frac{A_{0,k}}{2}\Big(\mathrm{e}^{-\mathrm{j}(\omega_{n,k}T_0+\phi_{0,k})}\Big),\\
&\qquad\mathrm{e}^{-\mathrm{j}\Omega T_0}\Big)\}-P_{q,k}\Big]\mathrm{e}^{-\mathrm{j}(\omega_{r,k}T_0)}=0.
\end{aligned}\tag{3.52}$$

Similarly to the DNF method, the bracketed terms in Eq. (3.52) are complex conjugates, both of which must be equated to zero. As such, the frequency-amplitude equation can be written as

$$\begin{aligned}
&(\omega_{n,k}^2-\omega_{r,k}^2)\Big(A_{0,k}\mathrm{e}^{+\mathrm{j}\phi_{0,k}}\Big)+(D_1A_{0,k}+\mathrm{j}\omega_{r,k}A_{0,k}D_1\phi_{0,k})\mathrm{e}^{+\mathrm{j}\phi_{0,k}}\\
&\quad+\mathrm{Res}\{\Gamma_{q,k}\Big(\frac{A_{0,k}}{2}\Big(\mathrm{e}^{+\mathrm{j}(\omega_{r,k}t+\phi_{0,k})}\Big),\mathrm{j}\omega_{r,k}\frac{A_{0,k}}{2}\Big(\mathrm{e}^{+\mathrm{j}(\omega_{r,k}t+\phi_{0,k})}\Big),\mathrm{e}^{+\mathrm{j}\Omega t}\Big)\}\\
&\qquad=P_{q,k}.
\end{aligned}\tag{3.53}$$

By considering the real and imaginary parts of Eq. (3.53) separately and equating each to

zero, it is possible to solve the system for $A_{0,k}$ and $\phi_{0,k}$.

Recall that the equivalent expression in the DNF method, Eq. (3.45), is written as

$$(\omega_{n,k}^2 - \omega_{r,k}^2)A_k \mathrm{e}^{-\mathrm{j}\phi_k} + \Gamma_{u,k}^{+} = P_{u,k}.$$

Now, it is possible to equate the equations found using the two techniques. In addition, recall from Eq. (3.24) that $\mathbf{P}_{\mathbf{q},k} = \mathbf{P}_{\mathbf{v},k} + (\omega_{n,k}^2 - \Omega^2)[e]_k$; for the resonant equation, $[e]_k = [0 \;\; 0]$. Therefore, $P_{u,k} = P_{q,k}$.

By definition, $\Gamma_{u,k}^{+}$ denotes the resonant terms of $\mathbf{\Gamma_u}$, which includes the damping and nonlinear terms. In the dMS case, this is represented by the term

$$\mathrm{Res}\{\Gamma_{q,k}\Big(\frac{A_{0,k}}{2}\Big(\mathrm{e}^{+\mathrm{j}(\omega_{r,k}t+\phi_{0,k})}\Big), \mathrm{j}\omega_{r,k}\frac{A_{0,k}}{2}\Big(\mathrm{e}^{+\mathrm{j}(\omega_{r,k}t+\phi_{0,k})}\Big), \mathrm{e}^{+\mathrm{j}\omega_{r,k}t}\Big)\}.$$

However, the additional term, $\mathrm{j}\omega_{r,k}(D_1 A_{0,k} + A_{0,k} D_1 \phi_{0,k})\mathrm{e}^{+\mathrm{j}\phi_{0,k}}$, is now also required to account for the fact that time and derivatives are now expressed as expansions in terms of bookkeeping parameter ε. Given that A_k and $A_{0,k}$ both denote the fundamental response, it can be concluded that the two expressions represent identical dynamics.

The solution for $\mathbf{q}_1$ can be determined in a similar way to the standard MS method by solving

$$(\mathbf{\Lambda} - \mathbf{\Upsilon})\mathbf{q}_1 = -\mathrm{NRes}\{\mathbf{\Gamma_q}\}. \tag{3.54}$$

Recall that the corresponding ε^1-order equation for the DNF method is

$$\ddot{\mathbf{h}}_1 + \mathbf{\Upsilon}\mathbf{h}_1 + \mathbf{\Gamma_v} = \mathbf{n}_{u1}. \tag{3.55}$$

It can be further noted that $\ddot{\mathbf{h}}_1 = -\mathbf{\Lambda}\mathbf{h}_1$ and that $\mathbf{\Gamma_v} - \mathbf{n}_{u1} = \boldsymbol{\beta}\mathbf{h}_1 = -\mathrm{NRes}\{\mathbf{\Gamma_q}\}$, so that the expression in Eq. (3.55) can be rewritten as

$$(\mathbf{\Lambda} - \mathbf{\Upsilon})\mathbf{h}_1 = -\mathrm{NRes}\{\mathbf{\Gamma_q}\}. \tag{3.56}$$

It is immediately clear that the solutions of Eqs. (3.54) and (3.56) must be identical.

3.3 Application to a forced Duffing oscillator

While the rigour of the comparison made in the previous section is important, the impact of this detuning is more easily visualised through the consideration of an example nonlinear structure. To this end, the current section will consider the application of these methods to a forced Duffing oscillator, a system that has been used extensively to investigate analytical approximations for nonlinear dynamical structures [217].

The Duffing oscillator can be thought of as a mass-spring system, in which the lumped mass is grounded by a spring with linear and nonlinear stiffness parameters, $k = \omega_n^2$ and α, respectively. Additionally, the system contains a dashpot with damping coefficient $c = 2\zeta\omega_n$ and experiences a periodic forcing with equation $F(t) = P\cos(\Omega t)$. The mass is taken to be unitary – i.e. $m = 1$ – and its time-dependent displacement is denoted $x(t)$. Therefore, the Duffing equation is written as

$$\ddot{x} + 2\zeta\omega_n\dot{x} + \omega_n^2 x + \alpha x^3 = P\cos(\Omega t). \tag{3.57}$$

3.3.1 Harmonic balance

As previously mentioned, the first step of the HB method is to assume a harmonic form for the trial solution, as demonstrated in Eq. (3.2). To ensure the same level of accuracy as in the MS and DNF methods, a single harmonic will be used in the trial solution for each technique. Therefore, the HB trial solution will takes the form

$$x = \frac{A}{2}\mathrm{e}^{+\mathrm{j}(\Omega t+\phi)} + \text{c.c.}, \tag{3.58}$$

where c.c. denotes the complex conjugate terms. Applying this solution in Eq. (3.57) gives

$$\left[(\omega_n^2 - \Omega^2)A + 2\mathrm{j}\zeta\omega_n A + \frac{3\alpha}{4}A^3\right]\mathrm{e}^{+\mathrm{j}(\Omega t+\phi)} + \mathcal{O}(\mathrm{e}^{+3\mathrm{j}(\Omega t+\phi)}) + \text{c.c.} = P\mathrm{e}^{+\mathrm{j}\Omega t}, \tag{3.59}$$

Note that, in the full expansion of Eq. (3.59), there are terms that respond at frequencies of 3Ω. Since these frequencies are not included in the trial solution, it is implicitly assumed that their influence on the system dynamics is negligible, so they are omitted henceforth.

For Eq. (3.59) to hold, the coefficients of the time-varying components must be balanced. Ignoring the complex conjugate terms, the expression in Eq. (3.59) gives rise to the balanced

equation:

$$\left(\omega_n^2 - \Omega^2\right)A + 2\mathrm{j}\zeta\omega_n\Omega A + \frac{3\alpha}{4}A^3 = P\mathrm{e}^{-\mathrm{j}\phi}, \tag{3.60}$$

It is possible to observe the fact that the inclusion of forcing and damping terms gives rise to a complex equation. Therefore, the real and imaginary parts can be thought of as two separate equalities. Bearing this in mind, and returning to trigonometric notation, Eq. (3.60) can be expressed as

$$\begin{aligned}\left(\omega_n^2 - \Omega^2\right)A + \frac{3\alpha}{4}A^3 &= P\cos(\phi),\\ 2\zeta\omega_n\Omega A &= P\sin(\phi).\end{aligned} \tag{3.61}$$

By squaring and summing these expressions, it is possible to establish an equation which is independent of the phase, ϕ; this strategy is used across all three techniques to find a single expression for the forced response. For the HB method, this is given by

$$\left[\left(\omega_n^2 - \Omega^2\right)A + \frac{3\alpha}{4}A^3\right]^2 + \left[2\zeta\omega_n\Omega A\right]^2 = P^2. \tag{3.62}$$

It is now possible to analytically solve Eq. (3.62) to give an expression for Ω in terms of A, or vice versa; that is, to express the forcing frequency and response amplitude in terms of one another. That being said, it is important to recall the trial solution given in Eq. (3.2), which assumes that the displacement, x, can be expressed as a series of harmonic terms. The fact that the expression in Eq. (3.62) can be solved analytically is, in part, due to the relative simplicity of the trial solution used. Therefore, the ease with which higher-order, analytical solutions can be found is likely to decrease when a greater number of harmonics is used. As such, it may prove necessary to utilise numerical methods to evaluate the forced response, see [107], for instance.

The steps in this section can be repeated, with the forcing and damping terms omitted, to find the backbone curves of this system. Alternatively, one can simply set $\zeta = P = 0$ in Eq. (3.62) to give

$$\left(\omega_n^2 - \Omega^2\right) + \frac{3\alpha}{4}A^2 = 0. \tag{3.63}$$

Now, the response of the system can be defined by Eq. (3.58), with Ω defined by solving either Eqs. (3.62) or (3.63).

3.3.2 Multiple scales

In the current, initial comparison, the MS and DNF methods will be considered up to ε^1-order, with higher-order behaviour considered later in this chapter. Therefore, the initial perturbations will be defined as

$$\begin{aligned} t &= T_0 + T_1 = t + \varepsilon t, \\ x &= x_0(T_0, T_1) + \varepsilon x_1(T_0, T_1). \end{aligned} \tag{3.64}$$

The multiple time scales defined in Eq. (3.64) lead to the following perturbed derivative expressions.

$$\begin{aligned} \tfrac{\mathrm{d}}{\mathrm{d}t} &= D_0 + \varepsilon D_1, \\ \tfrac{\mathrm{d}^2}{\mathrm{d}t^2} &= D_0^2 + \varepsilon(2D_0D_1). \end{aligned} \tag{3.65}$$

Implementing the perturbed expressions in Eqs. (3.64) and (3.65) in the equations of motion given in Eq. (3.57) results in the updated expression

$$\begin{aligned} (D_0^2 + 2\varepsilon D_0D_1)(x_0 + \varepsilon x_1) + 2\varepsilon\zeta\omega_n\Omega(D_0 + \varepsilon D_1)(x_0 + \varepsilon x_1) \\ + \omega_n^2(x_0 + \varepsilon x_1) + \varepsilon\alpha(x_0 + \varepsilon x_1)^3 = \varepsilon P\cos(\Omega(T_0 + T_1)). \end{aligned} \tag{3.66}$$

When this equation is expanded, terms with order higher than ε^1 will naturally occur. Therefore, by choosing to omit these, an assumption is made that the influence of higher-order, harmonic terms on the system dynamics is negligible.

It can also be noted that, in Eq. (3.66), the damping, nonlinear, and forcing terms are assumed to be weak, as denoted by the inclusion of ε in their coefficients. Balancing the terms of the ε-expansion in Eq. (3.66) leads to the following system of equations

$$\begin{aligned} \varepsilon^0: &\quad D_0^2x_0 + \omega_n^2x_0 = 0, \\ \varepsilon^1: &\quad D_0^2x_1 + \omega_n^2x_1 = -2D_0D_1x_0 - 2\zeta\omega_nD_1x_0 \\ &\qquad\qquad -\alpha x_0^3 + P\cos(\Omega T_0). \end{aligned} \tag{3.67}$$

It is immediately clear that a solution for the ε^0-order equation will take the form

$$x_0 = \frac{A(T_1)}{2}\big(e^{+\mathrm{j}(\omega_nT_0 + \phi(T_1))} + e^{-\mathrm{j}(\omega_nT_0 + \phi(T_1))}\big), \tag{3.68}$$

where a and α denote the response amplitude and phase, respectively. At this point, it is worth highlighting the fact that these parameters are functions of $T_1 = \varepsilon t$, allowing the user to model transient changes in the system dynamics. Although this is not pursued further in

this work, this ability is not present in the HB and DNF methods in their classical definition.

The emphasis of this study is on the comparison of steady-state behaviour. As such, the resonant, secular terms – i.e. those terms that respond at frequency ω_n – must be isolated and set to zero. Furthermore, as is often the case when considering the forced dynamics of a non-linear structure, the frequency interval of interest is that close to the linear natural frequency, ω_n. Hence, it is useful to consider the forcing frequency in terms of some small deviation, σ, from this value, writing $\Omega = \omega_n + \varepsilon\sigma$. Implementing this detuning and separating the real and imaginary components, the secular terms are given by

$$\begin{aligned} \frac{3\alpha}{4}A(T_1)^3 - 2\omega_n^2 A(T_1)(D_1\phi(T_1)) &= P\cos(\phi(T_1)), \\ -2\zeta\omega_n^2 A(T_1) - 2\omega_n(D_1 A(T_1)) &= P\sin(\phi(T_1)). \end{aligned} \tag{3.69}$$

For these equations to represent steady-state dynamics, one must enforce the fact that there are no changes in amplitude and phase with respect to T_1. Doing so is relatively straightforward for $A(T_1)$, but the phase term must be considered in conjunction with the detuning parameter, σ, since $\Omega T_0 = (\omega_n + \varepsilon\sigma)T_0 = \omega_n T_0 + \sigma T_1$. To this end, it is useful to define the following linear transformation of the phase angle

$$\psi = \sigma T_1 - \phi(T_1). \tag{3.70}$$

Thus, the conditions for steady-state behaviour are

$$\begin{aligned} D_1 A(T_1) &= 0, \\ D_1\psi(T_1) &= 0. \end{aligned} \tag{3.71}$$

From Eq. (3.71), it can be seen that $A(T_1) = A$ is constant, and that $D_1\phi(T_1) = \sigma$. Eq. (3.69) can now be rewritten in terms of these expressions

$$\begin{aligned} \frac{3\alpha}{4}A^3 - 2\omega_n^2 A\sigma &= P\cos(\alpha), \\ -2\zeta\omega_n^2 A &= P\sin(\alpha). \end{aligned} \tag{3.72}$$

As in the HB section, it is possible to collate these equations into a phase-independent expression by squaring and summing them. Recalling that the detuning parameter is given by

$\sigma = \frac{1}{\varepsilon}(\Omega - \omega_n)$, the final solution for the forced response is given by

$$\left[2\omega_n(\omega_n - \Omega)A + \varepsilon\frac{3\alpha}{4}A^3\right]^2 + [2\varepsilon\zeta\omega_n^2 A]^2 = (\varepsilon P)^2, \tag{3.73}$$

and the free vibration is defined by

$$2\omega_n(\omega_n - \Omega) + \varepsilon\frac{3\alpha}{4}A^2 = 0. \tag{3.74}$$

It can be seen that, in these final equalities, the weak nature of the damping, nonlinear, and forcing terms is maintained. Solving either Eq. (3.73) or (3.74) allows the user to define the forced or free frequency-amplitude relationship, respectively. Solving either of these, it is possible to find an expression for Ω, which can be immediately applied in the trial solution to give the ε^0-order approximation for x.

To find the solution for x_1, it is necessary to solve the non-resonant part of the ε-expansion. For the free response, this is given by

$$D_0^2 x_1 + \omega_n^2 x_1 = \text{NRes}\{-\alpha x_0^3\} = \frac{\alpha}{4}A^3 \mathrm{e}^{+3j(\Omega t+\alpha)} + \text{c.c.}. \tag{3.75}$$

Once this equation has been solved, it is possible to find the following ε^1-order solution for the free vibration of x:

$$x = x_0 + \varepsilon x_1 = A\cos(\Omega t + \alpha) + \varepsilon\frac{\alpha}{32\omega_n^2}A^3\cos(3(\Omega t + \alpha)). \tag{3.76}$$

3.3.3 Direct normal form

The initial stages of the DNF method are defined by three transforms: modal, forcing, and nonlinear near-identity. However, the Duffing oscillator contains only a single DOF, and the forcing frequency is assumed to be close to the linear natural frequency. Therefore, the first two transforms are simply the identity transform. As such, the displacement can be directly defined as

$$x = q = v = u + h, \text{ where } u = u_p + u_m = \frac{A}{2}\mathrm{e}^{+\mathrm{j}(\omega_r t+\phi)} + \frac{A}{2}\mathrm{e}^{-\mathrm{j}(\omega_r t+\phi)}, \tag{3.77}$$

where ω_r denotes the system response frequency; henceforth, it will be assumed that $\omega_r = \Omega$. It can be recalled that the general frequency response from the DNF method is given by

Eq. (3.45). Thus, to understand the nonlinear behaviour, it only remains to find Γ_u^+ and $\mathbf{u}^*$. These are found in the expansion of $\Gamma_q(q, \dot{q}, \mathbf{r})$. For the current structure, this is given by

$$\Gamma_q(q, \dot{q}, \mathbf{r}) = \Gamma_u(u, \dot{u}) = 2\zeta\omega_n\dot{u} + \alpha u^3. \tag{3.78}$$

By applying Eq. (3.77) and converting to matrix notation, it is possible to express Eq. (3.78) as

$$\Gamma_u(u, \dot{u}) = [\Gamma_u]\mathbf{u}^* = [-2\mathrm{j}\zeta\omega_n, -2\mathrm{j}\zeta\omega_n, \alpha, 3\alpha, 3\alpha, \alpha] \begin{bmatrix} u_p \\ u_m \\ u_p^3 \\ u_p^2 u_m \\ u_p u_m^2 \\ u_m^3 \end{bmatrix}. \tag{3.79}$$

Recalling the expression in Eq. (3.37) and the subsequent discussion thereof, the vectors $\boldsymbol{\beta}$, $[\Gamma_{u,1}]$, and $[h_1]$ are given by

$$\begin{aligned} \boldsymbol{\beta} = \Big[0, 0, 8\Omega^2, 0, 0, 8\Omega^2\Big] \implies [\Gamma_{u,1}] &= \Big[-2\mathrm{j}\zeta\omega_n, -2\mathrm{j}\zeta\omega_n, 0, 3\alpha, 3\alpha, 0\Big], \\ [h_1] &= \left[0, 0, \frac{\alpha}{8\Omega^2}, 0, 0, \frac{\alpha}{8\Omega^2}\right]. \end{aligned} \tag{3.80}$$

Implementing these definitions in Eq. (3.45) and treating the real and imaginary parts in the familiar way leads to the following expression for the forced response

$$\left[(\omega_n^2 - \Omega^2)A + \varepsilon\frac{3\alpha}{4}A^3\right]^2 + [2\varepsilon\zeta\omega_n\Omega A]^2 = (\varepsilon P)^2. \tag{3.81}$$

In addition, the free response is given by

$$(\omega_n^2 - \Omega^2) + \varepsilon\frac{3\alpha}{4}A^2 = 0. \tag{3.82}$$

Now, the free ε^1-order solution for x is given by

$$x = u + \varepsilon[h_1]\mathbf{u}^* = A\cos(\Omega t + \phi) + \frac{\alpha}{32\Omega^2}A^3\cos(3(\Omega t + \phi)). \tag{3.83}$$

3.3.4 Frequency detuning of the multiple scales method

As outlined in Section 3.2.4, the use of frequency detuning is commonplace in the application of the MS method, with the use of the physically-motivated detuning applied in the DNF

method identified as a potential candidate to refine the process. It has been demonstrated above that, for an arbitrary nonlinear system, the use of this detuning can bring the MS solution in line with that of the DNF technique. Here, this is illustrated for the Duffing oscillator.

Up until Eq. (3.67), the steps in the dMS method are identical to those in the classical MS method. It is at this point that the DNF detuning is applied; it should be noted that, in the forced case, this is given by $\Omega^2 = \omega_n^2 + \varepsilon\delta$. The ε-expansion in Eq. (3.67) is now given by

$$\begin{aligned} \varepsilon^0: \quad & D_0^2 x_0 + \omega_n^2 x_0 = 0, \\ \varepsilon^1: \quad & D_0^2 x_1 + \omega_n^2 x_1 = -\delta x_0 - 2D_0 D_1 x_0 - 2\zeta\omega_n (D_0 x_1 + D_1 x_0) \\ & \qquad\qquad -\alpha x_0^3 + P\cos(\Omega T_0). \end{aligned} \tag{3.84}$$

Once more, since it is the steady-state dynamics that are of interest, the conditions in Eq. (3.71) are applied. Separating the real and imaginary parts now leads to the following steady-state equations

$$\begin{aligned} \frac{3\alpha}{4} A^3 + a\delta &= P\cos(\alpha), \\ 2\zeta\omega_n \Omega a &= P\sin(\alpha). \end{aligned} \tag{3.85}$$

Combining these equations in the standard way results in forced and free responses which can be expressed as

$$\begin{aligned} \left[(\omega_n^2 - \Omega^2)a + \varepsilon\frac{3\alpha}{4}A^3\right]^2 + [2\varepsilon\zeta\omega_n\Omega a]^2 &= (\varepsilon P)^2, \\ (\omega_n^2 - \Omega^2) + \varepsilon\frac{3\alpha}{4}A^2 &= 0, \end{aligned} \tag{3.86}$$

respectively. It can immediately be noted that, for both cases, the response is identical to that given in the DNF method (see Eqs. (3.81) and (3.82)); these will be compared further in the following section. The process for finding the ε^1 component of the solution is identical to that in the MS method, though with a frequency-amplitude relationship identical to that of the DNF method.

3.3.5 Comparison of results at ε^1-order

Before comparing the results from these methods, it is first necessary to remove any ambiguity that could arise in doing so. It is widely accepted that, should any perturbation method consider a high enough order of ε or include enough harmonic terms in the trial solution, it

is theoretically possible that it produces results that are considered exact up to some small tolerance. However, it should be noted that a high number of iterations could actually be detrimental to the insight provided by these analytical methods; this is true for a number of reasons. Firstly, it could be argued that, if it is only the accuracy of the curve that is of interest, then numerical continuation is likely to be simpler and more accurate. Secondly, the complexity of the analytical solutions found using a large number of iterations can be extremely complex, and do not offer a great deal of insight to the user. Thus, it is desirable to obtain accurate curves with only a small number of iterations, which is the motivating factor for the comparison at ε^1-order in this section.

Technique	Free	Forced
HB	$\Omega^2 = \omega_n^2 + \frac{3\alpha}{4}A^2$	$\left[(\omega_n^2 - \Omega^2)A + \frac{3\alpha}{4}A^3\right]^2 + [2\zeta\omega_n\Omega A]^2 = P^2$
MS	$\Omega = \omega_n + \varepsilon\frac{3\alpha}{8\omega_n}A^2$	$\left[2\omega_n(\omega_n - \Omega)A + \varepsilon\frac{3\alpha}{4}A^3\right]^2 + [2\varepsilon\zeta\omega_n^2 A]^2 = (\varepsilon P)^2$
DNF/dMS	$\Omega^2 = \omega_n^2 + \varepsilon\frac{3\alpha}{4}A^2$	$\left[(\omega_n^2 - \Omega^2)A + \varepsilon\frac{3\alpha}{4}A^3\right]^2 + [2\varepsilon\zeta\omega_n\Omega A]^2 = (\varepsilon P)^2$
Technique	**Phase**	**Displacement**
HB	$\phi = \sin^{-1}\left(\frac{2\zeta\omega_n\Omega A}{P}\right)$	$A\cos(\Omega t + \phi)$
MS	$\phi = \sin^{-1}\left(\frac{2\varepsilon\zeta\omega_n^2 A}{P}\right)$	$A\cos(\Omega t + \phi) + \varepsilon\frac{\alpha}{32\omega_n^2}A^3\cos(3(\Omega t + \phi))$
DNF/dMS	$\phi = \sin^{-1}\left(\frac{2\varepsilon\zeta\omega_n\Omega A}{P}\right)$	$A\cos(\Omega t + \phi) + \varepsilon\frac{\alpha}{32\Omega^2}A^3\cos(3(\Omega t + \phi))$

Table 3.1: Summary of approximate solutions and expressions for backbone curves for the undamped, unforced Duffing oscillator.

The expressions for the free and forced dynamics from each method, as well as the forced phase and displacement expressions, are displayed in Table 3.1. Although the MS and DNF methods employ a bookkeeping parameter that is not typically present in the HB method, it is common practice to discard this once a truncation of the solution has been made. In doing this, it can be seen that the HB free and forced responses are identical to those found using the DNF method, but this is not the case for the MS method. In Table 3.1, the free vibration solutions have been formatted to represent the detuning nature of these expressions. However, it is useful to reconsider their original representations:

$$\begin{aligned} \text{HB}: &\quad (\omega_n^2 - \Omega^2) + \frac{3\alpha}{4}A^2 = 0, \\ \text{MS}: &\quad 2\omega_n(\omega_n - \Omega) + \varepsilon\frac{3\alpha}{4}A^2 = 0, \\ \text{DNF}: &\quad (\omega_n^2 - \Omega^2) + \varepsilon\frac{3\alpha}{4}A^2 = 0. \end{aligned} \tag{3.87}$$

Now, the nonlinear terms are identical across all three equations; the only difference is the first term in the MS expression. However, if one takes a Taylor expansion of the term $(\omega_n^2 - \Omega^2)$ at the point $\Omega = \omega_n$, the linear term is exactly $2\omega_n(\omega_n - \Omega)$, as seen in the MS expression. As such, for the case in hand, the MS solution can be thought of as a linearisation of the quadratic detuning of ω_n seen in the HB and DNF methods.

The influence of the difference in detunings – as summarised in Table 3.1 – can be noted in both the backbone curves and forced responses, as displayed in Fig. 3.1. This figure considers the expressions in Eq. (3.87), so that A is given as a function of Ω. Here, the parameter values are as follows: $\omega_n = 1$, $\alpha = 0.6$, with $\zeta = 0.005$, $P = 0.0015$ in the first case and $\zeta = 0.0015$, $P = 0.005$ in the second. Note that the bookkeeping parameter, ε, has been removed once the solutions has been truncated at the same order.

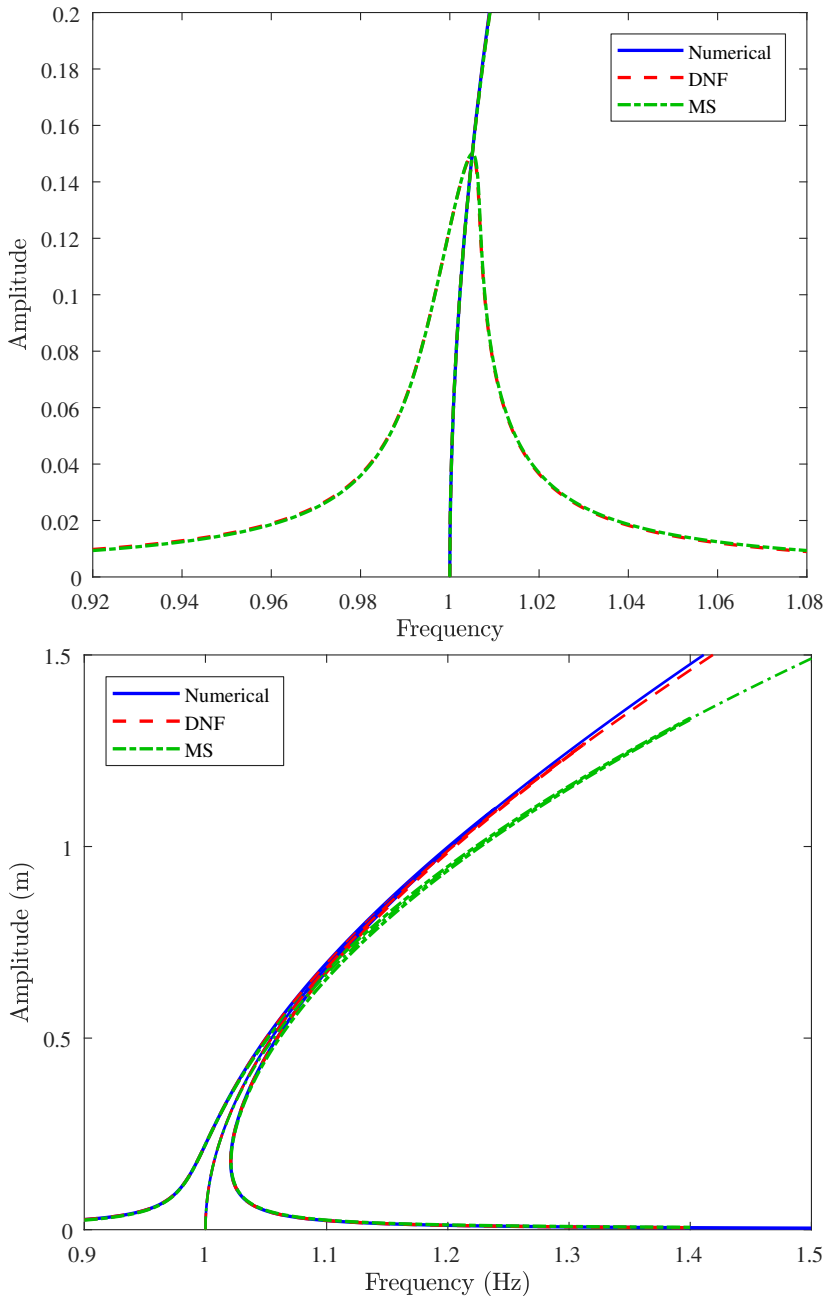

Figure 3.1: Free and forced responses at ε^1-order, for the HB, DNF, and MS methods, and numerically continued solutions. Case 1: $\zeta = 0.005$, $P = 0.0015$; Case 2: $\zeta = 0.0015$, $P = 0.005$.

In the first panel of Fig. 3.1, the smaller value of P naturally leads to a lower response amplitude. It can be seen that the results from all three methods give very close approximations to the black curve, which has been numerically continued using the software AUTO-07p [29]. In fact, it is difficult to categorically determine which analytical technique gives the better approximation. The differences are much clearer in the higher amplitude response displayed in the second panel, in which it can be seen that all of the methods eventually diverge from the true solution, though this happens at a much lower amplitude for the classical MS technique. This directly correlates with the previous discussion regarding the Taylor expansion in the

MS method. That is, as the amplitude increases, the validity of the linearised approximation decreases.

In Fig. 3.1, only the fundamental response is displayed, so the DNF curve is identical to both that of the dMS method (as, it has been shown, is always the case) and the HB method (which is specific to this example). However, Table 3.1 demonstrates the fact that the HB method does not produce any harmonic component when only a single term is used in the trial solution. Therefore, should harmonic behaviour be important to the user, it would be necessary to add an extra layer of complexity to the application of this technique.

3.3.6 Higher-order investigation of backbone curves

A key feature of perturbation methods is the possibility to iteratively apply their steps to achieve a more accurate solution. As previously discussed, with enough iterations of such techniques, the solution can potentially increase in accuracy to the extent that it can be considered exact up to some small tolerance. However, a primary motivation for using analytical approximation techniques is to gain a greater insight into the system dynamics than can be achieved by using numerical methods. As such, it is inconvenient to include too many ε terms, as this can make the solution needlessly complicated. As such, it is common practice to limit any perturbations to ε^2-order.

To investigate the influence that this may have on the obtained results, this higher-order is obtained for the methods shown here. However, it can clearly be seen that the forced response remains close to the corresponding backbone curve at any amplitude, so only the latter will be discussed. Note that the steps applied at ε^1-order are simply repeated here, so they will only be briefly outlined. Further, given that the HB method does not produce information regarding the harmonic content of the response, only the DNF and MS techniques will be given further consideration.

3.3.6.1 Multiple scales

The MS method can be applied in a number of ways, with variations seen in the assumptions made regarding the time scales, as well as in the notation. To demonstrate the generalised nature of the results presented here, a different MS variant will be used in this section. Namely, an expanded version of the *two-timing* MS method [26] will be applied. This method typically includes a fast time scale, $\tau = \omega t$, and a slow time scale, $T = \varepsilon t$. Here, this has been updated to allow ε^2-order solutions to be found by adding the extra slow time scale,

$T_s = \varepsilon^2 t$. The derivatives with respect to these time scales will be given by

$$\begin{aligned}\frac{\mathrm{d}x}{\mathrm{d}t} &= \omega\frac{\partial x}{\partial \tau} + \varepsilon\frac{\partial x}{\partial T} + \varepsilon^2\frac{\partial x}{\partial T_s},\\ \frac{\mathrm{d}^2x}{\mathrm{d}t^2} &= \omega^2\frac{\partial^2 x}{\partial \tau^2} + 2\omega\varepsilon\frac{\partial^2 x}{\partial T\partial \tau} + \varepsilon^2\Big(\frac{\partial^2 x}{\partial T^2} + 2\omega\frac{\partial^2 x}{\partial T_s\partial \tau}\Big).\end{aligned} \tag{3.88}$$

We introduce the following, more succinct notation for these derivatives: $\bullet^\dagger = \frac{\partial \bullet}{\partial \tau}$, $\bullet^\ddagger = \frac{\partial \bullet}{\partial T}$, and $\bullet^* = \frac{\partial \bullet}{\partial T_s}$. Now, for the unforced, undamped system, the ε-expansion is given by

$$\begin{aligned}\varepsilon^0:&\quad \omega_n^2 x_0^{\dagger\dagger} + \omega_n^2 x_0 = 0,\\ \varepsilon^1:&\quad \omega_n^2 x_1^{\dagger\dagger} + \omega_n^2 x_1 = -2\omega_n x_0^{\dagger\ddagger} - \alpha x_0^3,\\ \varepsilon^2:&\quad \omega_n^2 x_2^{\dagger\dagger} + \omega_n^2 x_2 = -2\omega_n x_1^{\dagger\ddagger} - x_0^{\ddagger\ddagger} - 2\omega_n x_0^{\dagger *} - 3\alpha x_0^2 x_1.\end{aligned} \tag{3.89}$$

The ε^1-order steps are not repeated here; however, it is useful to recall that the frequency-amplitude relationship for free vibration is given by

$$\omega_r = \omega_n + \varepsilon\frac{3\alpha}{8\omega_n}A^2, \tag{3.90}$$

where ω_r now denotes the response frequency, rather than the forcing frequency. It can also be noted that the solutions for frequency and displacement can be implemented to give the following expressions for the free vibration solution at ε^1-order

$$\begin{aligned}X_0 &= A(T_s)\cos\left(\omega_r t + \phi(T_s)\right),\\ X_1 &= \frac{\alpha}{32\omega_n^2}A(T_s)^3\cos(3(\omega_r t + \phi(T_s))),\\ &\text{with: } \omega_r = \omega_n + \varepsilon\frac{3\alpha}{8\omega_n}A(T_s)^2,\end{aligned} \tag{3.91}$$

Here, the very slow time scale has been reintroduced to allow higher-order solutions to be found. These solutions can now be utilised in Eq. (3.89). It is further possible to reapply these steps for the ε^2-order components of Eq. (3.89). Considering the right hand side and balancing the coefficients of $\cos(\omega_r t + \phi(T_s))$ and $\sin(\omega_r t + \phi(T_s))$ gives the following equations

$$\begin{aligned}\phi^\ddagger(T_s) &= \frac{3\alpha^2 A(T_s)^4}{256\omega_n^4},\\ A^\ddagger(T_s) &= 0,\end{aligned} \tag{3.92}$$

respectively. Solving these in parallel leads to the following solutions for displacement and phase

$$A(T_s) = A, \quad \phi(T_s) = -\frac{15\alpha^2 A^4}{256\omega_n^3} T_s + \phi. \tag{3.93}$$

Now, the updated form of Eq. (3.91) is given by

$$\begin{aligned} X_0 &= A\cos\left(\omega_r t + \phi\right), \\ X_1 &= \frac{\alpha}{32\omega_n^2} A^3 \left(1 - \varepsilon \frac{21\alpha}{32\omega_n^2} A^2\right) \cos(3(\omega_r t + \phi)), \\ X_2 &= \frac{\alpha^2 A^5}{1024\omega_n^4} \cos(5(\omega_r t + \phi)) \\ &\text{with: } \omega_r = \omega_n + \varepsilon \frac{3\alpha}{8\omega_n} A^2 - \varepsilon^2 \frac{15\alpha^2}{256\omega_n^3} A^4. \end{aligned} \tag{3.94}$$

3.3.6.2 Direct normal form

Although there have been other applications of the normal form technique to second-order equations [218], these are qualitatively different to the current DNF method, so are not considered here.

Similarly to the MS method, the frequency and amplitude expressions can be combined to give the following forms for the ε^1-solution

$$\begin{aligned} X_0 &= A\cos(\omega_r t + \phi), \\ X_1 &= \frac{\alpha}{32\omega_r^2} A^3 \cos(3(\omega_r t + \phi)), \\ &\text{with: } \omega_r^2 = \omega_n^2 + \varepsilon \frac{3\alpha}{4} A_c^2, \end{aligned} \tag{3.95}$$

Now, it can be recalled, from Eq. (3.37), that the ε^2-order homological equation is given by

$$[h_2]\ddot{\mathbf{u}}_2^* + \omega_r^2 [h_2]\mathbf{u}_2^* + [\Gamma_{v,2}]\mathbf{u}_2^* = [\Gamma_{u,2}]\mathbf{u}_2^*. \tag{3.96}$$

We now consider the *excitation* of these equations, as it is this that defines the vector $\mathbf{u}_2^*$. These are given by

$$\begin{aligned} \varepsilon^1 : &\quad [\Gamma_{u,1}]\mathbf{u}_1^* = \alpha u^3, \\ \varepsilon^2 : &\quad [\Gamma_{u,2}]\mathbf{u}_2^* = \delta[h_1]\mathbf{u}_1^* + 3\alpha u^2 [h_1]\mathbf{u}_1^*. \end{aligned} \tag{3.97}$$

Here, the $\delta[h_1]\mathbf{u}_1^*$ term arises as a result of the detuning present in the DNF method. Now,

by considering the excitation of the ε^2 equation in relation to the matrix formulation, it is possible to write

$$\begin{aligned}
[\Gamma_{u,2}] &= \frac{\alpha}{8\omega_r^2}\Big[\delta\ \ \delta\ \ 3\alpha\ \ 6\alpha\ \ 3\alpha\ \ 3\alpha\ \ 6\alpha\ \ 3\alpha\Big], \\
\mathbf{u}_2^* &= \Big[u_p^3\ \ u_m^3\ \ u_p^5\ \ u_p^4 u_m\ \ u_p^3 u_m^2\ \ u_p^2 u_m^3\ \ u_p u_m^4\ \ u_m^5\Big]^{\mathrm{T}}, \\
\therefore [h_2] &= \frac{\alpha}{64\omega_r^4}\Big[\delta\ \ \delta\ \ \alpha\ \ 6\alpha\ \ 0\ \ 0\ \ 6\alpha\ \ \alpha\Big].
\end{aligned} \tag{3.98}$$

Therefore, the ε^2-order expression for free vibration is given by

$$\begin{aligned}
q =& A\cos(\omega_r t + \phi) + \\
& \varepsilon\frac{\alpha}{32\omega_r^2}A^3\left(1 + \varepsilon\frac{3\alpha}{32\omega_r^2}A^2\right)\cos(3(\omega_r t + \phi)) \\
& + \varepsilon^2\frac{\alpha^2}{512\omega_r^4}A^5\cos(5(\omega_r t + \phi)). \\
& \text{with} \quad \omega_r^2 = \omega_n^2 + \varepsilon\frac{3\alpha}{4}A^2 + \varepsilon^2\frac{3\alpha^2}{128\omega_r^2}A^4.
\end{aligned} \tag{3.99}$$

3.3.6.3 Detuned multiple scales

To approximate the higher order exponents of ε, it is actually necessary to perturb δ, so that $\delta = \delta_0 + \varepsilon\delta_1 + \ldots$; this prevents the resulting system of equations from being over-defined. As such, the ε-expansion is now defined by

$$\begin{aligned}
\varepsilon^0 :&\ \ \omega_r^2 x_0^{\dagger\dagger} + \omega_r^2 x_0 = 0, \\
\varepsilon^1 :&\ \ \omega_r^2 x_1^{\dagger\dagger} + \omega_r^2 x_1 = \delta_0 x_0 - 2\omega_r x_0^{\dagger\ddagger} - \alpha x_0^3, \\
\varepsilon^2 :&\ \ \omega_r^2 x_2^{\dagger\dagger} + \omega_r^2 x_2 = \delta_0 x_1 + \delta_1 x_0 - 2\omega_r x_1^{\dagger\ddagger} - x_0^{\ddagger\ddagger} - 2\omega_r x_0^{\dagger *} - 3\alpha x_0^2 x_1.
\end{aligned} \tag{3.100}$$

In trigonometric form, the ε^0-order solution is simply given by $x_0 = A(T, T_s)\cos(\tau + \phi(T, T_s))$. This can be applied in the ε^1-order equation and, as has been done previously, the coefficients of $\cos(\tau + \phi(T, T_s))$ and $\sin(\tau + \phi(T, T_s))$ – i.e. the secular terms – can be balanced to give

$$\begin{aligned}
2\omega_r\phi^{\ddagger}(T, T_s) &= \delta_0 + \frac{3\alpha}{4}A(T, T_s)^2, \\
A^{\ddagger}(T, T_s) &= 0.
\end{aligned} \tag{3.101}$$

Note that it will again be assumed that the phase is constant. Furthermore, it can be seen from the second of these equations that A is constant with respect to T. Therefore, the detuning

parameter is given by

$$\delta_0 = -\frac{3\alpha}{4}A(T_s)^2. \tag{3.102}$$

Applying this equality in the non-resonant part of the ε^1-order equation allows x_1 to be defined by

$$x_1 = \frac{\alpha A(T_s)^3}{32\omega_r^2}\cos(3(\tau+\phi)). \tag{3.103}$$

Considering the ε^2-order equation in the same manner, the balance of the first harmonic terms gives

$$\begin{aligned} \delta_1 &= \frac{3\alpha}{128\omega_r^2}A(T_s)^4, \\ A^*(T_s) &= 0. \end{aligned} \tag{3.104}$$

As such, the second harmonic displacement is defined by

$$x_2 = \frac{\alpha^2 A^5}{1024\omega_r^2}(3\cos(3(\tau+\phi)) + \cos(5(\tau+\phi))). \tag{3.105}$$

Now, it is possible to define the full ε^2-order solution, which is given by

$$\begin{aligned} x =& x_0 + \varepsilon x_1 + \varepsilon^2 x_2 = A\cos(\omega_r t+\phi) + \\ & \varepsilon\frac{\alpha}{32\omega_r^2}A^3\left(1+\varepsilon\frac{3\alpha}{32\omega_r^2}A^2\right)\cos(3(\omega_r t+\phi)) + \varepsilon^2\frac{\alpha^2}{512\omega_r^4}A^5\cos(5(\omega_r t+\phi)). \\ & \text{with} \quad \omega_r^2 = \omega_n^2 + \varepsilon\delta_0 + \varepsilon^2\delta_1 = \omega_n^2 + \varepsilon\frac{3\alpha}{4}A^2 + \varepsilon^2\frac{3\alpha^2}{128\omega_r^2}A^4. \end{aligned} \tag{3.106}$$

3.3.6.4 Comparison of solutions

As in the previous section, the comparison of these methods assesses their ability to reproduce the numerical backbone curves within one or two applications of the steps of each respective method. The fundamental and harmonic projections for the Duffing oscillator backbone curves are given in Fig. 3.2, considering both the ε^1- and ε^2-order frequency-amplitude relationships. A comparison of the ε^2-order free response and displacement expressions is also given in Table 3.2.

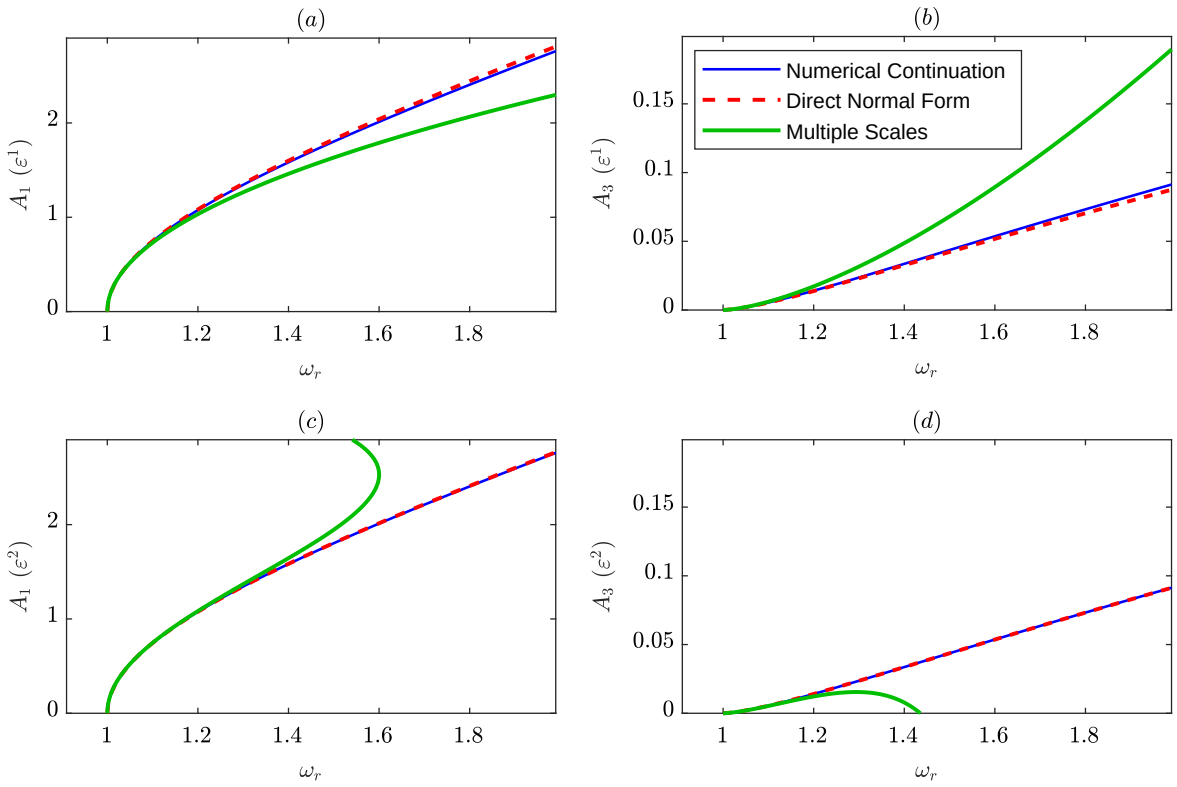

Figure 3.2: Comparison of first-order accurate (ε^1) and second-order accurate (ε^2) response curves found using approximate methods and numerical continuation for the undamped Duffing oscillator in terms of (a) the fundamental amplitude, (b) the third harmonic and (c) other harmonics, using $\omega_n = 1$ and $\alpha = 0.5$. *This figure has been reproduced from [1].*

Technique	Free
HB	$\omega_r^2 = \omega_n^2 + \frac{3\alpha}{4}A^2$
MS	$\omega_r = \omega_n + \varepsilon\frac{3\alpha}{8\omega_n}A^2 - \varepsilon^2\frac{15\alpha^2}{256\omega_n^3}A^4$
DNF/dMS	$\omega_r^2 = \omega_n^2 + \varepsilon\frac{3\alpha}{4}A^2 + \varepsilon^2\frac{3\alpha^2}{128\omega_r^2}A^4$
Technique	**Displacement**
HB	$A\cos(\omega_r t + \phi)$
MS	$A\cos(\omega_r t + \phi) + \varepsilon\frac{\alpha}{32\omega_n^2}A^3\left(1 - \varepsilon\frac{21\alpha}{32\omega_n^2}A^2\right)\cos(3(\omega_r t + \phi)) + \varepsilon^2\frac{\alpha^2}{1024\omega_n^4}A^5\cos(5(\omega_r t + \phi))$
DNF/dMS	$A\cos(\omega_r t + \phi) + \varepsilon\frac{\alpha}{32\omega_r^2}A^3\left(1 + \varepsilon\frac{3\alpha}{32\omega_r^2}A^2\right)\cos(3(\omega_r t + \phi)) + \varepsilon^2\frac{\alpha^2}{512\omega_r^4}A^5\cos(5(\omega_r t + \phi))$

Table 3.2: Summary of approximate solutions and expressions for backbone curves for the undamped, unforced Duffing oscillator.

Of particular note is the range of frequencies and amplitudes over which the analytical approximations remain close to the numerical solution, which has, again, been found using Auto 07p [29]. It can be seen, across all four panels, that the DNF (and, therefore, dMS) backbone curves remain accurate across the considered region. Although there is a minor improvement in this when the ε^2-order terms are considered, the ε^1-order curve gives a strong approximation, even as ω_r approaches $2\omega_n$.

In contrast, this trend does not hold true for the MS method. At ε^1-order, the curve begins to noticeably diverge from the numerical solution at $\omega_r \approx 1.2$. When the MS procedure is reapplied up to the ε^2-order, this increases to $\omega_r \approx 1.4$ in the fundamental backbone curve, as shown in panel (c). Beyond these points, the approximations diverge from the numerical curve. Interestingly, there is a variation in the qualitative behaviour of the MS solution as the considered order changes. More specifically, the ε^1-order approximation underestimates the fundamental backbone, but overestimates the harmonic response; further, it can be noted that the rate of divergence is greater in the latter of these. On the other hand, the ε^2-order approximation overestimates the fundamental response and underestimates the harmonic component, though it can be seen that the behaviour is more complicated in this case. In panel (c), there is a turning point in the MS response at $\omega_r \approx 1.6$, after which the approximation is noticeably distant from the numerical solution. In the harmonic contribution, this phenomenon manifests as a curve which appears to diverge at $\omega_r \approx 1.2$ and then reaches zero at $\omega_r \approx 1.45$.

3.4 Investigating alternative detunings

Up until this point, the consideration of detunings in analytical approximation methods has been limited to the application of the DNF detuning in the MS method. However, it is possible and enlightening to investigate this notion more generally. As such, this section will consider the implementation of arbitrary frequency detunings in both the MS and DNF methods. This section considers the equations up to ε^1-order for the sake of simplicity.

3.4.1 Direct normal form

First, it is necessary to define a general detuning that can be varied to investigate a number of scenarios. In [219], such a detuning was applied to the square of the natural frequency, as in the DNF method; i.e. $\omega_n^2 = \omega_d^2 + \delta_d$, where ω_d is the detuned frequency and δ_d is the corresponding detuning parameter. The paper concludes that, at ε^1-order, the fundamental

response found using the DNF method is independent of the choice of δ_d. This can be explained by considering the updated form of Eq. (3.35), which is now given by

$$\begin{aligned} \varepsilon^0 &: \ \mathbf{P_u r} = \mathbf{P_v r}, \\ \varepsilon^1 &: \ \ddot{\mathbf{h}}_1(\mathbf{u}, \dot{\mathbf{u}}, \mathbf{r}) + \boldsymbol{\Upsilon}_d \mathbf{h}_1(\mathbf{u}, \dot{\mathbf{u}}, \mathbf{r}) + \boldsymbol{\Gamma}_{\mathbf{v},1}(\mathbf{u}, \dot{\mathbf{u}}, \mathbf{r}) = \boldsymbol{\Gamma}_{\mathbf{u},1}(\mathbf{u}, \dot{\mathbf{u}}, \mathbf{r}), \end{aligned} \tag{3.107}$$

where $\boldsymbol{\Upsilon}_d$ takes the same form as $\boldsymbol{\Upsilon}$, but with diagonal entries $\omega_{d,k}^2$, as opposed to $\omega_{r,k}^2$. It is evident that the ε^0-order equation is the same as in the traditional application of the DNF method, so the fundamental response will be unaltered by the change in frequency detuning.

Recalling that $\ddot{\mathbf{h}}_1 = -\boldsymbol{\Lambda}\mathbf{h}_1$, it can be seen that the ε^1-order equation contains $(\boldsymbol{\Upsilon}_d - \Lambda)\mathbf{h}_1$ as one of its terms. Therefore, in this updated application, the elements of $\boldsymbol{\beta}$ are defined by

$$\beta_{k,i,\ell} = [\omega_{k,\ell}^*]^2 - \omega_{d,k}^2, \tag{3.108}$$

as opposed to $\beta_{k,i,\ell} = [\omega_{k,\ell}^*]^2 - \omega_{r,k}^2$, as in Eq. (3.40). As such, the role of the updated $\boldsymbol{\beta}$ matrix can be thought of as capturing those terms which respond at *approximately* ω_r, as opposed to *exactly*. This accounts for the fact that ω_d is within some neighbourhood of ω_r. Thus, there is a difference between the updated and classical applications of the DNF method in the ε^1-order homological equation, which may lead to a difference in the harmonic terms.

To explore this further, it is possible to apply this altered DNF method to the Duffing oscillator. In Eqs. (3.39) and (3.40), the definitions of $[\Gamma_{u,k}]$ and $[h_k]$ are dependent on whether $\beta_{k,i,\ell} = 0$. In applying the updated definition in Eq. (3.108) to the Duffing oscillator, the fundamental and harmonic vectors become

$$[\Gamma_{u,1}] = \begin{bmatrix} 0 & 3\alpha & 3\alpha & 0 \end{bmatrix}, \ [h_1] = \begin{bmatrix} \dfrac{\alpha}{9\omega_r^2 - \omega_d^2} & 0 & 0 & \dfrac{\alpha}{9\omega_r^2 - \omega_d^2} \end{bmatrix}, \tag{3.109}$$

respectively. Note that the entries of $[\Gamma_{u,1}]$ (with the damping terms now removed) remain unaltered, as predicted. However, while the fundamental response is invariant to changes in ω_d, this is not true of the harmonic response, which is now given by

$$A_3 = \frac{\alpha A^3}{4(9\omega_r^2 - \omega_d^2)}. \tag{3.110}$$

To investigate the influence of the choice of ω_d, the following parameterised frequency is introduced

$$\omega_d = \omega_r + \gamma(\omega_n - \omega_r), \tag{3.111}$$

where $\gamma \in [0, 1]$. The case $\gamma = 0$ represents the traditional DNF detuning, whereas $\gamma = 1$ leads to the case where no detuning is applied, as in the classical MS method. In Fig. 3.3, γ is varied between 0 and 1. As previously predicted, panel (a) shows no variation in the fundamental backbone curve, but it can be seen that, as γ increases, the A_3 response moves further from the true solution. It can be concluded that the DNF detuning is more accurate than any other parametrised detuning.

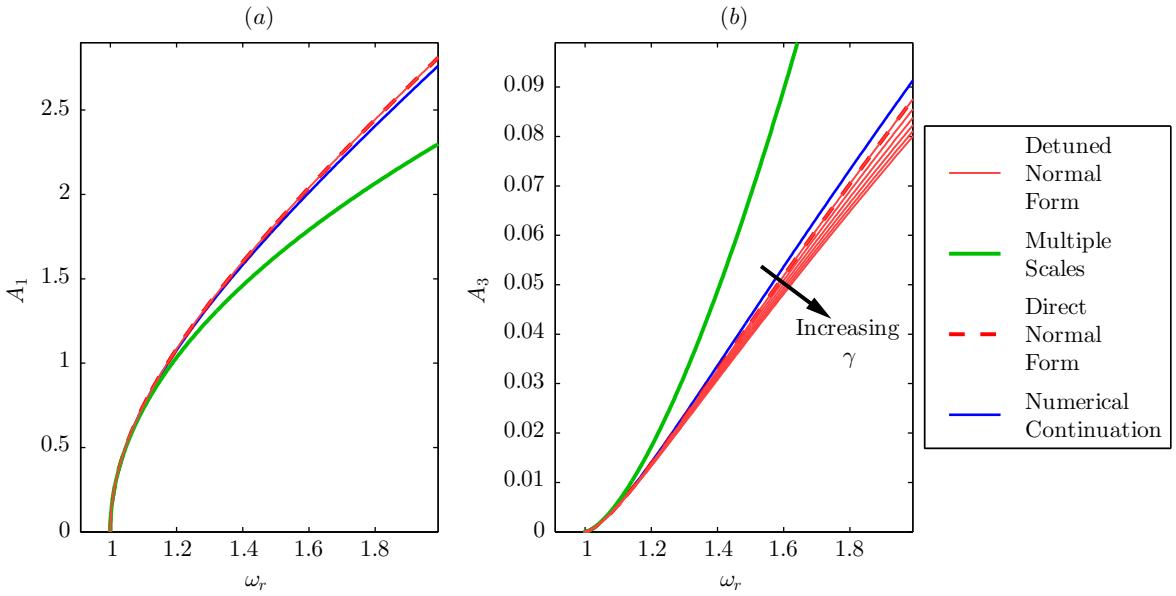

Figure 3.3: (a) Fundamental and (b) third harmonic amplitude response curves for the undamped Duffing oscillator, with variations in the DNF detuning, using $\omega_n = 1$, $\alpha = 0.5$, and $\gamma \in [0, 1]$. *This figure has been reproduced from [1].*

3.4.2 Multiple scales

Similar consideration is now given to the MS method, in which we will define the fast time as $\tau = \omega_d t$. As such, the ε-balance is now given by

$$\begin{aligned} \varepsilon^0 : &\quad \omega_d^2 x_0^{\dagger\dagger} + \omega_d^2 x_0 = 0, \\ \varepsilon^1 : &\quad \omega_d^2 x_1^{\dagger\dagger} + \omega_d^2 x_1 = \delta_d x_0 - 2\omega_n x_0^{\dagger\ddagger} - \alpha x_0^3, \\ &\vdots \end{aligned} \tag{3.112}$$

where it has been noted that $\varepsilon^i \omega_n^2 x_i = \varepsilon^i \omega_d^2 x_i + \varepsilon^{i+1} \delta_d x_i$. Further, ω_n has been removed from the slow dynamics term, $2\omega_n x_0^{\dagger\ddagger}$, through the Taylor expansion $\omega_n = \omega_d + \varepsilon \frac{\delta_d}{2\omega_d}$. Solving the ε^0-order equation now results in the trial solution $x_0 = A(T)\cos(\omega_d + \phi(T))$, which can be

implemented in the ε^1 equation to give

$$\begin{aligned} \phi^{\ddagger}(T) &= \frac{\delta_d}{2\omega_d} + \frac{3\alpha A(T)^2}{8\omega_d}, \\ A^{\ddagger}(T) &= 0, \end{aligned} \tag{3.113}$$

from which it can be deduced that

$$A(T) = A, \quad \phi(T) = \left(\frac{\delta_d}{2\omega_d} + \frac{3\alpha A^2}{8\omega_d}\right)T + \phi. \tag{3.114}$$

Implementing Eq. (3.114) in the trial solution results in the following ε^0-order expression

$$x_0 = A\cos(\omega t + \phi), \quad \text{with} \quad \omega = \omega_d + \varepsilon\left(\frac{\delta_d}{2\omega_d} + \frac{3\alpha A^2}{8\omega_d}\right). \tag{3.115}$$

At this point, one can recall that $\delta_d = \omega_n^2 - \omega_d^2$ and $\omega_d = \omega_r + \gamma(\omega_n - \omega_r)$, so that the response frequency equation is given by

$$(1-\gamma^2)\omega_r^2 + (2\omega_n\gamma^2)\omega_r - \left(\omega_n^2(1+\gamma^2) + \frac{3\alpha A}{4}\right) = 0. \tag{3.116}$$

Further, by solving the ε^1 expression, the corresponding harmonic response amplitude is given by

$$A_3 = \frac{\alpha A^3}{32\omega_d^2} = \frac{\alpha A^3}{32(\omega_r + \gamma(\omega_n - \omega_r))^2}. \tag{3.117}$$

The ε^1-order solution is now plotted, in Fig. 3.4, for a set of distributed values of $\gamma \in [0, 1]$. As predicted, it can be seen that increasing γ from 0 to 1 transforms the response from that of the DNF/dMS method to that of the classical MS technique. Although the values of γ are equally spaced, this is not true of the backbone curves, which reflects the quadratic nature of Eq. (3.116). It can be further concluded that this parameterised solution represents a continuum between the two limit cases.

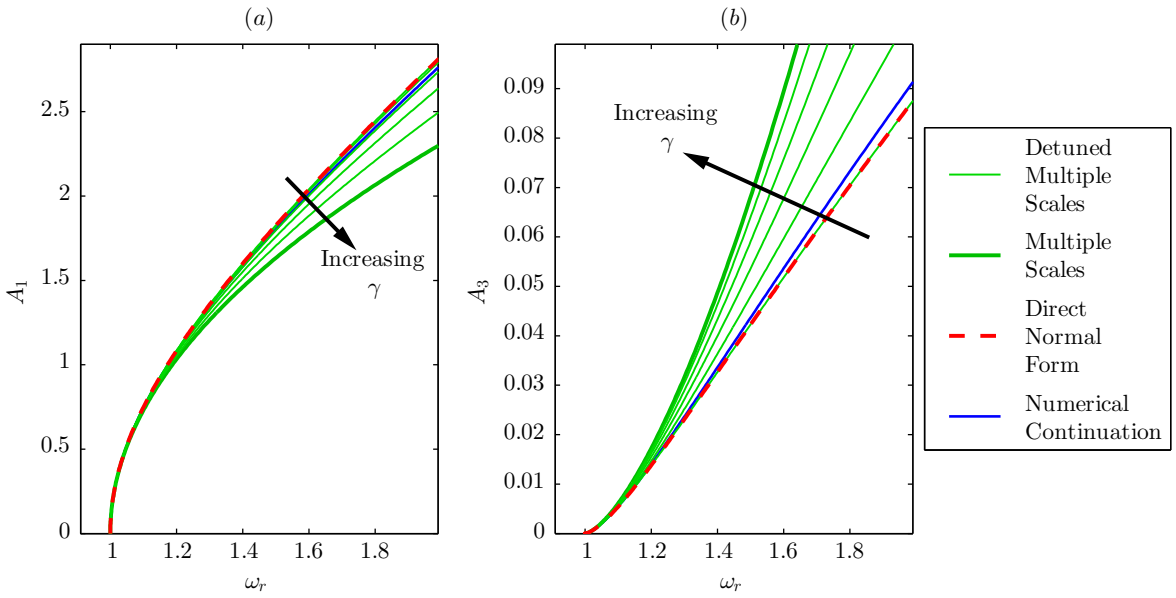

Figure 3.4: (a) Fundamental and (b) third harmonic amplitude response curves for the undamped Duffing oscillator, with variations in the MS detuning, using $\omega_n = 1$, $\alpha = 0.5$, and $\gamma \in [0, 1]$. *This figure has been reproduced from [1].*

3.5 Summary

In this chapter, the derivation and application of three analytical approximation methods have been considered. Namely, the harmonic balance, multiple scales, direct normal form methods have been applied to a general nonlinear system, before being applied to the forced, damped Duffing oscillator. To aid the comparison of these techniques, particular attention has been given to the manner in which the natural frequencies are detuned. In light of the assessment of the DNF detuning given in [136], this has been applied to the MS method, with more general detunings then being applied to both the MS and DNF techniques.

All three methods are able to produce good approximations of the numerical solution, though it has been seen that there are also limitations to each. Perhaps the strongest attribute of the HB method is its simplicity. By assuming a trial solution for the displacement and implementing this in the equations of motion, it is then only necessary to balance the coefficients of the time-dependent terms to find a solution. In fact, this step is ubiquitous across all three techniques. However, the equations found in the classical application of the HB method can include terms which are of a higher order than those in the trial solution. Therefore, it must be assumed that any components of the response that responds at a frequency different from those in the initial expression are negligible. This is shown not to be the case in the two more complex techniques. The relative size of the terms is managed through the use of a bookkeeping parameter, the coefficients of which are balanced in a similar way to

the aforementioned time-dependent terms. As well as this, the use of this parameter for the time scale allows the MS method to capture transient behaviour, a feat which is not typically achieved in the other two methods. In spite of this, the discussion of the steady-state dynamics given in this chapter reveals the disparity between the MS method and numerical solutions at higher amplitudes, which is significantly less pronounced for the DNF method. This increased accuracy after the same number of iterations occurs due to the aforementioned detuning, which is given considerable attention in this chapter.

In practice, although it is not strictly dictated in its definition, the MS method is regularly applied in conjunction with a detuning of the natural frequency. However, in this chapter, the detuning from the DNF method is introduced to remove the arbitrary nature in which this has typically been done, instead using a physically-interpretable expression – a series expansion about the square of the natural frequency – to advise this decision. With this simple change to the MS method, which only results in a minor change to the ε-balance in the method, it has been seen that the resulting free and forced responses are identical to those given by the DNF method itself. By considering a more general detuning, it has been shown that this detuning is a limit case of the accuracy for both methods.

This chapter provides agreement between the results of two prominent analytical approximation methods for nonlinear dynamical systems. Detuning techniques of the classical formulation have been developed and applied to allow the user to achieve identical results regardless of the choice of technique. This result goes some way to removing the doubt that the user may have when choosing an analytical approximation technique. It is possible to propose some potential rules-of-thumb that could be used. As has been observed in this chapter, the HB method assumes any harmonics higher than those in the trial solution are negligible, so this method can be most confidently used if the behaviour of these higher-order components are either not of interest or known to be negligible. Following the equivalence of results presented here, the MS and DNF method can effectively be used interchangeably. Thus, the user can make a decision based on the unique capabilities of each, such as the time-varying components of the MS method (which can be used for predicting time-dependent phenomena that may occur in acceleration), or the matrix formulation of the DNF technique.

Chapter 4

The Galerkin method

In this chapter:

- The Ritz-Galerkin method is introduced and applied to an Euler-Bernoulli beam.
- Particular attention is given to the way in which boundary conditions are treated and used to determine the mode shapes and natural frequencies.
- The importance of numerical accuracy in the calculation of these properties is discussed.
- Further, the influence that these attributes have on the system response, particularly in terms of the occurrence of modal interactions, is studied.
- A novel approach for defining the mode shapes and natural frequencies of beams with nonlinear boundary conditions is introduced.
- This methodology is then applied to a cantilever beam with a magnetic interaction at the tip to investigate the most appropriate way to approximate nonlinear boundary conditions.

4.1 Introduction

As seen in Chapter 3, complex dynamics can arise in even the simplest of nonlinear systems. In continuous structures, it is possible for this complexity to become even more pronounced, and the mathematical modelling required to fully capture such behaviour is a key challenge in the field. Commercial FE software can be used to address this issue, but these are typically

"black box" programmes, which do not allow the user to have total control and understanding of the way in which the nonlinear behaviour is treated. Furthermore, these commercial programmes can be computationally expensive for nonlinear structures, and their calculation in the time domain does not always allow for complete comprehension of the frequency behaviour. As such, it can be beneficial to adapt an analytical methodology for the structure, modelling the nonlinearities by considering the physical principles associated with the development of the model.

The focus of this chapter is on the Galerkin technique. This method is more thoroughly defined in the subsequent sections, but its underlying assumption (for the present application) is that a continuous function in terms of two variables can be discretised as an infinite series of products of projection functions. Each of these functions is then defined in terms of only one of the aforementioned variables. By truncating this expansion and utilising the orthogonality of the linear mode shapes, it becomes possible to express the equations of motion as a finite system of second-order differential equations.

As outlined in Chapter 2, the Galerkin approximation is particularly useful for modelling simple continuous systems, such as beams, plates, shells, and cables. Extensive consideration has been given to developing Galerkin models for these structures with a number of *classical* BCs, an expression that typically refers to clamped, pinned, free, and sliding beam tips. Further, the discussion outlined the notion of nonlinear BCs, in which the relationship is defined by a polynomial in terms of the deflection. This extends the mathematical complexity of the problem and has typically required an approximation approach to be taken. This chapter aims to address this issue and prevent such a step from being necessary.

This chapter will begin by discussing these classical BCs, allowing both the derivation and investigation of Galerkin methods to be established in §4.2. This provides a basis from which more complicated systems can be considered, allowing the introduction of non-symmetric BCs, so that the modelling of modal interactions can be investigated in §4.3. This discussion will pay particular attention to the relationship between the modal basis and the ability to predict internal resonances between modes. §4.4 briefly outlines an example of linear, non-classical BCs, so that the methodology can be expanded through the use of nonlinear algebraic techniques in §4.5. This final section proposes a methodology that can be applied to any nonlinear BC that can be approximated using a Taylor expansion, as will be demonstrated for a general spring-supported beam, and one with a magnetic BC.

Publications resulting from this work

Elliott, A. J., Cammarano, A., and Neild, S. A.. (2018). Investigating Modal Contributions Using a Galerkin Model. In *Nonlinear Dynamics, Volume 1*, Kerschen, G., ed., Conference Proceedings of the Society for Experimental Mechanics Series, 199-210.

– This paper investigates a Galerkin model for a clamped-clamped beam. As well as developing algebraic expressions for the cross-coupling terms, this study investigates the relationship between the order of the truncation and the accuracy of the solutions (discussions relating to this paper are presented in §4.2).

Elliott, A. J., Tartaruga, I., Cammarano, A., Dobson, P. S., and Neild, S. A.. (2018). Investigating reduced order models for nanoscale nonlinear structures. In *Proceedings of ISMA2018*.

– This paper applies the novel methodology derived in §4.5 as a nanoscale beam example. This example is used as the "full" model for the non-intrusive methods discussed in Chapter 5; this is due to the complex behaviour arise in systems with nonlinear BCs. It is concluded that, at this scale, the backbone curves give a close approximation for the forced response.

4.2 Overview of the Galerkin method

As this discussion has alluded to, the Galerkin method has been applied in a wide variety of systems. However, in this thesis, the primary focus will be on beam models, due to their broad application, most recently in micro- and nanoscale systems, but also in the more traditional exploration of structures such as bridges, wind turbine blades, and aeroplane wings. As such, it is necessary to begin by deriving a mathematical model for the behaviour of beams. Depending on the application, the user has the option to use either Euler-Bernoulli or Timoshenko beam theory, the key difference between them being that the latter takes into account shear deformation and rotational bending. An in-depth outline of the derivation and application of these can be found in [2, 140], for example, and a thorough discussion of their respective performance is given in [141]. Although this comparison concludes that the Timoshenko model is applicable across a wider range of systems, the Euler-Bernoulli beam theory is applicable for small deformations, as would be found in the weakly nonlinear structures considered in this thesis.

4.2.1 General beam theory

In this chapter, a general beam is considered to allow both the Euler-Bernoulli beam theory and the application of the Galerkin method to be illustrated more clearly. This beam will have length ℓ, Young's modulus E, second moment of intertia I, density ρ, and cross-sectional area $\hat{A}$. For this system, the deflection curve is given by

$$EI\frac{\partial^2 w}{\partial x^2} = -M, \tag{4.1}$$

where M is the bending moment, which is proportional to the curvature, $w(x,t)$ is the transverse displacement, which is dependent on the position along the beam x and time, t. By twice differentiating this equation with respect to x, the expression becomes

$$\begin{aligned} \frac{\partial}{\partial x}(EI\frac{\partial^2 w}{\partial x^2}) &= -\frac{\partial M}{\partial x} = -V, \\ \frac{\partial^2}{\partial x^2}(EI\frac{\partial^2 w}{\partial x^2}) &= -\frac{\partial V}{\partial x} = f, \end{aligned} \tag{4.2}$$

where V is the shearing force applied to the beam and f is a continuous load, with variable intensity along the beam. This force will be defined by

$$f = -\rho\hat{A}\frac{\partial^2 w}{\partial t^2}. \tag{4.3}$$

Applying f in Eq. (4.2) gives the general equation for transverse vibration:

$$EI\frac{\partial^4 w}{\partial x^4} + \rho\hat{A}\frac{\partial^2 w}{\partial t^2} = 0. \tag{4.4}$$

Alternatively, by introducing the parameter a, it is possible to rearrange this system as

$$\frac{\partial^2 w}{\partial t^2} + a^2\frac{\partial^4 w}{\partial x^4} = 0, \quad \text{where} \quad a^2 = \frac{EI}{\rho\hat{A}}. \tag{4.5}$$

4.2.2 Galerkin approximation

In the Galerkin method, it is further assumed that the transverse displacement can be expressed as a series of functions with distinct spacial and temporal parts, writing

$$w(x,t) = \sum_{j=1}^{\infty} \phi_j(x)q_j(t), \tag{4.6}$$

where $\phi_j(x)$ are the linear mode shapes of the system and $q_j(t)$ denotes the contribution of ϕ_j to the physical displacement; these modal coordinates are time-dependent and capture the periodic nature of the response. As such, they can be written in the form

$$q_j(t) = A\cos(p_j t) + B\sin(p_j t), \tag{4.7}$$

where p_j are constants that depend on the BCs; values for these are typically found numerically. Applying an arbitrary mode shape, $\phi(x)$, and the harmonic form in Eq. (4.7) allows the system equations of motion to be written as

$$\frac{d^4\phi}{dx^4} - \frac{p_j^2}{a^2}\phi = \frac{d^4\phi}{dx^4} - \kappa^4\phi = 0, \tag{4.8}$$

where the variable κ has been introduced so that $\sin(\kappa x)$, $\cos(\kappa x)$, $\sinh(\kappa x)$, and $\cosh(\kappa x)$ are particular solutions to Eq. (4.8), with

$$\kappa = \frac{p_j^2}{a^2} = \sqrt[4]{\frac{p_j^2\rho\hat{A}}{EI}}. \tag{4.9}$$

Now, the general solution to Eq. (4.8) allows the j^{th} mode shape to be written as

$$\phi(y) = c_1\cos(\kappa y) + c_2\sin(\kappa y) + c_3\cosh(\kappa y) + c_4\sinh(\kappa y). \tag{4.10}$$

Therefore, to find the mode shapes, it is simply necessary to apply the BCs and solve for the constants, c_n.

4.2.3 Constrained beam considerations

Up until this point, the derivation has been independent of the BCs used. In this section, it will be demonstrated that those supports which constrain the beam – and, therefore, cause the beam to stretch – can actually introduce an additional term to the equations of motion, which is associated with the geometric nonlinearity of the system. In constrained beams, if the deflection is great enough, the stretching of the beam leads to a non-negligible change in its geometry. Associated with this is an alteration of the vibration characteristics, particularly in terms of the natural frequencies. This also introduces a tension force, T, in the equations of motion, where it had previously been assumed that such a force would be negligible. The process of finding T begins with the consideration of a small length of beam, denoted Δs,

which can be approximated by

$$\Delta s \approx \sqrt{\Delta x^2 + \Delta w^2} \rightsquigarrow \frac{\partial s}{\partial x} = \sqrt{1 + \left(\frac{\partial w}{\partial x}\right)^2}. \tag{4.11}$$

Thus, the stretched beam length, L, is approximated by

$$L = \int_0^\ell \frac{\partial s}{\partial x} \mathrm{d}x = \int_0^\ell \sqrt{1 + \left(\frac{\partial w}{\partial x}\right)^2} \mathrm{d}x. \tag{4.12}$$

By invoking the small deflection assumption, it is possible to apply a Taylor expansion to the square root, so that Eq. (4.12) can be expressed as

$$L \approx \int_0^\ell 1 + \frac{1}{2}\left(\frac{\partial w}{\partial x}\right)^2 \mathrm{d}x = \ell + \frac{1}{2}\int_0^\ell \left(\frac{\partial w}{\partial x}\right)^2 \mathrm{d}x. \tag{4.13}$$

Therefore, the change in length can be written as

$$L - \ell = \frac{1}{2}\int_0^\ell \left(\frac{\partial w}{\partial x}\right)^2 \mathrm{d}x. \tag{4.14}$$

Now that a solution for $(L-\ell)$ has been obtained, it can be applied directly in the calculation of the tension, T:

$$T = E\hat{A}\frac{(L-\ell)}{\ell} = \frac{E\hat{A}}{2\ell}\int_0^\ell \left(\frac{\partial w}{\partial x}\right)^2 \mathrm{d}x. \tag{4.15}$$

Further details on this are given in [9]. The tension force arises due to the updated form of $\frac{\partial^2 M}{\partial x^2}$ (see Eq. (4.2)), which is now given by

$$\frac{\partial^2 M}{\partial x^2} = F_z - P\frac{\partial^2 w}{\partial x^2}. \tag{4.16}$$

Here, P is the compressive loading of the beam at the BCs, given by $P = -T\cos(\psi(0))$, where $\psi(x)$ is the rotation at point x. As such, this term can be approximated by $P = -T$ for relatively small deflections. Further, F_z is used to denote the combined external and internal forces, which are now expressed as

$$F_z = -\rho\hat{A}\frac{\partial^2 w}{\partial t^2} + f_{\text{ext}}, \tag{4.17}$$

where f_{ext} denotes an external force. Recalling that $M = \frac{\partial^2 w}{\partial x^2}$ and applying this in Eq. (4.16), the equation of motion may now be written as

$$EI\frac{\partial^4 w}{\partial x^4} + \rho\hat{A}\frac{\partial^2 w}{\partial t^2} - \frac{E\hat{A}}{2\ell}\int_0^\ell \left(\frac{\partial w}{\partial x}\right)^2 \mathrm{d}x\left(\frac{\partial^2 w}{\partial x^2}\right) = 0. \tag{4.18}$$

Comparing Eq. (4.18) with the expression in Eq. (4.4), it is possible to note that the third term of Eq. (4.18) arises as a direct consequence of the constrained BCs and associated geometric nonlinearities. Applying the Galerkin decomposition from Eq. (4.6), this system can be rewritten as

$$EI\sum_{j=1}^{\infty}\frac{d^4\phi_j}{dx^4}q_j + \rho\hat{A}\sum_{j=1}^{\infty}\phi_j\ddot{q}_j - \frac{E\hat{A}}{2\ell}\sum_{j=1}^{\infty}\sum_{i=1}^{\infty}\sum_{k=1}^{\infty}\int_0^\ell \frac{d\phi_i}{dx}\frac{d\phi_k}{dx}\mathrm{d}x\left(\frac{d^2\phi_j}{dx^2}\right)q_i q_j q_k = 0, \tag{4.19}$$

where $\ddot{\bullet}$ denotes the second derivative with respect to t. To simplify this equation, one can make use of the orthogonality of the mode shapes. By multiplying this equation by an arbitrary mode shape, ϕ_n, and integrating across the beam length, the system can be written as

$$\begin{aligned} EI\sum_{j=1}^{\infty}\int_0^\ell \frac{d^4\phi_j}{dx^4}\phi_n \mathrm{d}x q_j + \rho\hat{A}\sum_{j=1}^{\infty}\int_0^\ell \phi_j\phi_n\mathrm{d}x\ddot{q}_j \\ - \frac{E\hat{A}}{2\ell}\sum_{j=1}^{\infty}\int_0^\ell\left[\sum_{i=1}^{\infty}\sum_{k=1}^{\infty}\left(\int_0^\ell \frac{d\phi_i}{dx}\frac{d\phi_k}{dx}\mathrm{d}x q_i q_k\right)\left(\frac{d^2\phi_j}{dx^2}\right)q_j\phi_n\right]\mathrm{d}x = 0. \end{aligned} \tag{4.20}$$

By considering the various integrals in Eq. (4.20) separately, it is possible to decouple the system, so that the equation for the n^{th} modal coordinate is given by

$$\ddot{q}_n + \frac{EI\alpha_{4,n}}{\rho\hat{A}\ell}q_n + \frac{E\alpha_{2,j}}{2\rho\ell^2}\sum_{i=1}^{N}\sum_{j=1}^{N}\sum_{k=1}^{N}\alpha_{2,k,n}\beta_{i,j}q_i q_j q_k = 0, \tag{4.21}$$

where N is the order of the truncated model. The α and β terms are defined as follows

$$\begin{aligned}
&\int_0^\ell \phi_n \phi_j \mathrm{d}x = \begin{cases} \ell, & \text{if } n = j, \\ 0, & \text{otherwise,} \end{cases} \\
&\int_0^\ell \phi_n \frac{d^2\phi_j}{dx^2} \mathrm{d}x = \alpha_{2,n,j}, \\
&\int_0^\ell \phi_n \frac{d^4\phi_j}{dx^4} \mathrm{d}x = \begin{cases} \alpha_{4,j}, & \text{if } n = k, \\ 0, & \text{otherwise,} \end{cases} \\
&\int_0^\ell \frac{d\phi_i}{dx} \frac{d\phi_j}{dx} \mathrm{d}x = \beta_{i,j}.
\end{aligned} \tag{4.22}$$

Therefore, once the mode shapes have been found, it is possible to define the dynamics of the system in terms of a set of N equations in modal coordinates.

4.2.4 Example: clamped-clamped beam

Initially, the Galerkin methodology will be demonstrated for a relatively simple clamped-clamped beam (as displayed in Fig. 4.1), a structure which has been widely used across the literature and, more recently, for M/NEMS. Returning to Eq. (4.10), it is now possible to apply the BCs associated with this structure. These are given by

$$\phi(0) = 0, \quad \phi'(0) = 0, \quad \phi(\ell) = 0, \quad \phi'(\ell) = 0. \tag{4.23}$$

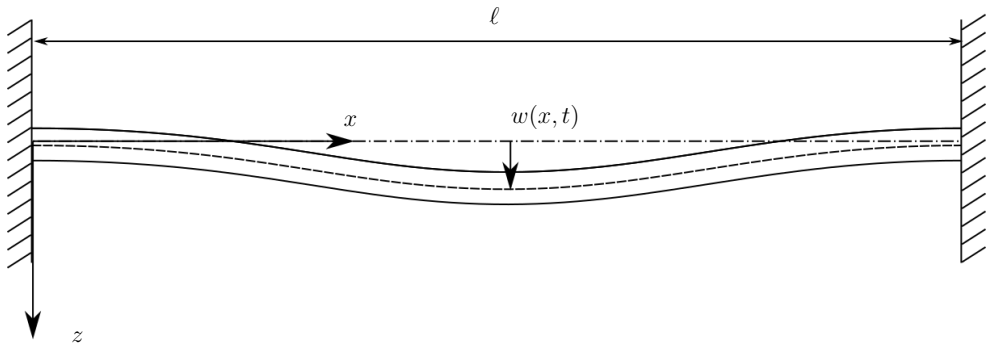

Figure 4.1: A diagram of a clamped-clamped beam. The physical coordinates x, z are defined; it is assumed that the beam only deflects in this plane.

By applying the first two conditions in Eq. (4.10), it can be noted that $c_3 = -c_1$ and $c_4 = -c_2$. As such, it is possible to express the mode shape, ϕ, as

$$\phi(y) = c_1\big[\cos(\kappa y) - \cosh(\kappa y)\big] + c_2\big[\sin(\kappa y) - \sinh(\kappa y)\big]. \tag{4.24}$$

Implementing this updated mode shape in the two remaining BCs, it is now possible to write

$$\phi(\ell) \ = c_1\big[\cos(\kappa\ell) - \cosh(\kappa\ell)\big] + c_2\big[\sin(\kappa\ell) - \sinh(\kappa\ell)\big] = 0, \tag{4.25}$$

$$\phi'(\ell) = -c_1\big[\sin(\kappa\ell) + \sinh(\kappa\ell)\big] + c_2\big[\cos(\kappa\ell) - \cosh(\kappa\ell)\big] = 0. \tag{4.26}$$

From either of these equations, it is now possible to express c_2 in terms of c_1. Choosing Eq. (4.26), this is given by

$$c_2 = c_1\frac{\sin(\kappa\ell) + \sinh(\kappa\ell)}{\cos(\kappa\ell) - \cosh(\kappa\ell)}. \tag{4.27}$$

This solution for c_2 can be applied in Eq. (4.25) to give the transcendental equation

$$\cos(\kappa\ell)\cosh(\kappa\ell) = 1. \tag{4.28}$$

This equation can now be solved numerically to find values of $\kappa\ell$ that correspond to mode shapes of the structure.

4.2.4.1 A note on numerical precision

The solution of Eq. (4.28) introduces an interesting discussion regarding the numerical accuracy with which it should be solved. In [2], these values are given to 8 decimal places for the first five modes, with the approximation $\kappa\ell \approx \frac{2k+1}{2}\pi$ for modes $k > 5$. The rational term in Eq. (4.27) is also numerically approximated at this level. These values are implemented in the clamped-clamped beam in Fig. 4.2. It can be seen, for modes 7 and 9, that $\phi(\ell) \neq 0$, even though this condition was explicitly imposed.

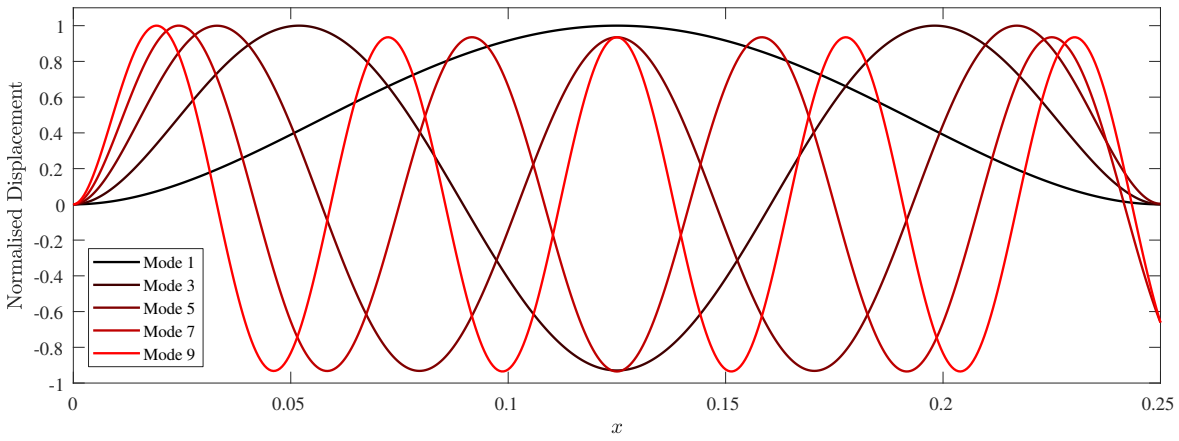

Figure 4.2: The first five symmetric mode shapes for the clamped-clamped beam, as found using the numerical values in [2].

Further investigation into this artefact is given in Fig. 4.3. Here, instead of the erroneous approximation of κ for modes $k > 5$, a numerical solution is used for all modes. As can be seen, focus is shifted solely to the relationship between the precision of numerical approximation and the accuracy with which the BC is captured. When 5 decimal places are used, the BC is approximately the same as that for the aforementioned approximation. There is a substantial increase in the accuracy once this is increased to 10 decimal places, with the true behaviour being captured once 15 are used. Note that the level of accuracy required is dependent on the mode shape under consideration, a point which is accounted for in the remainder of this thesis.

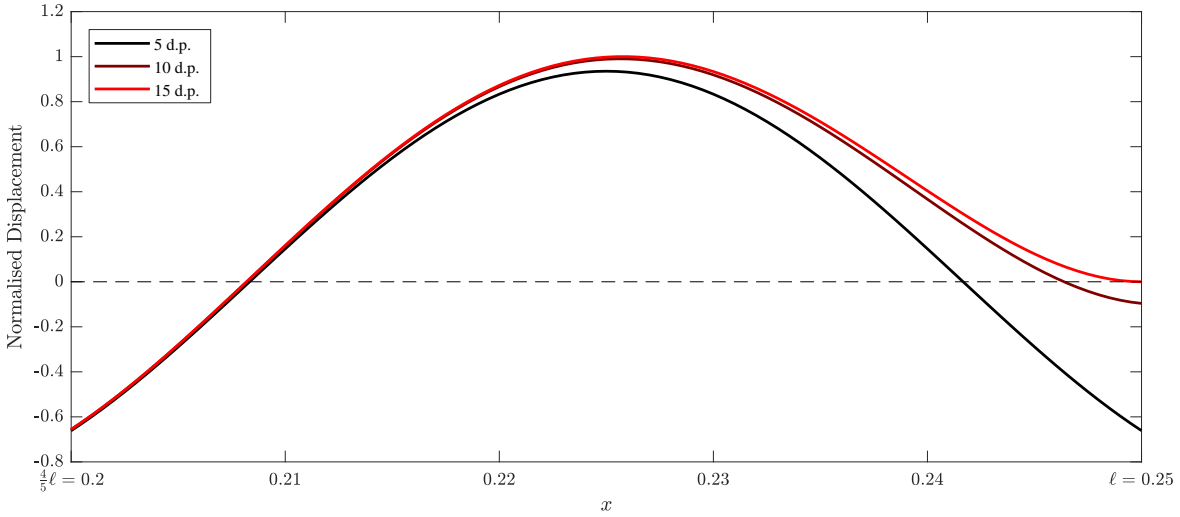

Figure 4.3: Variations in the numerical precision used to derive the seventh mode shape of the clamped-clamped beam. This figure displays the right-hand end of the beam.

4.2.4.2 Backbone curves and forced responses

Throughout this section, to allow numerical results to be generated, the following parameters will be assigned: $\ell = 0.25$ m, $E = 193$ GPa, $I = 10^{-11}$ m^4, $\rho = 8000$ kg/m^3, and $I = 3 \times 10^{-5}$ m^2. Applying these values, it is possible to obtain the first backbone curve, and related forced responses, of the system, given in Fig. 4.4; this is achieved through the numerical continuation of the appropriate equations of motion. It can be seen that the clamped-clamped beam exhibits a distinct hardening behaviour, caused by the stretching of the beam that is induced by the constraining of the BCs. This type of behaviour has already been seen Fig. 3.1, and is common in nonlinear structures. In the following section, a more complex nonlinear system is introduced, so that more complicated behavioural phenomena can be investigated.

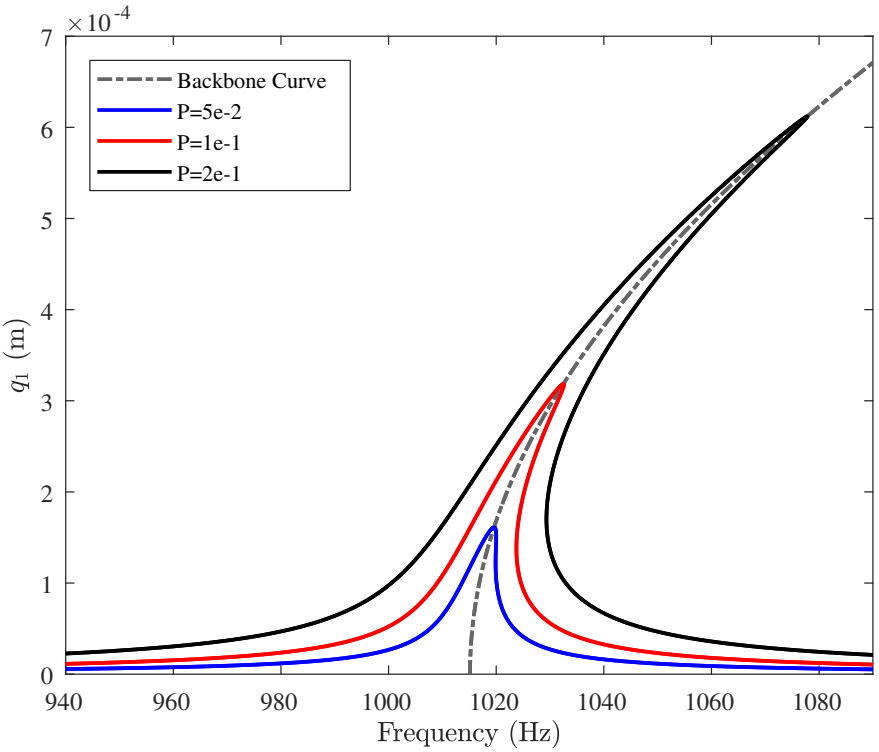

Figure 4.4: Backbone curve and a number of forced responses for the clamped-clamped beam, found using the Galerkin method.

4.3 Investigating modal interactions

4.3.1 Example: pinned-pinned beam with rotational spring

The clamped-clamped beam in the previous section provides an insight into the hysteretic nature of nonlinear systems, though further interesting, and potentially damaging, behaviour can be exhibited if the symmetry of the system is broken. To investigate this, the boundary conditions of the beam are changed. At both ends, the beam will rest upon pinned supports, so that the displacement is fixed, but the rotation is not. To break the symmetry, a rotational spring of stiffness $\hat{k}$ is added at the right-hand end. The schematic for this system is shown in Fig. 4.5.

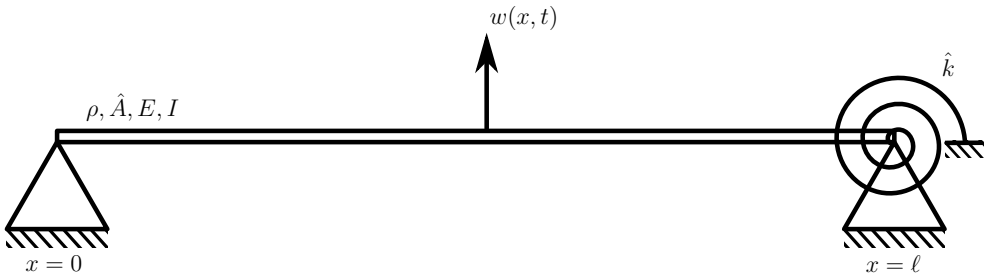

Figure 4.5: Schematic for a pinned-pinned beam with rotational spring at the right-hand tip.

This system has been more thoroughly derived in [159], and the approach taken in that paper

is summarised here. The equations of motion are now defined by

$$\rho\hat{A}\frac{\partial^2 w}{\partial t^2} + EI\frac{\partial^4 w}{\partial x^4} - \left[\frac{E\hat{A}}{2L}\int_0^\ell \left(\frac{\partial w}{\partial x}\right)^2 \mathrm{d}x\right]\frac{\partial^2 w}{\partial x^2} + \delta(x-\ell)\hat{k}\psi(\ell,t) = 0, \tag{4.29}$$

where $\psi(x,t)$ denotes the rotation of the beam and $\delta(\bullet)$ is the Dirac delta function, used here to represent the fact that there is only a spring at the tip. The spring stiffness, and associated asymmetry, can be incorporated into the mode shapes of the system, so that the i^{th} mode is defined by

$$\phi_i(x) = \sqrt{\frac{2}{1 - \frac{2EI}{\hat{k}\ell}\sin^2(\kappa\ell) - \left(\frac{\sin(\kappa\ell)}{\sinh(\kappa\ell)}\right)^2}}\left(\sin(\kappa x) - \frac{\sin(\kappa\ell)}{\sinh(\kappa\ell)}\sinh(\kappa x)\right). \tag{4.30}$$

This result is taken directly from [159], which also defines the solvability condition for κ, given by

$$\cot(\kappa) - \coth(\kappa) + \frac{2EI\kappa}{\hat{k}} = 0. \tag{4.31}$$

By projecting the system onto these mode shapes and applying the Galerkin approximation, the equations of motion in Eq. (4.30) can be written, in modal coordinates, as

$$\ddot{q}_n + \frac{EI\alpha_{4,n}}{\rho\hat{A}\ell}q_n + \frac{E}{2\rho\ell^2}\sum_{i=1}^{N}\sum_{j=1}^{N}\sum_{k=1}^{N}\beta_{i,j}\alpha_{2,k,n}q_i q_j q_k = 0, \tag{4.32}$$

where $\alpha_{4,n}$ has been updated to include the linear stiffness provided by the spring. As in the previous case, the terms denoted α and β are nonlinear coefficients that can be found by integrating products of mode shapes and their respective derivatives. Depending on the number of equations included in the model, N, these equations can now easily be solved either by the analytical methods discussed in Chapter 3 or via numerical continuation. The latter has been used to create the backbone curves in Fig. 4.6.

In [159], a two-mode model is used and a 1:3 internal resonance is observed, in which energy is transferred from the first to the second mode. In Fig. 4.6, an expanded modal basis is used and it can be seen that, as ω_r approaches 155 Hz, energy is actually transferred to the third and fourth mode. However, it should be noted that energy transfer to the former is relatively minimal.

This interaction between the modes is a behaviour that is not exhibited by the clamped-clamped beam, as seen in Fig. 4.4. Although not shown here, this absence of internal res-

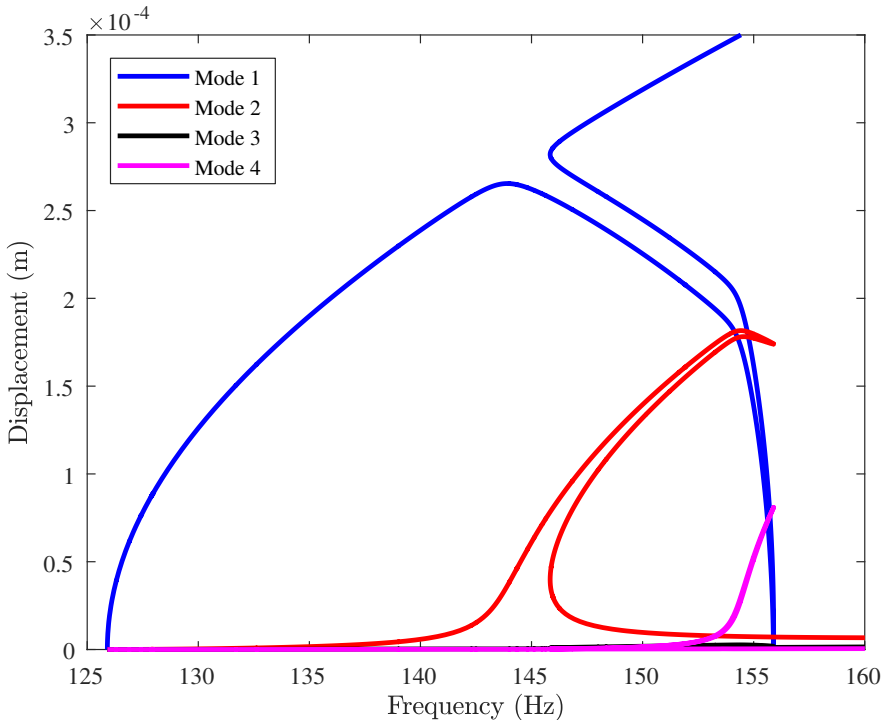

Figure 4.6: Modal contributions of the first four modes in the first backbone curve.

onance is also the case for the pinned-pinned beam without the rotational spring (see [9], for example). It is, therefore, possible to conclude that such an interaction is caused by the introduction of the symmetry-breaking, rotational spring. Further confirmation of this has been found by considering a pinned-pinned beam with identical rotational springs at both ends, which also shows no sign of such an interaction; due to this response and that of the clamped-clamped beam, it is not shown here.

Given that the only difference in these models is the BCs, it is the terms of Eqs. (4.21) and (4.32) defined by these expressions that must be investigated. Here, it should be noted that

$$\frac{EI\alpha_{4,n}}{\rho\hat{A}L} = \omega_n^2. \tag{4.33}$$

The only remaining terms to be considered are the nonlinear coupling terms and, in particular, the α_2 and β parameters by which these are defined. The values of $\alpha_{2,i,j}$ and $\beta_{i,j}$ are given in Tables 4.1 and 4.2 for the coupling between the first five modes in the pinned-pinned model, both with and without the rotational spring.

Since the only difference between these systems is the addition of the spring, the nature of these matrices offers some enlightening insight. This is summarised as follows:

- Although the order of the α_2 coefficients are consistent between the two systems, there

Table 4.1: Parameter values for $\alpha_{2,i,j}$ for $i, j \in \{1, 2, 3, 4, 5\}$.

Pinned-pinned				
8.8877E+09	-3.3059E+09	-2.9327E+09	-2.5354E+09	-2.2060E+09
-3.3059E+09	3.3116E+10	-6.0361E+09	-5.9017E+09	-5.5322E+09
-2.9325E+09	-6.0365E+09	7.2597E+10	-8.6215E+09	-8.7148E+09
-2.5354E+09	-5.9017E+09	-8.6209E+09	1.2732E+11	-1.1143E+10
-2.2060E+09	-5.5322E+09	-8.7155E+09	-1.1143E+10	1.9728E+11
Pinned-pinned with spring				
1.5183E+09	2.6873E+09	3.1945E+09	2.7973E+09	1.3608E+09
2.9764E+10	4.0117E+10	2.3824E+10	1.0268E+10	4.4290E+10
2.2281E+10	1.7504E+10	8.0044E+09	2.3590E+10	1.4446E+10
3.0198E+10	2.6464E+09	3.0099E+10	5.4013E+09	2.9842E+10
3.6546E+10	2.7304E+10	3.2184E+10	3.9700E+10	2.7516E+10

Table 4.2: Parameter values for $\beta_{i,j}$ for $i, j \in \{1, 2, 3, 4, 5\}$.

Pinned-pinned				
4.6050E+01	-1.7129E+01	-1.5195E+01	-1.3137E+01	-1.1430E+01
-1.7129E+01	1.7159E+02	-3.1276E+01	-3.0578E+01	-2.8664E+01
-1.5195E+01	-3.1276E+01	3.7615E+02	-4.4668E+01	-4.5158E+01
-1.3137E+01	-3.0578E+01	-4.4668E+01	6.5967E+02	-5.7735E+01
-1.1430E+01	-2.8664E+01	-4.5158E+01	-5.7735E+01	1.0222E+03
Pinned-pinned with spring				
2.6216E+04	4.5241E+04	3.4668E+04	-1.8453E+04	-1.6901E+05
4.5241E+04	7.8698E+04	6.0091E+04	-3.2040E+04	-2.9316E+05
3.4668E+04	6.0091E+04	4.6125E+04	-2.4564E+04	-2.2437E+05
-1.8453E+04	-3.2040E+04	-2.4564E+04	1.3155E+04	1.1940E+05
-1.6901E+05	-2.9316E+05	-2.2437E+05	1.1940E+05	1.0937E+06

are differences in their signs. In particular, in the no-spring system, only the lead diagonal terms are positive and the others are negative. In the spring case, all of the terms are positive.

- Furthermore, for each i, it is true that $\max_j\{|\alpha_{2,i,j}|\} = \alpha_{2,i,i}$ in the classical model, but this is not necessarily the case once the spring is added.

- The pinned-pinned α_2 matrix is symmetric, but the spring removes this symmetry.

- For the β matrix, there is a noticeable difference in the order of the terms, of the magnitude $10^2 - 10^4$.

- Once more, the only positive terms are on the lead diagonal for the pinned-pinned beam, but this is not true of the spring case.

The equivalent terms for the clamped-clamped beam are not given, though all of the properties of the pinned-pinned model listed here remain true for that case. As previously men-

Table 4.3: Linear natural frequencies for the clamped-clamped, pinned-pinned, and pinned-pinned with rotational spring beam configurations.

Mode	C-C	$\omega_{n,k}/\omega_{n,1}$	P-P	$\omega_{n,k}/\omega_{n,1}$	P-P w/ spring	$\omega_{n,k}/\omega_{n,1}$
1	1015.1	1	699.6	1	977.0	1
2	2798.3	2.757	2267.0	3.241	3246.8	3.323
3	5485.7	5.404	4730.0	6.761	6470.8	6.623
4	9068.1	8.933	8088.5	11.653	10557.9	10.806

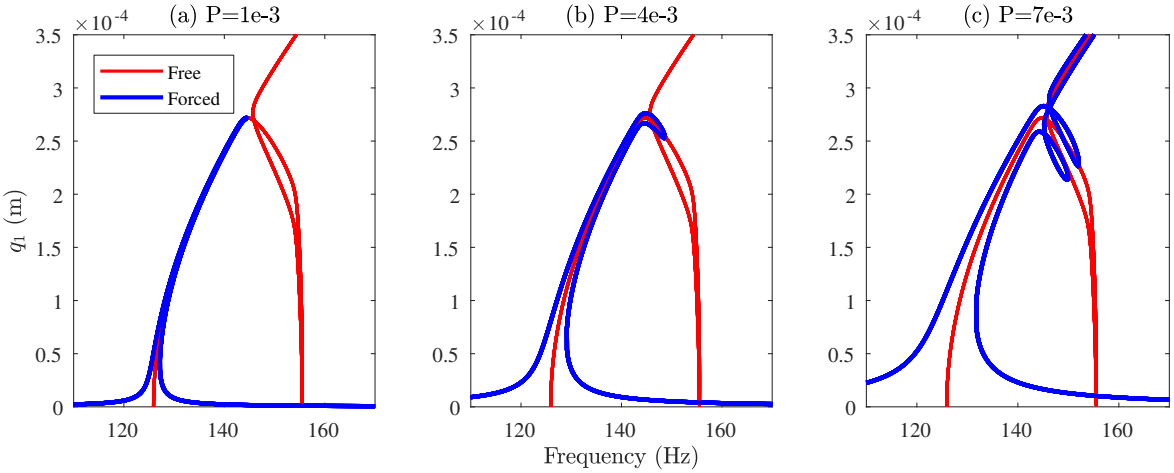

Figure 4.7: Forced responses for three forcing cases.

tioned, it is a 1:3 internal resonance in the spring beam, so the response frequency of the second mode is approximately three times that of the first. In fact, as shown in Table 4.3, $\omega_{n,2}$ is slightly greater than $3\omega_{n,1}$ for both pinned configurations, and there is minimal difference between the extent to which this is the case. As such, this highlights the importance of the nonlinear coupling coefficients, as discussed above.

The influence of the modal interaction on the forced response is presented in Fig. 4.7. The forcing levels, P, are varied and displayed in the figure, and the damping level across all three cases is $\zeta =$ 1e-3. The forcing in panel (b) is four times that in panel (a), but it can be seen that the maximum value of q_1 is only fractionally greater. This suggests that, for this beam, the internal resonance introduces some limiting behaviour in the modal displacement, so that the amount of energy required to reach the higher amplitudes of the fundamental tongue is greater than in the symmetric case with no rotational spring.

4.4 Linear, non-classical boundary conditions

4.4.1 Example: cantilever beam with linear compression spring support

In this section, the procedure for finding the natural frequencies and mode shapes of a cantilever beam supported by a linear spring (with spring constant $\hat{k}$) at the tip, as defined in [155], is recapped. This is necessary as it provides a useful starting point for the formulation of beams with nonlinear BCs, as will be shown in Section 4.5.

The clamped end of this beam retains the classical BCs, given by

$$\phi(0) = \phi'(0) = 0. \tag{4.34}$$

Applying these conditions allows Eq. (4.10) to be written in the form

$$\phi(y) = c_1(\cos(\kappa y) - \cosh(\kappa y) + \sin(\kappa y) - \sinh(\kappa y)) + 2c_2(\sin(\kappa y) - \sinh(\kappa y)) \tag{4.35}$$

For the linear spring support, the BCs are

$$\phi''(L) = 0, \quad \phi'''(L) = f = \hat{K}_L\phi(L), \text{ where } \quad \hat{K}_L = \frac{k_L L^3}{EI}. \tag{4.36}$$

Here, $\hat{K}_L$ is the non-dimensionalised linear spring constant. Defining ϕ as in Eq. (4.35), the tip BCs can be written as

$$\begin{aligned}
&(\cos(\kappa) + \sin(\kappa) + \cosh(\kappa) + \sinh(\kappa))c_1 + 2(\sin(\kappa) + \sinh(\kappa))c_2 = 0,\\
&(\kappa^3[-\cos(\kappa) - \cosh(\kappa)\sin(\kappa) - \sinh(\kappa)]\\
&\quad + \hat{K}_L[-\cos(\kappa) + \cosh(\kappa) - \sin(\kappa) + \sinh(\kappa)])c_1\\
&\quad - 2(\kappa^3[\cos(\kappa) + \cosh(\kappa)] + \hat{K}_L[\sin(\kappa) - \sinh(\kappa)])c_2 = 0.
\end{aligned} \tag{4.37}$$

Both of these equations are linear expressions in terms of $\mathbf{c} = [c_1, c_2]^T$, so it is possible to express this system as

$$\mathbf{Ac} = \begin{bmatrix} a_{11} & a_{12} \\ a_{21} & a_{22} \end{bmatrix} \begin{bmatrix} c_1 \\ c_2 \end{bmatrix} = \begin{bmatrix} 0 \\ 0 \end{bmatrix}, \tag{4.38}$$

where $\mathbf{A}$ is defined by the coefficients in Eq. (4.37); for instance, $a_{11} = (\cos(\kappa) + \sin(\kappa) +$

$\cosh(\kappa) + \sinh(\kappa)$). The system has non-trivial solutions if, and only if,

$$\det \mathbf{A} = 0. \tag{4.39}$$

This equation is defined solely in terms of κ, so it can be solved numerically to define the natural frequencies and mode shapes. The results of doing so are given in [155].

4.5 Nonlinear, non-classical boundary conditions

The final section of this chapter investigates the behaviour of beam configurations in which the BCs can not be expressed in terms of a linear function of the displacement and its derivatives. Boundary conditions such as these have a number of practical applications at the microscale, such as in non-contact atomic force microscopy. In addition, attention will be given to the influence these have on the natural frequencies and mode shapes of such a beam, as well as the possible issues that could arise if the linear mode shapes are used. BCs of this type can be found in systems with magnetic interactions at the tip, beams supported by springs with nonlinear stiffness, and in M/NEMS, as will be discussed in subsequent chapters.

The methodology proposed here is developed for a beam with two nonlinear BCs. In reality, it is perhaps more likely that one of them will be linear (clamped or pinned), but the general case is considered first to demonstrate the applicability of the technique. The BCs for this beam can be written as

$$\phi''(0) = \phi''(\ell) = 0, \quad \phi'''(0) = f_0(\phi(0)), \quad \phi'''(\ell) = f_\ell(\phi(\ell)), \tag{4.40}$$

where f_0 and f_ℓ are the functions defined by the nonlinear BCs. In the proposed technique, it is necessary to apply a Taylor expansion to both f_0 and f_ℓ. If these are assumed to be truncated at order N_0 and N_ℓ, respectively, then the only requirements on these functions are that $f_0 \in C^{N_0}$ and $f_\ell \in C^{N_\ell}$. Applying these Taylor expansions, it is possible to rewrite the BCs in Eq. (4.40) as

$$\phi''(0) = \phi''(\ell) = 0, \quad \phi'''(0) = \sum_{m=0}^{N_0} \mu_{0,m}\phi(0)^m, \quad \phi'''(\ell) = \sum_{n=0}^{N_\ell} \mu_{\ell,n}\phi(\ell)^n, \tag{4.41}$$

where $\mu_{0,m}$ and $\mu_{\ell,m}$ denote the coefficients that arise in the respective Taylor expansions of f_0 and f_ℓ. By implementing the general form given in Eq. (4.10), the first two equalities in

Eq. (4.41) can be written as

$$\begin{aligned}&\kappa^2(c_3 - c_1) = 0,\\ &\kappa^2(c_3\cosh(\kappa) - c_1\cos(\kappa) + c_4\sinh(\kappa) - c_2\sin(\kappa)) = 0.\end{aligned} \tag{4.42}$$

Thus, the expressions for c_3 and c_4 are given by:

$$\begin{aligned}&c_3 = c_1,\\ &c_4 = \frac{c_1(\cos(\kappa) - \cosh(\kappa)) + c_2\sin(\kappa)}{\sinh(\kappa)}.\end{aligned} \tag{4.43}$$

These expressions can be used to define $\phi(y)$ using only κ, c_1, and c_2, so that it is given by

$$\begin{aligned}\phi(y) = c_1&\left[\cos(\kappa y) + \cosh(\kappa y) + \frac{\cos(\kappa) - \cosh(\kappa)}{\sinh(\kappa)}\sinh(\kappa y)\right]\\ &+ c_2\left[\sin(\kappa y) + \frac{\sin(\kappa)}{\sinh(\kappa)}\sinh(\kappa y)\right].\end{aligned} \tag{4.44}$$

By representing the mode shape functions in this way, it is possible to massively simplify the polynomial series terms in Eq. (4.41), since the displacements at the boundaries can now be given by

$$\phi(0) = 2c_1, \quad \phi(\ell) = 2(c_1\cos(\kappa) + c_2\sin(\kappa)). \tag{4.45}$$

Further simplification is possible as the third derivatives can be written as

$$\begin{aligned}\phi'''(0) &= \kappa^3\left[c_1\frac{\cos(\kappa) - \cosh(\kappa)}{\sinh(\kappa)} + c_2\frac{\sin(\kappa) - \sinh(\kappa)}{\sinh(\kappa)}\right],\\ \phi'''(\ell) &= \kappa^3\left[c_1\left(\frac{(\cos(\kappa) - \cosh(\kappa)\cosh(\kappa))}{\sinh(\kappa)} + (\sin(\kappa) + \sinh(\kappa))\right)\right.\\ &\qquad\left. + c_2\left(\frac{\sin(\kappa)}{\tanh(\kappa)} - \cos(\kappa)\right)\right].\end{aligned} \tag{4.46}$$

Here, it is possible to note that these expressions take the form $\lambda^1_{\text{BC}}(\kappa)c_1 + \lambda^2_{\text{BC}}(\kappa)c_2$. Therefore, their contributions to the polynomial BCs will be linear and the full equations will be given by

$$\begin{aligned}x = 0: \quad &\lambda^1_0 c_1 + \lambda^2_0 c_2 = \sum_{m=0}^{N_0}\left[\sum_{k_1+k_2=m}\mu_0^{k_1k_2}c_1^{k_1}c_2^{k_2}\right],\\ x = \ell: \quad &\lambda^1_\ell c_1 + \lambda^2_\ell c_2 = \sum_{n=0}^{N_\ell}\left[\sum_{k_1+k_2=n}\mu_\ell^{k_1k_2}c_1^{k_1}c_2^{k_2}\right],\end{aligned} \tag{4.47}$$

where the notation $\mu_{\text{BC}}^{k_1k_2} = \mu_{\text{BC},k_1}$ has been used. The coefficients λ_{BC} are equivalent to the coefficients of c_1 and c_2 in Eq. (4.46). The expressions in Eq. (4.47) correspond to the linear conditions in Eq. (4.38), though tensors are now required, as opposed to matrices. Similarly to the linear case, it is useful to rewrite these equalities in the form $f(c_1, c_2) = 0$. For Eq. (4.47), this is done by writing

$$\begin{aligned} x = 0: &\quad \sum_{m=0}^{N_0} \left[\sum_{k_1+k_2=m} \hat{\mu}_0^{k_1k_2} c_1^{k_1} c_2^{k_2} \right] = 0, \\ x = \ell: &\quad \sum_{n=0}^{N_\ell} \left[\sum_{k_1+k_2=n} \hat{\mu}_\ell^{k_1k_2} c_1^{k_1} c_2^{k_2} \right] = 0, \end{aligned} \tag{4.48}$$

where

$$\hat{\mu}_{BC}^{k_1k_2} = \begin{cases} \mu_{\text{BC}}^{k_1k_2} - \lambda_{\text{BC}}^{j} & \text{if } k_1 + k_2 = 1, \\ \mu_{\text{BC}}^{k_1k_2} & \text{otherwise.} \end{cases} \tag{4.49}$$

The linear algebra methods used in the previous section must now be replaced by the non-linear algebra equivalents. These are thoroughly explained in [220], though it can be noted that the key difference is that the tensor *resultant* – an expansion of the matrix determinant – must now be used. Eq. (4.48) is now a non-homogeneous tensor system, which can be solved by applying Cramer's rule [220], which is outlined here.

Initially, it is assumed that (X, Y) represents a solution to the system in Eq. (4.47). Essentially, this is given by $(X, Y) = (c_1, c_2)$, though this will not be immediately implemented to avoid overcomplicating the discussion. By assuming this solution and applying a dummy variable, it is possible to rewrite the system in terms of two new variable pairs, namely (z, y) or (x, z). The variable z is the dummy variable that allows the system to be written in terms of one of the solutions from (X, Y). More explicitly, Eq. (4.48) can now be written either as

$$\begin{aligned} x = 0: &\quad \sum_{m=0}^{N_0} \left[\sum_{k_1+k_2=m} \hat{\mu}_0^{k_1k_2} X^{k_1} z^{k_1} y^{k_2} \right] = 0, \\ x = \ell: &\quad \sum_{n=0}^{N_\ell} \left[\sum_{k_1+k_2=n} \hat{\mu}_\ell^{k_1k_2} X^{k_1} z^{k_1} y^{k_2} \right] = 0, \end{aligned} \tag{4.50}$$

or

$$\begin{aligned} x = 0: \quad & \sum_{m=0}^{N_0} \left[\sum_{k_1+k_2=m} \hat{\mu}_0^{k_1 k_2} Y^{k_2} x^{k_1} z^{k_2} \right] = 0, \\ x = \ell: \quad & \sum_{n=0}^{N_\ell} \left[\sum_{k_1+k_2=n} \hat{\mu}_\ell^{k_1 k_2} Y^{k_2} x^{k_1} z^{k_2} \right] = 0. \end{aligned} \tag{4.51}$$

Eqs. (4.50) and (4.51) are necessarily solved by $(z, y) = (1, Y)$ and $(x, z) = (X, 1)$, respectively. It can be noted that these systems must both lead to the same overall solution; therefore, only Eq. (4.50) will be considered from this point forward.

As this derivation considers two independent nonlinear BCs, it is not necessarily true that $N_0 = N_\ell$. To aid the solution of this system, it is useful to define $N_{\text{max}} = \max\{N_0, N_\ell\}$, allowing the system to be written as two polynomials of order N_{max}:

$$\begin{aligned} x = 0: \quad & \sum_{m=0}^{N_{\text{max}}} \left[\sum_{k=0}^{m} \hat{\mu}_0^{k,(m-k)} X^{(m-k)} \right] z^{(N_{\text{max}}-m)} y^m \\ & = \sum_{m=0}^{N_{\text{max}}} \nu_0^{m,(N_{\text{max}}-m)} z^{(N_{\text{max}}-m)} y^m = 0, \\ x = \ell: \quad & \sum_{m=0}^{N_{\text{max}}} \left[\sum_{k=0}^{m} \hat{\mu}_\ell^{k,(m-k)} X^{(m-k)} \right] z^{(N_{\text{max}}-m)} y^m \\ & = \sum_{m=0}^{N_{\text{max}}} \nu_\ell^{m,(N_{\text{max}}-m)} z^{(N_{\text{max}}-m)} y^m = 0. \end{aligned} \tag{4.52}$$

Here, the assumed constant solution, X, is incorporated into the new tensor coefficients, ν_{BC}, to allow a simpler polynomial form to be used. These coefficients are now defined in terms of c_1 and κ. For the polynomial that was originally of a lower order, the coefficients of the new higher-order terms are zero, but it is beneficial to leave them in as it allows a simpler resultant expression to be used.

As previously mentioned, nonlinear algebraic systems can be solved through the use of the resultant, a formal definition of which can be found in [220]. The current procedure makes use of the fact that Eq. (4.52) comprises only two equations in two variables, each of order N_{max}. For such a system, one simply needs to find the ordinary resultant [221] of two polynomials in a single variable and can be solved using linear algebra in the following

fashion [220]

$$\mathcal{R}_{2|N_{\max}}(\nu) = \det_{2N_{\max}\times 2N_{\max}}(\nu_{\text{aug}}) =$$

$$\det_{2N_{\max}\times 2N_{\max}} \begin{bmatrix} \nu_0^{0,N_{\max}} & \nu_0^{1,N_{\max}-1} & \dots & \nu_0^{N_{\max}-1,1} & \nu_0^{N_{\max},0} & 0 & \dots & 0 \\ 0 & \nu_0^{0,N_{\max}} & \dots & \nu_0^{N_{\max}-2,2} & \nu_0^{N_{\max}-1,1} & \nu_0^{N_{\max},0} & \dots & 0 \\ & & & \dots & & & & \\ 0 & 0 & \dots & \nu_0^{0,N_{\max}} & \nu_0^{1,N_{\max}-1} & \nu_0^{2,N_{\max}-2} & \dots & \nu_0^{N_{\max},0} \\ \nu_\ell^{0,N_{\max}} & \nu_\ell^{1,N_{\max}-1} & \dots & \nu_\ell^{N_{\max}-1,1} & \nu_\ell^{N_{\max},0} & 0 & \dots & 0 \\ 0 & \nu_\ell^{0,N_{\max}} & \dots & \nu_\ell^{N_{\max}-2,2} & \nu_\ell^{N_{\max}-1,1} & \nu_\ell^{N_{\max},0} & \dots & 0 \\ & & & \dots & & & & \\ 0 & 0 & \dots & \nu_\ell^{0,N_{\max}} & \nu_\ell^{1,N_{\max}-1} & \nu_\ell^{2,N_{\max}-2} & \dots & \nu_\ell^{N_{\max},0} \end{bmatrix}$$

$$= 0, \tag{4.53}$$

where $\mathcal{R}_{n|s}(\bullet)$ is the tensor resultant of a system, $\bullet$, of n polynomials of order s, and ν_{aug} is the notation used for the augmented matrix defined in Eq. (4.53). It can now be recalled that the coefficient tensor ν_{BC} is defined in terms of c_1 and κ. Given that this model assumes that the mode shapes of the system will be scaled as the system vibrates, it is possible to obtain values for κ by setting $c_1 = 1$. In doing so, Eq. (4.53) provides a solvability condition that can be numerically solved, as has been seen in the linear BC models.

Although a numerical solution to Eq. (4.53) is possible, as $N_{\max}$ increases, it can become difficult to ensure the accuracy of the solution to a sufficient number of decimal places. As such, it can be useful to express this large determinant in terms of elementary, 2×2 determinants, called *Plücker relations*, as outlined in [220].

4.5.1 Example: nonlinear spring-supported beam

To further assess the ability of the proposed method for treating nonlinear BCs, it is useful to consider a model in which both BCs are nonlinear. To that end, the following beam configuration is introduced, in which both ends of the beam are supported by springs with linear, quadratic, and cubic stiffnesses. Although the consideration of this beam may seem somewhat theoretical, in reality, it can simply be thought of as an investigation into the

applicability of the method, giving insight into its validity for more complicated systems. In particular, there are multiple microscale BCs that can easily arise, and this methodology introduces an efficient way of investigating the associated dynamics. The BCs for this beam are given by

$$\begin{aligned}\phi''(0) = \phi''(\ell) = 0, \quad \phi'''(0) = \hat{K}_1^{(0)}\phi(0) + \hat{K}_2^{(0)}\phi(0)^2 + \hat{K}_3^{(0)}\phi(0)^3,\\ \phi'''(\ell) = \hat{K}_1^{(\ell)}\phi(\ell) + \hat{K}_2^{(\ell)}\phi(\ell)^2 + \hat{K}_3^{(\ell)}\phi(\ell)^3,\end{aligned} \tag{4.54}$$

where $\hat{K}_n^{(x)}$ defines the n^{th}-order spring stiffness at x.

By first addressing the second derivative BCs, it is possible to rewrite the mode shape equation in Eq. (4.10) as

$$\begin{aligned}\phi(y) = c_1\bigg(\cos(\kappa y) + \cosh(\kappa y) + \bigg[\frac{\cos(\kappa)}{\sinh(\kappa)} - \coth(\kappa)\bigg]\sinh(\kappa y)\bigg)\\ +c_2\bigg(\sin(\kappa y) + \frac{\sin(\kappa)}{\sinh(\kappa)}\sinh(\kappa y)\bigg).\end{aligned} \tag{4.55}$$

The BCs defined in Eq. (4.54) take the exact form given in Eq. (4.41), so the derivation is qualitatively identical to the general form given in Section 4.5 and is not repeated here. Instead, it is possible to immediately consider the system in the form given in Eq. (4.52). Once more, the coefficients in ν_0 and ν_ℓ are complicated expressions in terms of $\hat{K}_n^{(x)}$ and κ, but can be easily treated using symbolic mathematical solvers, such as Wolfram Mathematica or Maple. The explicit terms for these are as follows:

$$\begin{aligned}\nu_0^{0,3} &= \bigg[2\hat{K}_1^{(0)} + \kappa^3\bigg(\coth(\kappa) - \frac{\cos(\kappa)}{\sinh(\kappa)}\bigg)\bigg]X + 4\hat{K}_2^{(0)}X^2 + 8\hat{K}_3^{(0)}X^3,\\ \nu_0^{1,2} &= \kappa^3\bigg(1 - \frac{\sin(\kappa)}{\sinh(\kappa)}\bigg),\\ \nu_0^{2,1} &= 0,\\ \nu_0^{3,0} &= 0,\\ \nu_\ell^{0,3} &= (2\hat{K}_1^{(\ell)}\cos(\kappa) + \kappa^3[(\cosh(\kappa) - \cos(\kappa))\coth(\kappa) - \sin(\kappa) - \sinh(\kappa)])X\\ &\quad + 4\hat{K}_2^{(\ell)}\cos^2(\kappa)X^2 + 8\hat{K}_3^{(\ell)}\cos^3(\kappa)X^3,\\ \nu_\ell^{1,2} &= \kappa^3(\cos(\kappa) - \sin(\kappa)\coth(\kappa)) + 2\hat{K}_1^{(\ell)}\sin(\kappa) + 8\hat{K}_2^{(\ell)}\sin(\kappa)\cos(\kappa)X\\ &\quad + 24\hat{K}_3^{(\ell)}\sin(\kappa)\cos^2(\kappa)X^2,\\ \nu_\ell^{2,1} &= 4\hat{K}_2^{(\ell)}\sin^2(\kappa) + 24\hat{K}_3^{(\ell)}\sin^2(\kappa)\cos(\kappa)X,\\ \nu_\ell^{3,0} &= 8\hat{K}_3^{(\ell)}\sin^3(\kappa).\end{aligned} \tag{4.56}$$

The expressions in Eq. (4.56) are more algebraically complicated than in previous examples, leading to a resultant that can be particularly intensive to solve numerically. As an initial investigation into the validity of the proposed methodology, it is useful to consider the symmetric case of this beam, so that it may be compared to the classical free-free and pinned-pinned models. To that end, the beam stiffnesses will be set to $\hat{K}_n^{(0)} = \hat{K}_n^{(\ell)} = \hat{K}_n$, with the value of these constants being varied so that the classical cases can be approached. To aid this investigation, a single parameter, γ, will be used to express the spring stiffnesses as

$$\hat{K}_1 = \gamma, \quad \hat{K}_2 = 10\gamma, \quad \hat{K}_3 = 100\gamma. \tag{4.57}$$

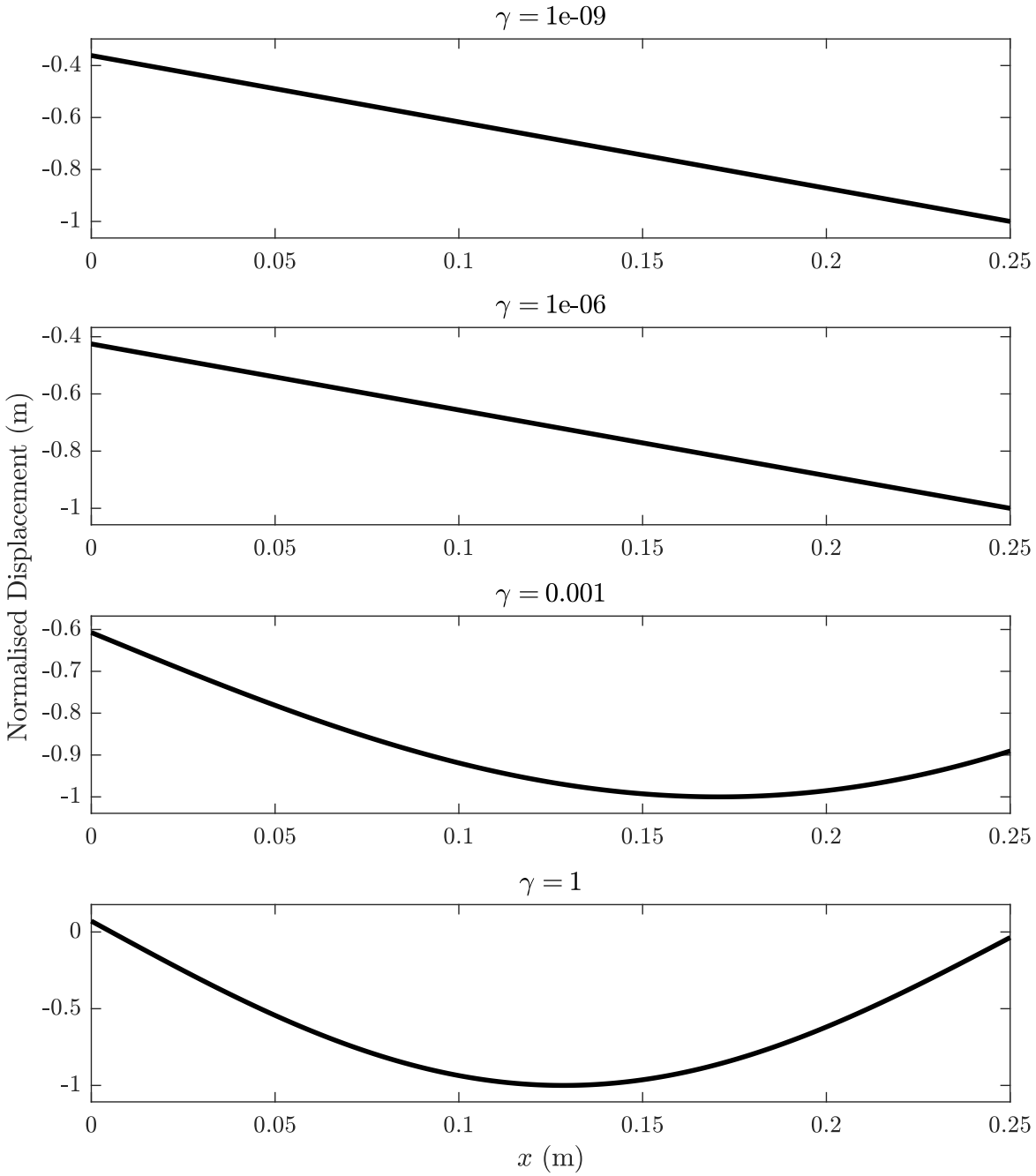

Figure 4.8: Normalised mode shapes of the first mode of the nonlinear spring-supported beam for $\gamma \in$ [1e-9, 1e-6, 1e-3, 1].

Figs. 4.8–4.10 display the first, second, and third mode shapes, respectively, for a number of values of γ. Namely, these are $\gamma \in$ [1e-9, 1e-6, 1e-3, 1]. As $\gamma \to \infty$, it is expected that the behaviour should become increasingly similar to that of the pinned-pinned beam. This trend is visible in Figs. 4.8–4.10, in which, for the case $\gamma = 1$, the mode shapes are very close to those expected from the fully pinned beam. Interestingly, although the beam tip supports are symmetric, the positions of the tips in the mode shapes are not. This suggests that the variable position of the beam tips allows the beam stiffness to influence the symmetry of the modes. This holds true even when the spring stiffnesses are extremely high. However, it

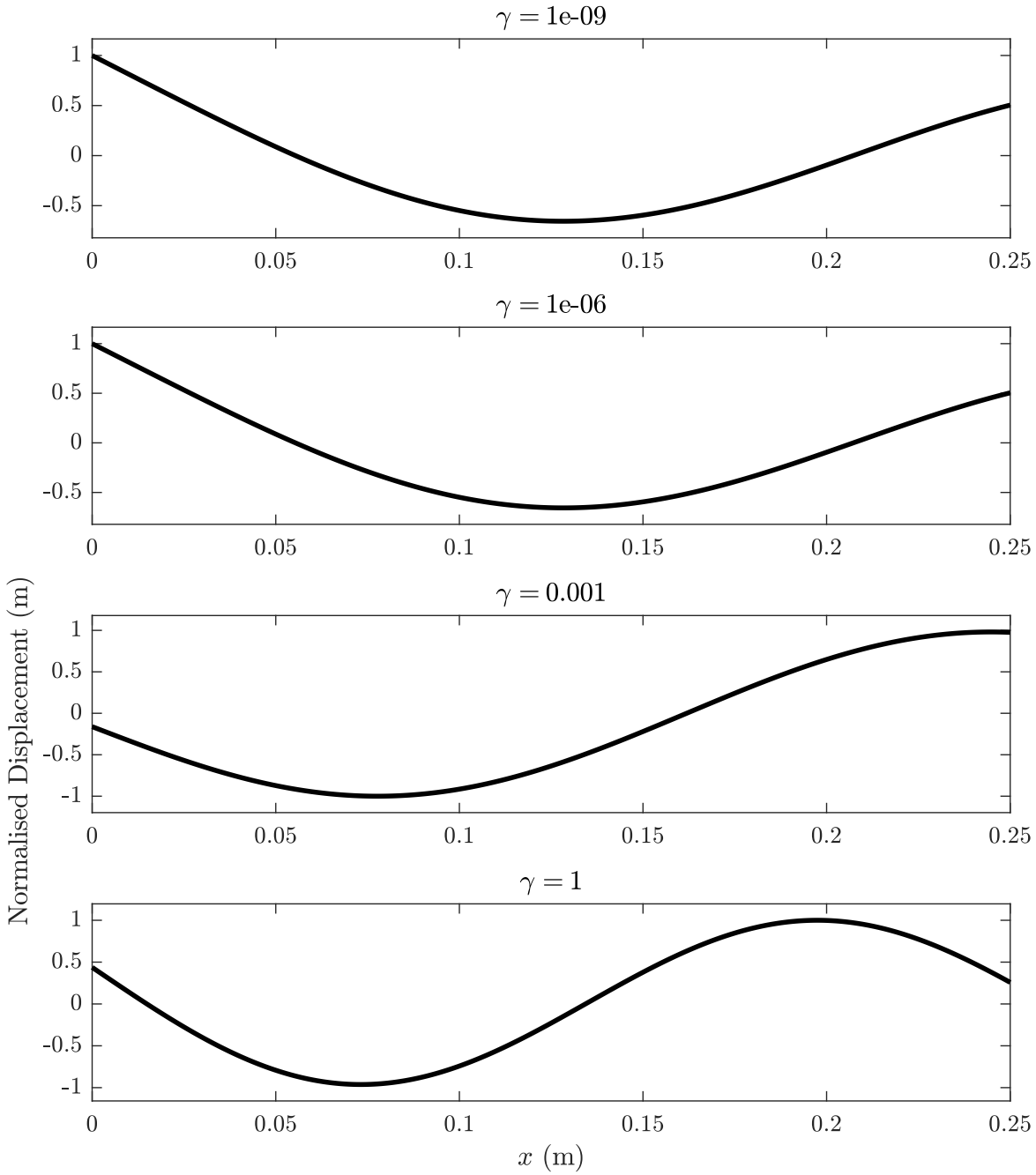

Figure 4.9: Normalised mode shapes of the second mode of the nonlinear spring-supported beam for $\gamma \in$ [1e-9, 1e-6, 1e-3, 1].

should be noted that, as γ is increased, they become closer to one another, suggesting that the pinned-pinned beam represents an upper limit case for this configuration. At the other end of the scale, one might expect the behaviour to tend to that of a free-free beam. However, it can be seen that the spring stiffnesses still have a significant influence. In fact, these shapes are qualitatively similar to those found if the spring-supported beam is assumed to be rigid, as there is negligible bending of the beam when $\gamma =$ 1e-6 or 1e-9.

The influence that the value of γ has on the free response of the system is investigated in Fig. 4.11 through the consideration of the backbone curves for $\gamma \in$ [1e-9, 1e-6, 1e-3]. As

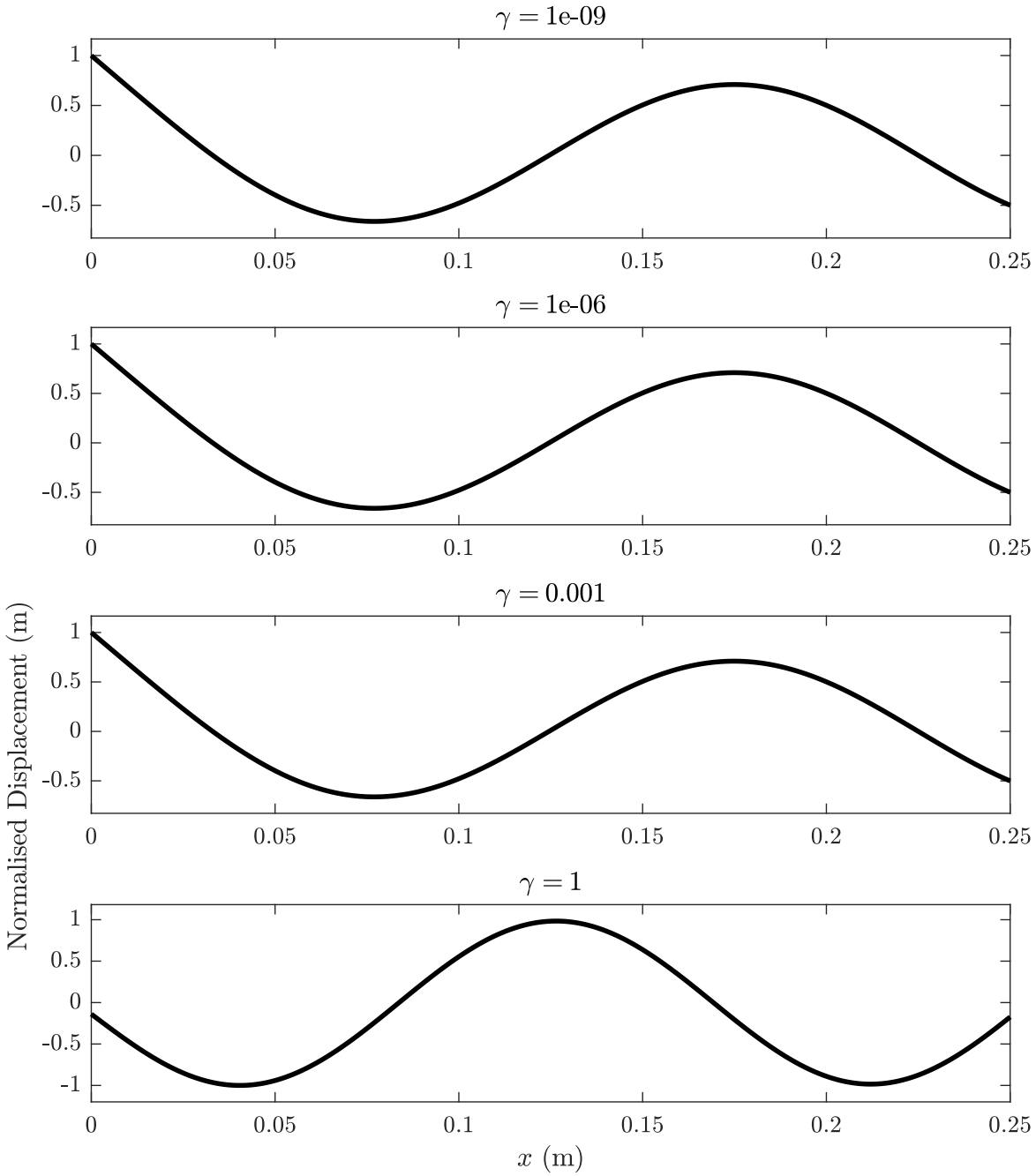

Figure 4.10: Normalised mode shapes of the third mode of the nonlinear spring-supported beam for $\gamma \in$ [1e-9, 1e-6, 1e-3, 1].

expected, the extent to which the system behaves nonlinearly increases with γ. Not only does the variation in frequency at higher amplitudes become more pronounced, but interactions between the modes also arise. In the previous section, it was noted that the introduction of a rotational spring at one end of a pinned-pinned beam leads to substantial changes in the α and β matrices, causing internal resonances to arise. In the current arrangement, the beam itself is symmetric. Therefore, it might understandably be assumed that it is unlikely that such a resonance would occur. However, the asymmetric nature of the mode shapes has a similar effect on the γ and β matrices. As such, it should be concluded that, in the initial discussion

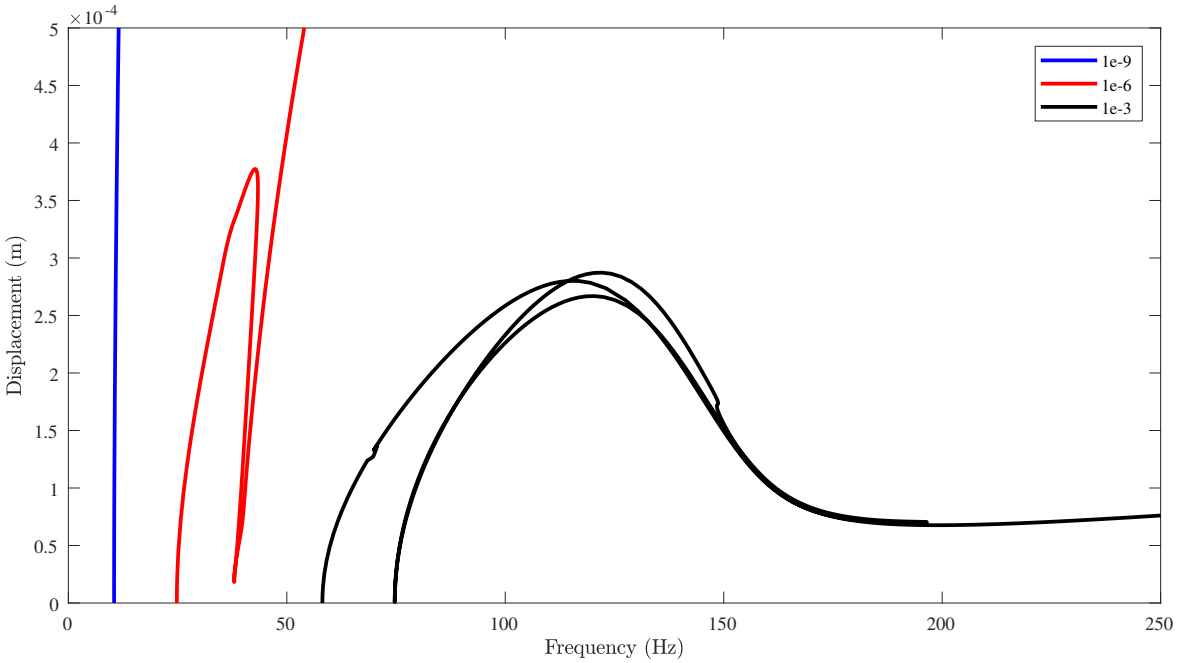

Figure 4.11: Backbone curves for the spring-supported beams with $\gamma \in$ [1e-9, 1e-6, 1e-3].

and prediction of modal interactions, it is important that the mode shapes are calculated, as opposed to simply considering the system configuration.

4.5.2 Example: cantilever beam with magnetic tip interaction

An immediate application of this method is to a beam configuration with a magnetic interaction at the tip. In this example, the magnet at the tip is aligned with an iron stator, at distance D from the beam tip. In this approximate model, the magnet and stator will be assumed to be covered by equally-distributed ideal charges. The stator charges facing the beam will be opposite to those of the magnet at the tip, so that the interaction is attractive. This example is illustrated in Fig. 4.12.

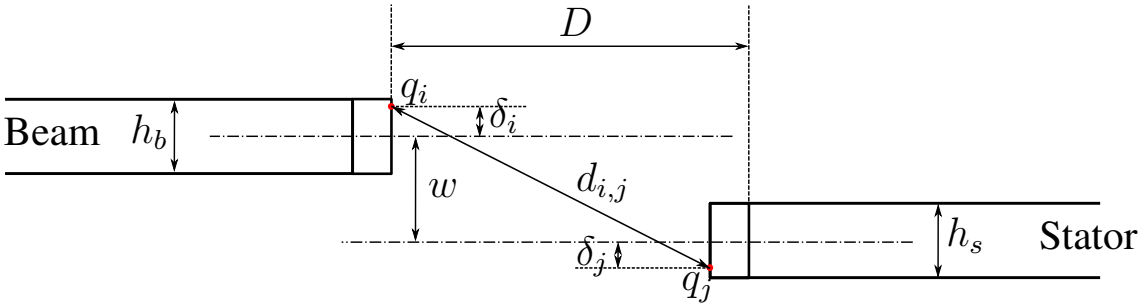

Figure 4.12: Schematic of a cantilever beam with a spring support at the free end.

Due to the complex nature of this BC, it is necessary to make a number of assumptions to investigate its dynamics. A summary of these is given here:

- The deflection of the beam will be small and, therefore, can be approximated as a pure

translation.

- Therefore, the faces of both magnet and the stator will always be parallel.
- Only the face of the stator facing the magnets is responsible for the attractive force.
- The magnetic properties of the magnet are concentrated at the face parallel to the stator.
- The attractive forces between the magnet and the stator are Coulomb-like in nature, so that $F_M \propto \frac{1}{d_{ij}^2}$.

We now consider two charges, q_i and q_j, which are from the beam and stator, respectively; these points are denoted by the red dots in Fig. 4.12. The attractive force between these charges is given by

$$\mathbf{F}_{i,j} = \frac{K_m}{|d_{i,j}|^3}\mathbf{d}_{i,j}, \tag{4.58}$$

where K_m is a constant that accounts for the characteristics of the magnets and $\mathbf{d}_{i,j}$ is the radius vector applied from the i^{th} charge to the j^{th} charge. It can be seen, in Fig. 4.12, that the distance between these charges is given by

$$d_{i,j} = \sqrt{D^2 + (w + \delta_i + \delta_j)^2}, \tag{4.59}$$

where δ_i denotes the distance of charge q_i from the vertical centre of the beam and δ_j is the equivalent for charge q_j, as depicted in Fig. 4.12. Therefore, Eq. (4.58) can now be expressed as

$$\mathbf{F}_{i,j} = K_m\left[\frac{D}{(D^2 + (w + \delta_i + \delta_j)^2)^{\frac{3}{2}}}\mathbf{i} + \frac{w + \delta_i + \delta_j}{(D^2 + (w + \delta_i + \delta_j)^2)^{\frac{3}{2}}}\mathbf{j}\right], \tag{4.60}$$

where **i** and **j** are unitary vectors that are orthogonal to and parallel to the vertical motion, respectively. The **i**-direction term in Eq. (4.60), although typically of greater magnitude than the parallel term, is largely counterbalanced by the longitudinal stresses in the beam. Therefore, its effect on the lateral displacement of the beam is small compared to the parallel term. As such, it is possible to neglect the orthogonal term and focus solely on the force component that is parallel to the motion of the beam.

Up until this point, the magnetic force calculations have considered the interaction between a single charge from each magnet. Considering that this type of interaction occurs between any such pair, it is necessary to calculate the net force that arises due to the magnetic BC. To do this, we integrate in the **j**-direction in Eq. (4.60) over the width of both the

beam and the stator:

$$F_M(w) = K_m \int_{-h_b/2}^{h_b/2} \int_{-h_s/2}^{h_s/2} \frac{w + \delta_i + \delta_j}{\sqrt{D^2 + (w + \delta_i + \delta_j)^2}} \mathrm{d}\delta_j \mathrm{d}\delta_i. \tag{4.61}$$

Here, h_b and h_s are the width of the beam and stator, respectively. It is possible to consider this double integral analytically, resulting in the following expression

$$\begin{aligned} F_M(w) = K_m \log \Bigg[& \frac{\left(h_s + h_b - 2w + \sqrt{4D^2 + (h_s + h_b - 2w)^2}\right)}{\left(h_s - h_b - 2w + \sqrt{4D^2 + (h_s - h_b - 2w)^2}\right)} \\ & \times \frac{\left(h_s - h_b + 2w + \sqrt{4D^2 + (h_s - h_b + 2w)^2}\right)}{\left(h_s + h_b + 2w + \sqrt{4D^2 + (h_s + h_b + 2w)^2}\right)} \Bigg]. \end{aligned} \tag{4.62}$$

Now that the tip forces have been quantified, it is possible to write the BCs for this system as

$$\phi(0) = \phi'(0) = \phi''(\ell) = 0, \quad \phi'''(\ell) = F_M(\phi(\ell)). \tag{4.63}$$

Therefore, we now have a classical, clamped BC at the left end and a nonlinear BC at the right, as alluded to at the beginning of this section. As suggested in the previous section, since $F_M \in C^\infty$, the function can be approximated through the use of a Taylor expansion. Due to the symmetry of the system, the coefficients of the even powers of $\phi(w)$ are seen to be zero, F_M can be approximated by

$$F_M(\phi(w)) = K_1\phi(w) - K_3\phi(w)^3 + K_5\phi(w)^5 - \ldots, \tag{4.64}$$

where K_n are the coefficients that arise in the Taylor expansion about the equilibrium point, $\phi(w) = 0$. By truncating the expression in Eq. (4.64), this model can be considered as an expansion of the linear spring-supported cantilever in [155], where, now, the supporting spring has higher order stiffness terms. In the subsequent calculations, the cubic truncation of Eq. (4.64) are utilised.

Given that the BCs at $x = 0$ are linear, it is immediately possible to recall, from Eq. (4.35), that the mode shape can be parametrised as

$$\phi(y) = c_1(\cos(\kappa y) - \cosh(\kappa y) + \sin(\kappa y) - \sinh(\kappa y)) + 2c_2(\sin(\kappa y) - \sinh(\kappa y)). \tag{4.65}$$

Considering the BCs at $x = \ell$ leads to the equations

$$\begin{aligned}
&\big(\cos(\kappa)+\sin(\kappa)+\cosh(\kappa)+\sinh(\kappa)\big)c_1 + 2\big(\sin(\kappa)+\sinh(\kappa)\big)c_2 = 0,\\
&\big(\kappa^3\big[-\cos(\kappa)-\cosh(\kappa)+\sin(\kappa)-\sinh(\kappa)\big]\\
&+\hat{K}_L\big[-\cos(\kappa)+\cosh(\kappa)-\sin(\kappa)+\sinh(\kappa)\big]\big)c_1\\
&\quad -2\big(\kappa^3\big[\cos(\kappa)+\cosh(\kappa)\big]+\hat{K}_L\big[\sin(\kappa)-\sinh(\kappa)\big]\big)c_2\\
&\qquad +\big(\big[\cos(\kappa)+\sin(\kappa)+\cosh(\kappa)+\sinh(\kappa)\big]c_1+2[\sin(\kappa)+\sinh(\kappa)]c_2\big)^3 = 0.
\end{aligned} \tag{4.66}$$

Expanding this expression, it is possible to collect the c_n terms, so that the system can be written as

$$\begin{aligned}
0 &= \sigma_0^1 c_1 + \sigma_0^2 c_2,\\
\mu_\ell^{111}c_1^3+\mu_\ell^{112}c_1^2c_2+\mu_\ell^{122}c_1c_2^2+\mu_\ell^{222}c_2^3 &= \sigma_\ell^1 c_1+\sigma_\ell^2 c_2,
\end{aligned} \tag{4.67}$$

where σ^i_{BC} and μ^{ijk}_{BC} are the collected coefficients from Eq. (4.66). Although it is possible to find the resultant of this tensor system, the process is aided by introducing dummy terms to the first of these equations, so that the system is written as

$$\begin{aligned}
\mu_0^{111}c_1^3+\mu_0^{112}c_1^2c_2+\mu_0^{122}c_1c_2^2+\mu_0^{222}c_2^3 &= \sigma_0^1 c_1+\sigma_0^2 c_2,\\
\mu_\ell^{111}c_1^3+\mu_\ell^{112}c_1^2c_2+\mu_\ell^{122}c_1c_2^2+\mu_\ell^{222}c_2^3 &= \sigma_\ell^1 c_1+\sigma_\ell^2 c_2,
\end{aligned} \tag{4.68}$$

where μ_0^{ijk} are dummy coefficients that allow Eq. (4.67) to be written in the form given in Eq. (4.47). By introducing the change in notation given in Eqs. (4.48) and (4.49), Eq. (4.68) can be written as

$$\begin{aligned}
\hat{\mu}_0^{111}c_1^3+\hat{\mu}_0^{112}c_1^2c_2+\hat{\mu}_0^{122}c_1c_2^2+\hat{\mu}_0^{222}c_2^3 &= 0,\\
\hat{\mu}_\ell^{111}c_1^3+\hat{\mu}_\ell^{112}c_1^2c_2+\hat{\mu}_\ell^{122}c_1c_2^2+\hat{\mu}_\ell^{222}c_2^3 &= 0,
\end{aligned} \tag{4.69}$$

It has been seen that, by assuming that $(c_1, c_2) = (X, Y)$ is a solution to this system, it is possible to express it in the following homogeneous form

$$\begin{aligned}
(\hat{\mu}_0^{111}X^3)z^3+(\hat{\mu}_0^{112}X^2)z^2y+(\hat{\mu}_0^{122}X)zy^2+(\hat{\mu}_0^{222})y^3 &= 0,\\
(\hat{\mu}_\ell^{111}X^3)z^3+(\hat{\mu}_\ell^{112}X^2)z^2y+(\hat{\mu}_\ell^{122}X)zy^2+(\hat{\mu}_\ell^{222})y^3 &= 0,
\end{aligned} \tag{4.70}$$

which is solved by $(z, y) = (1, Y)$. As such, the solvability condition for this system is found

by calculating

$$\mathcal{R}_{2|3}(\mu_{\text{aug}}) = \det \begin{bmatrix} \hat{\mu}_0^{111}X^3 & \hat{\mu}_0^{112}X^2 & \hat{\mu}_0^{122}X & \hat{\mu}_0^{222} & 0 & 0 \\ 0 & \hat{\mu}_0^{111}X^3 & \hat{\mu}_0^{112}X^2 & \hat{\mu}_0^{122}X & \hat{\mu}_0^{222} & 0 \\ 0 & 0 & \hat{\mu}_0^{111}X^3 & \hat{\mu}_0^{112}X^2 & \hat{\mu}_0^{122}X & \hat{\mu}_0^{222} \\ \hat{\mu}_\ell^{111}X^3 & \hat{\mu}_\ell^{112}X^2 & \hat{\mu}_\ell^{122}X & \hat{\mu}_\ell^{222} & 0 & 0 \\ 0 & \hat{\mu}_\ell^{111}X^3 & \hat{\mu}_\ell^{112}X^2 & \hat{\mu}_\ell^{122}X & \hat{\mu}_\ell^{222} & 0 \\ 0 & 0 & \hat{\mu}_\ell^{111}X^3 & \hat{\mu}_\ell^{112}X^2 & \hat{\mu}_\ell^{122}X & \hat{\mu}_\ell^{222} \end{bmatrix} = 0. \tag{4.71}$$

Although somewhat complicated, Eq. (4.71) can be solved through the use of algebraic software. As previously discussed, it it useful to utilise the Plücker relations to simplify this expression. For a system of two cubic polynomials, this is given by [220]

$$\mathcal{R}_{2|3}(\mu) = U_3^3 - U_2U_3U_4 + U_2^2U_5 - 2U_1U_3U_5 - U_1V_3U_5, \tag{4.72}$$

where

$$\begin{aligned} U_1 &= \begin{Vmatrix} \hat{\mu}_0^{122}X & \hat{\mu}_0^{222} \\ \hat{\mu}_\ell^{122}X & \hat{\mu}_\ell^{222} \end{Vmatrix}, \quad U_2 = \begin{Vmatrix} \hat{\mu}_0^{112}X^2 & \hat{\mu}_0^{222} \\ \hat{\mu}_\ell^{112}X^2 & \hat{\mu}_\ell^{222} \end{Vmatrix}, \\ U_3 &= \begin{Vmatrix} \hat{\mu}_0^{111}X^3 & \hat{\mu}_0^{222} \\ \hat{\mu}_\ell^{112}X^3 & \hat{\mu}_\ell^{222} \end{Vmatrix}, \quad V_3 = \begin{Vmatrix} \hat{\mu}_0^{112}X^2 & \hat{\mu}_0^{122}X \\ \hat{\mu}_\ell^{112}X^2 & \hat{\mu}_\ell^{122}X \end{Vmatrix}, \\ U_4 &= \begin{Vmatrix} \hat{\mu}_0^{111}X^3 & \hat{\mu}_0^{122}X \\ \hat{\mu}_\ell^{112}X^3 & \hat{\mu}_\ell^{122}X \end{Vmatrix}, \quad U_5 = \begin{Vmatrix} \hat{\mu}_0^{111}X^3 & \hat{\mu}_0^{112}X^2 \\ \hat{\mu}_\ell^{112}X^3 & \hat{\mu}_\ell^{112}X^2 \end{Vmatrix}. \end{aligned} \tag{4.73}$$

4.5.2.1 Results

As an initial investigation, the following system parameters will be used: $\ell = 0.25$ m, $E = 193$ GPa, $I = 10^{-11}$ m^4, and $\rho = 8000$ kg/m^3. Both the beam and the stator will have height $h_b = h_s = 0.002$ m and width $w_b = w_s = 0.015$ m, resulting in $\hat{A} = 3 \times 10^{-5}$ m^2. The distance between the beam and the stator will be set to $D = 0.04$ m and we choose $K_M = 10$.

Fig. 4.13 shows the first, second, and third mode shapes for the cantilever beam with

magnetic BC at the tip. Three approximations for F_M are utilised; namely, these are

$$\begin{aligned} &\text{Free:} && F_M(\phi(w)) = 0, \\ &\text{Linear:} && F_M(\phi(w)) = K_1\phi(w), \\ &\text{Cubic:} && F_M(\phi(w)) = K_1\phi(w) - K_3\phi(w)^3. \end{aligned} \tag{4.74}$$

It can clearly be seen that each of these cases represents a truncation of the Taylor series for F_M.

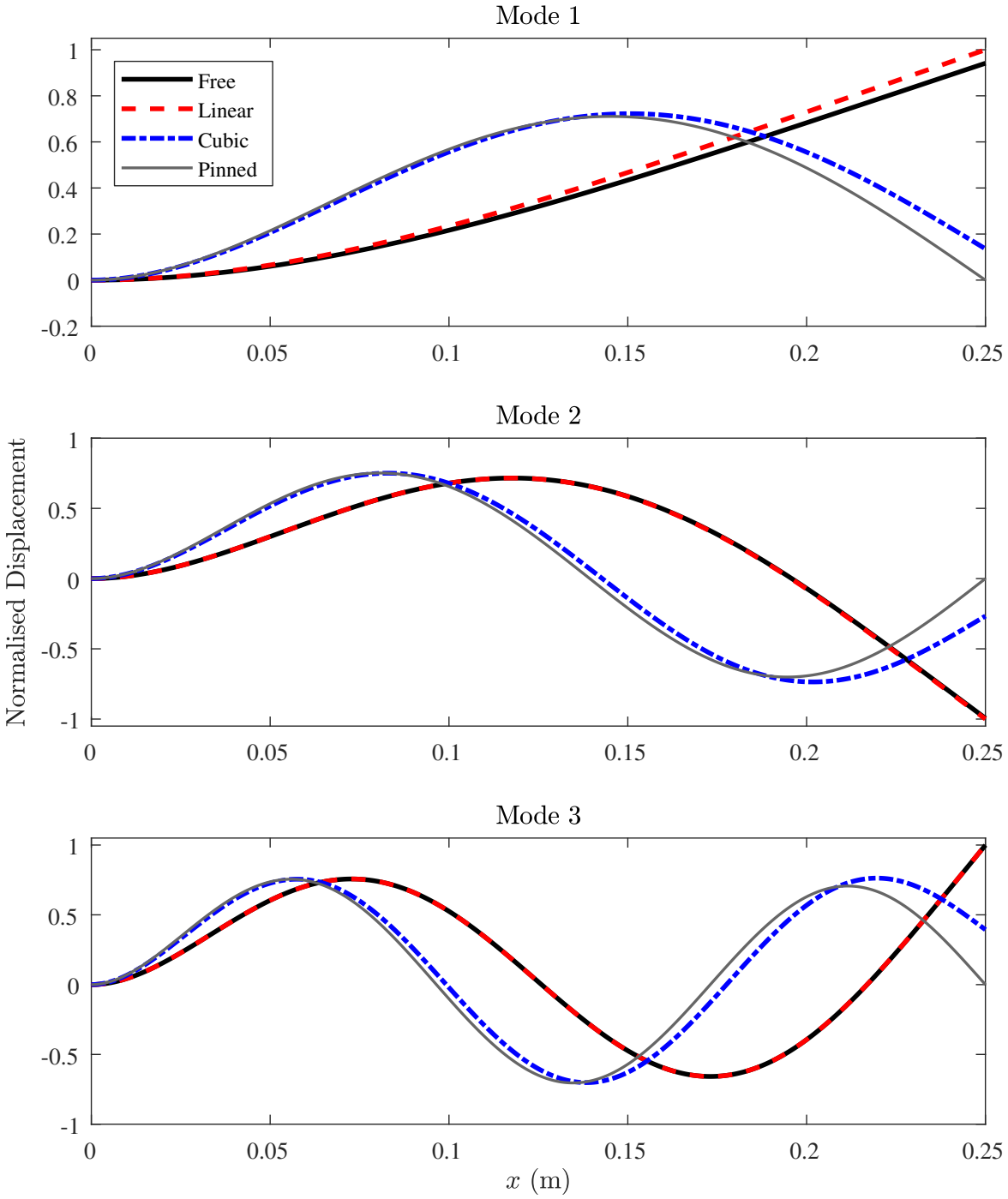

Figure 4.13: Normalised mode shapes for the first mode of the clamped-free, clamped-pinned, and clamped-spring support beams.

The mode shapes presented in Fig. 4.13 provide interesting insight into the variations in the model, should the system nonlinearity be included in the BCs, as opposed to simply the equations of motion. The disparity between the free, linear, and cubic approximations are noticeable across all three modes presented here (as well as those that are not shown), though these are most distinguishable for the first. Here, it can be seen that, while the linear truncation is close to the classical clamped-free mode shape, the cubic truncation is much closer to that of the clamped-pinned configuration, which is also shown for comparative purposes. The fact that both the free and linear cases are so dissimilar to the cubic approximation indicates that there are potentially concerning implications of using either of these approximations as a modal basis. That is, by either omitting the magnetic interaction from the modal calculations entirely, or by truncating it prematurely, the system could be vibrating in a shape that is considerably different to that predicted.

Of further interest is the fact the linear mode shapes approach those of the free cantilever as the mode number increases, suggesting that the influence of the magnetic BC is lost for higher modes. In contrast, this is not true for the cubic approximation, which remains close to the pinned cantilever model, but without approaching it. To investigate this further, it is useful to define a projection mode shape matrix for each mode number, n. This matrix is simply comprised of the n^{th} mode shape for the free and pinned cantilever, so that the relative contribution of each can be assessed. The matrix is given by:

$$\mathbf{\Phi}_{\text{comb},n} = \left[\phi_{\text{free},n}, \phi_{\text{pinned},n}\right], \tag{4.75}$$

where $\phi_{\text{BC},n}$ is the n^{th} mode shape of a particular BC. Therefore, by pre-multiplying the magnetic mode shapes in Fig. 4.13 by the pseudo-inverse of $\mathbf{\Phi}_{\text{comb},n}$, it is possible to assess the relative contribution of each classical BC. The results of doing so are presented in Table 4.5.

Table 4.4: Relative contributions of the free and pinned cantilever mode shapes in the magnetic tip model.

Approximation	Projection Model	Mode Number		
		1	2	3
Linear	*Free*	0.9921	0.9964	0.9993
	Pinned	0.0079	0.0036	0.0007
Cubic	*Free*	0.1389	0.1227	0.1546
	Pinned	0.8611	0.8773	0.8454

Table 4.4 provides support for a number of the points presented thus far. In particular, it can be seen that there is a large contribution of the free mode shape in the linear case, with the

same being true of the pinned mode shape in the cubic case. Furthermore, it can be seen that the contribution of $\phi_{\text{free},n}$ in $\phi_{\text{linear},n}$ grows as n is increased, whereas this is not true for the cubic BC expansion.

This difference in the mode shapes directly corresponds to a variation in their natural frequency, as displayed in Table 4.5. This is potentially more significant than the aforementioned issue regarding the shape of vibration. This comparison suggests that, by neglecting the influence of the cubic nonlinearity, the first natural frequency of the system could be over three times greater than predicted.

Table 4.5: Natural frequencies of the approximations of the cantilever with magnetic tip BC.

Approximation	$\omega_{n,1}$	$\omega_{n,2}$	$\omega_{n,3}$
Free	159.53	999.76	2799.4
Linear	174.80	1002.3	2800.3
Cubic	664.58	2146.2	4471.9
Pinned	699.56	2276.0	4730.0

The variation in mode shapes and natural frequencies can be observed in the free and forced responses. The nature of these responses in a neighbourhood of the first natural frequency are displayed in Fig. 4.14. Not only does the varying nature of $\omega_{n,1}$ change the frequency at which the backbone curves initiate, but it can be seen that the changes in the mode shapes influence the modal interaction behaviour which is predicted. The classical cantilever is completely linear, due to the lack of constraining and associated stretching. In the considered region, the linear truncation predicts a weak softening behaviour, in contrast with the hardening behaviour predicted by including the cubic term of the Taylor expansion. In addition, the linear approximation fails to predict the 1:3 modal interaction that is revealed in the higher-order model.

The importance of capturing modal interactions is highlighted in Fig. 4.15. Here, it can be seen that the transfer energy from the first to the second mode leads to a significant increase in its modal displacement. In can be further noted that this remains true away from the initial interaction. Therefore, for any higher amplitude response in this region, there will be a contribution of the second mode to the overall displacement.

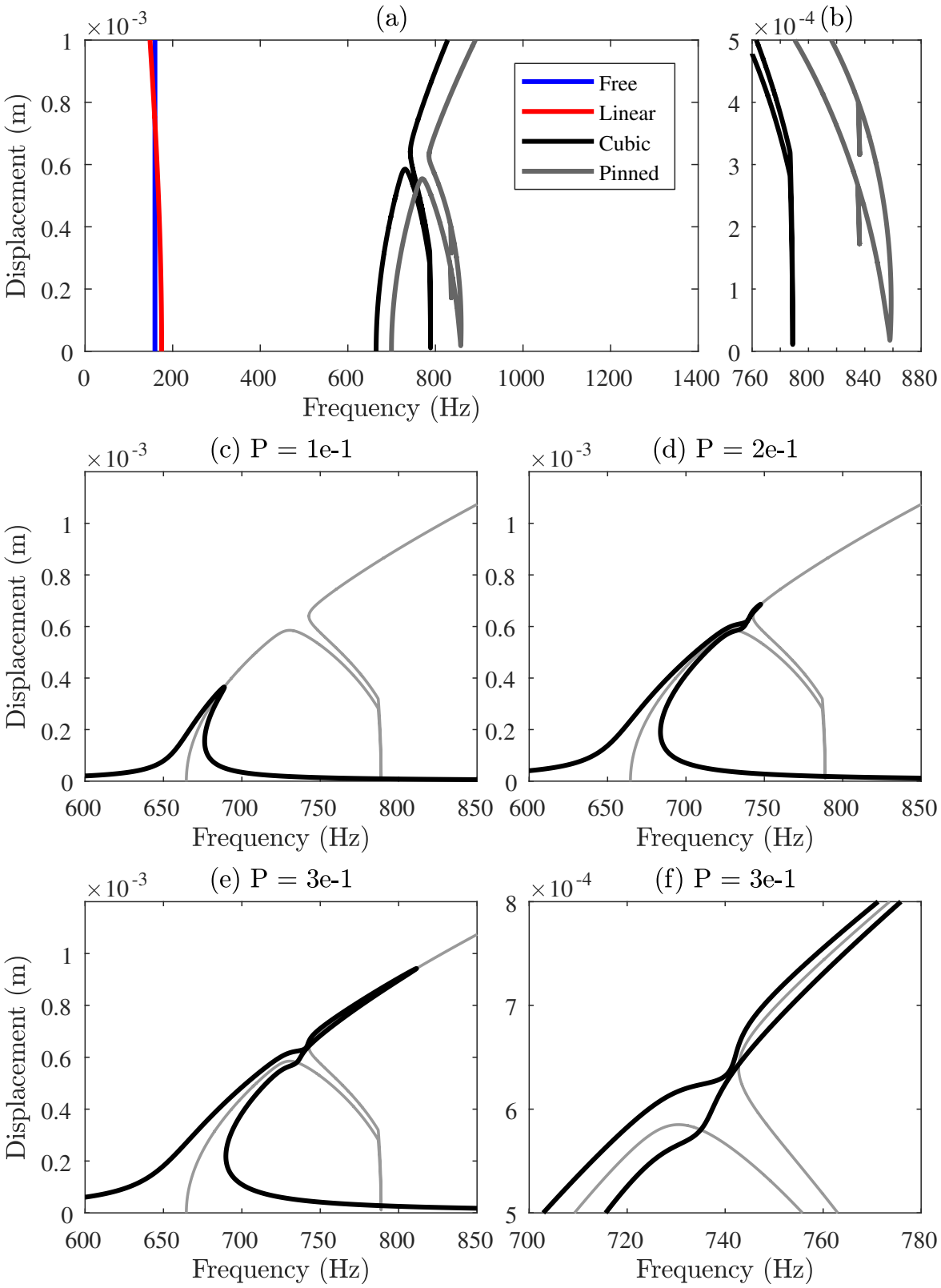

Figure 4.14: Free and forced responses for the considered beam configurations.

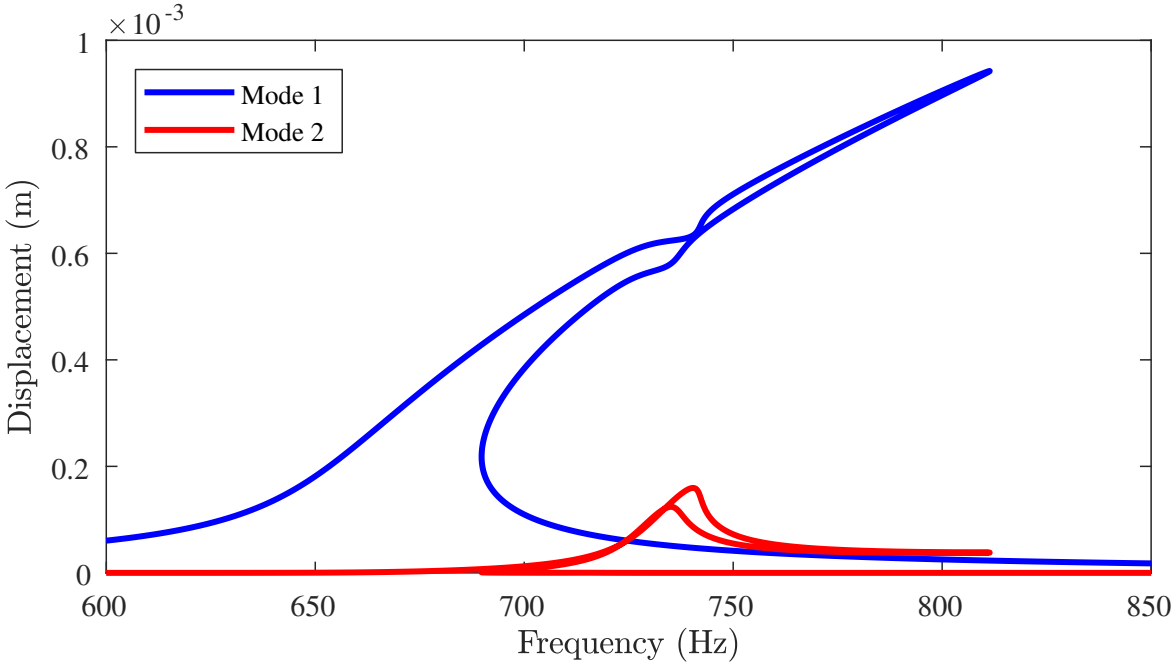

Figure 4.15: Modal projections of the forced response when P = 3e-1.

4.6 Summary

This chapter introduces and examines the Ritz-Galerkin method as a tool for modelling the nonlinear dynamical behaviour of beams. Since the focus of this thesis is on *weakly* nonlinear systems, Euler-Bernoulli beam theory is used to define the underlying beam equations to which the Galerkin approximation can be applied. It has been demonstrated, through the consideration of a number of configurations, that a standardised approach can be taken, with the only variation in the models resulting from the differences in their BCs. A primary focus of this chapter is the influence that these BCs have on the dynamics of the system and the best methodology for incorporating them into the equations of motion. This is particularly important for constrained beams, in which axial stretching results in cross-coupling terms between the modes, as these are defined entirely in terms of the mode shapes and, therefore, the BCs.

Of primary concern for nonlinear systems is the possibility that energy can be transferred between the modes as a result of an internal resonance. In §4.2.4, it has been shown that, although the clamped-clamped system exhibits a hardening nonlinearity at higher amplitudes, there is no modal interaction involving the first mode. It has been posited that this is a result of the symmetry of the system. To investigate this further, a pinned-pinned beam with rotational spring at the tip is also examined. With the symmetry broken, there is a 1:3 internal resonance between the first and second modes, which manifests as a tongue on the backbone curves. As such, the influence of the modal interactions on the forced response is entirely dependent on the balance between the forcing and damping levels. When the latter of these dominates, the amplitude at which the interaction occurs is not reached, so the system simply exhibits the hardening behaviour seen in the clamped-clamped case. As the interaction region is approached, a damping effect is introduced, increasing the forcing level at which the modal interaction is overcome.

As has already been established, there is a causal link between the BCs and the occurrence of modal interactions, which is captured by the cubic cross-coupling terms that arise in the equations of motion. These terms are defined as part of the Galerkin procedure and are calculated by taking integrals of products of particular derivatives of the mode shapes. By comparing the pinned beam with rotational spring with the unaugmented pinned beam, it is possible to give further insight into this discussion. It has been seen that the ratio $\omega_{n,2}/\omega_{n,1}$ is very similar between the two models, with values of 3.323 and 3.241, respectively. Given that no modal interaction is seen in the classical model, it can be concluded that the modal

ratio alone is not enough to predict an internal resonance. To aid this process, the α and β matrices have been considered, with attention given to the qualitative differences between them. A number of points have been made in §4.3, though chief among these is the observation that, in the classical case, all values of $\alpha_{2,i,j}$ are negative, unless $i = j$.

An updated version of the Galerkin approximation for beams is used to treat complicated BCs in this chapter. Motivated by the need for an accurate methodology to investigate the complex BC interactions that can occur in microscale structures, this procedure assumes that the BC force function can be accurately represented by a Taylor expansion. By doing so, it is possible to reduce the solvability condition to a tensor resultant. The application of this procedure has been illustrated initially through the investigation of a beam with both tips supported by identical, nonlinear springs. Despite its symmetry, the mode shapes of the system are asymmetric. At lower spring stiffnesses, the behaviour of the first mode is qualitatively similar to the spring-supported, rigid beam, whereas the behaviour converges to that of the fully pinned beam at higher stiffness values. This system also introduces an interesting case in which the symmetric structure exhibits similar internal resonance behaviour to that in the aforementioned non-symmetric beams, due to the asymmetry of the mode shapes.

In §4.5.2, this novel method is explored using a cantilever beam with a nonlinear, magnetic BC at the tip. Particular attention has been given to the impact of including the magnetic force in the BC, as opposed to in the equations of motion. This effect has been shown to be significant, changing both the shape and frequencies of vibration. Furthermore, when either the modal basis of the free cantilever or the linear truncation of the magnetic BC was used, the 1:3 modal interaction in the model was not captured. Finally, the importance of these modal interactions has been demonstrated, as higher amplitudes of vibration include modal contribution from the second mode, even when the frequency has moved away from the modal interaction region.

Chapter 5

Non-intrusive reduced-order modelling

In this chapter:

- The Implicit Condensation and Enforced Displacement reduced-order modelling techniques are introduced and assessed.
- The methods are applied to discrete systems to illustrate the differences in their approach, as well as to investigate the trends that arise in their application to a well-defined system.
- A cubic-order Galerkin model is used as a full nonlinear system to examine these trends in a continuous model.
- Higher-order nonlinear terms are then included in both the discrete and the continuous model, allowing the investigation of a case in which the order of the reduced-order model nonlinearities is lower than that of the full model.

5.1 Introduction

In the examples shown up to this point, the nonlinear components of the equation of motion have been well-defined, in that they are simply polynomial expressions in terms of the system displacements. When more complex structures are considered, this is not necessarily the case. The size and intricacy of mesh required to fully capture the physics of the system can lead to a significantly increased number of DOFs. Furthermore, while it is technically possible to use analytical finite element techniques to model such a system, for the most part, this will be prohibitively cumbersome. As such, it can be necessary to utilise bespoke finite

element software to develop the full model. Doing so allows a much simpler treatment of complex mechanical structures, but can require substantial computational expense when fine meshes or large systems are investigated.

As well as this increase in calculation time, there is also another drawback for nonlinear structures, as the full methodology used by commercial finite element software to calculate nonlinear behaviour is, typically, not provided to the user. When the source code of the software is available, it is possible to create an *intrusive* or *direct* ROM, as discussed in Chapter 2. For most commercial software, however, this information is inaccessible and a *non-intrusive* or *indirect* ROM technique is required; a useful overview of such methods is given in [56]. Broadly speaking, these non-intrusive ROM methods use a series of representative, static cases to approximate the nonlinear behaviour as a polynomial in terms of the modal displacements. Given that the evaluation of static cases is commonly available in commercial finite element software these techniques can be used in conjunction with any such programme or nonlinear solver.

The overarching aim of these indirect methods is to find an analytical approximation for the force-amplitude relationship of the structure. It follows that there are two obvious ways in which this can be achieved. Either a known set of displacements can be applied to the structure and the forces can be measured, known as the *Enforced Displacement* (ED) method, or vice versa, known as the *Implicit Condensation* (IC) method. In both methods, the nonlinear component of the ROM is approximated by a cubic-order polynomial. This assumption appears logical because, as shown in the previous chapters of this thesis, it is possible to capture a wide variety of nonlinear structural behaviour with such terms.

An overview of the development and, in particular, the application of these methods has been presented in Chapter 2, but they are more comprehensively defined in §5.2. Typically, the methodology with which commercial packages treat geometrically nonlinear structures is not know by the user. Thus, the purpose of these techniques is to allow this to be approximated using polynomial expressions. However, to further the fundamental understanding of these techniques, this chapter sees their application to analytical systems, so that any uncertainty pertaining to the opaque nature of finite element software is removed. In §5.3, 2- and 3DOF lumped-mass systems with cubic nonlinearities are considered, and this discussion is extended to a Galerkin model in §5.4. In both sets of examples, the order of the nonlinearity is cubic and, therefore, the same as that in the ROMs. Although this provides useful insight,

§5.5 expands these models up to quintic order, so that the ROM techniques are forced to condense the higher-order behaviour in a manner that may more closely mirror the application to software-based models.

Publications resulting from this work

Tartaruga, I., Elliott, A. J., Cammarano, A., , Hill, T. L., and Neild, S. A. (2019). The effect of nonlinear cross-coupling on reduced-order modelling. *International Journal of Non-Linear Mechanics*, 116:7-17.

– This paper applies the IC and ED method to three systems, two of which is discrete, the other is a continuous Galerkin model of a beam structure. This allowed the true values of the nonlinear coefficients to be know and compared to those found using the two ROM techniques. Discussions related to this work are presented throughout this chapter.

5.2 Overview of considered techniques

As mentioned above, the focus of this chapter will be on *indirect* ROM methods, as their compatibility with commercial FE software has led to their wide application across the literature. Namely, the techniques under consideration are the previously-discussed IC and ED methods, both of which apply a series of static cases and use regression analysis to approximate the nonlinear components, as will be outlined in this section.

These methods begin with the assumption that the equations of motion for the system can be written as

$$\mathbf{M}\ddot{\mathbf{x}} + \mathbf{C}\mathbf{x} + \mathbf{K}\mathbf{x} + \mathbf{F}_{\mathrm{NL}}(\mathbf{x}) = \mathbf{F}, \tag{5.1}$$

where, once more, $\mathbf{M}$, $\mathbf{C}$, and $\mathbf{K}$ are the linear mass, damping, and stiffness matrices, respectively. $\mathbf{F}$ is an external force and $\mathbf{F}_{\mathrm{NL}}$ denotes the function defining the nonlinearity of the model, in terms of displacement $\mathbf{x}$. This latter function is defined by the full FE model and, therefore, its form is not necessarily known by the user. As such, it is $\mathbf{F}_{\mathrm{NL}}$ which is approximated in these non-intrusive methods.

In order to allow the size of the model to be reduced, it is important to project the physical equations of motion in Eq. (5.1) onto a modal basis, defining $\mathbf{x} = \mathbf{\Phi q}$. This step is particularly important in the development of ROMs as it is the reduction of the modal basis, $\mathbf{\Phi}$, which allows the model to be reduced. The columns of $\mathbf{\Phi}$ – that is, the individual mode

shapes, ϕ_k – and the corresponding linear natural frequencies, $\omega_{n,k}$, must necessarily solve the eigenvalue problem $(\mathbf{K} - \omega_{n,k}^2\mathbf{M})\phi_k = 0$. The eigenvectors are then mass-normalised, so that $\mathbf{\Phi}^T\mathbf{M}\mathbf{\Phi} = \mathbf{I}$. Now, by implementing the modal projection and premultiplying the expression in Eq. (5.1) by $\mathbf{\Phi}^T$, the modal equations of motion are given by

$$\ddot{\mathbf{q}} + \mathbf{\Lambda}\mathbf{q} + \mathbf{F}_{\text{NL},q}(\mathbf{q}) = \mathbf{F}_q. \tag{5.2}$$

Here, $\mathbf{\Lambda}$ is the mass-normalised, modal stiffness matrix, as defined in Chapter 3 and $\mathbf{F}_{\text{NL},q}$ and $\mathbf{F}_q$ are the modal projections of the nonlinear and external forces, respectively. As with the physical nonlinear force, $\mathbf{F}_{\text{NL},q}$ is not necessarily known, such as in the case where commercial software is used to define the full model. To overcome this issue, it is useful to assume that the function can be accurately approximated by a polynomial, similar to the Taylor expansion applied in §4.5. Therefore, the n^{th} modal equation in Eq. (5.2) is approximated by

$$\ddot{q}_n + \omega_n^2 q_n + \sum_{i=1}^{N}\sum_{j=1}^{N}\sum_{k=1}^{N} A_{ijk}^{(n)} q_i q_j q_k + \sum_{i=1}^{N}\sum_{j=1}^{N} B_{ij}^{(n)} q_i q_j = F_{q,n}, \tag{5.3}$$

where the A and B terms are the coefficients of the cubic and quadratic terms in the expansion, respectively. Further, these coefficients are the only parameters in Eq. (5.3) which are not necessarily defined by the full model. It is at this stage that the aforementioned static cases are applied. In doing so, the $\ddot{q}_n$ term becomes zero, and the q_n and $F_{q,n}$ are simply numerical values, meaning that Eq. (5.3) is reduced to a linear equation in A and B, and each load case gives rise to a system of N such equations. As there are multiple summations in these expressions, the number of unknown coefficients exceeds N. Thus, it is necessary to impose a number of these static cases, so that regression analysis can be applied. In [60], it has been shown that the number of quadratic and cubic coefficients (denoted N_2 and N_3, respectively) are given by

$$\begin{aligned} N_2 &= \begin{cases} 1 & \text{if } N = 1, \\ 3 & \text{if } N = 2, \\ N + \binom{N}{2} & \text{if } N \geq 3, \end{cases} \\ N_3 &= \begin{cases} 1 & \text{if } N = 1, \\ 4 & \text{if } N = 2, \\ N^2 + \binom{N}{3} & \text{if } N \geq 3. \end{cases} \end{aligned} \tag{5.4}$$

The values in Eq. (5.4) represent upper limits to the number of unique coefficients. In fact, it is possible to reduce this number by considering the energy of the system, achieved here through the use of its Lagrangian. This is defined by the function $L = T - U$, where L is the Lagrangian, T is the kinetic energy, and U is the potential energy. Considering Lagrange's equation for the n^{th} mode, given by

$$\frac{d}{dt}\left(\frac{\partial L}{\partial \dot{q}_n}\right) - \frac{\partial L}{\partial q_n} = 0, \tag{5.5}$$

the following equation is obtained

$$\begin{aligned} L = \frac{1}{2}m_1\dot{q}_1^2 + \frac{1}{2}m_2\dot{q}_2^2 - \frac{1}{2}k_1q_1^2 - \frac{1}{2}k_2q_2^2 - \kappa_1q_1^4 - \kappa_2q_2^4 \\ - \lambda_1q_1^3q_2 - \lambda_2q_1q_2^3 - \mu q_1^2q_2^2 - \nu_1q_1^3 - \nu_2q_2^3 - \xi_1q_1^2q_2 - \xi_2q_1q_2^2. \end{aligned} \tag{5.6}$$

Here, the m_n and k_n represent the n^{th} mass and stiffness terms, respectively. The κ, λ, μ, ν, and ξ terms denote the coefficients of the various polynomial terms that arise in the expansion of Lagrange's equation. This expression can be applied, for both modes, in Eq. (5.5). The resulting expressions are then given by

$$m_1\ddot{q}_1 + k_1q_1 + 4\kappa_1q_1^3 + 3\lambda_1q_1^2q_2 + 2\mu q_1q_2^2 + \lambda_2q_2^3 + 3\nu_1q_1^2 + 2\xi_1q_1q_2 + \xi_2q_2^2 = 0, \tag{5.7}$$

$$m_2\ddot{q}_2 + k_2q_2 + \lambda_1q_1^3 + 2\mu q_1^2q_2 + 3\lambda_2q_1q_2^2 + 4\kappa_2q_2^3 + \xi_1q_1^2 + 2\xi_2q_1q_2 + 3\nu_2q_2^2 = 0. \tag{5.8}$$

Comparing these expressions with Eq. (5.3), it is possible to deduce the following relationships between the nonlinear coefficients

$$\begin{gathered} A_{112}^{(1)} = 3A_{111}^{(2)} = 3\lambda_1, \qquad A_{122}^{(1)} = A_{112}^{(2)} = 2\mu, \qquad 3A_{322}^{(1)} = A_{122}^{(2)} = 3\lambda_2, \\ B_{12}^{(1)} = B_{11}^{(2)} = 2\eta_1, \qquad 2B_{22}^{(1)} = B_{12}^{(2)} = 2\eta_2. \end{gathered} \tag{5.9}$$

5.2.1 Reduced-order modelling techniques

The static cases that determine the nonlinear coefficients are defined by linear combinations of the N mode shapes in the ROM basis. In any of these cases, the n^{th} mode can give a contribution of magnitude a_N in either the positive or negative direction, or not be included. Thus, the static case will take the form

$$\sigma = a_1\phi_1 + \cdots + a_N\phi_N. \tag{5.10}$$

Note that σ defines a modal shape, which could either be applied as a force or a displacement, depending on which method is used; this will be further reflected in the definition of the scaling factors, a_k. Now, the number of prescribed static cases can be given by

$$N_{\text{static}} = 3^N - 1, \tag{5.11}$$

where N is the number of modes in the ROM basis. Each of these modes can have either a positive or negative contribution to the static case, or can not be included at all. Thus, the total number of static cases would be 3^N. The negative unit term corresponds to the trivial case in which the contribution of all modes is zero.

At this stage, it is worth verifying that $N_{\text{static}} > N_2 + N_3$; this is easily done using proof by induction. The statement is clearly true for the cases $N = 1, 2$ and is also true for $N = 3$, since

$$(N_2 + N_3)|_{N=3} = 3 + \binom{3}{2} + 3^2 + \binom{3}{3} = 18 \leq 3^3 - 1 = N_{\text{static}}\big|_{N=3}. \tag{5.12}$$

To allow the proof by induction to be continued, it is necessary to assume that, for an arbitrary $k > 3$,

$$(N_2 + N_3)\big|_{N=k} \leq N_{\text{static}}\big|_{N=k}. \tag{5.13}$$

The proof continues by considering these expressions when $N = k + 1$, as follows

$$\begin{aligned}(N_2 + N_3)\big|_{N=k+1} &= (k+1) + \frac{(k+1)!}{2!(k-1)!} + (k+1)^2 + \frac{(k+1)!}{3!(k-2)!} \\ &= (k^2 + k) + 2(k+1) + \frac{(k+1)}{(k-1)}\frac{k!}{2!(k-2)!} + \frac{(k+1)}{(k-2)}\frac{k!}{3!(k-3)!}.\end{aligned} \tag{5.14}$$

Note that, since $k > 3$, it must hold that $2(k+1) < k(k+1)$ and $1 < \frac{(k+1)}{(k-1)}, \frac{(k+1)}{(k-2)} \leq 2$. Therefore, Eq. (5.14) can be developed to give

$$\begin{aligned}(N_2 + N_3)\big|_{N=k+1} \leq& 2\left(k^2 + k + \frac{k!}{2!(k-2)!} + \frac{k!}{3!(k-3)!}\right) \\ &\leq 2(3^k - 1) \leq 3(3^k - 1) + 2 = 3^{(k+1)} - 1 = N_{\text{static}}\big|_{N=k+1},\end{aligned} \tag{5.15}$$

as was required. Thus it can be concluded that defining the static cases in this manner guarantees that there are sufficient terms for the regression analysis. This analysis is discussed in subsequent sections, but it is first necessary to define the IC and ED methods used to create

these static cases.

Implicit condensation

Originally defined in [57], the IC method imposes a set of static, modal forces on the system and records the modal displacement. In this case, the modal shape defined in Eq. (5.10) is applied as a force. In this work, it will be assumed that the contribution of each mode will be equal, so that the force can be written, in physical coordinates, as

$$F = \sum_{k=1}^{N} \frac{C_k}{N_{\text{active}}} \phi_k, \tag{5.16}$$

where N_{active} denotes the number of modes with non-zero contributions to F, and C_k is the scale factor of the k^{th} mode, defined by

$$C_k = \frac{t_R}{\max_{disp}(|\phi_k|)} \omega_k^2. \tag{5.17}$$

Here, t_R is a variable, referential scale factor and $\max_{disp}(|\phi_k|)$ denotes the maximum deflection of the k^{th} mode. This referential scale factor is introduced so that the forcing level can be updated if the displacement does not fall in the desired region, as demonstrated in Fig. 5.1. This is important, as the nonlinear nature of the system means that the process of ensuring a specific displacement can be hampered by the indirect triggering of modes.

Enforced displacement:

The approach of the ED method is very similar to that of the IC technique, but, as suggested in its name, it is modal displacements that are imposed, as opposed to forces. As such, the definition of these displacements closely resembles the form of Eq. (5.16):

$$x = \sum_{k=1}^{N} \frac{C_k}{N_{\text{active}}} \phi_k. \tag{5.18}$$

However, it must be noted that the scale factors, C_k, are now defined by

$$C_k = \frac{t_R}{\max_{disp}(|\phi_k|)}. \tag{5.19}$$

The application of the ED method is summarised in Fig. 5.2.

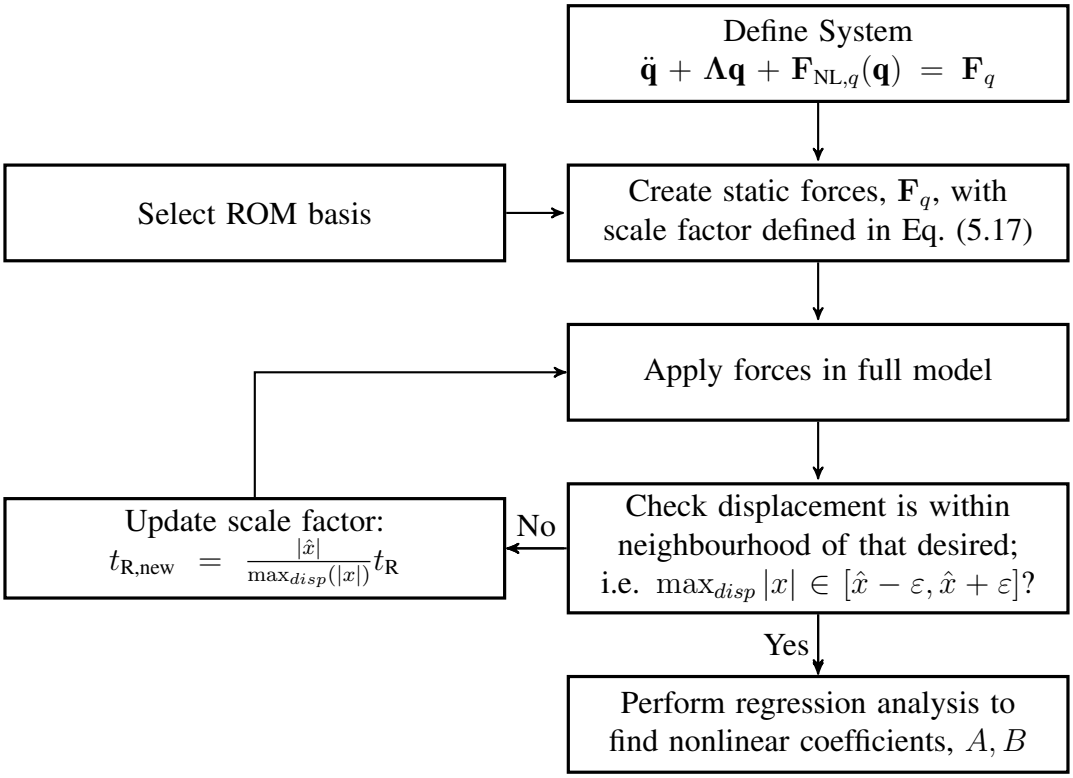

Figure 5.1: Flowchart for the iterative implementation of the IC method.

Therefore, C_k can be more generally written as

$$C_k = \begin{cases} \frac{t_R}{\max_{disp}(|\phi_k|)}\omega_k^2, & \text{for IC,} \\ \frac{t_R}{\max_{disp}(|\phi_k|)}, & \text{for ED,} \end{cases} \tag{5.20}$$

In both methods, the magnitude of these static cases must be carefully selected to obtain accurate values for the nonlinear coefficients. It has been theorised, in [60], that, if the displacements achieved are too low, the nonlinear contributions will not be great enough for the least-squares method to accurately capture the coefficients. However, higher amplitudes may lead to static cases that are unrealistic, in terms of the physical system. Essentially, the static loads must be great enough to trigger the influence of the modal cross-couplings, but without potentially damaging the structure itself. To this end, it is useful to follow the rule of thumb proposed in [60], which suggests that "a displacement of one panel thickness is sufficient for the primary modes to become nonlinear". The first of the aforementioned points is naturally guaranteed in the ED method, regardless of the displacement, though this is not necessarily the case for the IC technique. To achieve this, t_R can be iteratively adapted so that the displacement is within some neighbourhood of this value, as can be noted in Fig. 5.1.

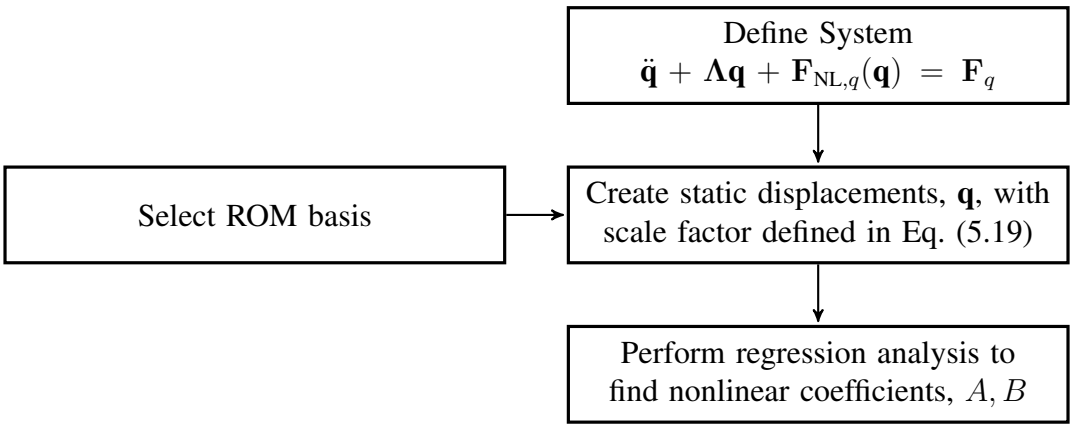

Figure 5.2: Flowchart for the iterative implementation of the IC method.

5.3 Application to a discrete system

To investigate the application of these techniques, it is useful to first consider a discrete system, in which the nonlinearities are known exactly. This initial step will allow the results of these non-intrusive methods to be considered without the uncertainty introduced through the use of commercial FE software. The system in question is shown in Fig. 5.3. The structure comprises three identical lumped masses, m, connected by springs with linear stiffness component k; such springs also ground the first and third masses. Nonlinearity is introduced to the system through the inclusion of cubic stiffnesses, k_{NL}, in the first two springs.

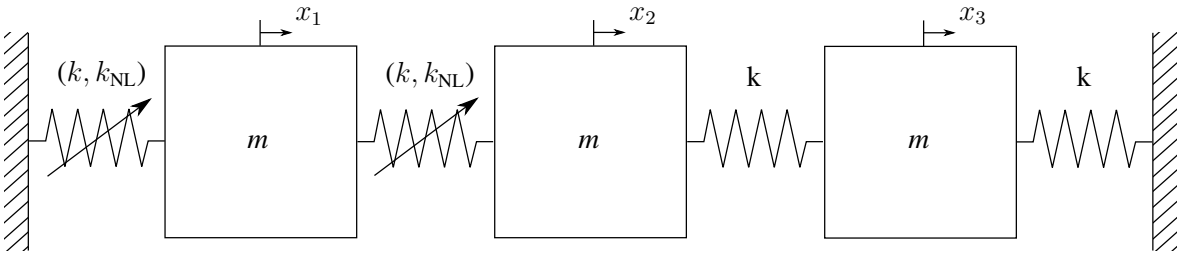

Figure 5.3: Schematic of a 3DOF mass-spring system with nonlinear springs grounding the first mass and connecting the first two.

The physical equations of motion for this system are of the form given in Eq. (5.1), with the various matrices defined by

$$\mathbf{M} = \begin{pmatrix} m & 0 & 0 \\ 0 & m & 0 \\ 0 & 0 & m \end{pmatrix}, \quad \mathbf{K} = \begin{pmatrix} 2k & -k & 0 \\ -k & 2k & -k \\ 0 & -k & 2k \end{pmatrix}, \quad \mathbf{F}_{\mathrm{NL}}(\mathbf{x}) = k_{\mathrm{NL}} \begin{pmatrix} (x_2 - x_1)^3 \\ -x_2^3 \\ 0 \end{pmatrix}. \tag{5.21}$$

As in §5.2, the system can be expressed in modal coordinates, giving the equations of motion

in Eq. (5.2). For the present system, the mass-normalised matrices are given by

$$\begin{aligned}\mathbf{\Lambda} &= \frac{1}{\sqrt{m}}\begin{pmatrix}\sqrt{(2-\sqrt{2})k} & 0 & 0\\ 0 & \sqrt{2k} & 0\\ 0 & 0 & \sqrt{(2+\sqrt{2})k}\end{pmatrix} = \begin{pmatrix}\omega_{n,1}^2 & 0 & 0\\ 0 & \omega_{n,2}^2 & 0\\ 0 & 0 & \omega_{n,3}^2\end{pmatrix},\\ \mathbf{\Phi} &= \frac{1}{\sqrt{2m}}\begin{pmatrix}\frac{1}{\sqrt{2}} & 1 & \frac{1}{\sqrt{2}}\\ 1 & 0 & -1\\ \frac{1}{\sqrt{2}} & -1 & \frac{1}{\sqrt{2}}\end{pmatrix},\end{aligned} \tag{5.22}$$

The full form of the nonlinear term, $\mathbf{F}_{\text{NL,q}} = \mathbf{\Phi}^T\mathbf{F}_{\text{NL}}$, is not shown here, but can be expressed as

$$\mathbf{F}_{\text{NL,q}} = \begin{pmatrix}\sum\limits_{\rho_i+\rho_j+\rho_k=3} A^{(1)}_{\rho_i\rho_j\rho_k} q_i^{\rho_i} q_j^{\rho_j} q_k^{\rho_k}\\ \sum\limits_{\rho_i+\rho_j+\rho_k=3} A^{(2)}_{\rho_i\rho_j\rho_k} q_i^{\rho_i} q_j^{\rho_j} q_k^{\rho_k}\\ \sum\limits_{\rho_i+\rho_j+\rho_k=3} A^{(3)}_{\rho_i\rho_j\rho_k} q_i^{\rho_i} q_j^{\rho_j} q_k^{\rho_k}\end{pmatrix}, \tag{5.23}$$

where ρ_i denotes the exponent of q_i in a particular nonlinear term and $\sum\limits_{\rho_i+\rho_j+\rho_k=3}$ denotes the summation of any terms in which $\rho_i + \rho_j + \rho_k = 3$. Implementing the matrix definitions in Eqs. (5.22) and (5.23) in this way, the static case in the IC and ED methods can now be written as

$$\omega_1^2 q_1 + \sum_{\rho_i+\rho_j+\rho_k=3} A^{(1)}_{\rho_i\rho_j\rho_k} q_i^{\rho_i} q_j^{\rho_j} q_k^{\rho_k} = F_{q,1}, \tag{5.24}$$

$$\omega_2^2 q_2 + \sum_{\rho_i+\rho_j+\rho_k=3} A^{(2)}_{\rho_i\rho_j\rho_k} q_i^{\rho_i} q_j^{\rho_j} q_k^{\rho_k} = F_{q,2}, \tag{5.25}$$

$$\omega_3^2 q_3 + \sum_{\rho_i+\rho_j+\rho_k=3} A^{(3)}_{\rho_i\rho_j\rho_k} q_i^{\rho_i} q_j^{\rho_j} q_k^{\rho_k} = F_{q,3}. \tag{5.26}$$

Considering this example in more general terms, these equations represent the full model, which would typically be calculated using FE software. Treating Eqs. (5.24-5.26), a number of sets of $\mathbf{q}$ and $\mathbf{F}_q$ will be applied, so that a ROM can be created. If a SDOF ROM were desired, it would be written in the form

$$\ddot{\tilde{q}}_1 + \omega_1^2\tilde{q}_1 + \tilde{A}^{(1)}_{300}\tilde{q}_1^3 = \tilde{F}_{q,1}, \tag{5.27}$$

where the notation $\tilde{\bullet}$ is used to highlight the approximate nature of the ROM; the static case is found by simply removing the $\ddot{\tilde{q}}_1$ term. This equation can be used to investigate the two non-intrusive methods considered in this chapter. In the ED method, a SDOF model will

result in static displacements of the form $\mathbf{q} = [\hat{q},\ 0,\ 0]^T$. Applying this displacement in Eq. (5.27) leads to the specific static case

$$\omega_1^2 \hat{q} + A_{300}^{(1)} \hat{q}^3 = F_{q,1}. \tag{5.28}$$

Comparing this expression with the static form of Eq. (5.27), it can be seen that the forms of both are identical. Therefore, if the displacement and force from the full static case are applied in the ROM static case, it can be concluded that $\tilde{A}_{300}^{(1)} = A_{300}^{(1)}$. Thus, in the correct implementation of the ED method in this model, there should be no variation in the nonlinear coefficients if the scale factor is varied.

The IC method prescribes a set of static modal forces, as opposed to displacements. Therefore, each static force will be of the form $\mathbf{F}_q = [\hat{F},\ 0,\ 0]^T$. Noting that this system is weakly nonlinear, it can be assumed that $A_{0\rho_j\rho_k}^{(n)} \approx A_{1\rho_j\rho_k}^{(n)} \approx 0$. That is, for any cubic term in which $\rho_1 = 0$ or 1, it holds that $\rho_2 + \rho_3 \in \{2, 3\}$. This term will be negligible due to the small nature of q_2 and q_3. As such, the static cases will now take the form

$$\omega_1^2 q_1 + A_{300}^{(1)} q_1^3 + A_{210}^{(1)} q_1^2 q_2 + A_{201}^{(1)} q_1^2 q_3 = \hat{F}, \tag{5.29}$$

$$\omega_2^2 q_2 + A_{300}^{(2)} q_1^3 + A_{210}^{(2)} q_1^2 q_2 + A_{201}^{(2)} q_1^2 q_3 = 0, \tag{5.30}$$

$$\omega_3^2 q_3 + A_{300}^{(3)} q_1^3 + A_{210}^{(3)} q_1^2 q_2 + A_{201}^{(3)} q_1^2 q_3 = 0. \tag{5.31}$$

Eqs. (5.30) and (5.31) can be solved as a separate system to give q_2 and q_3 in terms of q_1. Further, if these displacements and forces are applied in the ROM, it is possible to approximate $\tilde{A}_{300}^{(1)}$ as

$$\begin{aligned}\tilde{A}_{300}^{(1)} \approx A_{300}^{(1)} &- \frac{A_{210}^{(1)} A_{300}^{(2)} q_1^2}{A_{210}^{(2)} q_1^2 + \omega_{n,2}^2} \\ &+ \frac{q_1^2 (A_{210}^{(1)} A_{201}^{(2)} q_1^2 - A_{201}^{(1)} (A_{210}^{(2)} + \omega_{n,2}^2))(-A_{300}^{(2)} A_{210}^{(3)} q_1^2 + A_{300}^{(3)} (A_{210}^{(2)} + \omega_{n,2}^2))}{(A_{210}^{(2)} q_1^2 + \omega_{n,2}^2)((A_{210}^{(2)} q_1^2 + \omega_{n,2}^2)(A_{201}^{(3)} q_1^2 + \omega_{n,3}^2) - A_{201}^{(2)} A_{210}^{(3)} q_1^4)}.\end{aligned} \tag{5.32}$$

It can be seen, in Eq. (5.32), that any term containing $A_{0\rho_j\rho_k}^{(n)}$ or $A_{1\rho_j\rho_k}^{(n)}$ has been omitted. This approximation is compared with the true IC coefficients, as well as the ED coefficients, in Fig. 5.4. It can be seen that the approximation is accurate across the considered region of C_1, so it can be concluded that, if the static cases are too large, the IC will give an inaccurate prediction of the nonlinear coefficients. Further, this figure confirms the invariant nature of

the ED coefficients.

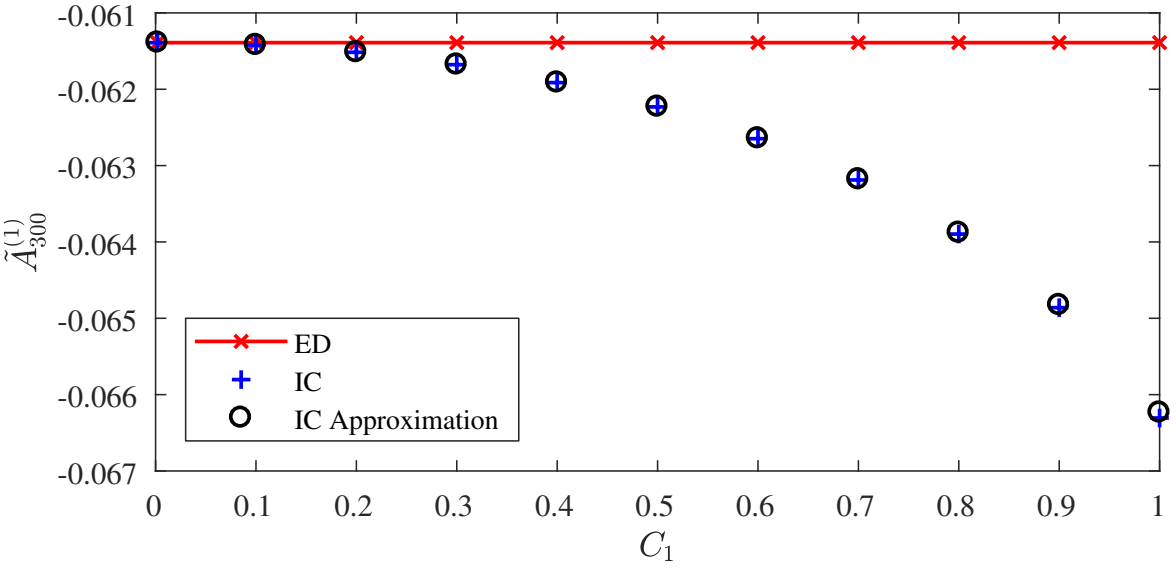

Figure 5.4: Calculated values for the first coefficient using the ED and IC method, as well as using the IC approximation.

The discussion in this section alludes to an inherent difference between the IC and ED methods. Namely, in the IC method, the ROM for the 3DOF system is highly dependent on the maximum displacement permitted, whereas this is not the case in the equivalent ED model. This can be attributed to the calculation of the modal displacements and the condensation of membrane effects in the IC technique. For the ED method, it is the displacements that are prescribed, so that the only active modes are those in the ROM, and in-plane deflections are not included. However, for the IC method, applying a modal force can trigger the deflection of modes which are not directly forced, due to modal coupling. While this may appear prohibitive in this case, it may be useful for cases in which the exact nature of the nonlinearity is unknown.

The influence of these differences on the 3DOF system can be seen in Fig. 5.5, in which the backbone curves for a number of IC ROMs are compared with those of the ED ROM and the full model. As expected from the nonlinear coefficients, the ED method produces a curve which remains close to the full model in a close neighbourhood of the linear natural frequency, though begins to diverge at $\sim$0.9 Hz, as the influence of the coupled modes becomes more prominent. For lower scale factors (given in the legend), the IC backbone curves remain close to the ED model. However, it can be seen that, as this factor is increased, there is a rapid divergence from the correct behaviour, with higher scale factors incorrectly predicting a softening nonlinearity. The second panel of Fig. 5.5 provides an interesting discussion point with regard to the judgement of accuracy in ROMs. As has been

mentioned, the coefficients diverge from the $A_{30}^{(1)}$ at higher amplitudes, as forcing one mode can trigger the displacement of others. This influence is now reflected in the backbone curve. For a maximum displacement of 0.7, it can be seen that the predicted backbone curve actually diverges at a later point. Although the region in which the backbone is captured exactly (up to a certain tolerance) is reduced in the IC method, the overall region in which it predicts a reasonable prediction of the response is expanded.

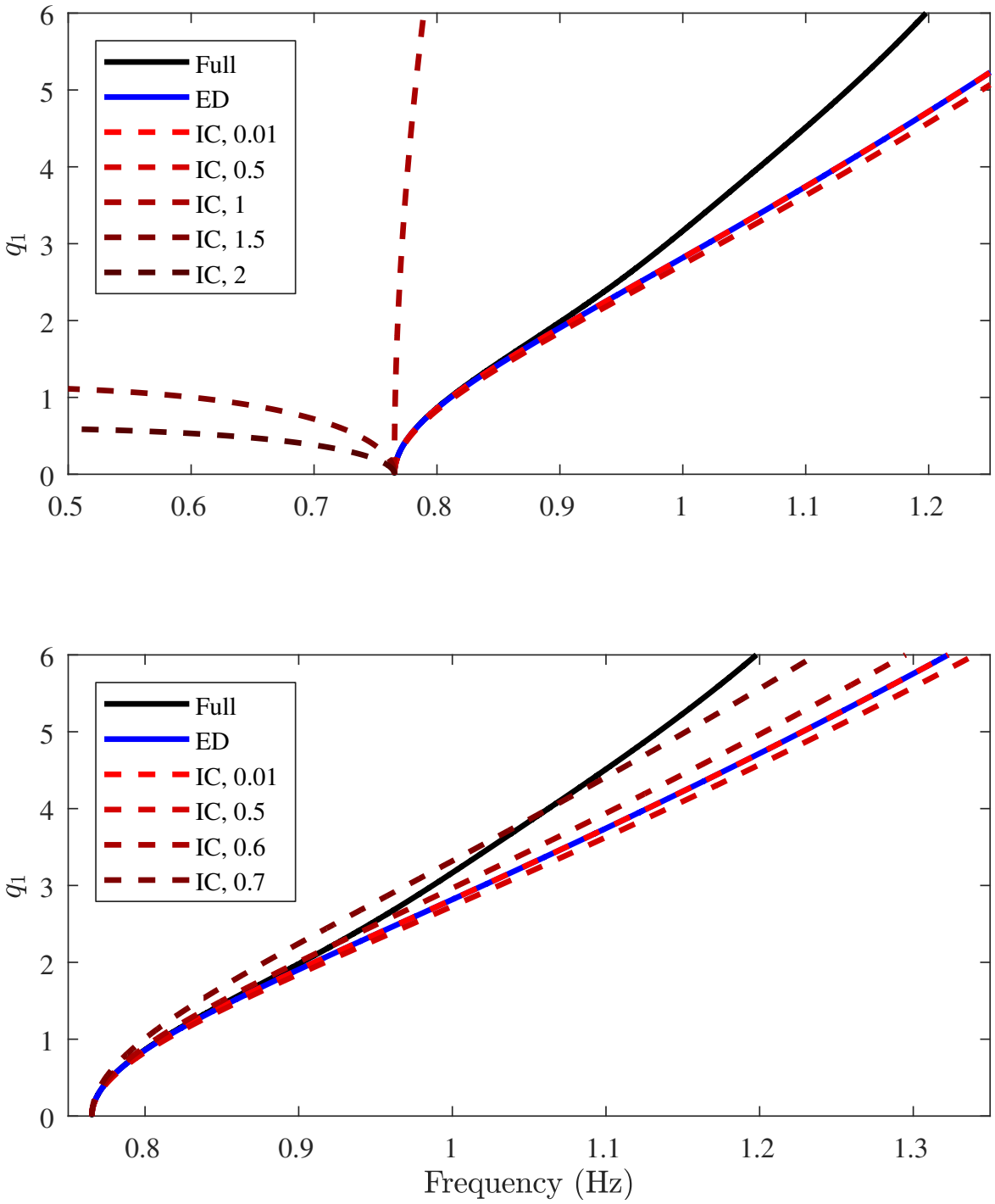

Figure 5.5: Backbone curves for the 3DOF spring-mass model, generated using the full model, as well as with the IC and ED methods.

To further investigate this behaviour, it is useful to consider the same system, but with only

two masses. In this case, the approximation for the IC coefficient is given by

$$\tilde{A}_{30}^{(1)} \approx A_{30}^{(1)} - \frac{A_{21}^{(1)} A_{30}^{(2)} q_1^2}{A_{21}^{(2)} q_1^2}. \tag{5.33}$$

It can be seen that this is similar to the corresponding expression in the 3DOF model – as presented in Eq. (5.32) – but without the complicated final term. The relative simplicity of this expression leads to reduced variation in the coefficients of the system for higher scale factors, as is reflected in the backbone curves displayed in Fig. 5.6. This decreased difference suggests that the addition of the third mass strengthens the coupling of the modes.

In the inset plot in Fig. 5.6, it can be seen that, at lower amplitudes, the IC model created with a scale factor of 1 actually remains closer to the true solution than the ED model. This highlights the fact that the IC method has greater potential to capture the influence of modal couplings, which is particularly important for those systems in which the exact nature of the nonlinearity is not known *a priori*.

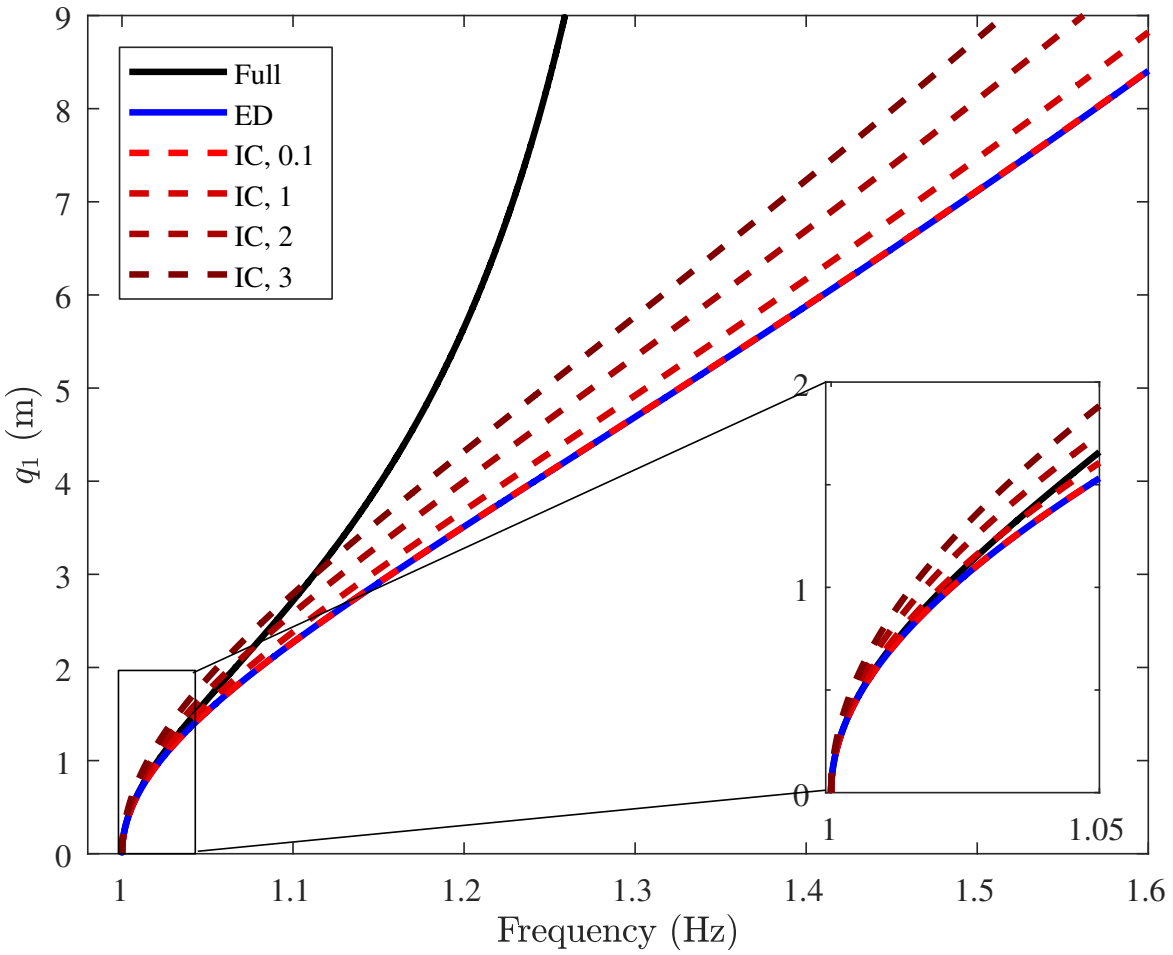

Figure 5.6: Backbone curves for the 2DOF spring-mass model, generated using the full model, as well as with the IC and ED methods.

5.4 Continuous systems

Although the theoretical example in §5.3 provides useful insight into the mechanisms of these techniques, the true motivation for their use is the ability to reduce the order of complex, continuous models. As has been discussed earlier in this chapter, this approach is typically applied using commercial FE software, meaning that the treatment of nonlinearities can not be directly assessed. Although there have undoubtedly been interesting results using this methodology, this section looks to bridge the gap between these studies and the knowledge obtained for the discrete system above, allowing the IC and ED methods to be applied to a more complex system. To do so, the Galerkin method, discussed in the previous chapter, will be used as the "full" model[1].

Of particular interest is the ability of the IC and ED methods to accurately predict and capture internal resonances between the modes. The motivation for this is that, if they are unable to accurately model this type of behaviour for systems in which the nonlinearity is completely understood, it is difficult to place a great deal of confidence in those models developed using commercial software. To this end, the relatively simple pinned-pinned beam model with an asymmetric rotational spring configuration at the tips (see §4.3.1) will be used, due to the 1:3 modal interactions that occur.

As with the discrete case, initial consideration is given to the calculation of the coefficients for a range of scale factors. The process is identical to that of the previous section and is not repeated; the results are displayed in Fig. 5.7. It can be seen that the trends are similar to those in the mass-spring system. In particular, the ED method coefficients are invariant to changes in the static displacement. However, at higher amplitudes the IC diverges from the correct solution as modes not included in the modal basis are triggered. It can further noted that, for static displacements higher than 10^{-3} m, there is minimal variation in the calculated value of the coefficient.

As demonstrated in Fig. 4.6, it is modes 1, 2, and 4 that are involved in the internal resonance behaviour of this system. The influence that these modes have on the ROM is investigated, for both techniques, in Fig. 5.8. Here, the single-thickness rule of thumb from [60] is used in each case. Naturally, the single-mode ROM is unable to capture the modal interaction. Interestingly, the addition of the second mode to the modal basis is not sufficient to fully

[1]Recall that this "full" model is technically still a truncated version of the infinite system defined by the Galerkin approximation.

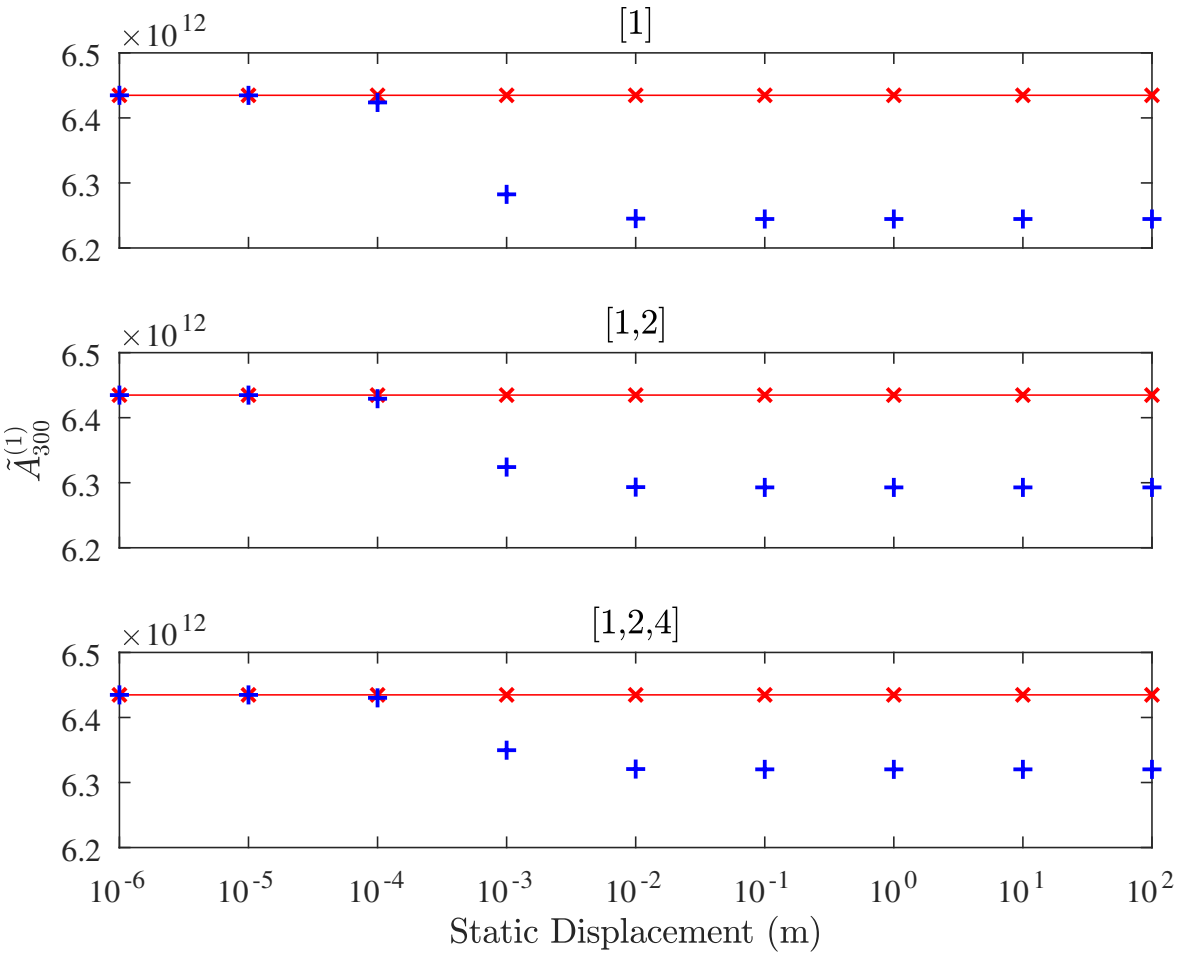

Figure 5.7: Calculated values for the first coefficient using the ED and IC method. The red line denotes the invariant value obtained using the ED method, with the red crosses being specific comparison points. The blue plus symbols denote values from the IC method.

capture the modal interaction tongue. The true behaviour is only successfully encapsulated once the fourth mode is included. The reason for this is that there is a second 1:3 modal interaction between modes 2 and 4. As such, this transfer of energy can not be captured by the modal basis [1,2]. This behaviour is, arguably, more readily observed through the consideration of Fig. 5.8, as opposed to Fig. 4.6.

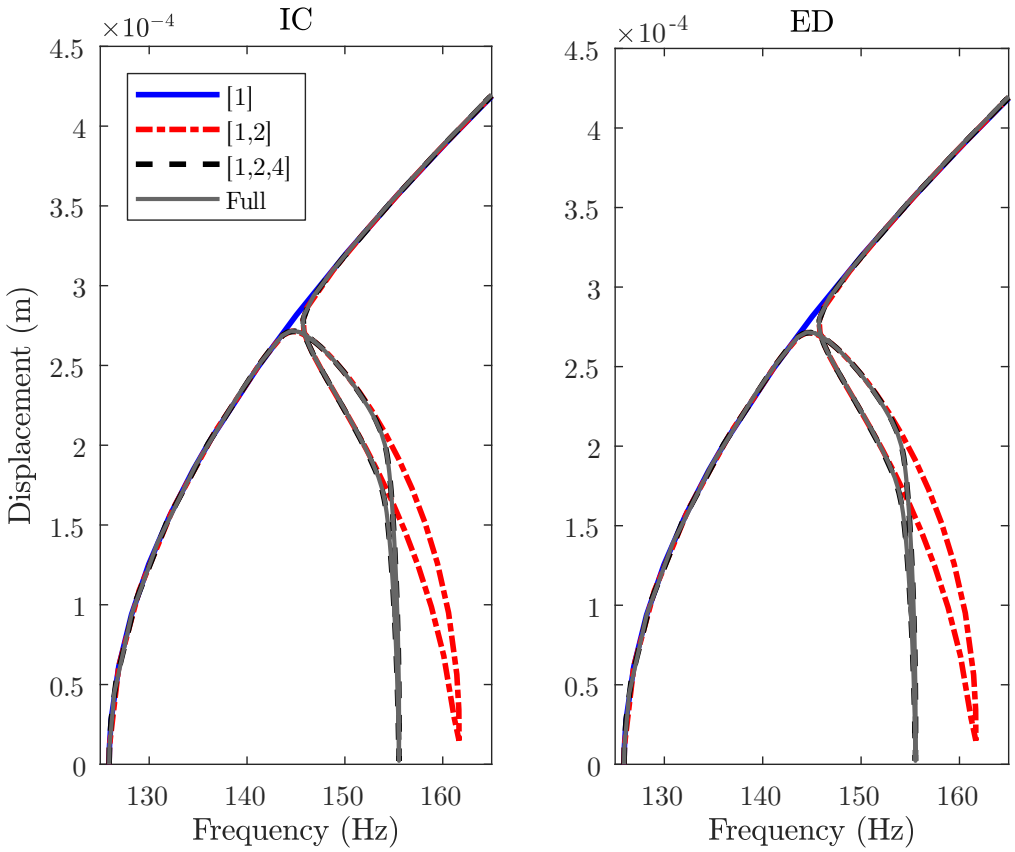

Figure 5.8: Variation in the first backbone curve for the beam with changes in the number of modes in the ROM in the (a) IC and (b) ED methods.

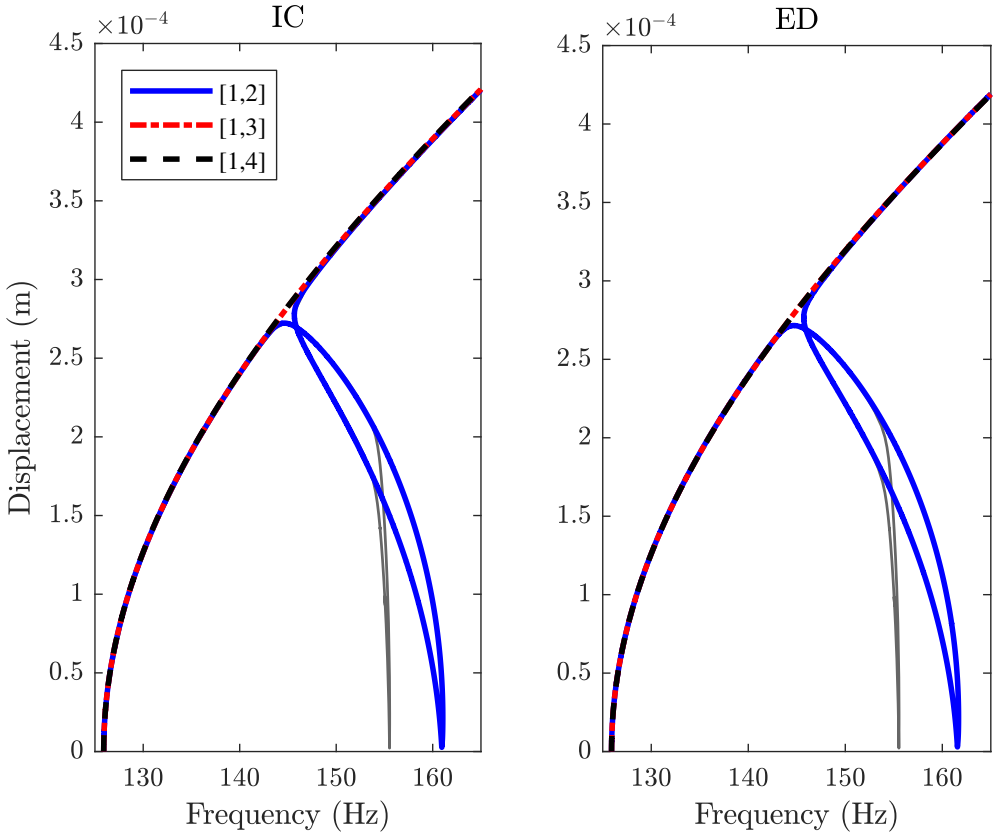

Figure 5.9: Variation in the first backbone curve for the beam with changes in the second mode selected for the ROM in the (a) IC and (b) ED methods.

This discussion is further investigated in Fig. 5.9, in which all three ROMs include the first mode and one other mode. As expected, the only model capable of capturing the internal resonance behaviour is the model including both of the first two modes. This confirms the fact that energy can not be directly transferred from mode 1 to mode 4 without the intermediary energy transfer between modes 1 and 2.

In addition, a visual representation of the ED cubic coefficients is given in Fig. 5.10, so that the trends can be more easily explored. The left column of this figure displays the full matrix, as it is applied in the ROM, whereas the right column shows the absolute value of this matrix so that the relative magnitude of the coefficients can be compared.

Perhaps the most intriguing behaviour is found in the [1,3] model, in which it can be seen that there are no negative coefficient values, in stark contrast to the other two ROMs. The reason for this is not immediately clear, though it is likely to be related to the fact that there is no way in which energy can be transferred from mode 1 to mode 3. In these models, there is an alternating pattern of positive and negative values between adjacent coefficients. Interestingly, considering Fig. 5.9, it can be seen that there is negligible difference between ROMs [1,3] and [1,4], despite this contrast. What is consistent across these models is the value of $A_{30}^{(1)}$, once more highlighting the fact that only the accuracy of this leading coefficient is important for modelling the main tongue.

Considering solely the left column, the qualitative similarity of the [1,2] and [1,4] matrices might suggest that the backbone curves from these ROMs would be similar. However, this trend is less true in the right hand column, though there are some similarities. The variation in the magnitude of the coefficients is more pronounced in the latter of these, and there is also some change in the relative magnitudes of the coefficients. For instance, $A_{21}^{(1)}$ and $A_{03}^{(1)}$ are of similar magnitudes in the first ROM, but this is not true when mode 4 is used in place of mode 2. This demonstrates the fact that these ROM methods adapt the coefficients in an attempt to fully capture the system behaviour, but are unable to do so when the relevant modes are not included.

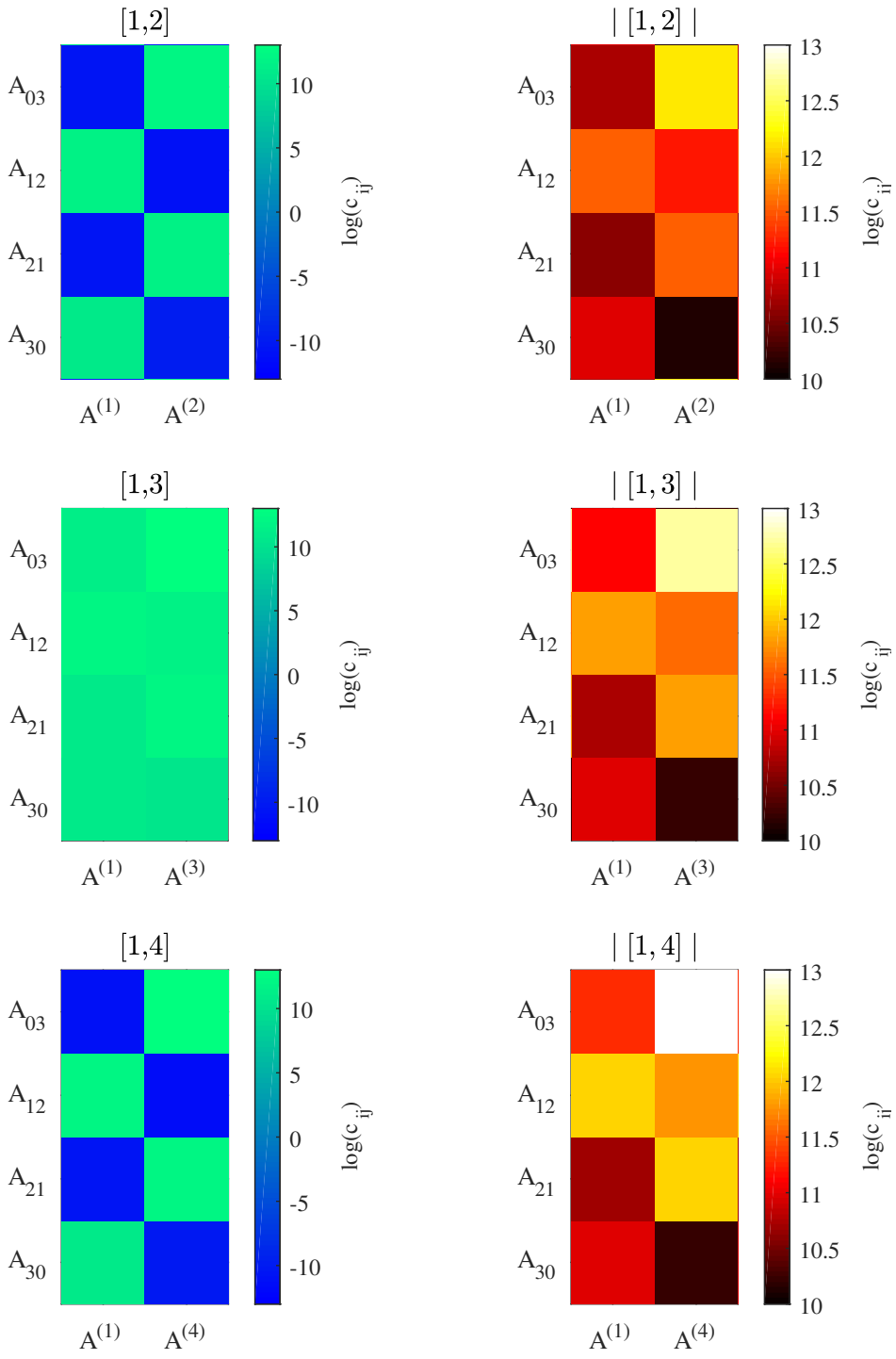

Figure 5.10: Graphic representation of the value (left column) and magnitude (right column) of the nonlinear coefficients for two-mode ROMs.

5.5 Application to higher-order systems

At this point, it is important to note that both models considered have only included nonlinearities up to the cubic order. The motivating factor for this decision is that it simplifies the model and provides a theoretical ideal to test the full capabilities of the techniques, even though it is highly unlikely that these exact results will occur in more complex models. With this in mind, the current section will use an expanded model with higher-order nonlinear terms. Although this expansion does not necessarily provide a perfect parallel to the nonlinear solvers found in commercial FE software, it will still offer an initial insight into the capabilities of the two ROM methods to condense higher-order behaviour in their quadratic and cubic terms.

5.5.1 Higher-order discrete system

The most simple implementation of higher-order terms can be achieved by introducing quintic terms to the nonlinear springs in the discrete system in §5.3. As such, the nonlinear force term will be refined as

$$\mathbf{F}_{\mathrm{NL}}(\mathbf{x}) = k_3 \begin{pmatrix} (x_2 - x_1)^3 \\ -x_2^3 \\ 0 \end{pmatrix} + k_5 \begin{pmatrix} (x_2 - x_1)^5 \\ -x_2^5 \\ 0 \end{pmatrix}, \tag{5.34}$$

where k_3 and k_5 are constant coefficients. As in the lower-order example, these will be projected onto the modal basis to give

$$\mathbf{F}_{\mathrm{NL,q}} = \begin{pmatrix} \sum_{\rho_i+\rho_j+\rho_k=3} R^{(1)}_{\rho_i\rho_j\rho_k} q_i^{\rho_i} q_j^{\rho_j} q_k^{\rho_k} + \sum_{\rho_i+\rho_j+\rho_k+\rho_l+\rho_m=5} S^{(1)}_{\rho_i\rho_j\rho_k\rho_l\rho_m} q_i^{\rho_i} q_j^{\rho_j} q_k^{\rho_k} q_l^{\rho_l} q_m^{\rho_m} \\ \sum_{\rho_i+\rho_j+\rho_k=3} R^{(2)}_{\rho_i\rho_j\rho_k} q_i^{\rho_i} q_j^{\rho_j} q_k^{\rho_k} + \sum_{\rho_i+\rho_j+\rho_k+\rho_l+\rho_m=5} S^{(2)}_{\rho_i\rho_j\rho_k\rho_l\rho_m} q_i^{\rho_i} q_j^{\rho_j} q_k^{\rho_k} q_l^{\rho_l} q_m^{\rho_m} \\ \sum_{\rho_i+\rho_j+\rho_k=3} R^{(3)}_{\rho_i\rho_j\rho_k} q_i^{\rho_i} q_j^{\rho_j} q_k^{\rho_k} + \sum_{\rho_i+\rho_j+\rho_k+\rho_l+\rho_m=5} S^{(3)}_{\rho_i\rho_j\rho_k\rho_l\rho_m} q_i^{\rho_i} q_j^{\rho_j} q_k^{\rho_k} q_l^{\rho_l} q_m^{\rho_m} \end{pmatrix}, \tag{5.35}$$

where the R and S coefficients arise in the conversion to modal coordinates.

It is now possible to examine the calculation of coefficients at varying maximum static displacements. The results from doing so are presented in Fig. 5.11. In this figure, the system has the same parameter values as the cubic model, with the values chosen for the newly-introduced nonlinear coefficient given in the title of the figure panels. While the

coefficients of the ED method were previously invariant to changes in the static displacement, it can be seen that this is no longer the case. Now, as the displacement is increased, the magnitude of the cubic coefficient also increases to account for the additional nonlinear stiffness introduced by the quintic term.

The trend is similar for the IC results, though the difference between these and the lower-order model results is much less significant than for the ED method. This can be explained by the fact that the IC coefficients are influenced not only by the $S^{(n)}_{11111}q_1^5$ term introduced (as is the case for the ED technique), but also by the aforementioned triggering of multiple modal displacement from a single modal force. This similarity not only explains why the IC coefficients diverge at a higher rate than the corresponding ED values, but also suggests that it is the coupling of modes by the lower-order nonlinear terms which has the greater influence on the definition of the IC ROM.

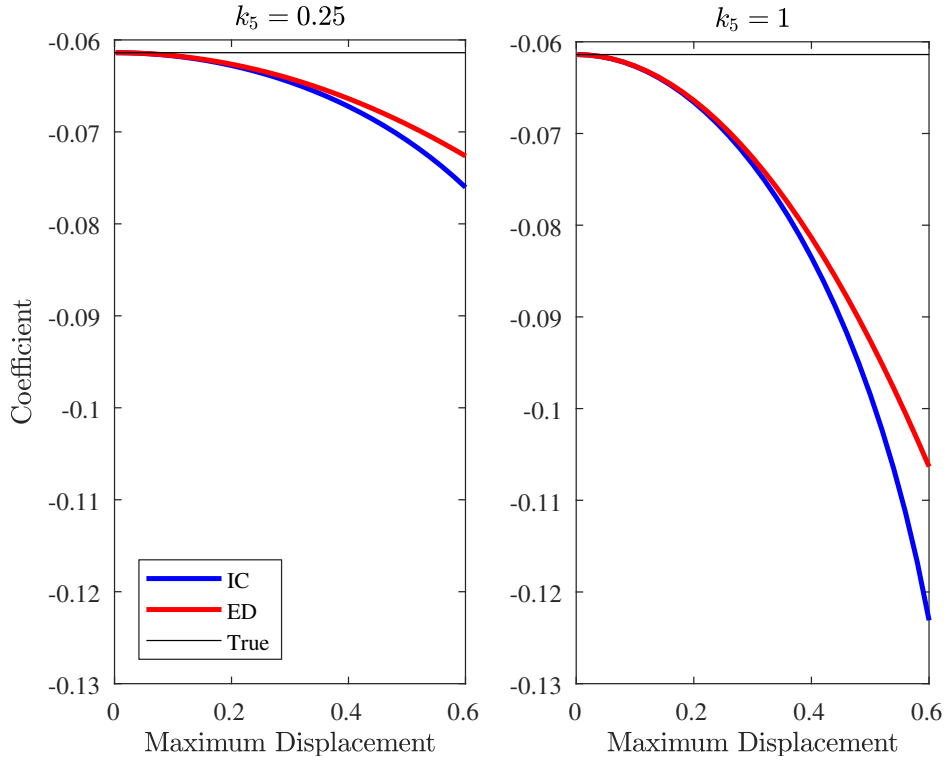

Figure 5.11: Variations in the coefficients approximated by the IC and ED methods for a 3DOF mass-spring system with cubic and quintic nonlinearities.

The backbone curves of the SDOF ROMs when $k_5 = 1$ are shown in Fig. 5.12. The stiffening behaviour of these curves mirrors the increasing magnitude of the cubic coefficient seen in Fig. 5.11. In particular, the rate at which this shift takes place is slightly higher for the IC method. At the base of the backbone curves, the approximation of the full model behaviour is accurately approximated by both methods, though there is some variation in the frequency interval in which this is true. In the cubic model, at lower amplitudes, the ROM curves

remained close to the full solution, before diverging as the frequency increases. In the higher-displacement ROMs, there is a similar behaviour, but with a more rapid rate of divergence. However, the curve then intersects that of the full model once more at a higher frequency; beyond this point, the models will again diverge.

At this point, it is useful to consider the manner in which these backbone curves are assessed. The decreased rate of divergence in the cubic model leads to an initial frequency range over which the ROM could be considered 'exact' to some very small tolerance. This is not true of the faster divergence in the quintic model. However, if this tolerance was increased, the interval in which the quintic model ROM is considered accurate is greater than in the cubic case, due to the fact that the curves intersect at a higher frequency. This second example better illustrates the more realistic scenario in which higher-order nonlinear attributes are condensed into the quadratic and cubic ROM terms.

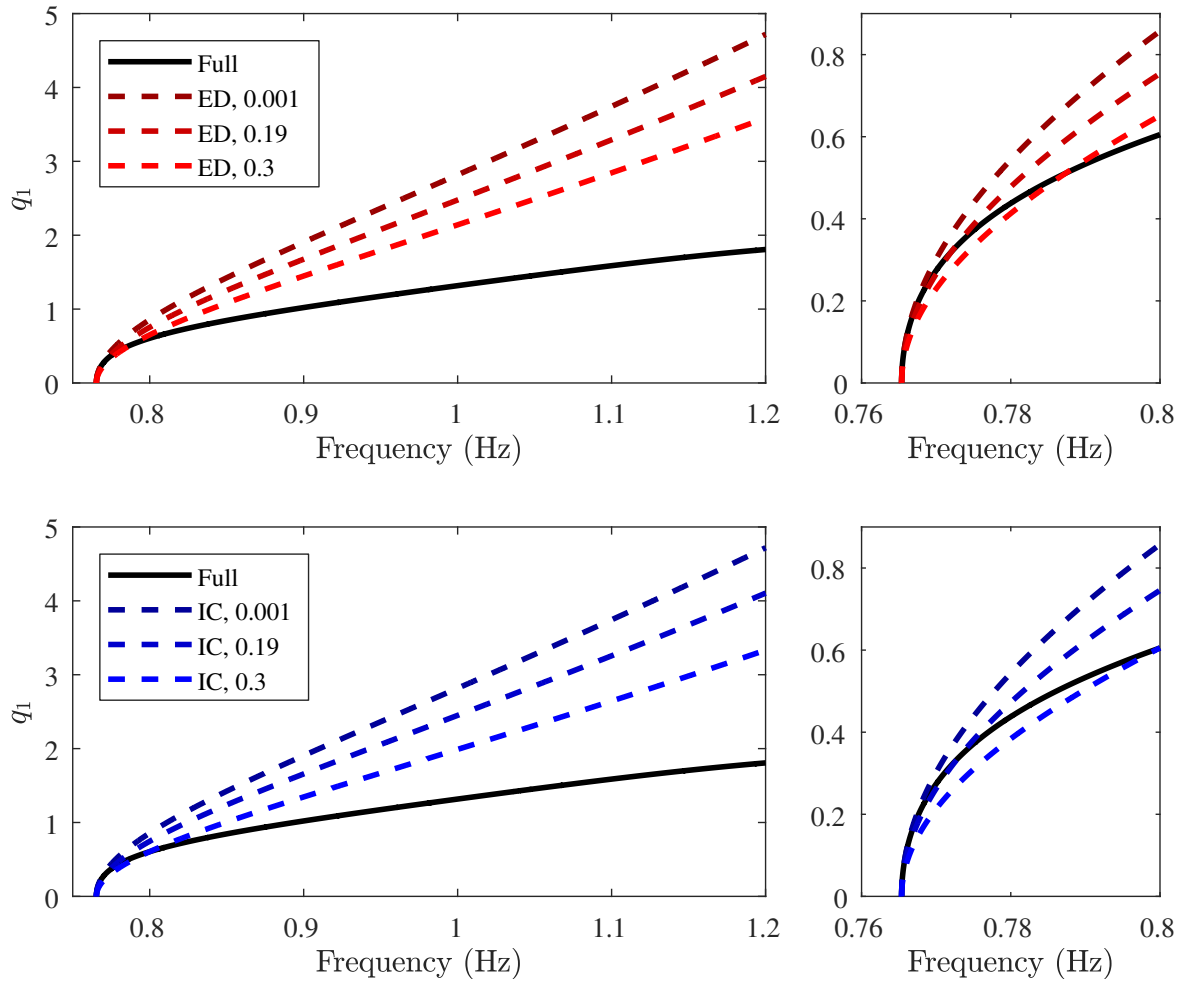

Figure 5.12: Backbone curves for the 3DOF spring-mass model, generated using the full model, as well as with the IC and ED methods.

5.5.2 Higher-order Galerkin model

In this section, the same beam configuration as above will be used here, but with the Taylor expansion in Eq. (4.13) now expanded to give

$$L \approx \int_0^\ell 1 + \frac{1}{2}\left(\frac{\partial w}{\partial x}\right)^2 - \frac{1}{8}\left(\frac{\partial w}{\partial x}\right)^4 \mathrm{d}x = \ell + \frac{1}{2}\int_0^\ell \left(\frac{\partial w}{\partial x}\right)^2 - \frac{1}{8}\int_0^\ell \left(\frac{\partial w}{\partial x}\right)^4 \mathrm{d}x. \quad (5.36)$$

Thus, the higher-order tension force is given by

$$T = E\hat{A}\frac{(L-\ell)}{\ell} = \frac{E\hat{A}}{2\ell}\int_0^\ell \left(\frac{\partial w}{\partial x}\right)^2 \mathrm{d}x - \frac{E\hat{A}}{8\ell}\int_0^\ell \left(\frac{\partial w}{\partial x}\right)^4 \mathrm{d}x. \quad (5.37)$$

The full Galerkin model is developed in the same way as in §4.2.3, so is not repeated here. The final form of the model is now given by

$$\begin{aligned}\ddot{q}_n + \frac{EI\alpha_{4,n}}{\rho\hat{A}\ell}q_n - \frac{E}{2\rho\ell^2}\sum_{i=1}^{N}\sum_{j=1}^{N}\sum_{k=1}^{N}\alpha_{2,k,n}\beta_{i,j}q_iq_jq_k \\ + \frac{E}{8\rho\ell^2}\sum_{i=1}^{N}\sum_{j=1}^{N}\sum_{k=1}^{N}\sum_{l=1}^{N}\sum_{m=1}^{N}\alpha_{2,m,n}\gamma_{i,j,k,l}q_iq_jq_kq_lq_m = 0,\end{aligned} \quad (5.38)$$

where

$$\gamma_{i,j,k,l} = \int_0^\ell \frac{d\phi_i}{dx}\frac{d\phi_j}{dx}\frac{d\phi_k}{dx}\frac{d\phi_l}{dx}\mathrm{d}x. \quad (5.39)$$

Although the scope of this model has now been expanded, the number of terms and, hence, the computational expense have also been dramatically increased. For the 19-mode "full" model considered previously, there are now $19^5 = 2,476,099$ possible values for $\alpha_{2,m,n}\gamma_{i,j,k,l}$. As such, it is useful to address the way in which these quintic terms are implemented. For the newly-defined cross-coupling term, $\gamma_{i,j,k,l}$, the value is equal for any permutation of the set $I = \{i, j, k, l\}$. Therefore, for any fixed index, m, there are potentially $4! = 24$ coefficients which will contribute to the coefficient of $q_iq_jq_kq_lq_m$. When it is further noted that this m could also be one of the indices of γ, it can be seen that there is a great deal of repetition in the definition of the quintic coefficients.

To simplify this, it is useful to calculate a single coefficient for any quintic product of modal displacements. Consider the set of indices $J = \{i, j, k, l, m\}$. Then, considering the possible combinations discussed above, the coefficient for $\prod_{x\in J} q_x$ can be defined by

$$\eta_J = \sum_{x \in J} \frac{4!}{(N_{J\setminus\{x\}})!} \alpha_{2,x,n} \gamma_{J\setminus\{x\}}, \tag{5.40}$$

where $\setminus$ denotes the set difference operator, and $(N_{\{a,b,c,d\}})! = N_a! N_b! N_c! N_d!$, with N_y denoting the number of element of $A = \{a, b, c, d\}$ that are equal to y. As an example, for the set $\{1, 2, 1, 1\}$, this value would be $3! \times 1!$, since $N_1 = 3$ and $N_2 = 1$. Effectively, this term is used to capture the number of unique permutations of the index set.

Incorporating this notation, Eq. (5.38) can be rewritten as

$$\begin{aligned} \ddot{q}_n + \frac{EI\alpha_{4,n}}{\rho \hat{A} \ell} q_n - \frac{E}{2\rho\ell^2} \sum_{i=1}^{N} \sum_{j=1}^{N} \sum_{k=1}^{N} \alpha_{2,k,n} \beta_{i,j} q_i q_j q_k \\ + \frac{E}{8\rho\ell^2} \sum_{i=1}^{N} \sum_{j=1}^{N} \sum_{k=1}^{N} \sum_{l=1}^{N} \sum_{m=1}^{N} \eta_{\{i,j,k,l,m\}} q_i q_j q_k q_l q_m = 0, \end{aligned} \tag{5.41}$$

The number of coefficients can now be calculated as $\binom{19+5-1}{5} = 33,649$, i.e. only 1.4% of the total possible calculations.

This system can now be considered as the "full" nonlinear model, in place of the nonlinear solver in commercial FE software. As mentioned previously, this new model provides a case in which the nonlinearities are of a higher order than those in the proposed ROM. While it is technically possible to expand this ROM to include quartic and quintic terms, this would require a significantly greater number of static solutions, reducing the utility and saving provided by the use of a ROM technique. As such, the original quadratic and cubic terms will be used, as in the traditional application of the techniques. However, it is likely that these coefficients will differ from those in the full model, as they must adapt to capture the higher-order behaviour.

The results from the pinned-pinned beam with rotational spring, as applied above and with the same system parameters, are displayed in Fig. 5.13. For the IC method, as shown in the first panel, the results are largely consistent with those from the original model, which is unsurprising, as the influence of the quintic terms is unlikely to be of the same magnitude as that of the cubic terms. More interestingly, it can be seen that these higher-order terms introduce a divergent behaviour in the ED method, as the influence of these terms is captured in the ROM. ED ROMs created with higher static displacements are displayed in the second panel. Here, it can be seen that, at very high amplitudes, it is possible to achieve nonlinear coefficients that are several orders of magnitude greater than those found at lower deflection

levels. This presents a potentially hazardous possibility for the accuracy of the ROMs. That is, when the stiffness is overestimated, the prediction of the hysteresis behaviour may be incorrect, as this greater stiffness will lead to lower amplitudes. In this case, where there is a difference by several orders of magnitude, the real displacement could be significantly larger than that predicted, which could lead to unexpected levels of stress in the system.

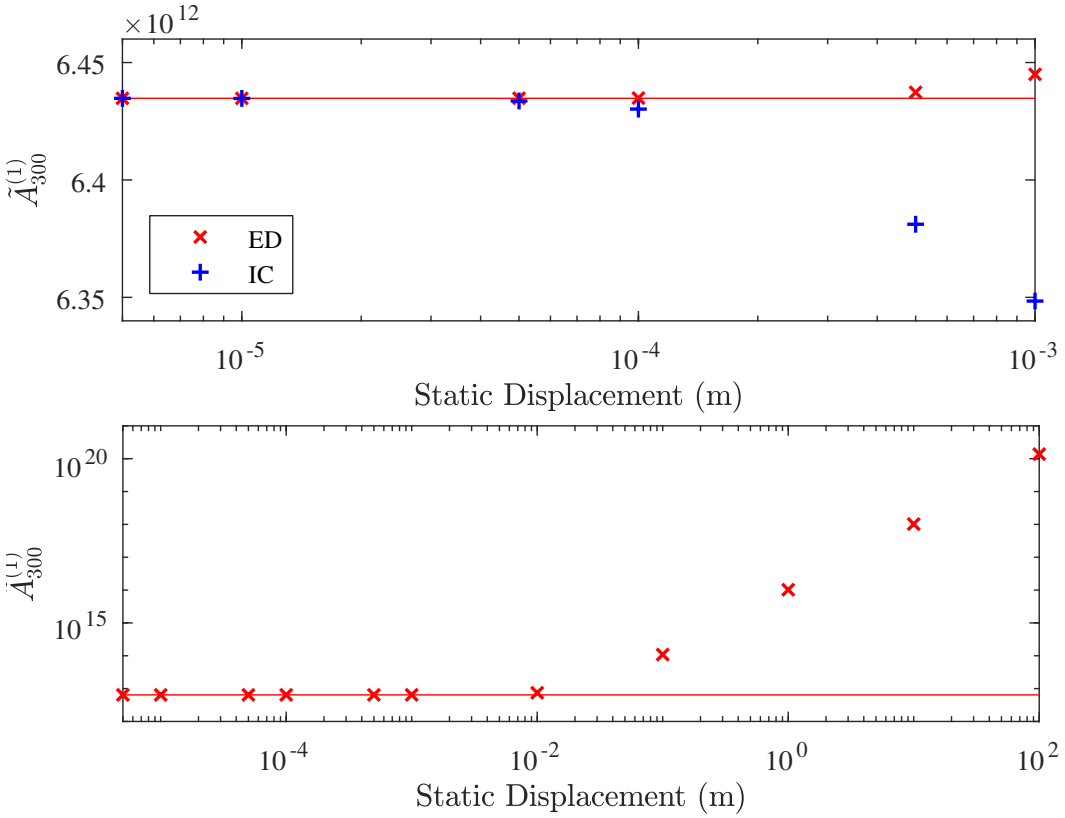

Figure 5.13: Calculated values for the first coefficient using the ED and IC method for the higher-order Galerkin model.

The backbone curves produced using these ROMs found are given in Fig. 5.14; note that the behaviour of the IC curves is qualitatively similar to the cubic case and is, therefore, not presented. As predicted, the ROMs with smaller deflections produce a more accurate prediction of the 'Full' curve (found using numerical continuation [29]). All of the ROMs utilised in this figure are able to accurately predict that a modal interaction occurs at a frequency of around 145-150 Hz, though this does not ensure that the behaviour will be captured accurately, as can be seen at very high amplitudes. That being said, because the ROMs shown only include the first two modes, the model is unable to correctly predict the 1:3 internal resonance between the second and fourth modes. The ED method seems to implicitly capture this behaviour, as the inset figure shows the internal resonance tongue moving towards that of the numerical curve when the static displacement initially increases. However, the predicted ROM tongue then begins to move away from the true solution, before the behaviour changes

completely when the static displacement is greater than 1e-2 m. Therefore, as predicted, at higher amplitudes, the over-prediction of the nonlinear coefficients introduces a stiffening effect that does not accurately represent the system behaviour. In addition, the seemingly incomplete curves in Fig. 5.14 are due to the fact that the numerical continuation software used [29] was unable to proceed past the end point, even though the continuation parameters used were consistent in each case. Therefore, it can be concluded that, at these higher amplitudes, it is no longer possible to assume that the membrane effects are negligible.

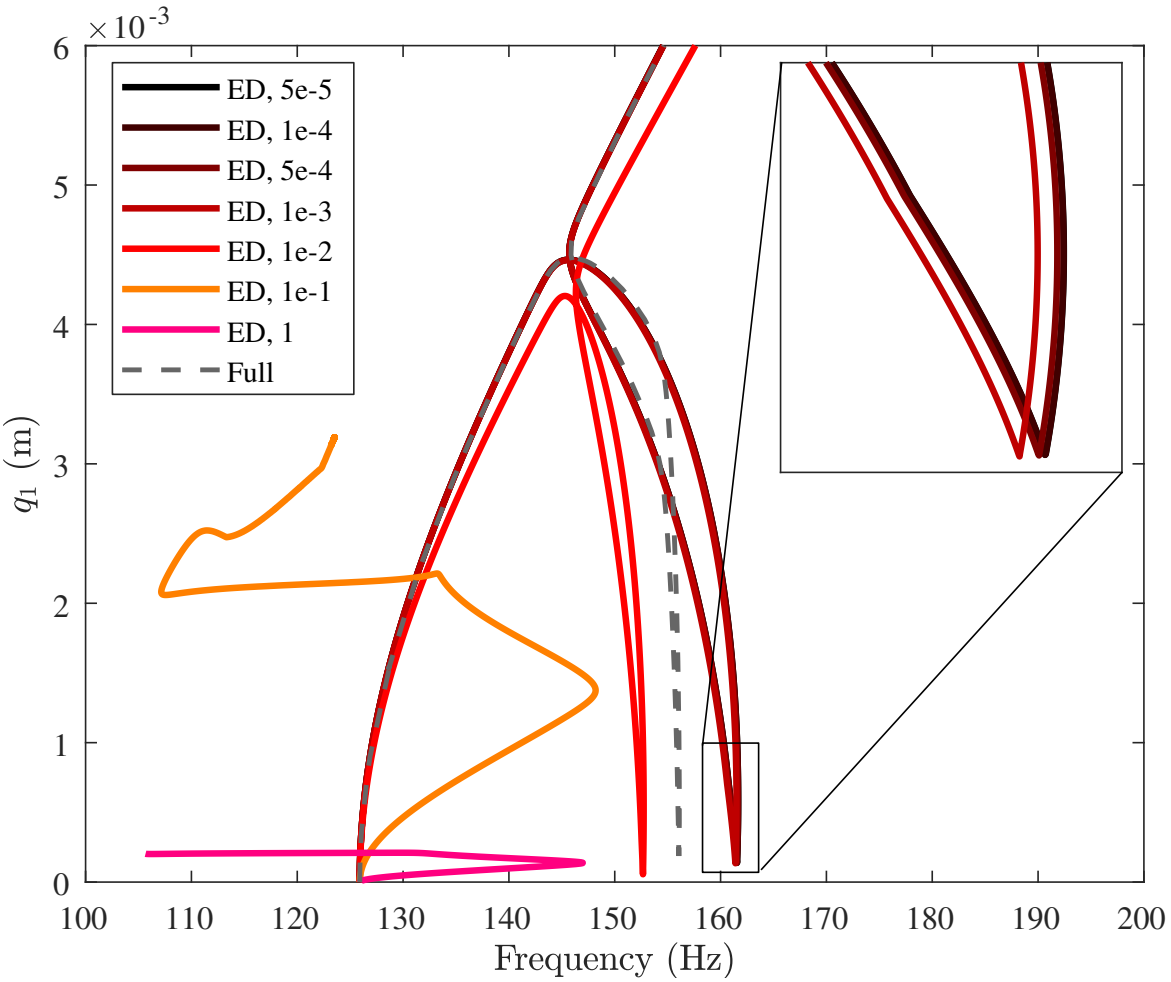

Figure 5.14: Backbone curves calculated by applying the ED method to the higher-order Galerkin model.

5.6 Summary

An analytical consideration of two non-intrusive reduced-order modelling techniques is presented in this chapter; namely the implicit condensation and enforced displacement methods are explored. While these techniques have been used extensively in the literature, they are typically used in conjunction with commercial finite element software. Given that the source code of these software packages is not commonly available, any discussion regarding the

application of these ROM techniques is limited by the uncertainties relating to the nonlinear solver. That is, it can be difficult to isolate the characteristics which are dependent solely on the methods, as opposed to being influenced by the software in some way. It is for this reason that the analytical discussion in this chapter is given, as the use of a fully-defined algebraic system eliminates this lack of clarity.

This discussion begins with a simple mass-spring system, similar to those examined in Chapter 3, this time comprising three masses connected by linear springs, with two cubic stiffnesses introduced to the first two springs, mirroring the type of nonlinearities that might occur in a continuous system. Initial analytical investigations into the application of the non-intrusive methods in this model predict that the coefficients would be invariant to changes in the static case in the ED method. However, the approximation to the IC solutions predicts that the value would actually diverge from that of the real coefficient as the static displacement (or scale factor) is increased. This prediction has been shown to be true when the method is applied, with the reason being that higher levels of forcing can trigger displacements in multiple modes, some of which may not be included in the ROM modal basis. The influence of this modal coupling is then condensed into the coefficients of the ROM. This discussion raises an interesting point regarding the assessment of these techniques. While the ED method has been shown to accurately capture the corresponding cubic coefficient for this example, there is no guarantee that this will necessarily lead to the most accurate backbone curves, especially in cases where the influence of higher modes play a major role in defining the system dynamics.

For the structures considered in this chapter, the prediction of the backbone curves is used as a metric for comparing the accuracy of the ROMs, as is common practice across the literature. In the 3DOF system, both methods were used to create SDOF ROMs. In each of these, regardless of the static displacement, there is a point at which the predicted backbone curve diverges from the full solution. The invariant ED curve gives an accurate prediction of the dynamic behaviour at low amplitudes, but then diverges from the full solution as the influence of other modes increases. This remains true for the IC method, if the static displacements are sufficiently low. However, when these displacements are increased, it can be seen that the ROM becomes largely inaccurate, leading to softening behaviour, as opposed to hardening.

This theoretical, discrete system provides a motivation for investigating whether similar

conclusions can be drawn for continuous systems. A Galerkin model for a pinned-pinned beam with a rotational spring at one tip is used, the motivation for doing so being the internal resonances that the structure was shown to exhibit in the previous chapter. This adds a further criterion by which the accuracy of ROMs can be assessed, as any model which is unable to capture this modal interaction behaviour must be considered inaccurate to some extent. Initially, the effect of the static displacement on the coefficients has been investigated, displaying the invariant behaviour in the ED method and divergent behaviour in the IC method that was seen in the discrete model. However, it must be noted that the rate of this divergence is diminished when the size of the ROM basis is increased.

In discretising the continuous system and transforming the model into modal coordinates, a much larger "full" model is produced, though it has been remarked that this model is not full in the true sense, as the Galerkin method technically produces an infinite system. Due to this increased model magnitude, it has been possible to compare the responses predicted by ROMs of different sizes. In this case, even with only a single DOF, it is possible to accurately capture the primary tongue of the backbone curve. This is a reassuring result for those models that either do not possess internal resonances, or will not be excited to a great enough displacement to trigger them. When predicting the resonance tongue, it has been seen that it is only necessary to include those modes involved in the aforementioned interaction to accurately predict the behaviour of the full model. As an interesting aside, this model includes two 1:3 modal interactions, between the first and second, and second and fourth modes, respectively. However, this may not necessarily be recognised by predicting the full model response. Alternatively, by first comparing the full model behaviour with that of the ROM consisting of modes 1 and 2, the difference in the resonance tongue is indicative that a third mode is required to fully capture the behaviour of this frequency range.

As has already been addressed, elements of the discussion in this chapter could be considered somewhat artificial. More precisely, the use of a system in which the nature of the nonlinearities is identical to that of the ROM provides a useful setting for a fundamental examination of the techniques, but the extent to which these results may be generalised is not necessarily obvious. In particular, the order of the polynomials defining the full nonlinear model is equal to that included in the IC and ED methods, meaning that there are no higher-order effects that must be captured by the low-order terms. As a preliminary investigation, the Galerkin model has been expanded by using a higher-order Taylor expansion in its derivation. The divergent trends seen in the IC method were largely similar to those

in the lower-order case, albeit slightly more pronounced as a result of the additional terms. More intriguingly, although perhaps expectedly, the invariant nature of the prediction of the coefficients is no longer true for the updated ED model. It has been demonstrated that the higher-order terms can dramatically increase the stiffness of the cubic terms, as they attempt to capture the membrane effects of the beam stretching. Furthermore, it has been shown that this may actually be detrimental to the model prediction: if the higher displacement leads to very large amounts of stretching, the overcompensation that this leads to in the cubic coefficients can lead to large under-predictions of the system displacements and, hence, the levels of stress observed.

Chapter 6

Understanding reduced-order modelling techniques

In this chapter:

- The discussion of the Implicit Condensation and Enforced Displacement is expanded to address pronounced differences between their results in finite element software.
- Observations are made regarding the challenges faced in attempting to prescribe a static displacement in finite element software.
- An explanation is given for the discontinuous forces observed in the Enforced Displacement method
- An iterative application of modal forces is applied to improve the results of the Enforced Displacement method
- The modal composition of the static cases in the two methods is varied to investigate the influence this has on the reduced-order model

6.1 Introduction

While the previous chapter introduced an analytical framework in which to apply and assess ROM techniques, the current chapter returns to the more traditional case, in which they are applied in finite element software. The comparison made here has been motivated by observations that were initially made in [46], where a numerical continuation method for full

finite element models was used to determine the "true" system response; this method is an expansion of the NNMcont method defined in [44]. It was seen that the ED method solution deviated from the true backbone curve much faster than that of the IC method. Similar trends to those in [46] are observed in [47, 62], with the IC ROMs providing a more accurate approximation of that found using numerical continuation. Since this result contrasts the analytical findings of the previous chapter, in which it was seen that the solutions of the two techniques were reasonably consistent, this chapter will explore the reasons behind the disparity. Note that results from [46, 47] have been used to verify the application of the IC and ED methods in this thesis.

The discussion in this chapter notes that both ROM methods can be considered somewhat artificial. In particular, the static cases suggest that either a modal displacement or a modal force can be statically applied to the structure, when, in reality, the realisation of this presents a number of significant challenges and uncertainties. For instance, the enforcement of static modal displacements would likely require the introduction of further machinery or equipment to maintain the desired shape. However, the inclusion of these constraints would effectively introduce a complex set of BCs to the structure, which would undoubtedly alter its structural response. Should the same be true of the finite element model, as will be investigated in this chapter, the methodology and its associated applicability would be brought into question.

A further, implicit assumption of these techniques is that a modal input would necessarily lead to a modal output; this conclusion can be drawn from the fact that the physical forces and displacements are projected onto the modal basis prior to the regression analysis. While this assumption seems intuitive, it neglects the discussion above regarding, for instance, the alteration of the structure as a result of effectively enforcing a displacement by introducing a set of BCs. This chapter will investigate the effect of this implementation and its influence on the results found by each method.

An initial overview of the differences observed between the analytical and traditional applications of the IC and ED methods is given in §6.2. The reasons behind this are investigated in §6.3, which addresses the shortcomings of the application of these methods in finite element software, proposing ways in which these could influence the accuracy of the model. These hypotheses are investigated in §6.4 and are used to verify the reasons for the disparity suggested in §6.2.

6.2 Qualitative differences between analytical and numerical nonlinear models

As discussed above, the FE software implementation of these ROM methods is more complicated than the analytical counterpart, due to the opaque nature of the source code and iterative methods applied to capture nonlinearity. As a result, this section begins with a qualitative comparison between results for the same beam modelled in both ways. This will allow an initial insight into the key differences and will direct the subsequent research.

To this end, the clamped-clamped beam defined in [46] is used, as this paper provides validation for the software implementation of these methods. The results from both applications are presented in Fig. 6.1, in which a single beam thickness has again been used as the static displacement. It can be seen that, as in the previous chapter, the difference between the two methods is negligible for the Galerkin model. However, as was also seen in [46], this is not the case when FE software is used. In fact, the ED method can be seen to over-predict the cubic stiffness, so that the amplitude is under-calculated at higher frequencies. This trend is present across the literature [46, 47] and warrants further investigation into the causes and treatment of this disparity.

The results of [46] are expanded in Fig. 6.2. In this figure, the static displacement is varied, considering the cases when the scale factor is half and double a single beam thickness. Since the Galerkin model used only contains cubic terms, the ED curve in this case is invariant to the static displacement, though there is some minor variation for the IC method. In the results from the Abaqus model, the discrepancy between the two methods, observed in [46], is shown to hold true in all three cases.

It can be further noted that, while there is some variation as a result of varying the static case scale factor, this is relatively minimal. Interestingly, it is the ED method that shows the greatest variation, in contrast with the invariant results seen in the Galerkin panel. Although this difference is minor, it further suggests that there is a fundamental difference in the treatment of the structure when it is considered using Abaqus software, rather than analytically.

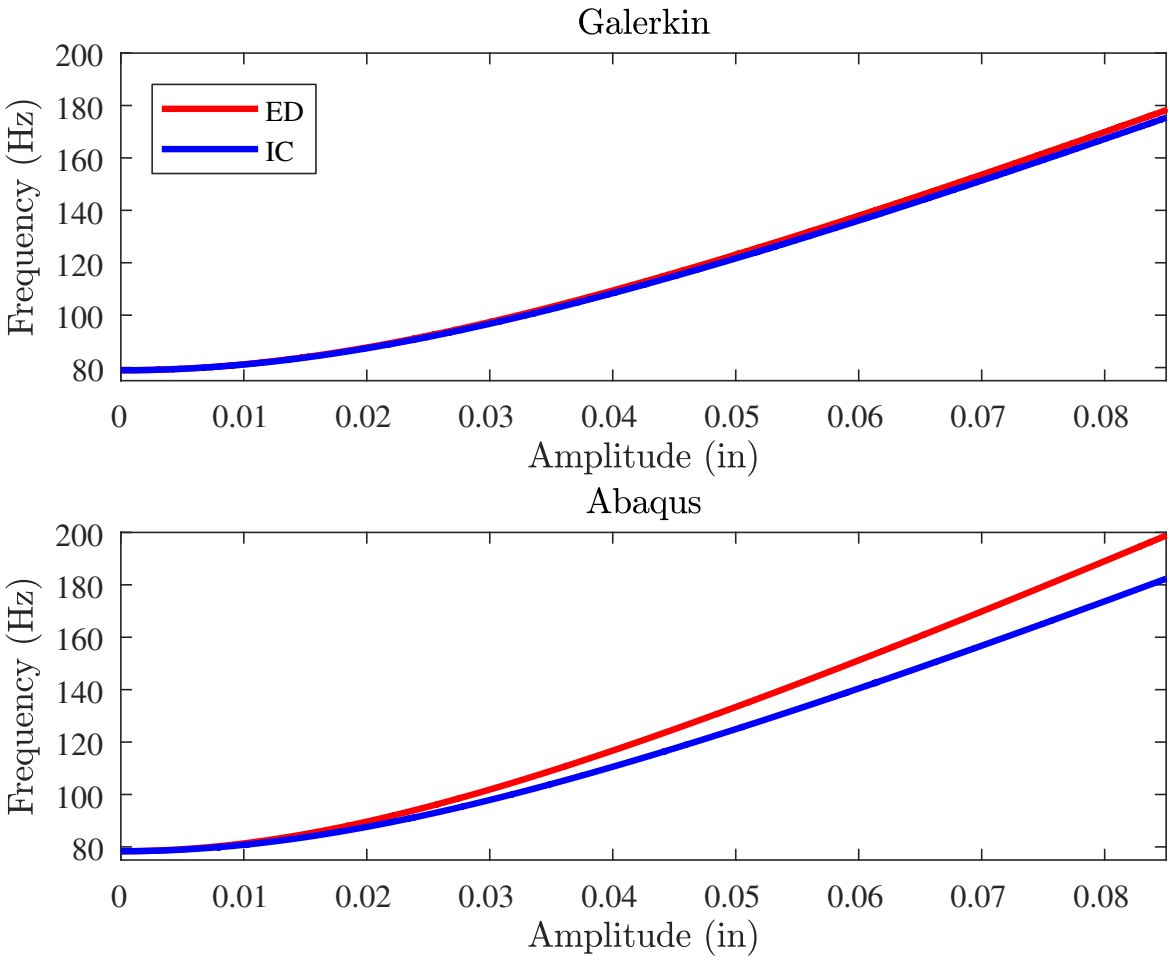

Figure 6.1: Backbone curves of a clamped-clamped beam predicted by ROMs obtained using the IC and ED methods in analytical and software based frameworks.

6.3 Appropriating forces in finite element software

6.3.1 Overview of force calculations

In light of this discussion and the apparent disparity between the IC and ED results, further consideration is given to the relationship between forces and displacements in the two methods. It is useful to keep in mind the fact that both of these can be considered somewhat artificial when compared to a physical system. In particular, the application of a modal force or the enforcement of a modal displacement is difficult to realise for a physical structure and doing so statically would require the use of external equipment which would alter the structural characteristics of the structure. The use of FE software allows these drawbacks to be overcome numerically to provide useful insight that could not otherwise be obtained. However, as is discussed in this section, this can still lead to difficulties.

In the IC method, the application of a modal force leads to displacement that can also be considered modal, even though the relative contributions of each mode in the two cases

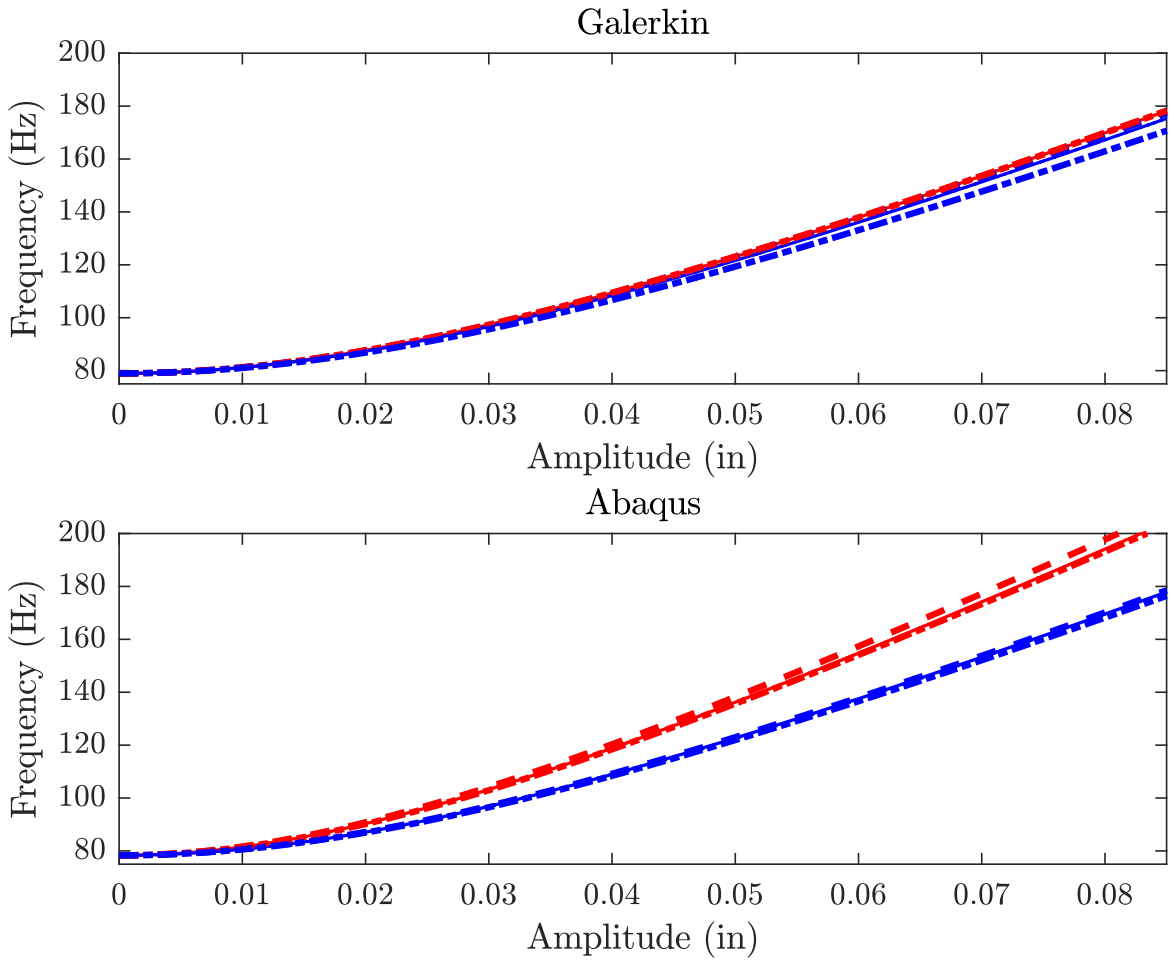

Figure 6.2: Backbone curves of a clamped-clamped beam predicted by ROMs obtained using various scaling factors in the IC and ED methods in analytical and software based frameworks. Red lines denote solutions found with the ED method, whereas blue lines denote the IC method. Thin, solid lines use a single beam thickness for the static case, dashed lines use half a beam thickness, and dot-dashed lines use twice the beam thickness.

may differ. However, the ED technique relies on the ability of the FE software to resolve forces. As demonstrated in Fig. 6.3, this can lead to a discontinuous force profile, as observed in panel (b). This section explores the theory of FE modelling to explain the unusual force distribution. The original application of both methods in this thesis utilises Matlab code that writes the necessary Abaqus input file (.inp) for the static cases and, then, runs the file; Matlab files have also been developed to read the data file (.dat). The static cases themselves either apply a force or displacement field. The former simply uses the Abaqus `*FORCE` function, whereas the latter requires the use of the `*BOUNDARY` function to define the displacement or moment of each DOF as a BC; see [222] for further details on this implementation.

It is first necessary to outline the appropriation of forces for a general FE beam model; this is presented in Fig. 6.4. This methodology can be thought of both in terms of a system

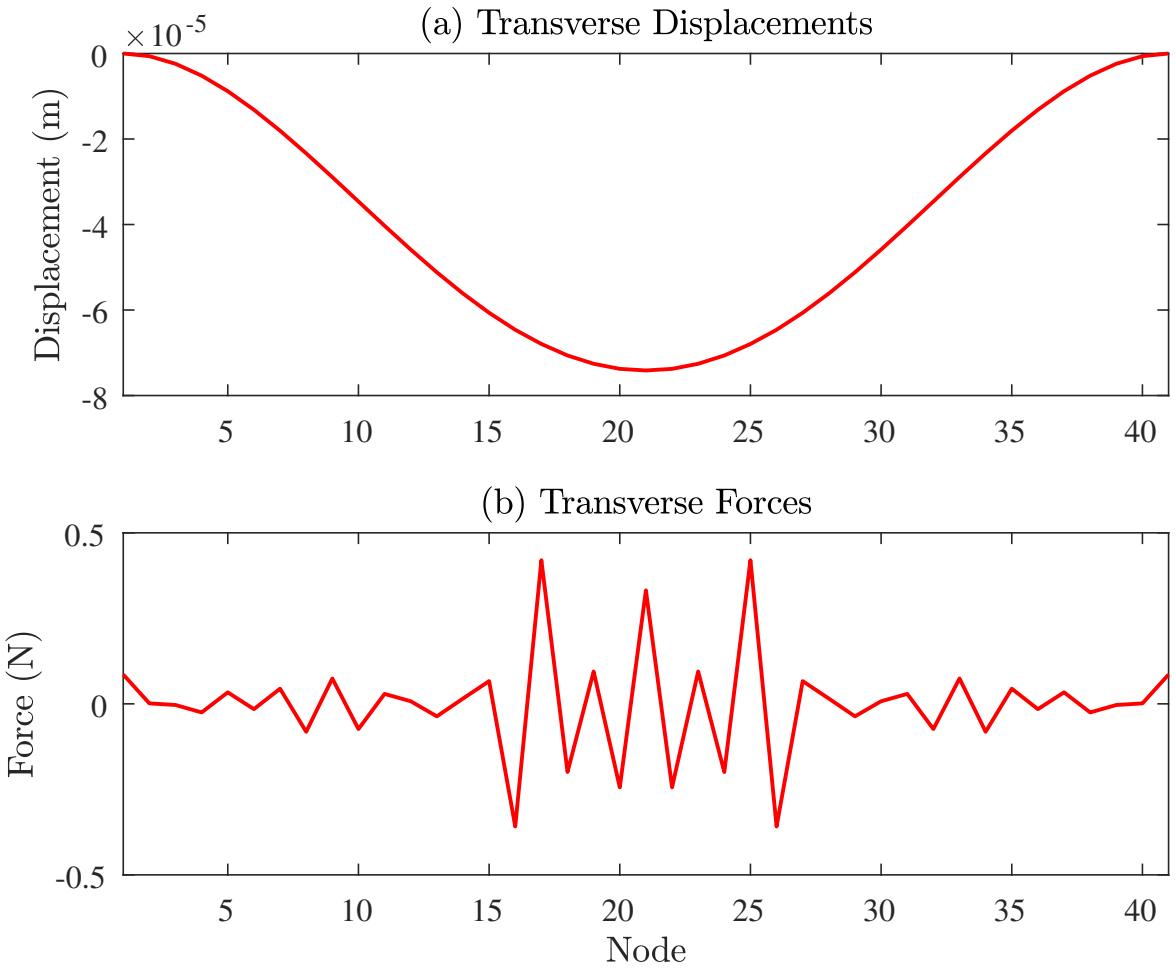

Figure 6.3: A transverse displacement applied to a clamped-clamped beam in Abaqus, and the resultant outputted forces.

of elements or a system of nodes. The forces in a FE model are calculated first in terms of the elements, and then converted into nodal coordinates. The shape functions, i.e. the coloured lines denoted N_i, represent interpolations between the values at the nodes; in this example, these interpolations are linear, though this does not necessarily have to be the case. It can be seen that, since these are both representations of the same system, we must have $N_2(x) = N_2^{(1)}(x)+N_1^{(2)}(x)$. That is, for any node along a beam which is not on the boundary, the nodal shape functions is the sum of contributions of the element shape function on either side. Similarly, for any node on the boundary, the nodal and element shape functions are equal.

By extension, the same relationship occurs for the stiffness matrix and, in particular, the force vector. In summary, the force in any node, u_k, is the sum of the forces in the elements either side of it. This can be written as

$$F_k = F_k^e + F_{(k+1)}^e \tag{6.1}$$

The linear force and displacement vectors are related by the equation

$$\mathbf{Kw} = \mathbf{F} + \mathbf{r}, \tag{6.2}$$

where $\mathbf{r}$ denotes the vector of residual forces, i.e. the out-of-balance forces conjugate to each element. This vector is minimised in the resolution of the forces and, for the sake of this discussion, it will be assumed to be zero.

Therefore, we assume that the forces can be calculated as $\mathbf{F} = \mathbf{Kw}$, which appears to be a relatively straightforward calculation. However, it must be noted that this becomes less straightforward as the ED method is applied. The stiffness matrix, $\mathbf{K}$, is calculated based on the elements and constraints of the undeformed beam.

An enforced static displacement is effectively achieved by ensuring that each node is not allowed to translate or rotate in any direction. Thus, the process is identical to imposing a fully-clamped BC at each node. This leads to an updated stiffness matrix for the deformed beam, which will be used in the FE software calculations.

By considering the simple four-element beam in Fig. 6.5, it can be seen that these pseudo-BCs can be used to explain the unusual force profile seen in Fig. 6.3. In this beam, the end points are not displaced, but an enforced displacement is applied to nodes 2, 3, and 4; their new position is denoted using the prime ($\bullet'$) notation. Focus is now given to the central node, 3', which is displaced by a force F_3 in panel (a). This represents the force that would displace the node from its unperturbed position. However, in panel (d), it must be noted that nodes 2' and 4' are fixed, and the dotted line represents a new undeformed beam configuration consisting of only two elements. This emphasizes the difficulty that arises due to the lack of a physical parallel for this methodology. That is, the force required displace node 3 in panel (d) may be more representative, while the force in panel (a) is recorded. Note that, depending on the software used, it could be the case that the force in (d) is recorded. Regardless of which of these is true, this downward force applied to node 3' must be some fraction of F_3, which can be denoted $\delta_{3,3}F_3$.

This issue is made more complex when panels (b) and (c) are introduced. Similarly to (d), each of these subfigures can be considered as a two-element beam, due to the fixed nature of nodes 1 and 3' (nodes 3' and 5). The vertical force required to displace node 2' (node 4') must be balanced in nodes 1 and 3' (nodes 3' and 5). Therefore, denoting these two forces

by $-\delta_{3,2}F_2$ and $-\delta_{3,4}F_4$, the balanced force at node 3' must be given by

$$f_3 = \delta_{3,3}F_3 - \delta_{3,2}F_2 - \delta_{3,4}F_4. \tag{6.3}$$

More generally, any interior node k (i.e. a node that is not at the boundary) will experience the force

$$f_k = \delta_{k,k}F_k - \delta_{k,k-1}F_{k-1} - \delta_{k,k+1}F_{k+1}. \tag{6.4}$$

At the boundary, there is no force applied directly to the nodes, so the only force in the balance is the reaction to the displacement of the first internal node; i.e. $f_1 = -\delta_{1,2}F_2$. This can be seen in Fig. 6.3. Given that F_2 is in the negative x direction, it holds that f_1 is positive.

For the second node, Eq. (6.4) is simply given by

$$f_2 = \delta_{2,2}F_2 - \delta_{2,3}F_3. \tag{6.5}$$

Now, it can be seen that the sign of f_2 is defined primarily by the δ terms. Similar conclusions can be drawn regarding the expression for f_k in Eq. (6.4). At this point in the discussion, it is useful to return to Fig. 6.4 and recall that the nodal forces are defined by the element forces, which are in turn defined by the stresses. For element (k), the shape functions are defined so that $N_1^{(k)}(x) = -N_2^{(k)}(x)$; effectively, the magnitude of the elemental force at each end of the element is the same, but in opposite directions.

Considering a series of such elements, particularly in the complicated ED configuration, it can be noted that the δ terms must be dictated by the relative contributions of the elements either side of each node. Therefore, if the stress of an element is particularly large, it will give a large positive contribution at one node and an equally large negative contribution at the other. This stress will be inherently linked to the beam deflection, which provides a reasonable explanation for the seemingly erratic force profile in Fig. 6.3, particularly as the magnitude of the deflection increases toward the centre of the beam.

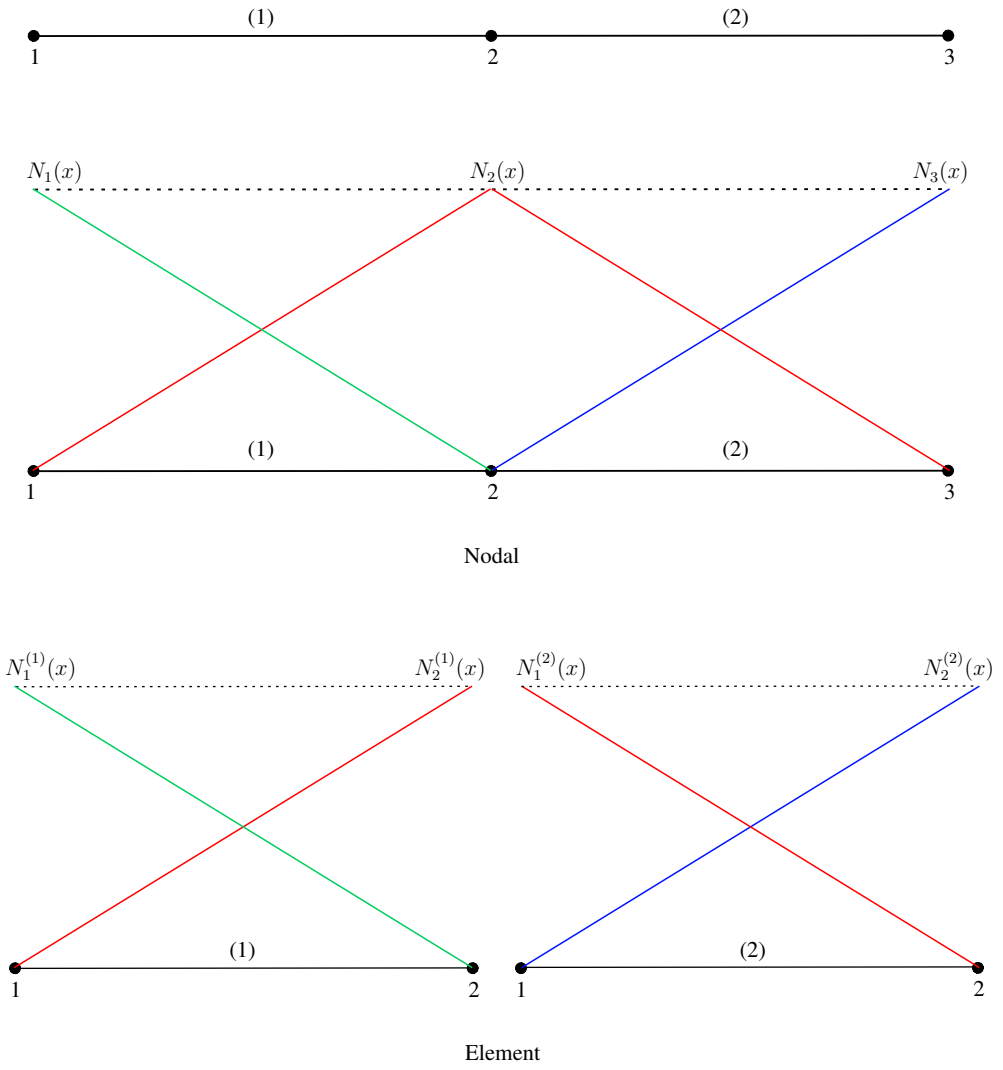

Figure 6.4: Nodal and element overview of shape functions in a FE beam.

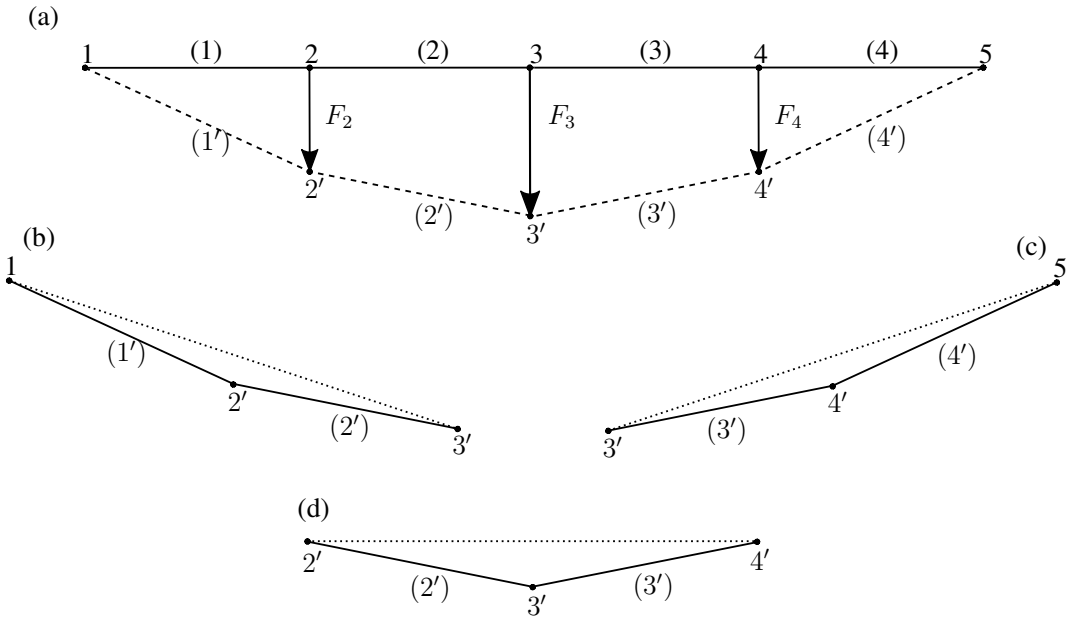

Figure 6.5: Overview of the distribution of forces in a FE beam model.

This discussion is now investigated further in Fig. 6.6. In this figure, cantilever beams consisting of nodes $\{1, 2, \ldots, n\}$ are subjected to transverse displacement vectors of the form $w = -[0, 1/1000, \ldots, (n-1)/1000]$. In Fig. 6.6, it is only the boundary nodes in which the resultant force is non-zero. This can be explained by the linearity of the enforced displacements. For any interior node, the relative displacement of the adjacent modes will be of equal magnitude, but in opposite directions. Therefore, the sum of these forces must be zero, as can be seen in the figure.

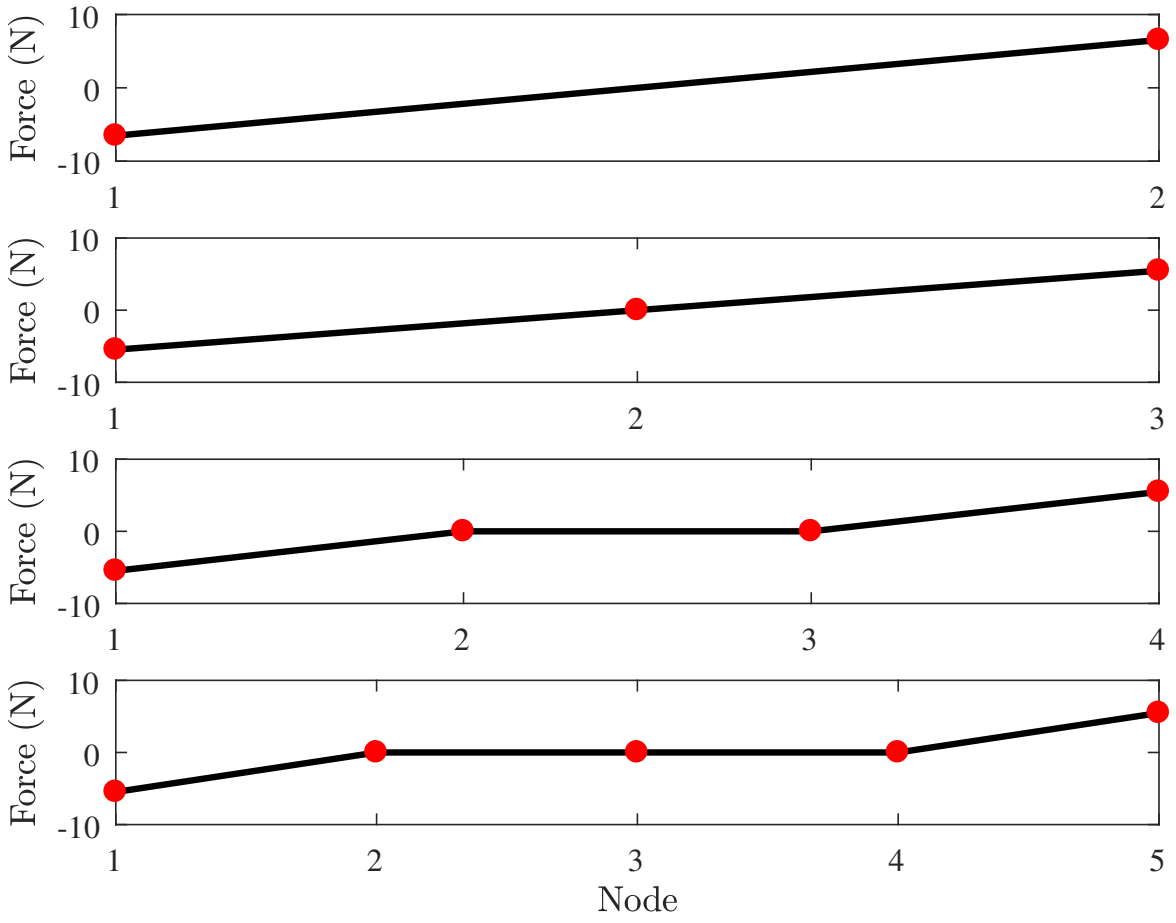

Figure 6.6: Reaction forces of cantilever beams consisting of an increasing number of nodes, subjected to linear displacements.

Fig. 6.7 focuses on a five-node cantilever beam with two sets of enforced displacements. Namely, these will be a linear case, $w_{\text{lin}} = -1/1000[0, 1, 2, 3, 4]$, and an incremental case, $w_{\text{inc}} = -1/1000[0, 1, 3, 6, 10]$. From these, it is possible to define a parameterised combination of the two, given by $w_i = iw_{\text{lin}} + (1-i)w_{\text{inc}}$, where $i \in [0, 1]$. Increasing the value of i from 0 to 1 moves the displacements from the linear case to the incremental case. While the former is identical to the behaviour in Fig. 6.6, the latter introduces a force profile which more closely resembles the behaviour seen in Fig. 6.3. The force at the tip increases incrementally, as expected. Since the distance between nodes 4 and 5 is now greater than that

between nodes 3 and 4, the reaction to F_5 in node 4, $\delta_{4,5}F_5$,is now greater than the force required to displace the node, $\delta_{4,4}F_4$. In fact, it can be seen that $|\delta_{4,4}F_4| < |\delta_{4,5}F_5 + \delta_{4,3}F_3|$, which explains why the balanced force at node 4 is negative. Furthermore, this becomes more pronounced as i is increased.

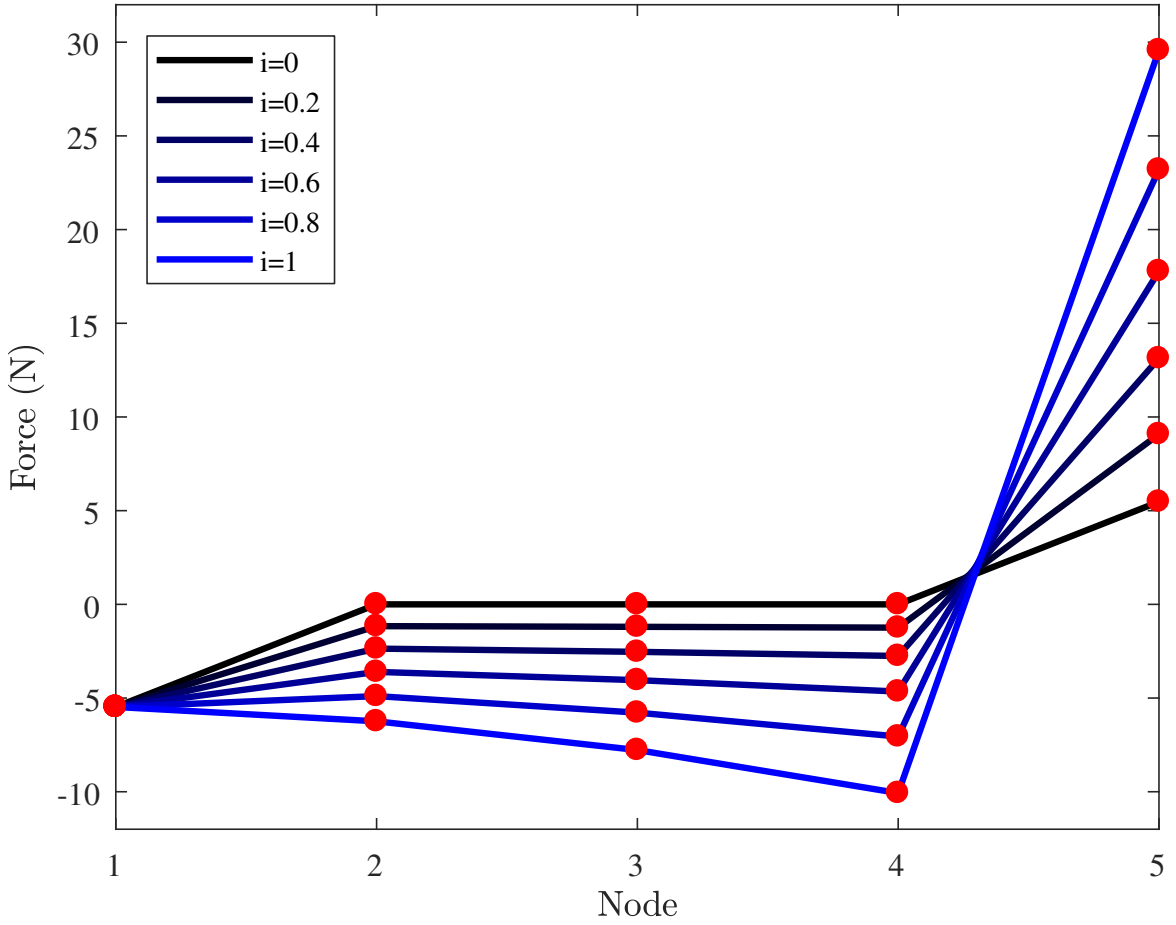

Figure 6.7: Reaction forces of a five-node cantilever beam subjected to a displacement defined by $w_i = iw_{\text{lin}} + (1-i)w_{\text{inc}}$.

At this stage, it is important to recall that a key step in both techniques is projection of both the forces and the displacements onto the modal basis. As has been addressed above, this does not necessarily arise if it is the displacements that are imposed, in which case the force can be considered highly non-modal. If we consider static cases for a single-mode ROM in which the deflections are below a certain level, then, up to some tolerance, both methods will produce static displacements with only a single mode triggered. Assume that this displacement is the same in each case. For the IC method, the corresponding static force will be modal, by definition. However, in the ED technique, we have already seen that there will be a discontinuous force outputted by the FE software. Thus, there are two forces that are vastly difference in both appearance and magnitude, but that result in the same displacement, as can be seen in Fig. 6.8. This means that the relationship between static forces and displacements is not bijective and, naturally, the force used will lead to differences in the ROM produced, as discussed above.

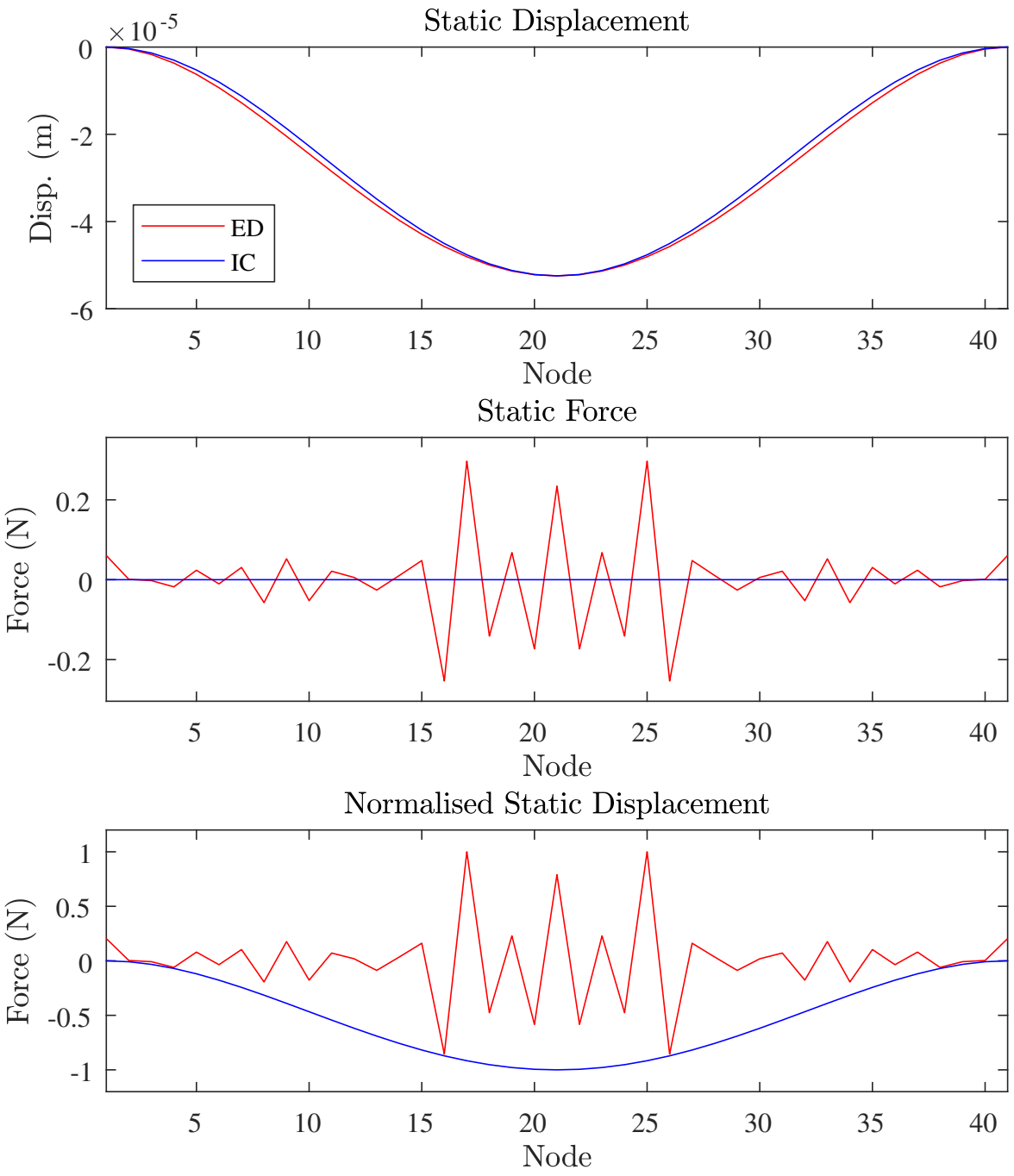

Figure 6.8: Static displacements and forces for two cases with displacements that can be considered equal up to a small tolerance.

6.4 Resolving issues in the ED method

With these results in mind, the ED method is more thoroughly considered in terms of the relationship between its displacements and forces. In particular, the influence of this relationship on the apparent underperformance of the technique is investigated. The most logical initial test is to concoct a methodology that will allow a modal force to be obtained in the ED method, while maintaining its other aspects. There are a number of ways in which this could be achieved, with varying degrees of complexity and time expense. In an initial test,

the efficiency of the methodology is not a priority, as it is first simply necessary to establish whether there is any change in behaviour as a result of altering the force.

To achieve this, the modal forcing is applied iteratively until the correct displacement has been achieved. The first applied load is comprised by a unitary forcing of a single mode; for instance, in the calculation of a two-mode ROM, this would take the form $F_{q,n} = [1, 0]^T$, where n denotes the iteration in which the force is applied. Thus, the applied, physical force in the n^{th} iteration is given by

$$F_n = \Phi F_{q,n}. \tag{6.6}$$

Having applied this load, the corresponding displacement, x_n, is then found and the greatest difference between the current and desired displacements is recorded; the latter is denoted x_{des}. If this difference is smaller than a certain tolerance, the modal force can be used in the linear least-squares method. If not, the force must be updated. This is done by introducing the updating parameter α_n, defined as

$$\alpha_n = \frac{q_{\text{des}} - q_n}{|q_n|}, \tag{6.7}$$

where $q_{\text{des}} = \Phi^+ x_{\text{des}}$ and $q_n = \Phi^+ x_n$, and $\bullet^+$ denotes the Moore-Penrose pseudoinverse. This parameter can then be used to update the force, writing

$$F_{q,n+1} = F_{q,n} + \frac{\alpha_n}{|\alpha_n|} \frac{\max\{F_{q,n}\}}{N}. \tag{6.8}$$

In essence, it is the ratio of the elements of α_n that is important in the updating of the force. This ratio dictates the relative change of each modal contribution, which can then be scaled according to $\max\{F_{q,n}\}$ and some value N, used to control the rate of convergence. As mentioned above, the optimisation of this process is not a priority. The convergence of this procedure is illustrated for a single-mode force in Fig. 6.9.

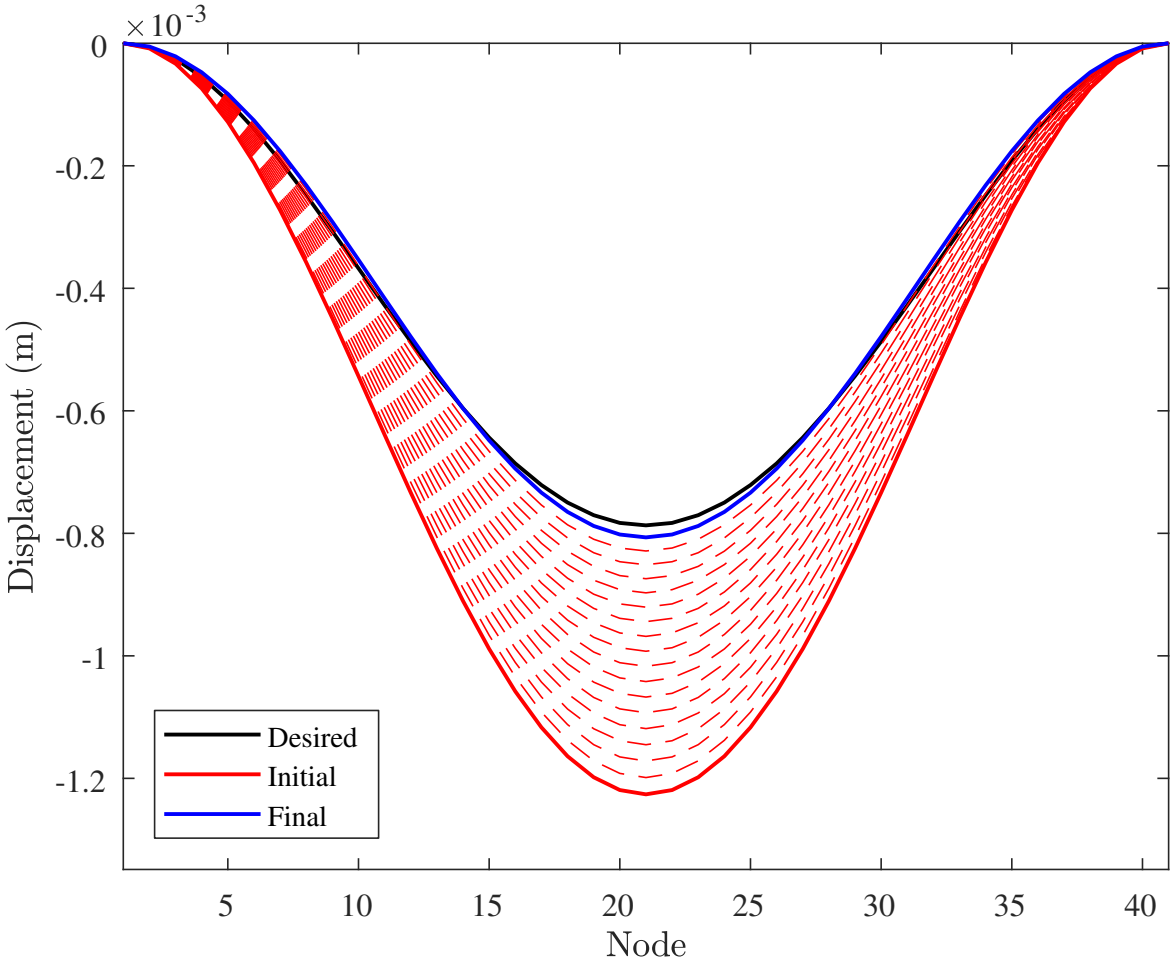

Figure 6.9: Progression of iterative methodology for approximating a modal displacement with a modal force.

This approach has been applied to a clamped-clamped beam to create both single-mode and two-mode ROMs. The cubic coefficients from the two models are as follows:

Single-mode:

$$\mathbf{A}_{\text{IC}} = 4.2648\text{e+}13, \quad \mathbf{A}_{\text{ED}} = 5.8852\text{e+}13, \quad \mathbf{A}_{\text{ED,iter}} = 4.3913\text{e+}13. \tag{6.9}$$

Two-mode:

$$\begin{gathered}\mathbf{A}_{\text{IC}} = \begin{bmatrix} 4.0317\text{e+}13 & -3.1217\text{e+}13 \\ -9.3651\text{e+}13 & 3.7232\text{e+}14 \\ 3.7232\text{e+}14 & -7.5240\text{e+}14 \\ -2.5080\text{e+}14 & 2.6765\text{e+}15 \end{bmatrix}, \ \mathbf{A}_{\text{ED}} = \begin{bmatrix} 5.8872\text{e+}13 & -4.1093\text{e+}13 \\ -1.2328\text{e+}14 & 9.4978\text{e+}14 \\ 9.4978\text{e+}14 & -1.9495\text{e+}15 \\ -6.4982\text{e+}14 & 4.1655\text{e+}15 \end{bmatrix}, \\ \mathbf{A}_{\text{ED,iter}} = \begin{bmatrix} 3.9760\text{e+}13 & -3.1246\text{e+}13 \\ -9.3739\text{e+}13 & 3.87834\text{e+}14 \\ 3.87834\text{e+}14 & -7.4046\text{e+}14 \\ -2.6640\text{e+}14 & 2.6640\text{e+}15 \end{bmatrix}.\end{gathered} \tag{6.10}$$

It can now be noted that the percentage differences between $\mathbf{A}_{\text{IC}}$ and $\mathbf{A}_{\text{ED,iter}}$ are much smaller than between $\mathbf{A}_{\text{ED}}$ and $\mathbf{A}_{\text{ED,iter}}$:

$$\mathbf{A}_{\%,\text{IC}} = \begin{bmatrix} -1.38 & 0.09 \\ 0.09 & 4.03 \\ 4.03 & -1.59 \\ -1.59 & -0.47 \end{bmatrix} \%, \quad \mathbf{A}_{\%,\text{ED}} = \begin{bmatrix} -32.2 & -24.2 \\ -24.2 & -59.3 \\ -59.3 & -62.0 \\ -62.0 & -36.0 \end{bmatrix} \%, \tag{6.11}$$

In these matrices, each entry denotes the percentage change of the respective coefficient between $\mathbf{A}_{method}$ and $\mathbf{A}_{\text{ED,iter}}$.

In the derivation of $\mathbf{A}_{\text{ED}}$ and $\mathbf{A}_{\text{ED,iter}}$, the displacements used are identical, while the forces differed significantly, as was observed in Fig. 6.8. This suggests that it is the non-modal forcing outputted from finite element software that leads to the apparent underperformance in the ED method. Furthermore, the highest percentages errors, relative to the classical ED method, occur in the cross-coupling coefficients. As has been demonstrated in Chapter 5, these terms are particularly important in the modelling of modal interactions. Thus, a failure to address this difference in force may lead to the inaccurate prediction of internal resonance

behaviour.

6.4.1 Varying the modal composition of the static cases

Further investigation of the static cases can be achieved by varying the relative contributions of each mode in the modal shape (force or displacement). This variation is performed in the development of a two-mode model using both the IC and ED methods. As has been discussed, the modal shape in each of these currently takes the form

$$\Sigma = a(\hat{\phi}_1 + \hat{\phi}_2), \tag{6.12}$$

where $\hat{\phi}_k$ is the displacement-normalised form of the k^{th} mode shape and a is some scaling factor used to ensure the displacement is within the desired region. Recall that this modal shape can be applied as a force or a displacement, depending on the choice of ROM method. In the current investigation, the shape in Eq. (6.12) is updated, so that it takes the form

$$\Sigma = a(\hat{\phi}_1 + \gamma\hat{\phi}_2), \tag{6.13}$$

where γ is used to vary the relative contributions of the two modes.

Interestingly, it can be seen that the coefficients from both methods are invariant to changes in the static modal composition, even when the contribution of one is relatively small. This implies that it is the modal nature of the forces in the ED method that is important for obtaining accurate results, as opposed to the specific modal structure thereof.

6.5 Summary

An expanded investigation into discrepancies between the IC and ED methods is presented in this chapter. This discussion has been motivated by the fact that the fundamental steps of the two techniques are largely the same. In particular, the two methods both create corresponding sets of static forces and displacements, to which a linear regression procedure is applied. Given that the two methods both apply the static case using a modal shape and then assume a modal output, there is no apparent reason as to why there should be differences between the results. Although some variation between the methods was observed in Chapter 5, the distinction is much more pronounced in the software-based models.

Given these observations, the cause of the differences could be isolated to the acquisition

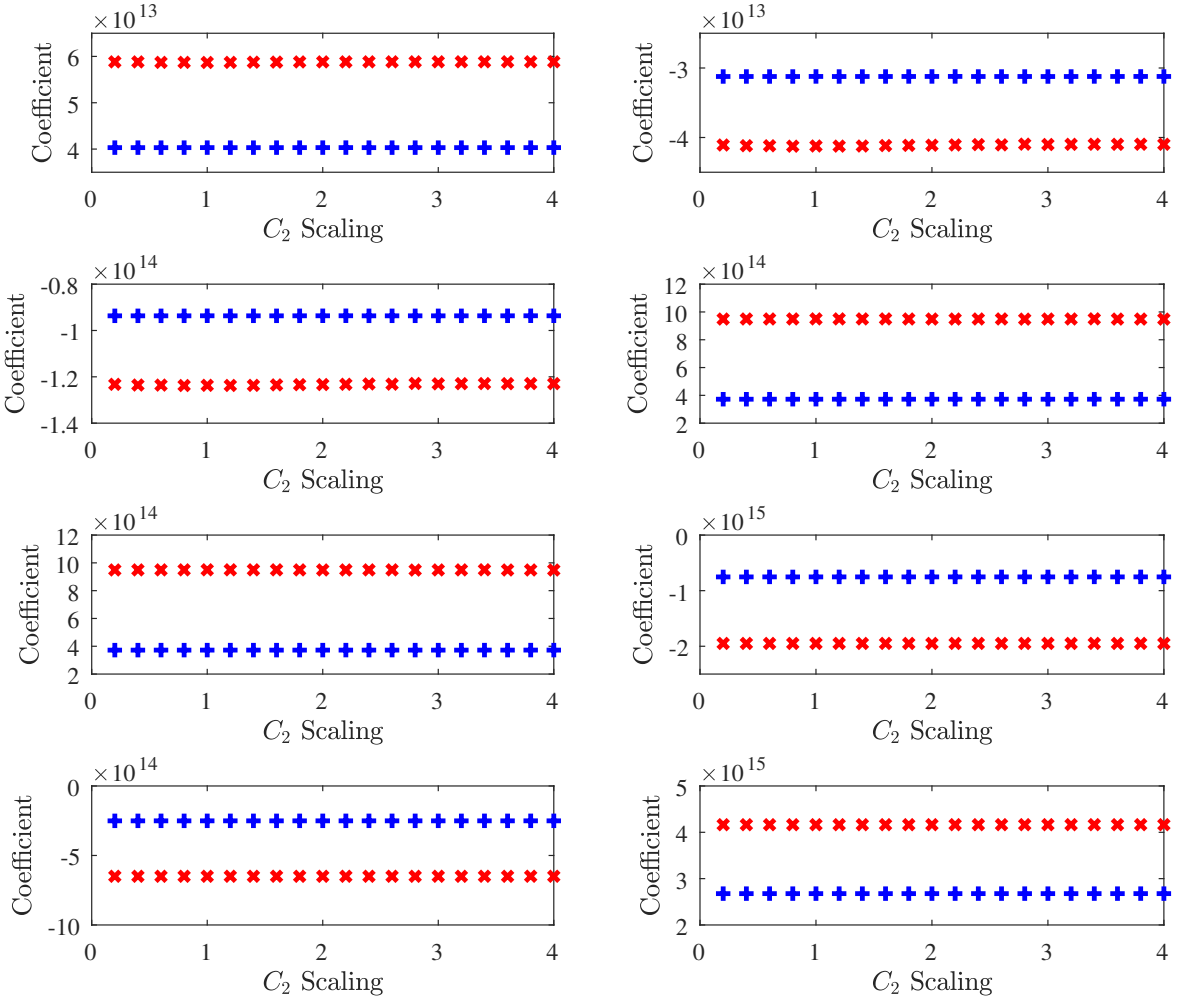

Figure 6.10: Nonlinear coefficients for a 2DOF ROM, found by varying the relative contributions of the two modes in the static cases.

of output data from the finite element software. Since the prescribed forces or displacements are necessarily modal by definition, it can be concluded that the leading cause of the deviations must be the treatment and calculation of the outputs by the nonlinear solver; this holds particularly true as this methodology is not readily available to the user. It has been concluded that, while a modal force leads to a modal displacement, the same can not be said when it is a linear displacement that is applied.

The displacements acquired in the ED method were observed to be largely discontinuous, an unexpected result, given that the displacements prescribed were smooth. Building on the fundamental theories underpinning the development of finite element models, this chapter proposes an explanation as to why this seemingly sporadic result occurs. This explanation is inherently linked to the notion that there is no physical equivalent to some of the steps proposed in this methodology. In particular, the application of a static displacement would require the constraining of a number of points along the beam. These are qualitatively

no different from the application of BCs and would, therefore, have a similar influence on the mechanical properties of the system; that is, the structure in the constrained and unconstrained configurations must be considered as separate systems, rather than different cases of the same system. Further, this discussion proposes that the introduction of BCs along the span of the beam effectively discretises the structure into a series of systems that are largely independent of one another.

To investigate this hypothesis, the ED is applied twice, with the recorded force acquired differently in both cases. Of course, the first, benchmark case is the traditional finite element application. In the latter, identical displacements are used, however, an iterative approach to calculate purely modal forces is introduced and applied. The predicted coefficients from the two applications are not identical, despite the similarity of their displacements. The results found using the novel, iterative approach are shown to be the same as those found using the IC method. Thus, it can be concluded that it is the attainment of the forces directly from the finite element software that leads to the inaccuracy.

A separate, but related, study into the modal composition of the static cases has also been undertaken. By varying the relative contributions of the two modes in a 2DOF ROM, it was concluded that the coefficients obtained in both techniques is independent of the these contributions, so long as they are both active to some extent. It is noted that these results may not hold true for more complicated structures; this would provide a beneficial expansion of this work.

Chapter 7

Conclusions and future work

In this thesis, a number of modelling techniques for nonlinear vibrations have been investigated and expanded. This has helped to further understand their theoretical understanding and has contributed to their ability to accurately and efficiently understand complex dynamic phenomena that may occur. This chapter provides a summary of the findings presented in this thesis, before outlining a number of ways in which the research could be expanded.

7.1 Conclusions

As discussed in Chapter 1 and throughout this thesis, the work presented aims to contribute to the understanding and modelling of nonlinear vibrations, so that they may, eventually, be predicted with the same ease and accuracy as linear modal analysis. This would allow the safe and practical design of nonlinear systems, resulting in great savings in efficiency. The key ways in which this has been achieved can be outlined as follows.

- By focusing on frequency tuning in the multiple scales method, it has been possible to bring its solutions in line with those of the direct normal form method. This allows the user to choose either technique without having to compromise on accuracy.

- Through the consideration of the modal coupling parameters in Galerkin models, it has been possible to ascertain a number of trends that could alert the user to possible modal interactions. This is extremely useful in predicting destructive behaviour that could occur, for instance, in ultralight or microscale mechanical structures.

- A novel method for incorporating nonlinear boundary conditions into Galerkin models

has been developed. Given the strong influence of such interactions at the microscale – for instance, in atomic force microscopy – this methodology could prevent damage to highly expensive systems.

- The implicit condensation and enforced displacement techniques have been fundamentally assessed through their application to an analytical nonlinear system. These methods present exciting reduced-order modelling techniques for structural engineers, but their use is predominantly observed in academic studies. As such, the discussions of this work further the understanding of the methods, contributing to their potential to be used on a much wider scale.

7.1.1 Analytical approximation methods

In Chapter 3, the harmonic balance, multiple scales, and direct normal form methods were derived and compared in terms of the accuracy of their predicted response found using only one or two iterations of the methodology. Although it has been shown that all three techniques are capable of producing accurate results, the discussion in this chapter highlights a number of benefits and limitations associated with the application of each, using two lumped-mass systems to demonstrate these via comparison with numerical solutions. The HB method is by far the simplest of those considered, as it effectively only requires a single major step, in which a trial sinusoidal solution is applied and the coefficients of the harmonic expansion are balanced. This means that results can quickly be found, but higher-order terms that occur in nonlinear structures are implicitly assumed to be negligible as they are not represented in the trial solution. As such, the method lacks the ability to model structures with significant harmonic responses without expanding this initial solution.

The MS and DNF methods both address this issue, though they do so using different strategies. The MS technique applies perturbations to key parameters, such as time and displacement, using a bookkeeping parameter to monitor the relative contribution of each term. In applying this parameter, it becomes possible to predict the aforementioned harmonic components of the response without making changes to the trial solution. Furthermore, the inclusion of time-dependent displacement parameters allows the modelling of transient behaviour, which is not possible in the standard implementation of the other techniques. In addition, this thesis has demonstrated that a key aspect in simplifying the methodology of this technique is to linearise the frequency term; this step is not utilised in the other methods considered.

Finally, the DNF method applies the classical normal form method directly to the second-order equations of motion of a nonlinear system, applying three transformations to ensure that only those terms that are resonant are retained. This method also uses a bookkeeping parameter to monitor the contribution of each term, though these are only included in the equations of motion, rather than in parameter perturbations. Chapter 3 outlined two major advantages of using the DNF method. The first is the matrix framework, used to track the fundamental and harmonic components of the response. The second is the frequency detuning applied during the technique, which has been shown in previous studies to explain the greater accuracy observed, compared to similar applications to the first-order system of equations.

In Chapter 3, it has been demonstrated that, if this detuning is chosen as the tuning applied in the MS method, it is possible to make the solutions of the two techniques identical to one another. This presents the user with the possibility of using either of these widely-applied techniques and the accuracy being independent of this choice. This also presents the opportunity to combine the accurate results typically obtained using the DNF method with the ability to model transient behaviour.

7.1.2 Analytical finite element modelling

While the previous discussion focused on lumped-mass systems, Chapter 4 addressed the development and application of analytical models for continuous structures, focussing particularly on the Galerkin method, due to its recent applications in M/NEMS structures. The development of an Euler-Bernoulli beam model is used to illustrate the implementation of the Galerkin assumption and the dependence of the model on its BCs. Particular focus was given to the comparison between symmetric and asymmetric beam configurations, in light of observations made in the literature, in which asymmetric systems have exhibited internal resonances between the modes. A key component of this investigation was the in-depth comparison between two similar models by studying a pinned-pinned beam with and without a rotational spring at one end. Confirmation of a 1:3 modal interaction between the first two modes, in the former case, is presented and supplemented by the observation of a second internal resonance between the second and fourth modes. This study outlined a number of key observations regarding the nonlinear coefficients, as well as the influence on the structure of the natural frequencies when the symmetry is broken.

Following this discussion, Chapter 4 addressed the notion that it may not be possible

for all physical structures to be accurately modelled using a combination of classical BCs and linear springs, particularly as the method is applied to M/NEMS structures. To this end, a novel, nonlinear algebraic approach for treating BCs defined by polynomial expressions of the displacement is introduced. As such, the technique can be used to approximate any system in which the behaviour at the boundary can be accurately represented by a Taylor expansion. This methodology can effectively be considered as a nonlinear algebra extension of the linear methods traditionally used, utilising the tensor resultant in place of the matrix determinant to develop the solvability condition; a number of results from the field of nonlinear algebra are utilised to simplify this step.

A practical example of the implementation of this method is presented, using a symmetric beam supported at both ends by springs with quadratic and cubic stiffnesses. The calculation of the elastic properties for this structures demonstrates that, while the system itself may be symmetric, the mode shapes may not be, as is seen in this case. It is further concluded that this asymmetry arises as a result of the relative contributions to the stiffness from the beam and the supports. By increasing the spring stiffnesses, the first mode shape varies from that of a rigid, spring-supported beam to that of a pinned-pinned beam. The mode shapes of a pinned-pinned beam can therefore be considered as a limit case as the spring stiffnesses tend to infinity. Note that, within this transition, a large amount of modal interaction behaviour is observed.

Following this theoretical example, a cantilever beam with an attractive magnetic reaction at the tip is modelled. The interaction itself actually takes a complex, logarithmic form, so this is approximated by a cubic truncation of its Taylor expansion. The mode shapes found using this approximation are compared with those found using a linear truncation and those of the underlying linear equations. A number of interesting observations are made from this comparison. First, it must be noted that both the underlying linear natural frequency and the ability to predict modal interactions are inhibited by the exclusion of higher-order terms. Further, the higher frequency mode shapes found using the linear approximation are effectively identical to those of the linear system. In contrast, no such trend is observed for the cubic approximation. These observations highlight the importance of properly including boundary interactions in the calculation of the elastic properties, if the nonlinear behaviour is to be accurately captured.

7.1.3 Reduced-order modelling

The work of Chapters 5 and 6 undertook a fundamental investigation into non-intrusive reduced-order modelling technique, focussing particularly on the implicit condensation and enforced displacement methods. The derivation and application of these techniques were initially outlined and it was noted that a key motivation for their use is their ability to approximate the nonlinear behaviour without requiring access to the source code. To provide more fundamental insight into the abilities and shortcomings of these methods, Chapter 5 considers their application to analytical nonlinear systems, as opposed to the typical implementation, in which the static cases are applied using finite element software; the motivation for doing so is that it removes the uncertainty that is introduced due to the lack of access to the source code in commercial software.

Initially, a 3DOF lumped-mass system with cubic nonlinearities was used to demonstrate and explain a case in which the coefficients found using the ED method are invariant to changes in the scaling of the static cases, whereas the IC method deviates from the full model value as the scaling factor is increased. While this example may be considered somewhat artificial, it provides a useful explanation of how the IC method condenses the effect of the interaction between the modes. These results suggest that the ED is less suited to capturing such effects. This poses the user with an interesting decision to be made. It has been shown that, for this case, the ED backbone curve is initially closer to the numerical solution, but deviates from this at higher amplitudes. In contrast, the IC curve initially appears to be less accurate, but the difference in its curvature provides a close representation of the true behaviour for a longer period. This is a result of the aforementioned ability of the method to condense the membrane effects that arise as a result of applying a force instead of a displacement.

This investigation was expanded by applying the two methods to the Galerkin model of the previously-discussed asymmetric pinned-pinned beam with rotational spring. Not only does this provide the ability to vary the size of the ROM, but it also allows the investigation of modal interaction behaviour. With regard to the former, it has been demonstrated that the condensation effect observed for the IC method in the lumped-mass system holds true in the continuous case, though it becomes less pronounced as more modes are added to the basis. It was further demonstrated that only those modes involved in an internal resonance need to be included in this basis for the behaviour to be captured almost exactly. However, this also highlighted an element of uncertainty, should such interactions not be known *a priori*. As

mentioned above, there was a second modal interaction between modes two and four, but the ROM is unable to predict this with only the fourth mode included, despite the structure of the nonlinear coefficient matrices being similar to that of the model including modes 1 and 2.

Both of the analytical models discussed in this section have been expanded further through the inclusion of higher-order nonlinear terms; more precisely, they were expanded up to quintic order. These updated models provide a case that is qualitatively closer to the traditional implementation, in that the ROM is not of the same polynomial order as the full model. In both cases, the invariance property previously observed in the ED method was no longer present and it followed a similar, albeit less pronounced, trend to that seen in the IC method. There were, however, some key differences between the two cases. For the lumped-mass system, both the IC and ED method exhibited a stiffening of the coefficients as the maximum static displacement was increased. This trend remained true when the IC method was applied to the continuous system (as was the case in the cubic model), but the opposite was true for the ED method.

The influence of these trends on the system behaviour was also observed. Naturally, the condensation of the nonlinear effects that were originally observed in the discrete model for the IC method were also seen to hold true for the ED technique, though the variation between the three cases considered was less obvious. While this was also initially true for the beam model, it has been observed that the presence of a modal interaction can somewhat hinder this procedure, if the displacements enforced are too great. In particular, the typical tongue observed on the backbone curve instead manifests as a hardening-to-softening behaviour, which is unrepresentative of the true response.

7.2 Future work

As has been demonstrated in §7.1, this thesis has presented a number of important results for the understanding, development, and refinement of nonlinear modelling techniques. As the field of nonlinear dynamics expands, it is important that this process continues to adapt to new challenges, with the ultimate goal being for nonlinear modal analysis techniques to be applied with the same confidence and understanding as corresponding linear techniques. This section presents a number of ways in which the research of this thesis could be continued to move towards this target.

7.2.1 Expanding the use of analytical approximation methods

In this thesis, it has been demonstrated that results from the MS and DNF methods can be identical to one another, should the frequency detuning from the second be used in both cases; it has been concluded that this allows the user to choose either technique and still be able to ensure the same level of accuracy. This development highlights the fact that, although there are a number of established methods, it is important to remember that these are not perfect. In fact, it is possible that they could be improved and refined by considering the positive aspects of other techniques. Although not pursued in this thesis, a key attribute of the MS method is the ability to capture transient behaviour, as a result of the inclusion of time-dependent displacement variables. This quality continues to be a benefit, for instance in the introduction of time-varying temperature dependence, so it is proposed that the introduction of a temporal component to the displacements of the DNF method would expand its potential scope.

The simplicity of the HB method has allowed its application to large-scale nonlinear systems, though the complexity of the MS and DNF method currently limits their use to much smaller-scale applications. While the possibility of developing similar automations of these techniques is valid, it should be noted that non-intrusive ROMs have been shown to provide accurate results using systems that closely resemble those seen in Chapter 3. As such, it may be much less computationally expensive to develop an integrated application of these techniques with analytical methods. So long as the necessary modes are included in the basis, these analytical methods (particularly DNF) offer the possibility of predicting isolas without the need for extensive full-model computation.

7.2.2 Developing the role of Galerkin models

The nonlinear algebra approach outlined in Chapter 4, as well as the associated results regarding the influence of nonlinear BCs on the system dynamics, present an interesting development of analytical methods, particularly as they continue to be applied to the relatively young field of micro- and nanomechanical structures. It must first be noted that these developments are currently limited to beam structures, so an obvious initial expansion should be to apply the same procedure to more complex mechanical elements, such as plates, shells, and pipes. As well as this, although some preliminary validation has been provided by the consideration of parameter limit cases, the stature of this procedure would benefit from experimental confirmation. This could be readily provided by the cantilever with magnetic

interaction at the tip, as outlined in Chapter 4, and further investigated for M/NEMS devices.

Chapter 4 also highlights a number of trends in the integral terms that define the nonlinear behaviour (the α and β terms) that occur when the symmetry is broken and modal interactions occur. Further investigation into these trends may lead to the development of a rigorous framework for predicting such behaviour without the need to run any simulations of the system response; it may also be possible to isolate the modes that would be involved in these interactions. Although these trends have only been considered for analytical models, it is a distinct possibility that they may hold true more generally and could also be investigated. Furthermore, for engineers developing designs that actively utilise nonlinearities (such as nonlinear tuned-mass dampers), these trends may represent a useful initial tool to ensure the correct nonlinear properties; therefore, further development of their understanding could reduce the computational expense of the design process.

7.2.3 Refining the application of non-intrusive reduced-order models

Despite the increasing application of the non-intrusive ROM techniques discussed, this tends to be in academic studies that aim to contribute to the development of the technique by comparing the results with those of the full model. As such, it is possible to conclude that, for the methods to become widely used for design purposes (as they have the potential to do), a more fundamental understanding of the intricacies of their methodology must be developed. The work of this thesis has aided this process by introducing the application of the methods to analytical structures, in which the full model is completely understood. That being said, there are a number of ways in which this discussion could be applied. For instance, although higher-order terms are added to the analytical systems, the results are qualitatively different to the application in commercial software. It may be beneficial to develop an analytical (or semi-analytical) system that more closely approximates the treatment of nonlinearities by these programmes. This could be achieved, for example, through the piecewise linearisation of the nonlinear components, or by utilising open source finite element software.

A number of studies have observed that solutions found using the ED method are somewhat less accurate than those found using the IC method. This thesis concludes that this is a result non-modal response forces in finite element software, an issue which appears to arise a consequence of the method used by commercial finite element software in their calculation. The unavailability of the source code, therefore, suggests that the ED method could be refined by establishing a reliable methodology for finding modal forces. While the iterative

method proposed in Chapter 6 provides one such strategy, it is time-consuming and effectively removes any benefit of using the ED method instead of the IC technique. A summary of potential alternative strategies is now provided:

- If translation at the BCs is restricted, the only reaction force observed at these nodes would be as a result of the displacement of the adjacent node. If, further, it is possible to characterise the relationship between relative displacement and the distribution of the associated reaction force, the 'true', modal force could be isolated through the simple application of matrix operations.
- If a force is applied at each node in turn, it should be possible to create a database of the relative contributions to the displacement of all the nodes. Thus, the force appropriation would be reduced to a surface fitting problem that could be solved numerically.
- An initial approximation could be obtained by applying each nodal displacement in turn and then scaling the resultant force. However, initial investigations into this strategy suggested that this may overestimate the force close to the boundary.

7.2.4 Final thoughts

The suggestions made in this final section summarise some of the simplest and most effective ways in which the work of this thesis could be expanded to the aforementioned confidence and reliability required of nonlinear modal analysis. To truly achieve this goal, a final suggestion for future work would be the unification of these techniques, both among themselves and with the other methods that continue to be developed. The results and methodology of this thesis provide a useful starting point for achieving this.

Bibliography

[1] A. J. Elliott, A. Cammarano, S. A. Neild, T. L. Hill, and D. J. Wagg. Comparing the direct normal form and multiple scales methods through frequency detuning. *Journal of Sound and Vibration*, 94:2919–2935, 2018.

[2] R. D. Blevins. *Formulas for Natural Frequency and Mode Shape*. Van Nostrand Reinhold Company, 1979.

[3] View from the academy: Engineering to mitigate climate change. `https://www.theengineer.co.uk/engineering-to-mitigate-climate-change`. Accessed: 06/08/19.

[4] New un climate change report demonstrates need for global engineering congress. `https://www.ice.org.uk/news-and-insight/latest-ice-news/new-un-climate-change-report`. Accessed: 06/08/19.

[5] Institution of Mechanical Engineers report. Population: One planet, too many people? 2011. Available at: `https://www.imeche.org/docs/default-source/1-oscar/reports-policy-statements-and-documents/population---one-planet-too-many-people.pdf?sfvrsn=0`. Accessed: 06/08/19.

[6] Atkins report. Current and emerging trends in the aerospace sector. 2018. Available at: `https://www.atkinsglobal.com/~/media/Files/A/Atkins-Corporate/aviation-trends-white-paper-digital.pdf`. Accessed: 06/08/19.

[7] Royal Academy of Engineering report. Innovation in aerospace. 2014. Available at: `https://www.raeng.org.uk/publications/reports/innovation-in-aerospace`. Accessed: 06/08/19.

[8] MIT and NASA engineers demonstrate a new kind of airplane wing. http://news.mit.edu/2019/engineers-demonstrate-lighter-flexible-airplane-wing-0401. Accessed: 06/08/19.

[9] D. J. Wagg and S. A. Neild. *Nonlinear Vibration with Control*. Springer-Verlag, 2009.

[10] X-43A Mishap Investigation Board. Report of findings, x-43a mishap. 1, 2003.

[11] J. J. McNamara and P. P. Friedmann. Aeroelastic and aerothermoelastic analysis in hypersonic flow: Past, present, and future. *AIAA Journal*, 49:1089–1122, 2011.

[12] S. Ataya and M. M. Z. Ahmed. Damages of wind turbine blade trailing edge: Forms, location, and root causes. *Engineering Failure Analysis*, 35:480–488, 2013.

[13] P. U. Haselbach, M. A. Eder, and F. Belloni. A comprehensive investigation of trailing edge damage in a wind turbine rotor blade. *Wind Energy*, 19:1871–1888, 2016.

[14] K. Elser, S. Hendricks, A. Golder, D. Bale, I. Fotsing, and T. McNulty. Damages of wind turbine blade trailing edge: Forms, location, and root causes. *Garrad Hassan America, Inc.*, 701005-USSD-R-01, 2013.

[15] F. Afonso, J. Vale, É. Oliveira, F. Lau, and A. Suleman. A review on non-linear aeroelasticity of high aspect-ratio wings. *Progress in Aerospace Sciences*, 89:40–57, 2017.

[16] S. Sharma, E. B. Coetzee, M. H. Lowenberg, S. A. Neild, and B. Krauskopf. Numerical continuation and bifurcation analysis in aircraft design: an industrial perspective. *Philolsophical Transactions of the Royal Society A*, 373:20140406, 2015.

[17] CIAIAC. Accident of aircraft fokker mk-100, registration i-alpl, at barcelona airport (barcelona), on 7 november 1999. *Technical Report A-068/1999. Civil Aviation Accident and Incident Investigation Commission, Madrid, Spain.*

[18] D. Rezgui and M. H. Lowenberg. On the nonlinear dynamics of a rotor in autorotation: a combined experimental and numerical approach. *Philosophical Transactions of the Royal Society of London A: Mathematical, Physical and Engineering Sciences*, 373, 2015.

[19] T. Richard, C. Germay, and E. Detournay. Self-excited stick–slip oscillations of drill bits. *C. R. Mecanique*, 332:619–626, 2004.

[20] G. Quintana and J. Ciurana. Chatter in machining processes: A review. *International Journal of Machine Tools and Manufacture*, 51:363–376, 2011.

[21] K. L. Turner, S. A. Miller, P. G. Hartwell, N. C. MacDonald, S. H. Strogatz, and S. G. Adams. Five parametric resonances in a microelectromechanical system. *Nature*, 396:149–152, 1998.

[22] J. R. Rhoads, S. W. Shaw, and K. L. Turner. Nonlinear dynamics and its applications in micro- and nanoresonators. *Journal of Dynamic Systems, Measurement, and Control*, 132, 2010.

[23] E. R. Jørgensen, K. K. Borum, M. McGugan, C. L. Thomsen, F. M. Jensen, C. P. Debel, and B. F. Sørensen. Full scale testing of wind turbine blade to failure - flapwise loading. *Denmark. Forskningscenter Risoe. Risoe-R*, 1392, 2004.

[24] D. J. Ewins. *Modal Testing: Theory, Practice and Application*. Research Studies Press Ltd., 2000.

[25] W. Lacarbonara. *Nonlinear Structural Mechanics: Theory, Dynamical Phenomena and Modeling*. Springer Science and Business Media, 2013.

[26] S. H. Strogatz. *Nonlinear Dynamics and Chaos*. Perseus Books, 1994.

[27] J. V. Carroll and R. K. Mehra. Bifurcation analysis of nonlinear aircraft dynamics. *Journal of Guidance, Control and Dynamics*, 5:529–536, 1982.

[28] C. Chen, D. H. Zanette, D. A. Czaplewski, S. Shaw, and D. López. Direct observation of coherent energy transfer in nonlinear micromechanical oscillators. *Nature Communications*, page 15523, 2017.

[29] E. J. Doedel, A. R. Champneys, T. F. Fairgrieve, Y. A. Kuznetsov, F. Dercole, B. E. Oldeman, R. C. Paffenroth, B. Sandstede, X. J. Wang, and C. Zhang. Auto-07p: Continuation and bifurcation software for ordinary differential equations, Montreal, Concordia University, Canada, 2008. Available at: http://cmvl.cs.concordia.ca.

[30] E. J. Doedel. Auto: A program for the automatic bifurcation analysis of autonomous systems. *Congressus Numerantium*, 30:265–384, 1980.

[31] W. Govaerts, Y. A. Kuznetsov, O. De Feo, A. Dhooge, V. Govorukhin, R. K. Ghaziani, H. G. E. Meijer, W. Mestrom, A. Riet, and B. Sautois. Matcont continuation software in matlab. Available at: http://www.matcont.ugent.be/.

[32] A. Dhooge, W. Govaerts, and Y. A. Kuznetsov. Matcont: A matlab package for numerical bifurcation analysis of odes. *ACM Transactions on Mathematical Software*, 29:141–164, 2003.

[33] F. Schilder and H. Dankowicz. Continuation core (coco). Available at: https://sourceforge.net/projects/cocotools/.

[34] H. Dankowicz and F. Schilder. *Recipes for Continuation*. Philadelphia, PA: Society for Industrial and Applied Mathematics., 2013.

[35] C. R., Kirkendall, and J. W. Kwon. Multistable internal resonance in electroelastic crystals with nonlinearly coupled modes. *Scientific Reports*, 6:22897, 2016.

[36] D. I. Caruntu and I. Martinez. Reduced order model of parametric resonance of electrostatically actuated mems cantilever resonators. *International Journal of Non-Linear Mechanics*, 66:28–32, 2014.

[37] D. I. Caruntu and L. Luo. Frequency response of primary resonance of electrostatically actuated cnt cantilevers. *Nonlinear Dynamics*, 78:1827–1837, 2014.

[38] D. I. Caruntu, M. Botello, C. A. Reyes, and J. Beatriz. Voltage–amplitude response of superharmonic resonance of second order of electrostatically actuated mems cantilever resonators. *Journal of Computational and Nonlinear Dynamics*, 14:031005, 2019.

[39] D. I. Caruntu and R. Oyervides. Frequency response reduced order model of primary resonance of electrostatically actuated mems circular plate resonators. *Communications in Nonlinear Science and Numerical Continuation*, 43:261–270, 2017.

[40] M. Botello, J. Beatriz, and D. I. Caruntu. Voltage response of circular plate mems resonators under superharmonic resonance. In *Proceedings of the ASME 2018 International Mechanical Engineering Congress and Exposition*, 2018.

[41] H. Farokhi and M. H. Ghayesh. Nonlinear size-dependent dynamics of microarches with modal interactions. *Journal of Vibration and Control*, 22:3679–3689, 2016.

[42] D. J. Skubov, A. V. Lukin, and L. V. Shtukin. Nonlinear dynamics of microelectromechanic element. *International Journal of Mathematics and Computers in Simulation*, 12:88–95, 2018.

[43] M. Peeters, L. Renson, and G. Kerschen. Nnmcont: A matlab package for the continuation of nonlinear normal modes. Available at: http://www.ltasvis.ulg.ac.be/cmsms/index.php?page=nnm.

[44] M. Peeters, R. Viguié, G. Kerschen, G. Sérandour, and J. C. Golinval. Nonlinear normal modes, part ii: Toward a practical computation using numerical continuation techniques. *Mechanical Systems and Signal Processing*, 23:195–216, 2009.

[45] D. Piombino, M. S. Allen, D. Ehrhardt, T. Beberniss, and J. J. Hollkamp. System identification to estimate the nonlinear modes of a gong. In G. Kerschen, editor, *Nonlinear Dynamics, Volume 1*, pages 121–136. Springer International Publishing, 2019.

[46] M. S. Allen, R. J. Kuether, B. J. Deaner, and M. W. Sraric. A numerical continuation method to compute nonlinear normal modes using modal reduction. In *53rd AIAA/ASME/ASCE/AHS/ASC Structures, Structural Dynamics and Materials Conference, Structures, Structural Dynamics, and Materials and Co-located Conferences*, 2012.

[47] R. J. Kuether and M. S. Allen. A numerical approach to directly compute nonlinear normal modes of geometrically nonlinear finite element models. *Mechanical Systems and Signal Processing*, 46:1–15, 2014.

[48] J. Sieber and B. Krauskopf. Control based bifurcation analysis for experiments. *Nonlinear Dynamics*, 51:365–377, 2008.

[49] D. A. W. Barton and S. G. Burrows. Numerical continuation in a physical experiment: Investigation of a nonlinear energy harvester. *Journal of Computational and Nonlinear Dynamics*, 6:011010, 2010.

[50] D. A. W. Barton and J. Sieber. Systematic experimental exploration of bifurcations with noninvasive control. *Physical Review E*, 87:052916, 2013.

[51] E. Bureau, F. Schilder, I. F. Santos, J. J. Thomsen, and J. Starke. Experimental bifurcation analysis of an impact oscillator — tuning a non-invasive control scheme. *Journal of Sound and Vibration*, 332:5883–5897, 2013.

[52] E. Bureau, F. Schilder, M. Elmegård, I. F. Santos, J. J. Thomsen, and J. Starke. Experimental bifurcation analysis of an impact oscillator — determining stability. *Journal of Sound and Vibration*, 333:5464–5474, 2014.

[53] D. A. W. Barton. Control-based continuation: Bifurcation and stability analysis for physical experiments. *Mechanical Systems and Signal Processing*, 84:54–64, 2017.

[54] L. Renson, A. Gonzalo-Buelga, D. A. W. Barton, and S. A. Neild. Robust identification of backbone curves using control-based continuation. *Journal of Sound and Vibration*, 367:145–158, 2016.

[55] A. D. Shaw, T. L. Hill, S. A. Neild, and M. I. Friswell. Periodic responses of a structure with 3:1 internal resonance. *Mechanical Systems and Signal Processing*, 81:19–34, 2016.

[56] M. P. Mignolet, A. Przekop, S. A. Rizzi, and S. M. Spottswood. A review of indirect/non-intrusive reduced order modeling of nonlinear geometric structures. *Journal of Sound and Vibration*, 332:2437–2460, 2013.

[57] M. I. McEwan, J. R. Wright, J. E. Cooper, and A. Y. Y. Leung. A combined modal/finite element analysis technique for the dynamic response of a non-linear beam to harmonic excitation. *Journal of Sound and Vibration*, 243:601–624, 2001.

[58] M. I. McEwan, J. R. Wright, J. E. Cooper, and A. Y. T. Leung. A finite element/modal technique for nonlinear plate and stiffened panel response prediction. In *Proceedings of the 42nd Structures, Structural Dynamics, and Materials Conference*, 2001.

[59] J. J. Hollkamp and R. W. Gordon. Reduced-order models for nonlinear response prediction: Implicit condensation and expansion. *Journal of Sound and Vibration*, 318:1139–1153, 2008.

[60] R. W. Gordon and J. J. Hollkamp. Reduced-order models for acoustic response prediction. *Air Force Research Laboratory (AFRL), Wright-Patterson Air Force Base, OH AFRL-RB-WP-TR-2011-3040*, 2011.

[61] A. A. Muravyov and S. A. Rizzi. Determination of nonlinear stiffness with application to random vibration of geometrically nonlinear structures. *Computers and Structures*, 81:1513–1523, 2003.

[62] R. J. Kuether, B. J. Deaner, J. J. Hollkamp, and M. S. Allen. Evaluation of geometrically nonlinear reduced-order models with nonlinear normal modes. *AIAA Journal*, 53:3273–3285, 2015.

[63] R. J. Kuether, M. R. W. Brake, and M. S. Allen. Evaluating convergence of reduced order models using nonlinear normal modes. *Model Validation and Uncertainty Quantification*, 3:287–300, 2014.

[64] R. J. Kuether, M. R. W. Brake, and M. S. Allen. Numerical methods for assessing response metrics. In M. R. W. Brake, editor, *The Mechanics of Jointed Structures*, pages 539–560. 2017.

[65] S. M. Spottswood and R. J. Allemang. Identification of nonlinear parameters for reduced order models. *Journal of Sound and Vibration*, 295:226–245, 2006.

[66] P. R. Cunningham and R. G. White. A review of analytical methods for aircraft structures subjected to high-intensity random acoustic loads. *Proceedings of the Institution of Mechanical Engineers, Part G: Journal of Aerospace Engineering*, 218:231–242, 2014.

[67] J. J. Hollkamp, R. W. Gordon, and S. M. Spottswood. Nonlinear modal models for sonic fatigue response prediction: a comparison of methods. *Journal of Sound and Vibration*, 284:1145–1163, 2005.

[68] R. W. Gordon and J. J. Hollkamp. Coupled structural-acoustic response prediction with complex modal models. In *50th AIAA/ASME/ASCE/AHS/ASC Structures, Structural Dynamics and Materials Conference*, 2009.

[69] S. A. Rizzi and A. Przekop. The effect of basis selection on static and random acoustic response prediction using a nonlinear modal simulation. *NASA/TP-2005-213943*, 2011.

[70] S. A. Rizzi and A. Przekop. System identification-guided basis selection for reduced-order nonlinear response analysis. *Journal of Sound and Vibration*, 315:467–485, 2008.

[71] S. A. Rizzi and A. Przekop. Estimation of sonic fatigue by reduced-order finite element based analysis. In M.J. Brennan and S. Liguore, editors, *Proceedings of the 9th International Conference on Recent Advances in Structural Dynamics*, 2006.

[72] R. Perez, X. Q. Wang, and M. P. Mignolet. Reduced order modeling for the nonlinear geometric response of cracked panels. In *52nd AIAA/ASME/ASCE/AHS/ASC Structures, Structural Dynamics and Materials Conference*, 2011.

[73] L. Liu, J. Ren, T.-R. He, and G. Kardomateas. Nonlinear dynamic response of acoustically excited and thermally loaded composite plates resting on elastic foundations. *International Journal of Solids and Structures*, 148-149:44–66, 2018.

[74] R. Perez, X. Q. Wang, and M. P. Mignolet. Steady and unsteady nonlinear thermoelastodynamic response of panels by reduced order models. In *51st AIAA/ASME/ASCE/AHS/ASC Structures, Structural Dynamics and Materials Conference*, 2010.

[75] R. Perez, X. Q. Wang, and M. P. Mignolet. Nonlinear reduced-order models for thermoelastodynamic response of isotropic and functionally graded panels. *AIAA Journal*, 49:630–641, 2011.

[76] M. Matney, R. A. Perez, S. M. Spottswood, X. Q. Wang, and A. M. P Mignolet. Nonlinear structural reduced order modeling methods for hypersonic structures. In *53rd AIAA/ASME/ASCE/AHS/ASC Structures, Structural Dynamics and Materials Conference*, 2012.

[77] A. Matney, S. M. Spottswood, and R. Perez abd M. Mignolet. Nonlinear unsteady thermoelastodynamic response of a panel subjected to an oscillating flux by reduced order models. In *52nd AIAA/ASME/ASCE/AHS/ASC Structures, Structural Dynamics and Materials Conference*, 2011.

[78] T. E. Noll, J. M. Brown, M. E. Perez-Davis, S. D. Ishmael, G. C. Tiffany, and M. Gaier. Investigation of the helios prototype aircraft mishap. volume i . mishap report. *Technical report, NASA*, 2004.

[79] M. Y. Harmin and J. E. Cooper. Aeroelastic behaviour of a wing including geometric nonlinearities. *The Aeronautical Journal*, 115:767–777, 2011.

[80] N. A. Rosly and M. Y. Harmin. Finite element analysis of high aspect ratio wind tunnel wing model: A parametric study. *IOP Conference Series: Materials Science and Engineering*, 270, 2017.

[81] K. Ahmad, Z. G. Wu, and H. J. Hasham. Fe-modal approach to model geometric nonlinearities of high aspect ratio wing. *Applied Mechanics and Materials*, 390:28–32, 2013.

[82] X. Q. Wang, R. A. Perez, M. P. Mignolet, R. Capillon, and C. So. Nonlinear reduced order modeling of complex wing models. In *54th AIAA/ASME/ASCE/AHS/ASC Structures, Structural Dynamics and Materials Conference*, 2013.

[83] P. Ribeiro. Free periodic vibrations of beams with large displacements and initial plastic strains. *International Journal of Mechanical Sciences*, 52:1407–1418, 2010.

[84] R. Perez, X. Q. Wang, and M. P. Mignolet. Nonintrusive structural dynamic reduced order modeling for large deformations: Enhancements for complex structures. *Journal of Computational and Nonlinear Dynamics*, 9, 2014.

[85] E. Manoach and P. Ribeiro. Coupled, thermoelastic, large amplitude vibrations of timoshenko beams. *International Journal of Mechanical Sciences*, 46:1589–1606, 2004.

[86] Y. Y. Lee, C. F. Ng, and X. Guo. Nonlinear random response of cylindrical panels to acoustic excitations using finite element modal method. *Nonlinear Dynamics*, 31:327–345, 2003.

[87] M. S. Allen, R. M. Lacayo, and M. R. Brake. Quasi-static modal analysis based on implicit condensation for structures with nonlinear joints. In *The 2016 Leuven Conference on Noise and Vibration Engineering*, 2016.

[88] A. Lazarus, O. Thomas, and J.-F. De u. Finite element reduced order models for nonlinear vibrations of piezoelectric layered beams with applications to nems. *Finite Elements in Analysis and Design*, 49:35–51, 2012.

[89] R.J. Kuether, M.S. Allen, and J.J. Hollkamp. Modal substructuring of geometrically nonlinear finite-element models with interface reduction. *AIAA Journal*, 55:1695–1706, 2017.

[90] R. J. Kuether, M. S. Allen, and J. J. Hollkamp. Modal substructuring of geometrically nonlinear finite-element models. *AIAA Journal*, 54:691–702, 2016.

[91] R. J. Kuether and M. S. Allen. Nonlinear modal substructuring of systems with geometric nonlinearities. In *54th AIAA/ASME/ASCE/AHS/ASC Structures, Structural Dynamics and Materials Conference*, 2013.

[92] T. Detroux, J.-P. Noël, L. N. Virgin, and G. Kerschen. Experimental study of isolas in nonlinear systems featuring modal interactions. *PLoS One*, 13:e0194452, 2018.

[93] T. L. Hill, S. A. Neild, and A. Cammarano. An analytical approach for detecting isolated periodic solution branches in weakly nonlinear structures. *Journal of Sound and Vibration*, 379, 2016.

[94] A. H. Nayfeh and D. T. Mook. *Nonlinear Oscillations*. Wiley, 1979.

[95] N. M. Krylov and N. N. Bogoliubov. *Introduction to Non-linear Mechanics*. Princeton University Press, 11 edition, 1949.

[96] N. N. Bogoliubov and Y. A. Mitropolskii. *Asymptotic Methods in the Theory of Non-linear Oscillations*. Gordon and Breach, 1961.

[97] A. H. Nayfeh and D. T. Mook. *Nonlinear Oscillations*. John Wiley and Sons, 1979.

[98] G. Kerschen, M. Peeters, J. C. Golinval, and A. F. Vakakis. Nonlinear normal modes, part i: A useful framework for the structural dynamicist. *Mechanical Systems and Signal Processing*, 23:170–194, 2009.

[99] J. P. Noël and G. Kerschen. Nonlinear system identification in structural dynamics: 10 more years of progress. *Mechanical Systems and Signal Processing*, 83:2–35, 2017.

[100] M. B. Özer and H. Nevzat Özgüven. A new method for localization and identification of non-linearities in structures. In *Proceedings of ESDA 2002: 6th Biennial Conference on Engineering Systems*, 2002.

[101] M. B. Özer, H. Nevzat Özgüven, and T. J. Royston. Identification of structural non-linearities using describing functions and the sherman–morrison method. *Mechanical Systems and Signal Processing*, 23:30–44, 2009.

[102] M. Aykan and H. Nevzat Özgüven. Parametric identification of nonlinearity in structural systems using describing function inversion. *Mechanical Systems and Signal Processing*, 40:356–376, 2013.

[103] M. D. Narayanan, S. Narayanan, and C. Padmanabhan. Parametric identification of nonlinear systems using multiple trials. *Nonlinear Dynamics*, 48:341–360, 2007.

[104] M. D. Narayanan, S. Narayanan, and C. Padmanabhan. Multiharmonic excitation for nonlinear system identification. *Journal of Sound and Vibration*, 311:707–728, 2008.

[105] S. Karkar, B. Cochelin, and C. Vergez. A comparative study of the harmonic balance method and the orthogonal collocation method on stiff nonlinear systems. *Journal of Sound and Vibration*, 333:2554–2567, 2014.

[106] B. Zaghari, M. Ghandchi-Tehrani, and E. Rustighi. Mechanical modeling of a vibration energy harvester with time-varying stiffness. In A. Cunha, E. Caetano, P. Ribeiro, and G. Müller, editors, *Proceedings of the 9th International Conference on Structural Dynamics, EURODYN 2014*, pages 2079–2085, 2014.

[107] T. Detroux, L. Renson, L. Masset, and G. Kerschen. The harmonic balance method for bifurcation analysis of large-scale nonlinear mechanical systems. *Computer Methods in Applied Mechanics and Engineering*, 296:18–38, 2015.

[108] J. A. Murdock. *Perturbations: Theory and Methods*. SIAM, 1999.

[109] J. A. Sanders, F. Verhulst, and J. Murdock. *Averaging Methods in Nonlinear Dynamical Systems*. Springer, 2007.

[110] E. C. Miranda and J. J. Thomsen. Vibration induced sliding: Theory and experiment for a beam with a spring-loaded mass. *Nonlinear Dynamics*, 16:167–186, 1998.

[111] A. H. Nayfeh. *Introduction to Perturbation Techniques*. Wiley, 1981.

[112] A.H. Nayfeh. *Perturbation Methods*. Wiley, 2000.

[113] R. E. Mickens. *Oscillations in Planar Dynamic Systems*. World Scientific, 1996.

[114] F. Benedettini, G. Rega, and R. Alaggio. Non-linear oscillations of a four-degree-of-freedom model of a suspended cable under multiple internal resonance conditions. *Journal of Sound and Vibration*, 182:775–798, 1995.

[115] C. L. Lee and N. C. Perkins. Nonlinear oscillations of suspended cables containing a two-to-one internal resonance. *Nonlinear Dynamics*, 3:465–490, 1992.

[116] A. H. Nayfeh. Quenching of primary resonance by a superharmonic resonance. *Journal of Sound and Vibration*, 92:363–377, 1982.

[117] A. Luongo and A. Di Egidio. Perturbation methods for bifurcation analysis from multiple nonresonant complex eigenvalues. *Nonlinear dynamics*, 14:193–210, 1997.

[118] A. Luongo, A. Paolone, and A. Di Egidio. Multiple timescales analysis for 1:2 and 1:3 resonant hopf bifurcations. *Nonlinear dynamics*, 34:269–291, 2003.

[119] A. Luongo and A. Paolone. Bifurcation equations through multiple-scales analysis for a continuous model of a planar beam. *Nonlinear dynamics*, 41:171–190, 2005.

[120] W. Wang and J. Xu. Multiple scales analysis for double hopf bifurcation with 1:3 resonance. *Nonlinear dynamics*, 66:39–51, 2011.

[121] T.L. Hill, S.A. Neild, and D.A.W. Barton. Comparing the direct normal form method with harmonic balance and the method of multiple scales. *Procedia Engineering 199*, pages 869–874, 2017.

[122] Z. Rahman and T. D. Burton. On higher order methods of multiple scales in non-linear oscillations-periodic steady state response. *Journal of Sound and Vibration*, 133:369–379, 1989.

[123] A. H. Nayfeh. *Method of normal forms*. Wiley, 1993.

[124] S. A. Neild, A. R. Champneys, D. J. Wagg, T. L. Hill, and A. Cammarano. The use of normal forms for analysing nonlinear mechanical vibrations. *Philosophical Transactions of the Royal Society A*, 373(2051):20140404, 2015.

[125] L. Jezequel and C. H. Lamarque. Analysis of nonlinear dynamic systems by the normal form theory. *Journal of Sound and Vibration*, 149(3):429–459, 1991.

[126] B. Qinsheng, C. Yushu, and W. Zhiqiang. Local bifurcation analysis of strongly non-linear duffing system. *Applied Mathematics and Mechanics*, 17:837–845, 1996.

[127] L. Cheikh, C. Pauchon, C.-H. Lamarque, A. Combescure, and R. J. Gibert. Nonlinear stability of a defective cylindrical shell. *Mechanics Research Communications*, 23:151–164, 1996.

[128] F. Pellicano and F. Mastroddi. Applicability conditions of a non-linear superposition technique. *Journal of Sound and Vibration*, 200:3–14, 1997.

[129] C. Touzé, O. Thomas, and A. Chaigne. Hardening/softening behaviour in non-linear oscillations of structural systems using non-linear normal modes. *Journal of Sound and Vibration*, 273:77–101, 2004.

[130] S. A. Neild and D. J. Wagg. Applying the method of normal forms to second-order nonlinear vibration problems. *Proceedings of the Royal Society of London A*, 467(2128):1141–1163, 2011.

[131] T. L. Hill, A. Cammarano, S. A. Neild, and D. J. Wagg. Out-of-unison resonance in weakly nonlinear coupled oscillators. *Proceedings of the Royal Society of London*

A: Mathematical, Physical and Engineering Sciences, 471, pp. 20140659. The Royal Society, 2015b.

[132] T. L. Hill, P. L. Green, A. Cammarano, and S. A. Neild. Fast bayesian identification of a class of elastic weakly nonlinear systems using backbone curves. *Journal of Sound and Vibration*, 360:156–170, 2016.

[133] A. Cammarano, T.L. Hill, S.A. Neild, and D.J. Wagg. Bifurcations of backbone curves for systems of coupled nonlinear two mass oscillators. *Nonlinear Dynamics*, 77:311–320, 2014.

[134] C.-H. Lamarque, C. Touzé, and). Thomas. An upper bound for validity limits of asymptotic analytical approaches based on normal form theory. *Nonlinear Dynamics*, 70:1931–1949, 2012.

[135] M. Eugeni, E. H. Dowell, and F. Mastroddi. Post-buckling longterm dynamics of a forced nonlinear beam: A perturbation approach. *Journal of Sound and Vibration*, 333:2617–2631, 2014.

[136] Z. Xin, S. A. Neild, and D. J. Wagg. The selection of the linearized natural frequency for the second-order normal form method. In *ASME 2011 International Design Engineering Technical Conferences and Computers and Information in Engineering Conference*, pages 1211–1218, 2011.

[137] A. Hassan. Use of transformations with the higher order method of multiple scales to determine the steady state periodic response of harmonically excited non-linear oscillators, part i: transformation of derivative. *Journal of Sound and Vibration*, 178:1–19, 1994.

[138] A. Hassan. Use of transformations with the higher order method of multiple scales to determine the steady state periodic response of harmonically excited non-linear oscillators, part ii: transformation of detuning. *Journal of Sound and Vibration*, 178:21–40, 1994.

[139] O. Zienkiewicz, R. Taylor, and J. Z. Zhu. *The Finite Element Method: Its Basis and Fundamentals*. Butterworth-Heinemann, 2013.

[140] W. Weaver Jr., S. P. Timoshenko, and D. H. Young. *Vibration Problems in Engineering*. Wiley, fifth edition, 1990.

[141] A. Labuschagne, N. F. J. van Rensburg, and A. J. van der Merwe. Comparison of linear beam theories. *Mathematical and Computer Modelling*, 49:20–30, 2009.

[142] A. Yashar, N. Ferguson, and M. Ghandchi-Tehrani. Simplified modelling and analysis of a rotatin euler-bernoulli beam with a single cracked edge. *Journal of Sound and Vibration*, 420:346–356, 2018.

[143] I. Romero. A comparison of finite elements for nonlinear beams: the absolute nodal coordinate and geometrically exact formulations. *Multibody System Dynamics*, 20:51–68, 2008.

[144] J. S. Rao and W. Carnegie. Solution of the equations of motion of coupled-bending bending torsion vibrations of turbine blades by the method of ritz-galerkin. *International Journal of Mechanical Sciences*, 12:875–882, 1970.

[145] T. J. R. Hughes. *The Finite Element Method: Linear Static and Dynamic Finite Element Analysis*. Courier Company, 2012.

[146] C. Touzé, O. Thomas, and A. Chaigne. Asymmetric non-linear forced vibrations of free-edge circular plates. part 1: theory. *Journal of Sound and Vibration*, 258:649–676, 2002.

[147] S.-S. Chen. Vibration and stability of a uniformly curved tube conveying fluid. *The Journal of the Acoustical Society of America*, 51:223–232, 1972.

[148] S.-S. Chen. Out-of-plane vibration and stability of curved tubes conveying fluid. *Journal of Applied Mechanics*, 40:362–368, 1973.

[149] C. O. Chang and K. C. Chen. Dynamics and stability of pipes conveying fluid. *Journal of Pressure Vessel Technology*, 116:57–66, 1994.

[150] R. A. Stein and M. W. Tobriner. Vibration of pipes containing flowing fluids. *Journal of Applied Mechanics*, 37:906–916, 1970.

[151] C. Semler, G. X. Li, and M. P. Païdoussis. The non-linear equations of motion of pipes conveying fluid. *Journal of Sound and Vibration*, 169:577–599, 1994.

[152] M. P. Païdoussis and J.-P. Denise. Flutter of thin cylindrical shells conveying fluid. *Journal of Sound and Vibration*, 20:9–26, 1972.

[153] B. Porter and R. A. Billett. Harmonic and sub-harmonic vibration of a continuous system having non-linear constraint. *International Journal of Mechanical Sciences*, 7:431–439, 1965.

[154] A. Rutenberg. Vibration frequencies for a uniform cantilever with a rotational constraint at a point. *ASME Journal of Applied Mechanics*, 45:422–423, 1978.

[155] J. H. Lau. Vibration frequencies and mode shapes for a constrained cantilever. *Journal of Applied Mechanics*, 51:182–187, 1984.

[156] C. Kameswara Rao and S. Mirza. A note on vibrations of generally restrained beams. *Journal of Sound and Vibration*, 130:453–465, 1989.

[157] W. L. Li. Free vibrations of beams with general boundary conditions. *Journal of Sound and Vibration*, 237:709–725, 2000.

[158] A. Bokaian. Natural frequencies of beams under compressive axial loads. *Journal of Sound and Vibration*, 126:49–65, 1989.

[159] T.L. Hill, A. Cammarano, S.A. Neild, and D.A.W. Barton. Identifying the significance of nonlinear normal modes. *Proceedings of the Royal Society A*, 473, 2017.

[160] W. Szemplinska-Stupnicka. "Non-linear normal modes" and the generalized Ritz method in the problems of vibrations of non-linear elastic continuous systems. *International Journal of Non-Linear Mechanics*, 18:149–165, 1983.

[161] W. L. Li. Vibration analysis of rectangular plates with general elastic boundary supports. *Journal of Sound and Vibration*, 273:619–635, 2004.

[162] X. Zhang and W. L. Li. Vibrations of rectangular plates with arbitrary non-uniform elastic edge restraints. *Journal of Sound and Vibration*, 326:221–234, 2009.

[163] G. Jin, Z. Su, S. Shi, T. Ye, and S. Gao. Three-dimensional exact solution for the free vibration of arbitrarily thick functionally graded rectangular plates with general boundary conditions. *Composite Structures*, 108:565–577, 2014.

[164] Z. Su, G. Jin, S. Shi, T. Ye, and X. Jia. A unified solution for vibration analysis of functionally graded cylindrical, conical shells and annular plates with general boundary conditions. *International Journal of Mechanical Sciences*, 80:62–80, 2014.

[165] M. Xu. Free transverse vibrations of nano-to-micron scale beams. *Proceedings of the Royal Society of London A: Mathematical, Physical and Engineering Sciences*, 462, 2006.

[166] W. K. Lee and M. H. Yeo. Two-mode interaction of a beam with a nonlinear boundary condition. *Journal of Vibration and Acoustics*, 121:84–88, 1999.

[167] G.-C. Zhang, L.-Q. Chen, and H. Ding. Forced vibration of tip-massed cantilever with nonlinear magnetic interactions. *International Journal of Applied Mechanics*, 6, 2014.

[168] T. F. Ma and J. da Silva. Iterative solutions for a beam equation with nonlinear boundary conditions of third order. *Applied Mathematics and Computation*, 159:11–18, 2004.

[169] Q. A. Dang and N. T. Huong. Iterative method for solving a beam equation with nonlinear boundary conditions. *Advances in Numerical Analysis*, 2013.

[170] Q. Gao. The solvability and numerical simulation for the elastic beam problems with nonlinear boundary conditions. *Abstract and Applied Analysis*, 2014.

[171] S. Heidarkhani, M. Ferrara, A. Salari, and M. Azimbagirad. A variational approach to perturbed elastic beam problems with nonlinear boundary conditions. *Mathematical Reports*, 18:573–589, 2016.

[172] R. C. Batra, M. Porfiri, and D. Spinello. Reduced-order models for microelectromechanical rectangular and circular plates incorporating the casimir force. *International Journal of Solids and Structures*, 45:3558–3583, 2008.

[173] T. Ikehara, J. Lu, M. Konno, R. Maeda, and T. Mihara. A high quality-factor silicon cantilever for a low detection-limit resonant mass sensor operated in air. *Journal of Micromechanics and Microengineering*, 17:2491–2494, 2007.

[174] I. Voiculescu and M. Zaghloul. *Nanocantilever Beams: Modeling, Fabrication, and Applications*. CRC Press, 2015.

[175] A. Raman and D. Kiracofe. Nonlinear dynamics of atomic force microscope microcantilevers in liquid environments - a review. *Nonlinear Theory and Its Applications, IEICE*, 4:184–197, 2013.

[176] A. J. Putman, K. O. Van der Werf, B. G. De Grooth, N. F. Van Hulst, and J. Greve. Tapping mode atomic force microscopy in liquid. *Applied Physics Letters*, 64:2454–2456, 1994.

[177] S. Basak and A. Raman. Dynamics of tapping mode atomic force microscopy in liquids: Theory and experiments. *Applied Physics Letters*, 91:064107, 2007.

[178] D. Kiracofe and A. Raman. Nonlinear dynamics of the atomic force microscope at the liquid-solid interface. *Physical Review B*, 86:205405, 2012.

[179] C.-Y. Chen, M.-H. Li, and S.-S. Li. Cmos-mems resonators and oscillators: A review. *Sensors and Materials*, 30:733–756, 2018.

[180] C. R. Kirkendall, D. J. Howard, and J. W. Kwon. Internal resonance in quartz crystal resonator and mass detection in nonlinear regime. *Applied Physics Letters*, 103:223502, 2013.

[181] C. Gui, R. Legtenberg, H. A. C. Tilmans, J. H. J. Fluitman, and M. Elwenspoek. Nonlinearity and hysteresis of resonant strain gauges. *Journal of Microelectromechanical Systems*, 7:122–127, 1998.

[182] T. Bourouina, A. Garnier, H. Fujita, T. Masuzawa, and J.-C. Peuzin. Mechanical nonlinearities in a magnetically actuated resonator. *Journal of Micromechanics and Microengineering*, 10:265–270, 2000.

[183] S.-B. Shim, M. Imboden, and P. Mohanty. Synchronized oscillation in coupled nanomechanical oscillators. *Science*, 316:95–99, 2007.

[184] H. A. C. Tilmans and R. Legtenberg. Electrostatically driven vacuum-encapsulated polysilicon resonators, part ii: Theory and performance. *Sensors and Actuators A*, 45:67–84, 1994.

[185] K. F. Wang, S. Zeng, and B. L. Wang. Large amplitude free vibration of electrically actuated nanobeams with surface energy and thermal effects. *International Journal of Mechanical Sciences*, 131-132:227–233, 2017.

[186] R. Almog, S. Zaitsev, O. Shtempluck, and E. Buks. Noise squeezing in a nanomechanical duffing resonator. *Physical Review Letters*, 98:078103, 2007.

[187] L. G. Villanueva, E. Kenig, R. B. Karabalin, M. H. Matheny, R. Lifshitz, M. C. Cross, and M. L. Roukes. Surpassing fundamental limits of oscillators using nonlinear resonators. *Physical Review Letters*, 110:177208, 2013.

[188] D. Antonio, D. H. Zanette, and D. López. Frequency stabilization in nonlinear micromechanical oscillators. *Nature Communications*, 3, 2017.

[189] L. G. Villanueva, R. B. Karabalin, M. H. Matheny, E. Kenig, R. Lifshitz, M. C. Cross, and M. L. Roukes. A nanoscale parametric feedback oscillator. *Nano Letters*, 11:5054–5059, 2011.

[190] B. E. DeMartini, J. F. Rhoads, K. L. Turner, S. W. Shaw, and J. Moehlis. Linear and nonlinear tuning of parametrically excited mems oscillators. *Journal of Microelectromechanical Systems*, 16:310–318, 2007.

[191] B. Zaghari, E. Rustighi, and M. Ghandchi-Tehrani. Dynamic response of a nonlinear parametrically excited system subject to harmonic base excitation. *Journal of Physics: Conference Series*, 744:012125, 2016.

[192] B. Zaghari, E. Rustighi, and M. Ghandchi-Tehrani. Improved modelling of a nonlinear parametrically excited system with electromagnetic excitation. *Vibration*, 1:157–171, 2018.

[193] N. Kacem, S. Hentz, D. Pinto, B. Reig, and V. Nguyen. Nonlinear dynamics of nanomechanical beam resonators: improving the performance of nems-based sensors. *Nanotechnology*, 20:275501, 2009.

[194] F. Ayela and T. Fournier. An experimental study of anharmonic micromachined silicon resonators. *Measurement Science and Technology*, 9:1821–1830, 1998.

[195] H. A. C. Tilmans, M. Elwenspoek, and J. H. J. Fluitman. Micro resonant force gauges. *Sensors and Actuators A*, 30:35–53, 1992.

[196] S. Evoy, D. W. Carr, L. Sekaric, A. Olkhovets, J. M. Parpia, and H. G. Craighead. Nanofabrication and electrostatic operation of single-crystal silicon paddle oscillators. *Journal of Applied Physics*, 86:6072–6077, 1999.

[197] W. Zhang, R. Baskaran, and K. L. Turner. Effect of cubic nonlinearity on auto-parametrically amplified resonant mems mass sensor. *Sensors and Actuators A*, 102:139–150, 2013.

[198] J. R. Rhoads, S. W. Shaw, K. L. Turner, J. Moehlis, B. E. DeMartini, and W. Zhang. Generalized parametric resonance in electrostatically actuated microelectromechanical oscillators. *Journal of Sound and Vibration*, 296:797–829, 2006.

[199] D. K. Agrawal, J. Woodhouse, and A. A. Seshia. Modeling nonlinearities in mems oscillators. *IEEE Transactions on Ultrasonics, Ferroelectrics, and Frequency Control*, 60:1646 – 1659, 2013.

[200] M. I. Younis, E. M. Abdel-Rahman, and A. H. Nayfeh. A study of the nonlinear response of a resonant microbeam to an electric actuation. *Nonlinear Dynamics*, 31:91–117, 2003.

[201] J. F. Rhoads, V. Kumar, S. W. Shaw, and K. L. Turner. The non-linear dynamics of electromagnetically actuated microbeam resonators with purely parametric excitations. *International Journal of Non-Linear Mechanics*, 55:79–89, 2013.

[202] S. W. Shaw, J. F. Rhoads, K. L. Turner, J. Moehlis, B. E. DeMartini, and W. Zhang. Generalized parametric resonance in electrostatically actuated microelectromechanical oscillators. *Journal of Sound and Vibration*, 296:797–829, 2016.

[203] X. Chen and S. A. Meguid. Dynamic behavior of micro-resonator under alternating current voltage. *International Journal of Mechanics and Materials in Design*, 13:481–497, 2017.

[204] X. Chen and S. A. Meguid. Nonlinear vibration analysis of a microbeam subject to electrostatic force. *Acta Mechanica*, 228:1343–1361, 2017.

[205] M. I. Younis, E. M. Abdel-Rahman, and A. H. Nayfeh. A reduced-order model for electrically actuated microbeam-based mems. *Journal of Microelectromechanical Systems*, 12, 2003.

[206] A. R. Askari and M. Tahani. An alternative reduced order model for electrically actuated micro-beams under mechanical shock. *Mechanics Research Communications*, 57:34–39, 2014.

[207] L. Ruzziconi, M. I. Younis, and S. Lenci. An efficient reduced-order model to investigate the behavior of an imperfect microbeam under axial load and electric excitation. *Journal of Computational and Nonlinear Dynamics*, 8, 2013.

[208] L. Ruzziconi, M. Bataineh, M. I. Younis, W. Cui, and S. Lenci. Nonlinear dynamics of an electrically actuated imperfect microbeam resonator: experimental investigation and reduced-order modeling. *Journal of Micromechanics and Microengineering*, 23, 2013.

[209] Y. Song and B. Bhushan. *Modeling of Tip-Cantilever Dynamics in Atomic Force Microscopy*, pages 149–223. Springer Berlin Heidelberg, 2007.

[210] A. Delnavaz, S. N. Mahmoodi, N. Jalili, M. M. Ahadian, and H. Zohoor. Nonlinear vibrations of microcantilevers subjected to tip-sample interactions: Theory and experiment. *Journal of Applied Physics*, 106, 2009.

[211] Y. Song and B. Bhushan. Atomic force microscopy dynamic modes: modeling and applications. *Journal of Physics: Condensed Matter*, 20, 2008.

[212] E. J. Doedel, H. B. Keller, and J. P. Kernevez. Numerical analysis and control of bifurcation problems (i) bifurcation in finite dimensions. *International Journal of Bifurcation and Chaos*, 1:493–520, 1991.

[213] E. J. Doedel, H. B. Keller, and J. P. Kernevez. Numerical analysis and control of bifurcation problems (i) bifurcation in finite dimensions. *International Journal of Bifurcation and Chaos*, 1:745–772, 1991.

[214] G. Veronis. A note on the method of multiple scales. *Quarterly of Applied Mathematics*, pages 363–368, 1980.

[215] D. P. Mason. On the method of strained parameters and the method of averaging. *Quarterly of Applied Mathematics*, pages 77–85, 1984.

[216] Z. Rahman and T. D. Burton. Large amplitude primary and superharmonic resonances in the duffing oscillator. *Journal of Sound and Vibration*, 110:363–380, 1986.

[217] I. Kovacic and J. J. Brenna. *The Duffing Equation: Nonlinear Oscillators and their Behaviour*. John Wiley & Sons, 2011.

[218] C. Touzé and M. Amabili. Nonlinear normal modes for damped geometrically nonlinear systems: Application to reduced-order modelling of harmonically forced structures. *Journal of Sound and Vibration*, 298:958–981, 2006.

[219] S. A. Neild and D. J. Wagg. A generalized frequency detuning method for multi-degree-of-freedom oscillators with nonlinear stiffness. *Nonlinear Dynamics*, 73:649–663, 2013.

[220] V. Dolotin and A. Morozov. *Introduction to Non-Linear Algebra*. World Scientific Publishing Co Inc, 2007.

[221] S. Lang. *Algebra*. Addison-Wesley Publishing, third edition, 2002.

[222] Michael Smith. *ABAQUS/Standard User's Manual, Version 6.9*. Dassault Systèmes Simulia Corp, United States, 2009.